SYNTHESIS AND BIOLOGICAL EVALUATION OF POLYNUCLEAR CYCLOMETALATED RUTHENIUM, RHODIUM AND IRIDIUM COMPLEXES BASED ON A PPI DENDRITIC SCAFFOLD

Lara Cathryn Sudding

University of Cape Town 2013

Synthesis and biological evaluation of polynuclear cyclometalated ruthenium, rhodium and iridium complexes based on a PPI dendritic scaffold

Lara Cathryn Sudding

A dissertation presented in fulfilment of the requirements for the degree

Master of Science

Department of Chemistry

University of Cape Town

2013

Supervisor: Dr Gregory S. Smith

Declaration

I declare that "**Synthesis and biological evaluation of polynuclear cyclometalated ruthenium, rhodium and iridium complexes based on a PPI dendritic scaffold***"* is my own work and to the best of my knowledge has never been reported or submitted for any degree or examination in any university. All sources of information used are cited, acknowledged and completely referenced at the end of each chapter. I grant the University of Cape Town free license to reproduce the dissertation in whole or in-part for the purpose of research.

.....

Lara Cathryn Sudding

..../..../.....

Dedication

This dissertation is dedicated to my family, thank you for all the love and support that has gotten me through the past 2 years. Through the good times and the tough times, you have been behind me every step of the way.

Acknowledgements

I would like to express my sincere gratitude to the following people, without whom this dissertation would not have been possible: My supervisor Dr Gregory Smith, for his optimism, guidance and encouragement throughout my Master's project, as well as my time with him before that. I would also like to thank Ms Deidre Brooks for her constant administrative support.

The Swiss collaborators, Dr Bruno Therrien (University of Néuchatel) for the X-ray crystallography analysis and Prof Paul Dyson (Ecole Polytechnique Fédérale de Lausanne) for the *in vitro* anticancer testing and DNA binding experiments. As well as a big thank you for inviting me into their labs for 3 months whereby I was under great supervision of two colleagues and friends, Anais & Yo.

The analytical staff at the University of Cape Town, Mr Pete Roberts for running the spectroscopic data and Mr Gianpierro Benincasa for recording the elemental analysis data.
For financial support the NRF. My deepest gratitude to Dr Prinessa Chellan for proof reading my dissertation. For the invaluable advice from my colleagues, Preshendren, Prinessa, Sisa and Irwin for his constant willingness to help me out. As well as the rest of the Synthetic Organometallic and Bioorganometallic Research Group.

And finally and most importantly to my family, Dad, Hil, Matt, Creagh, Nics, KJ & Tim, I thank you for your unconditional support throughout my academic career and especially during my Master's project.

Table of Contents

Publications

Journal Article:

Published in the Journal of Dalton Transactions,

P. Govender, L. C. Sudding, C. M. Clavel, P. J. Dyson, B. Therrien and G. S. Smith, *The influence of RAPTA moieties on the antiproliferative activity of peripheral-functionalised poly(salicylaldiminato) metallodendrimers*, 2013, **42**,1267-1277.

Conference Contributions

July 2013 - Poster Presentation:

'Synthesis and biological evaluation of polynuclear cyclometalated ruthenium, rhodium and iridium complexes based on a PPI dendritic scaffold' presented at the **INORG2013 Conference** hosted by the the South African Chemical Institute (SACI) 30 June - 4 July 2013 at the Southern Sun Elangeni Hotel, Durban, South Africa.

Abstract

A series of chelating, bidentate (*C,N*-) monomeric and dendritic ligands based on a poly(propyleneimine) dendritic scaffold were synthesized via a Schiff-base condensation reaction of the relevant amine and either naphthaldehyde or benzaldehyde. These reactions yielded air- and moisture-stable solids or oils. These compounds were isolated in good yields and characterized using standard spectroscopic and analytical techniques.

The monomeric and dendritic ligands were reacted via a bridge-splitting reaction with the dimeric metal precursors, either $[Ru(p\text{-cymene})Cl_2]_2$, $[Rh(\eta^5\text{-}C_5Me_5)Cl_2]_2$ or $[Ir(\eta^5\text{-}C_5Me_5)Cl_2]_2$, generating a series of new mono- and polynuclear ruthenium(II), rhodium(III) and iridium(III) cyclometalated complexes. The naphthaldimine complexes were isolated as air- and moisture-stable solids, while the benzaldimine complexes were slightly hygroscopic and decomposed in solution over time. All the complexes were obtained in poor to good yields, and were fully characterized using ^{1}H-, ^{13}C-NMR and IR spectroscopies, as well as elemental analysis and mass spectrometry. The molecular structures of selected neutral mononuclear complexes were determined using single crystal X-ray crystallography.

Selected transition metal complexes, based only on the naphthaldimine ligand, underwent reactivity studies with PTA to afford a series of cationic chelating bidentate (*C,N*-) complexes. These complexes were also isolated as air- and moisture-stable solids, in poor to good yields, and were fully characterized using ^{1}H-, ^{13}C-, ^{31}P{^{1}H}-NMR and IR spectroscopies, as well as elemental analysis and mass spectrometry. Further to this, a series of chelating bidentate (*C,N*-) cationic heterometallic rhodium(III) and iridium(III) complexes were synthesized based on the monomeric and dendritic naphthaldimine ligands, through the incorporation of a ferrocenyl-pyridine moiety. The desired complexes were obtained as air- and moisture-stable solids, in poor to moderate yields. These complexes were fully characterized using a series of spectroscopic and analytical techniques.

The cytotoxicities of the mononuclear and dendritic ruthenium(II), rhodium(III) and iridium(III) complexes were evaluated against the cisplatin-sensitive (A2780) and cisplatin-resistant (A2780cisR) human ovarian cancer cells, as well as the non-cancerous human

embryonic kidney (HEK) and KMST-6 cell line. The higher-generation metallodendrimers showed superior biological activity over the mononuclear analogues. The cationic complexes also showed increased activity over the neutral complexes, as well as the metallodendrimers showing the best activity, versus the mononuclear analogues. The cationic octanuclear ruthenium(II) and rhodium(III) metallodendrimers were found to be the most active, with IC_{50} values in the low micromolar range. These *in vitro* studies show a clear correlation between the size of the metallodendrimer and cytotoxicity, as well as between the charge on the complex and cytotoxicity.

Abbreviations

°	degrees
°C	degrees Celsius
Å	angstrom(s)
Ar	aromatic
bipy	4-4'-bipyridine
br	broad
^{13}C-NMR	carbon nuclear magnetic resonance
calc	calculated
COSY	correlation spectroscopy
Cp*	pentamethylcyclopentadienyl
d	doublet
DAB	1,4-diaminobutane
DCM	dichloromethane
dendr	dendrimer
dfphpy	2-(2,4-difluorophenyl) pyridine
DMSO	dimethyl sulfoxide
DNA	deoxyribonucleic acid
dppe	bis(diphenylphosphine)ethane
EA	elemental analysis
en	ethylenediamine
EPR	enhanced permeability and retention
ESI-MS	electrospray ionization - mass spectrometry
EtOH	ethanol
Et_2O	diethyl ether
FCS	foetal calf serum

Fc-py	ferrocenyl-pyridine
FT-IR	fourier transform infrared spectroscopy
g	gram(s)
h	hour(s)
^{1}H-NMR	proton nuclear magnetic resonance
HMB	hexamethylbenzene
HR-ESI	high resolution-electrospray ionization
HSQC	heteronuclear single quantum correlation
Hz	hertz
IC_{50}	50% inhibitory concentration
IR	infrared
JAK-STAT	Janus kinase and signal transducers and activators of transcription
μM	micromolar
m	multiplet
Me	methyl
MeOH	methanol
min	minute(s)
mol	mole(s)
mmol	millimole(s)
MP	melting point
MS	mass spectrometry
MTT	3-(4,5-dimethylthiazol-2-yl)-2,5-diphenyltetrazolium bromide
m/z	mass to charge ratio
NA	not active
nM	nanomolar
NMR	nuclear magnetic resonance
ORTEP	Oak Ridge Thermal Ellipsoid Plot

$^{31}P\{^{1}H\}$-NMR	phosphorous nuclear magnetic resonance
p	para
PAMAM	poly(amidoamine)
PGM	platinum group metal
phpy	phenylpyridine
phq	2-phenylquionoline
PKC	protein kinase-C
PPh_3	triphenylphosphine
PPI	poly(propyleneimine)
ppm	parts per million
PTA	1,3,5-triaza-7-phosphaadamantane
pyr	pyridine
pyz	pyrazine
q	quartet
RAPTA	ruthenium-arene PTA
RNA	ribonucleic acid
RT	room temperature
s	singlet (^{1}H-NMR)
sep	septet
t	triplet
TAM	tamoxifen
TNF-α	tumour necrosis factor-α
tpy	2-(*p*-tolyl)pyridine
WHO	World Health Organization

Chapter 1: A Review of Ruthenium(II), Rhodium(III) and Iridium(III) Organometallic Complexes and their Anti-Cancer Properties

1. Introduction

1.1 Cancer and chemotherapy

According to the WHO, there are more than 6 million deaths each year attributed to cancer.[1] Cancer is a disease known to affect any part of the human body due to the formation and accumulation of abnormal cells.[1] The ability of these cells to invade and spread throughout the body is known as metastasis and is the leading cause of death from cancer.[1] Chemotherapy, radiation therapy, and immunotherapy[2] are a few therapies that have been developed for the treatment and regulation of cancer, although there are many harsh side-effects that are associated with these therapies.[3]

Chemotherapy is not very selective to cancer cells as the chemotherapeutic drugs cannot always distinguish between cancerous and healthy cells, which cause undesirable side effects and systemic toxicity.[4] For instance its mode of action is to kill cells that divide rapidly, which is characteristic of cancer cells, whereas certain healthy cells also divide rapidly, for example, cells in the bone marrow.[3] Hence healthy cells can also be damaged in the process.

Therefore these therapies require excessive doses which will cause side effects that are intolerable for the human body and causes more damage than the cancer itself.[4] Organic compounds have been and are widely used in the pharmaceutical world, but there has been motivation for the development of metal-based drugs and drug delivery vehicles as potential anticancer treatments.[5] A metal-based drug, cisplatin ((*cis*-diamminedichloro-platinum(II)) was discovered by Rosenberg[6-8] in the 1960s for its use in anti-cancer treatment.[6]

1.2 Clinical success of platinum-based drugs

The most common metal-based drug that has been used for the past 30 years is cisplatin.[9,10] cisplatin, amongst other platinum-based drugs derived from cisplatin, have been used for the treatment of ovarian, testicular and other cancers.[9] Besides cisplatin, carboplatin and oxaliplatin are platinum-based complexes that have also received global attention (**Figure 1.1**).[9, 10]

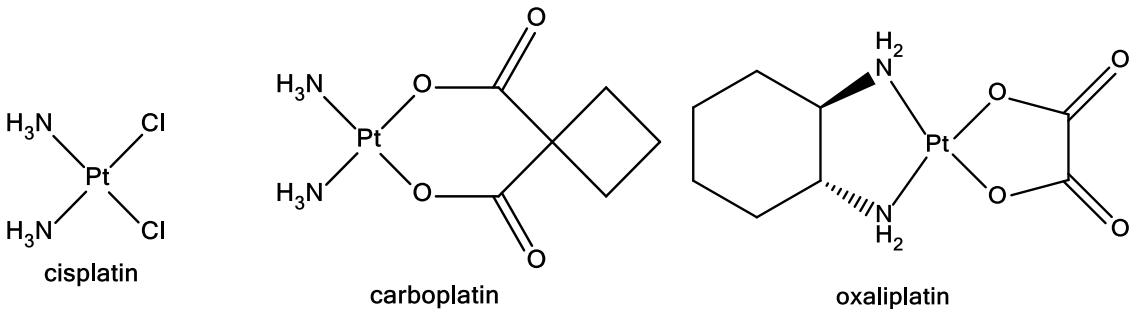

Figure 1.1: Three platinum-based anticancer drugs.[9]

Carboplatin and oxaliplatin were designed based on cisplatin, with modifications that attempted to eliminate the side effects associated with cisplatin. As can be seen in **Figure 1.1**, the chloride ligands have been replaced by less labile ligands. This is because the toxicity of platinum-based drugs is related to the ease with which the leaving groups (chloride and ammonia) are aquated, i.e. the ease with which these groups are replaced with a water molecule once the molecule enters the cell.[9] The slower the ligands are aquated, the less toxic the platinum-based drug, hence the presence of the less labile ligands on carboplatin and oxaliplatin.

One of the targets of cisplatin is supposed to be DNA. It is suspected that cisplatin targets and binds cellular DNA once aquated, whereby it interferes with DNA replication and transcription, and to some degree interferes with RNA processing, therefore the cancerous cells cannot replicate and apoptosis occurs.[9,10]

Besides the notable success of these platinum-based drugs, particularly cisplatin, as anti-cancer drugs, they have their limitations.[9] These include non-specific targeting of unhealthy as well as non-cancerous cells, dose-limiting side effects and drug resistance.[9]

A series of platinum(IV) drugs have demonstrated increased stability and lipophilicity *in vitro*, versus their platinum(II) counterparts.[10, 11] However, *in vivo* studies demonstrated the opposite effect. The platinum(IV) complexes showed little to no activity and hence these molecules have not advanced to clinical trials.[10, 11] In the case of *in vitro* studies, the cells in monolayer cultures tend to be exposed to uniform conditions which is not analogous to the tumour microenvironment, whereas *in vivo,* the cells are exposed to a large concentration gradient as the drug diffuses from the blood vessels.[10]

1.3 Platinum-like drug candidates (Ruthenium, rhodium and iridium-based drug candidates)

1.3.1 Ruthenium-based drug candidates

In light of the issues associated with platinum-based drugs, ruthenium-based drugs have received considerable attention due to their variety of available oxidation states,[12] similar ligand exchange abilities,[12] better selective cytotoxicity toward cancer cells allowing them to overcome cisplatin resistance[12-14] and their high affinity towards proteins making it easier for them to enter the cancerous tissue.[12, 15, 16]

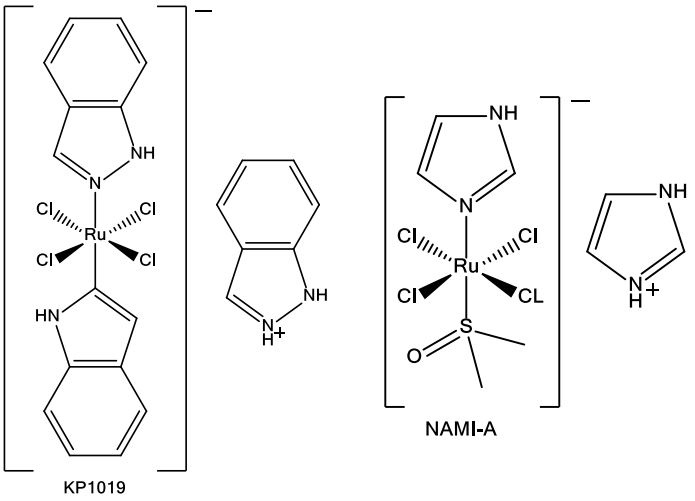

Figure 1.2: Structure of KP1019 and NAMI-A.[14]

Two mononuclear ruthenium complexes have completed phase I clinical trials and are undergoing phase II trials, namely Indazolium trans-[tetrachlorobis(1H-indazole)ruthenate(III)] (KP1019) and New Anti-tumour Metastasis Inhibitor-A (NAMI-A) (**Figure 1.2**).[17] Their potential anticancer activity can be accredited to the affinity of Ru(III) for proteins which can selectively enter cancerous tissue.[18] NAMI-A is not very toxic to cancer cells but it does show promising anti-metastatic activity.[19]

Ruthenium complexes are able to mimic the behaviour of iron under physiological conditions, making them more susceptible to be taken up by cancer cells via endocytosis by means of attaching themselves to albumin or transferrin.[12, 18, 20] The ability of ruthenium complexes to target cancer cells versus non-cancerous cells could be due to the fact that cancer cells have a high iron requirement and therefore express a large number of transferrin receptors on the cell surface. Therefore it has been proposed that there is cellular accumulation of ruthenium(III) in cancerous cells.[12, 18, 20] Once the ruthenium anti-cancer

agent has entered the cell, it has been proposed that the pH and redox potential within the cell can act as drug release triggers.[4] The speculated mode of action of ruthenium-based molecules is their ability to damage DNA and to some extent inhibit enzyme action.[9,10,21,22] The mononuclear complexes, NAMI-A and KP1019 (**Figure 1.2**), undergo *in vivo* reduction from ruthenium(III) to ruthenium(II) which is the suggested active species, as it is expected to bind and interfere with DNA. Therefore the ruthenium metal centre can be stabilized in the +2 oxidation state with coordinated arene ligands through pi-bonding.[13, 18, 23]

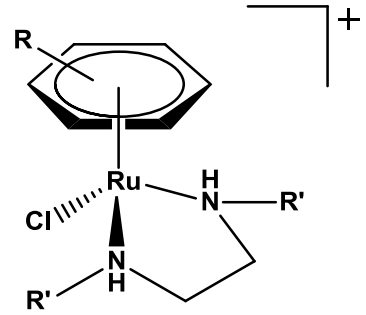

Figure 1.3: General structure of Sadler *et al.*[24] ruthenium(II)-arene complexes with promise for clinical trials.

Since the discovery of the proposed metal active species, there has been a shift in focus towards ruthenium(II)-arene type complexes.[20] Cationic complexes of the type [η-(arene)RuCl(en)]PF_6 (**Figure 1.3**)[20, 24] have shown *in vitro* and *in vivo* anticancer activity against many cell lines, more specifically against secondary metastatic tumours.[15, 24, 25] The arene-ring not only provides stabilization of the ruthenium in the +2 oxidation state but also provides a lipophilic face which can enhance molecular recognition and transport the ruthenium through cell membranes giving these complexes promising anti-tumour properties.[26]

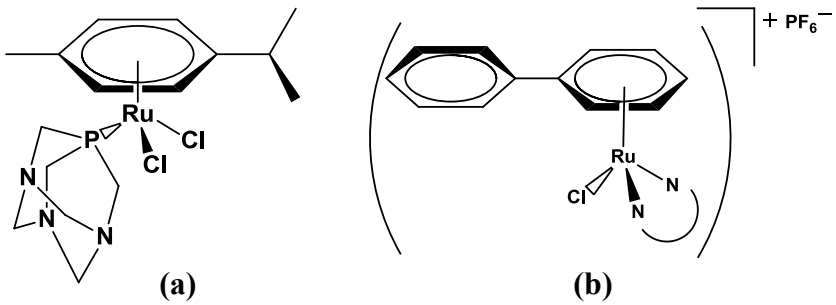

Figure 1.4: Ruthenium mononuclear complexes that exhibit *in vivo* and *in vitro* activity, respectively.[15,26]

Dyson *et al*.[25] synthesized and studied the anti-cancer activity of half-sandwich ruthenium-(II)-arene-PTA (RAPTA) complexes (**Figure 1.4a**) which exhibited dose-dependent *in vivo* activity against secondary metastatic tumours.[25] The success of these RAPTA-type compounds has been proposed to be because of their increased water solubility[25] as well as demonstrating pH-dependent activity.[22, 25] In an acidic environment, analogous to hypoxic cancerous cells, the nitrogen atom on the PTA ligand is protonated to the proposed active species and there is evidence of DNA damage.[27, 28] At a pH similar to that of healthy cells, pH above 7, there is little to no DNA damage therefore making these compounds more selective towards cancer cells versus non-cancerous cells.[22, 25, 27, 28]

Other ruthenium-(II)-arene complexes, that contain different functional groups, such as ethylenediamine in $[(\eta^6\text{-biphenyl})Ru(en)Cl][PF_6]$ (**Figure 1.4b**), have shown IC_{50} values as low as carboplatin, when tested against the human ovarian cancer cell line A2780.[26]

1.3.2 Rhodium-based drug candidates

Metal-based chemotherapeutics containing rhodium(III) and iridium(III) have also sparked interest in the field of anticancer therapy.[15] They possess similar properties to ruthenium where rhodium(III) complexes are isoelectronic to ruthenium(II).[20, 29] Their reactivity can be adjusted from kinetically labile to inert, but recently it has been proposed that their activity is due to their kinetic inertness.[20, 29] These rhodium and iridium complexes are also readily available and show high water solubility.[30]

As previously mentioned rhodium(III) and ruthenium(II) are isoelectronic and therefore are worth looking at as potential anticancer agents. In one study, rhodium and ruthenium complexes were tested against the ovarian cancer cell line, A2780 and cisplatin-resistant A2780cisR.[8, 14] The cluster complex $[Rh_3(\mu^3\text{-}S)_2(\eta^5\text{-}C_5Me_5)_3]^{2+}$ exhibited cytotoxicity similar to that of the ruthenium analogue, $[Ru_3(CO)_9(PTA)_3]$ indicating that rhodium(III) complexes can be considered for potential anticancer drugs.[8, 14]

With the success of incorporating 1,3,5-triaza-7-phosphaadamantane (PTA) into ruthenium(II) mononuclear complexes, a group of rhodium(III)-arene complexes, $[Rh(\eta^5\text{-}C_5Me_5)(PTA)Cl_2]$, showed similar cytotoxicities to the ruthenium analogue, against the HT29 colon cancer cell line (**Figure 1.5**).[15]

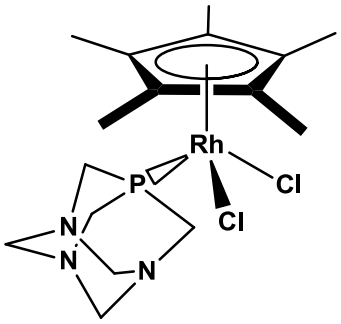

Figure 1.5: Rhodium(III) arene-PTA complex showing similar cytotoxicity's to the ruthenium(II) analogues.[15]

In this study, the focus is on bidentate-cyclometalated complexes. Meggers and co-workers developed a rhodium(III)-based bidentate cyclometalated complex to target protein kinase-C (PKC) active sites.[31] PKC is important for the regulation of a variety of cellular functions. Therefore if the complex inhibits the activity of the enzymes, apoptosis may occur.[32]

Complexes can be designed for a particular target and in this case a phenylquinoline motif was incorporated with the intention for these complexes (**Figure 1.6**) to be able to form hydrogen bonds with the ATP-binding site.[31] This is ideal as protein kinases are responsible for dephosphorylating the ATP group and transferring it to other substrates for important metabolic pathways. This process will be inhibited by these complexes and apoptosis of cancerous cells may occur.[31] The results showed that in the complex where R=H, an IC_{50} value of 30 μM was obtained.[31]

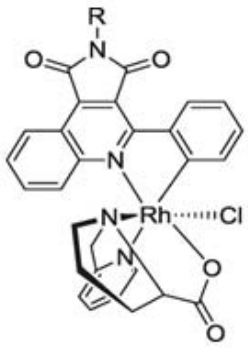

Figure 1.6: Rhodium(III) complexes as PKC inhibitors (where R = benzyl or H).[31, 33]

In a similar study, the intended target was the Janus kinase and signal transducers and activators of transcription (JAK-STAT) pathway, which is directly linked to the regulation and signalling of cell proliferation and apoptosis.[34] Enzyme and cellular assays were performed using two charged cyclometalated rhodium(III) complexes (**Figure 1.7**) and each complex showed inhibition of the JAK's pathway.[33]

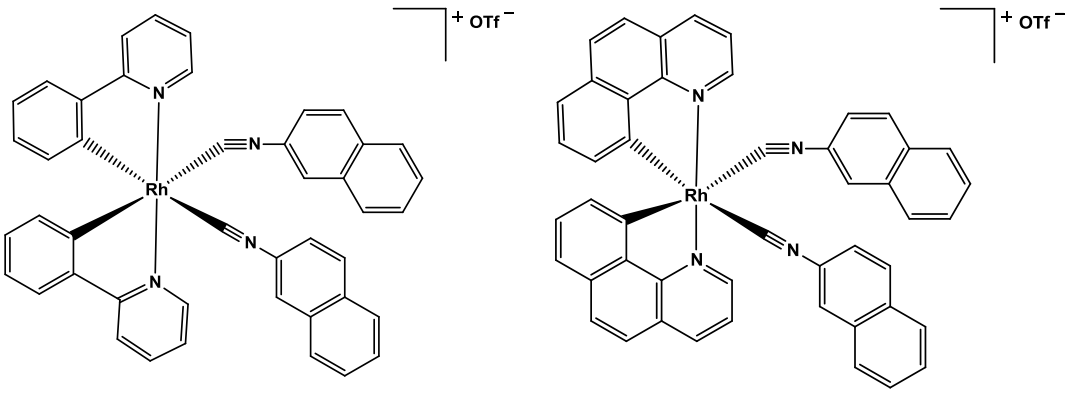

Figure 1.7: Rhodium(III) complexes as JAK-STAT pathway inhibitors.[33, 35]

A rhodium(III) *C,N*-chelating mononuclear complex was synthesized and its anticancer activity was evaluated. These complexes showed good stability due to the pentamethylcyclopentadienyl (Cp*) ring and showed activity similar to that of cisplatin.[20, 36]

This evidence demonstrates that rhodium(III) complexes have the potential to act as anti-cancer agents, focussing on targeted pathways different to that of cisplatin.

1.3.3 Iridium-based drug candidates

As discussed above, targeting a variety of kinases important for pathways within the cell is vital in the design of potential anti-cancer complexes.[31] VEGFR3 or FLT4 is a Fms-related tyrosine kinase 4 that plays a role in maintaining lymphatic vessels.[37] Meggers and co-workers designed and synthesized a series of iridium(III) pyridocarbazole complexes containing a 1,5-cyclooctadiene ligand and these complexes showed tyrosine kinase inhibition.[38] All the complexes showed good activity with the iridium(III) complex in **Figure 1.8** showing the best activity with an IC_{50} value in the nanomolar range. This complex also did not show the toxicity associated with other metallodrugs.[33, 38]

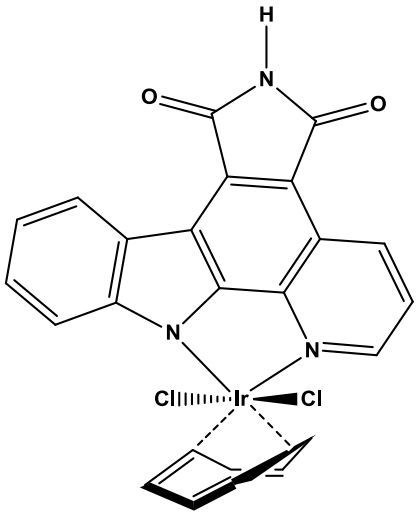

Figure 1.8: Iridium(III) pyridocarbazole complex showing tyrosine kinase inhibition.[33, 35, 38]

In another study, a cationic cyclometalated iridium complex was studied as a potential tumour necrosis factor-α (TNF-α) inhibitor.[39] TNF-α is a cytokine that regulates cell processes such as cell apoptosis and survival.[40] *In vitro* results confirmed that the iridium complex (**Figure 1.9**) interferes with TNF-α binding in the TNF-α binding pocket, which is necessary for it to perform its functions.[33] The authors proposed via molecular modelling analysis, that the complex coordinates to the binding pocket of the TNF-α dimer therefore preventing TNF-α from binding.[33] Further studies confirmed that the inhibition was dependent on the iridium metal centre and its affinity for the binding pocket, making this complex a specific inhibitor of TNF-α.[33]

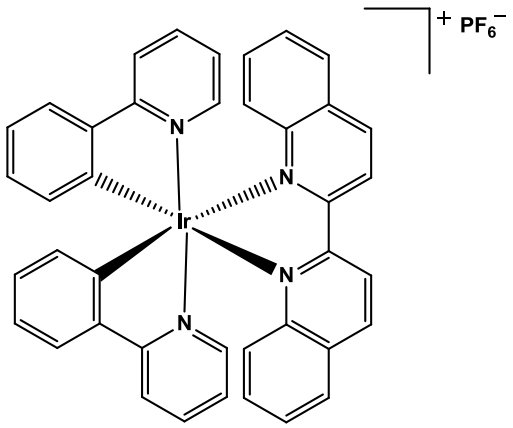

Figure 1.9: Ir(III) complex as an inhibitor of the TNF-α cytokine.[33, 35, 38, 39]

Sadler *et al*. synthesized a series of mononuclear iridium complexes and their cytotoxicity against the A2780 ovarian cancer cell line was examined.[41] Three complexes with the general formula [Ir(η^5-C_5Me_5)(C^N)Cl] (**Figure 1.10**) exhibited IC_{50} values similar to that of cisplatin.[41, 42] One iridium complex with the extended Cp* moiety exhibited an IC_{50} value of 0.70±0.04 μM, which is lower than cisplatin.[41, 42] There has been evidence that there is a

direct correlation between the cytotoxicity and the size of the ligands attached to the metal centre.[22] It is proposed that the larger ligands are able to intercalate into DNA therefore disrupting the DNA structure.[41] It was also proposed that the replacement of the *N,N*-chelating ligand with the *C,N*-chelating ligand switches on biological activity.[20, 42] Therefore there is promising evidence that iridium complexes can be used in biological applications, such as anticancer treatment.[41, 42]

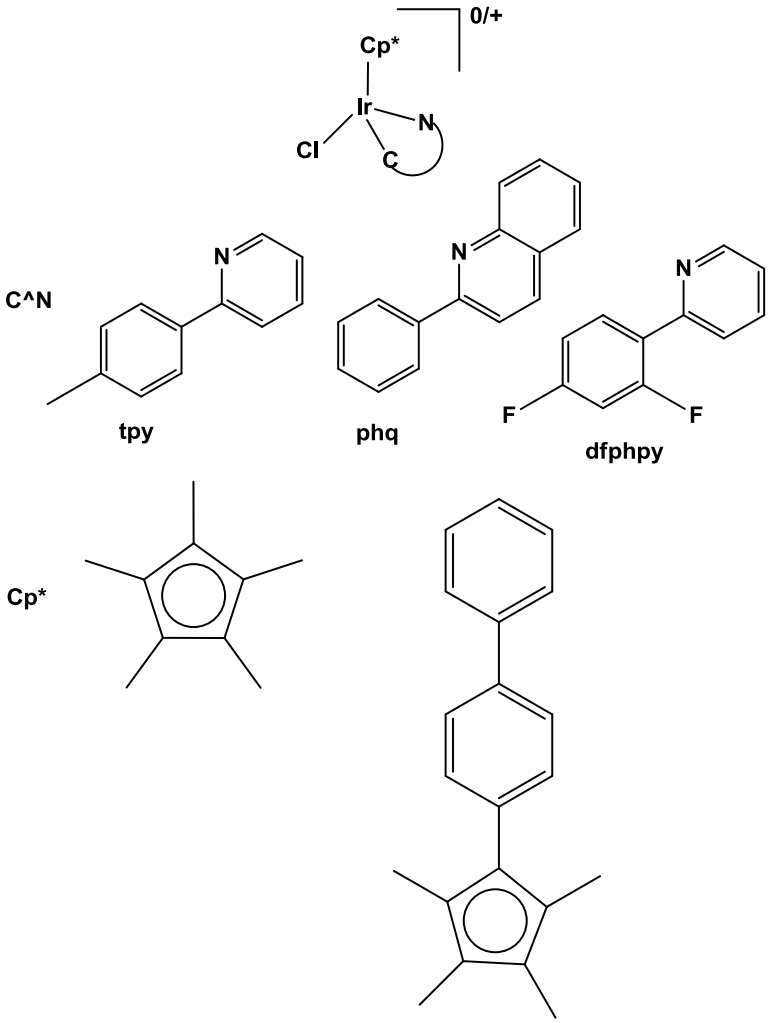

Figure 1.10: Iridium complexes showing *in vitro* activity against the A2780 human ovarian cancer cell line (cisplatin IC_{50} - 1.19±0.12 μM).[41]

There is sufficient evidence that molecules that contain ruthenium, rhodium and iridium have shown *in vitro* and to some extent *in vivo* cytotoxicity against a variety of cancer cell lines.[20, 33] There have been recent reviews on rhodium and iridium specifically.[33,35] It is also speculated that these metal-complexes affect and bind DNA, RNA and other proteins in a different and improved mechanism in comparison to platinum-based drugs.[22,41] However the

incorporation of multiple metal atoms has only been briefly looked into and so there is space for investigations into such complexes. The aim of this project is to incorporate all three transition metals in macromolecules such as dendrimers, as these molecules have the advantage of being morphologically similar to biological macromolecules, and therefore can be taken up into the human body relatively effortlessly.

1.4 Multinuclear metal-based drug candidates for clinical applications

1.4.1 Platinum-based drug candidates

After the success of cisplatin, it was suggested that increasing the number of metal centres may increase the biological activity of the platinum complexes.

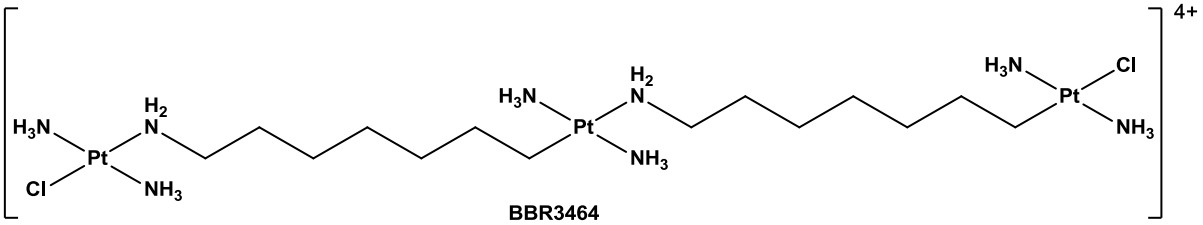

Figure 1.11: Trinuclear cationic platinum(II) compound, BBR3464.[44]

Synthesis of multinuclear complexes was initiated by Farrell *et al*.[44] who synthesized the platinum complex BBR3464 ([μ-*trans*-$Pt(NH_3)_2${*trans*-$PtCl(NH_3)_2${$NH_2(CH_2)_6$-NH_2}$}_2$][NO_3]) (**Figure 1.11**) which is a trinuclear complex that entered phase I clinical trials and the results showed that its *in vitro* activity was greater than that of cisplatin as well as showing a different mechanism of action by overcoming cisplatin-resistant mechanisms.[43, 44] From these results it has been established that multinuclear complexes show improved anti-cancer activity versus the mononuclear analogues.[44]

Platinum-based drugs have proven that the incorporation of metal centres into potential anti-cancer drugs has a desirable effect. Unfortunately, platinum-based drugs have developed a variety of limitations such as toxic side effects and acquired resistance, hence the shift in focus away from platinum-based drugs towards other transition metal-based drugs.[9, 17]

1.4.2 Palladium-based drug candidates

From what has been discussed so far, incorporating metals from the PGM series other than platinum has led to an increase in anti-cancer activity as well as potentially overcoming resistance. Palladium(II) is structurally and thermodynamically similar to platinum(II) therefore the incorporation of palladium(II) has been investigated.[20] A series of dimeric palladium(II) complexes (**Figure 1.12**) showed promising antitumor activity by inhibiting cathepsin B which is an enzyme that is expressed in cancer cells, showing both *in vitro* and *in vivo* anticancer activity.[45]

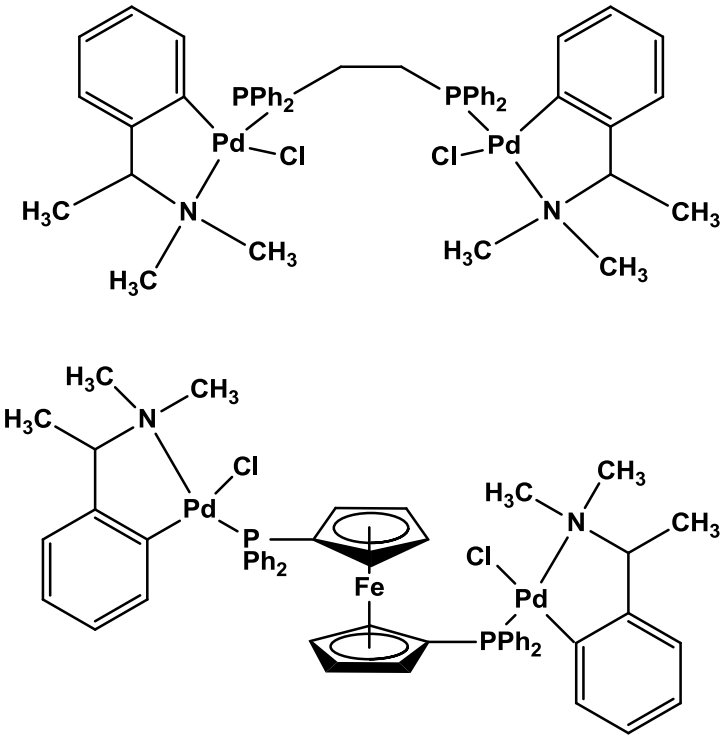

Figure 1.12: Examples of *C,N*-palladium(II) complexes.[20]

1.4.3 Osmium-based drug candidates

Another such example is osmium, which has been incorporated into metalla-rectangles as potential multinuclear anti-cancer agents.[46] One tetranuclear complex (**Figure 1.13a**) showed an IC_{50} value of 5.4 ± 0.6 μM, which was comparable with a series of ruthenium analogues (**Figure 1.13b**).[46, 47] Osmium complexes tend to be less cytotoxic than ruthenium complexes and therefore there has been more focus on ruthenium complexes.[46]

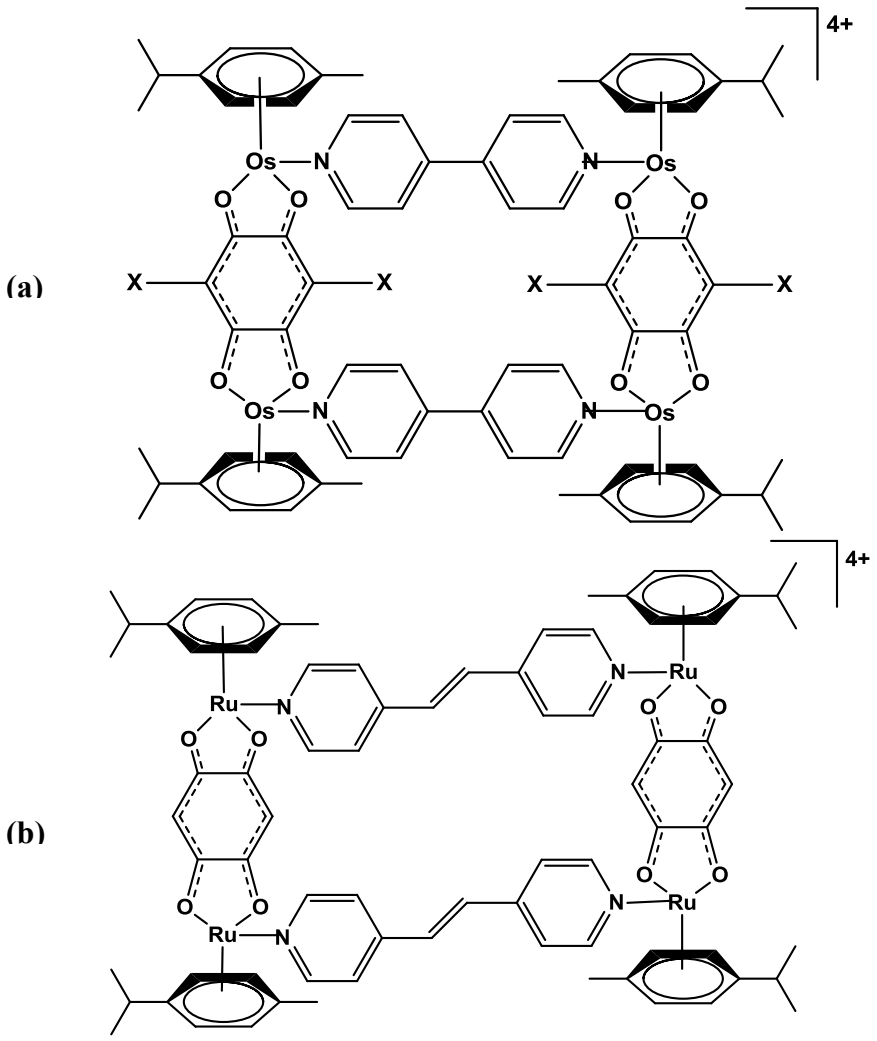

Figure 1.13: Multinuclear osmium and ruthenium metalla-rectangle (X = H) showing the highest *in vitro* activity.[46]

1.4.4 Ruthenium-based drug candidates

A series of multinuclear ruthenium analogues of the above mentioned compounds (**Figure 1.13b**) were also synthesized and showed even more promising *in vitro* activity.[47] These complexes showed a smaller range of IC_{50} values, from 6-50 μM whereas the osmium complexes showed a larger range from 5-223 μM.[47]

Dinuclear complexes have also been investigated for their biological properties. A series of ruthenium dinuclear complexes (**Figure 1.14**) were synthesized based on the mononuclear NAMI-A ruthenium(III) complex and their cytotoxicity was studied at different concentrations.[48]

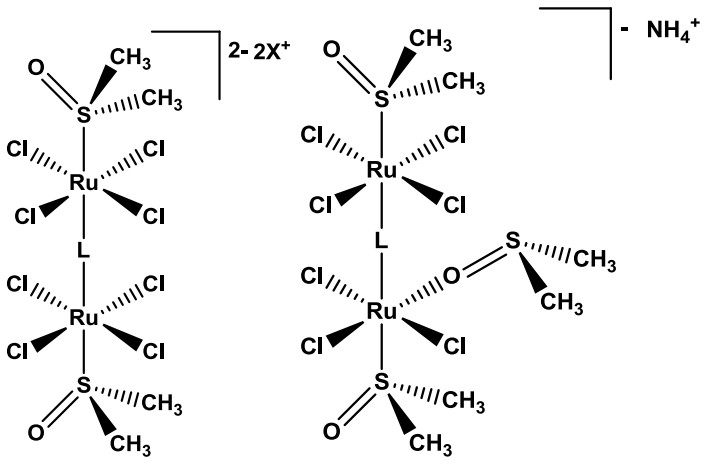

Figure 1.14: Two dinuclear ruthenium(III) complexes showing similar activity to NAMI-A (where X=Na and L=bipy (4-4'-bipyridine) and pyz (pyrazine)).[48]

Similarly to NAMI-A, the complexes *in vitro* activity was not promising even with an increase in the number of ruthenium atoms, although there was a correlation between the modification of the cell cycle with an increase in concentration of ruthenium uptake in tumour cells.[48] They were therefore able to conclude that these two dinuclear complexes (**Figure 1.14**) were able to modify the cell cycle and behave similarly to that of NAMI-A, which is able to inhibit the growth of new metastases as well as the growth of already established metastases.[49]

Dinuclear complexes have also been designed and synthesized with the purpose to target different pathways to that of cisplatin.[50] A di-ruthenium(II) triple-stranded helicate was obtained based on a bis(pyridylimine) ligand with a hexafluorophosphate counterion and exhibited IC_{50} values better than ruthenium(III) complexes (**Figure 1.15**). The complexes were tested against two breast cancer cell lines (HBL100 and T47D) and exhibited IC_{50} values of 22 and 53 μM, respectively, versus 4.9 and 28 μM for cisplatin, respectively. They also demonstrated that the helicate is able to bind and coil DNA.[50]

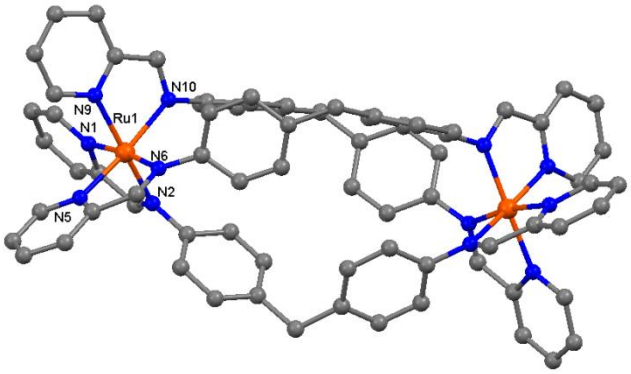

Figure 1.15: X-ray crystal structure of a di-ruthenium(II) triple stranded helicate.[50]

Increasing the number of metal atoms incorporated into an organic framework can potentially increase its anticancer and biological properties. These dinuclear complexes didn't show activity as high as that of the tetranuclear complexes but ruthenium has shown great potential when incorporated into potential anti-cancer agents.

1.5 Ferrocene-based anticancer drugs

Since the discovery of platinum-based anticancer drugs there has also been an increasing interest in ferrocene-based complexes to be used as potential anti-cancer drugs.[51] It is understood that the oxidised analogue of ferrocene, the ferrocenium ion (**Figure 1.16**), acts as the antitumor agent as it is proposed that this oxidised analogue generates active radicals which in turn form radical metabolites which are responsible for the damage in cancer cells.[51,52]

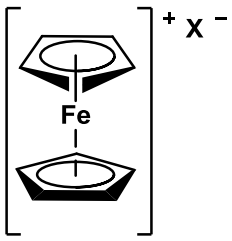

Figure 1.16: Active ferrocenium ion.[53]

In addition to this, the ferrocenyl moiety contains two cyclopentadienyl rings in a sandwiched arrangement, which prevents the iron from forming further bonds with any nearby molecules.[54] The oxidised ferrocenium ion seems to be more active than the ferrocene molecule. This could be due to solubility issues, but it has also been proposed that the

ferrocene is oxidised to the ferrocenium ion *in vivo* so the solubility of ferrocene may not be a critical issue.[51,54]

(a)

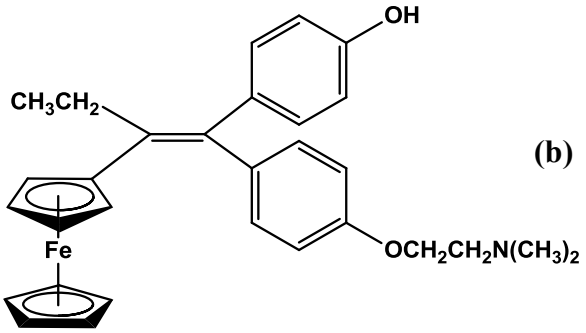

(b)

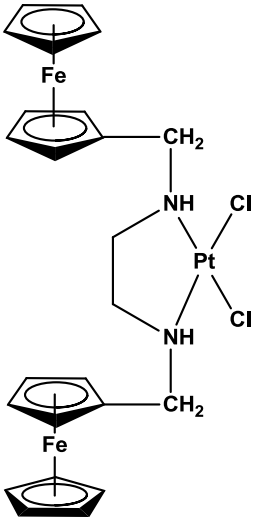

Figure 1.17: Ferrocene derivatives of known anticancer drugs **(a)** tamoxifen and **(b)** cisplatin, respectively.[51, 52]

Ferrocifen (**Figure 1.17a**) is a ferrocenyl derivative of tamoxifen (TAM), and has entered clinical trials and other related ferrocenyl derivatives are in clinical trials for malaria.[52] Ferrocene has also been incorporated in another well-known anti-cancer drug, cisplatin, in an attempt to develop dual action drugs (**Figure 1.17b**).[36,52,40]

TAM (**Figure 1.18**) is an anti-oestrogen drug that has been used in the treatment of breast cancer.[52] Its proposed mechanism of action is to inhibit the progression of tumours rather than eliminating them all together. This action is aided by the hydroxyl group which enhances recognition of the oestadiol receptor, which is an oestrogen receptor.[52] This gives the potential drug more than one functionality which can be involved in the anticancer activity, which decreases the chances of developed resistance and increases the activity of the molecule.[52] However in the case where it was coupled to cisplatin, it was found to be only slightly cytotoxic towards breast cancer cell lines.[16]

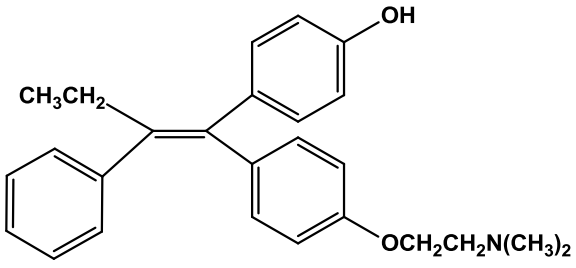

Figure 1.18: Structure of the TAM, which is used in the treatment of breast cancer.

In conjunction with this particular study, there is evidence that organometallic tamoxifen derivatives have been prepared that show considerable promise, of which the ferrocenyl derivatives are ready for entry into clinical trials therefore evidence that the incorporation of a ferrocene derivative can enhance the anticancer activity.[16]

1.6 Dendrimers in biology

Dendrimers are a group of macromolecules that are well-defined, highly branched, three-dimensional, globular polymers that consist of a central core with side chains that branch from it (**Figure 1.19**).[55-57] The periphery of the dendrimer can be comprised of different functional groups, which plays an important role in determining the physical properties of dendrimers, such as those that make dendrimers better drug delivery agents.[55-57]

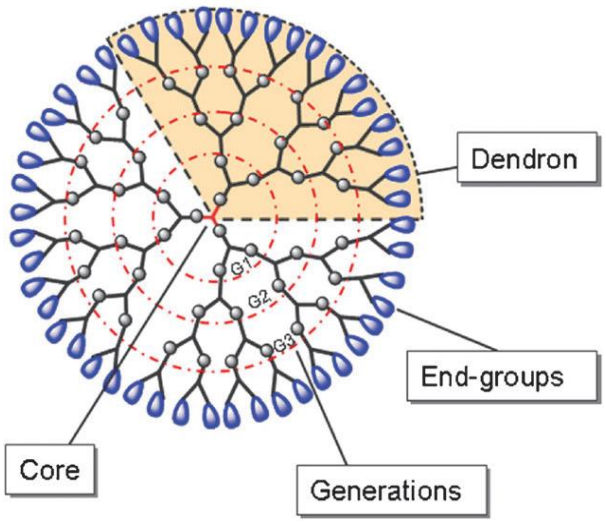

Figure 1.19: General structure of dendrimers.

Dendrimers possess properties such as high polyvalency, which means that a variety of targeting moieties, solubilising elements or drug molecules can be covalently attached to the periphery of the macromolecule to improve the performance of the drug carrier.[58]

1.6.1 Synthesis of dendrimers - the convergent and divergent synthetic routes

There are two main approaches to the synthesis of dendrimers. The first approach involves the initiation of synthesis at the core of the molecule and then progresses outwards, which is known as the divergent approach and was established by Tomalia *et al.*[59] While Frechét *et*

al.[60] introduced the convergent approach where synthesis starts off at the periphery of the molecule and progresses inward via a step addition of branching molecules which are finally attached to a central core (**Figure 1.20**).

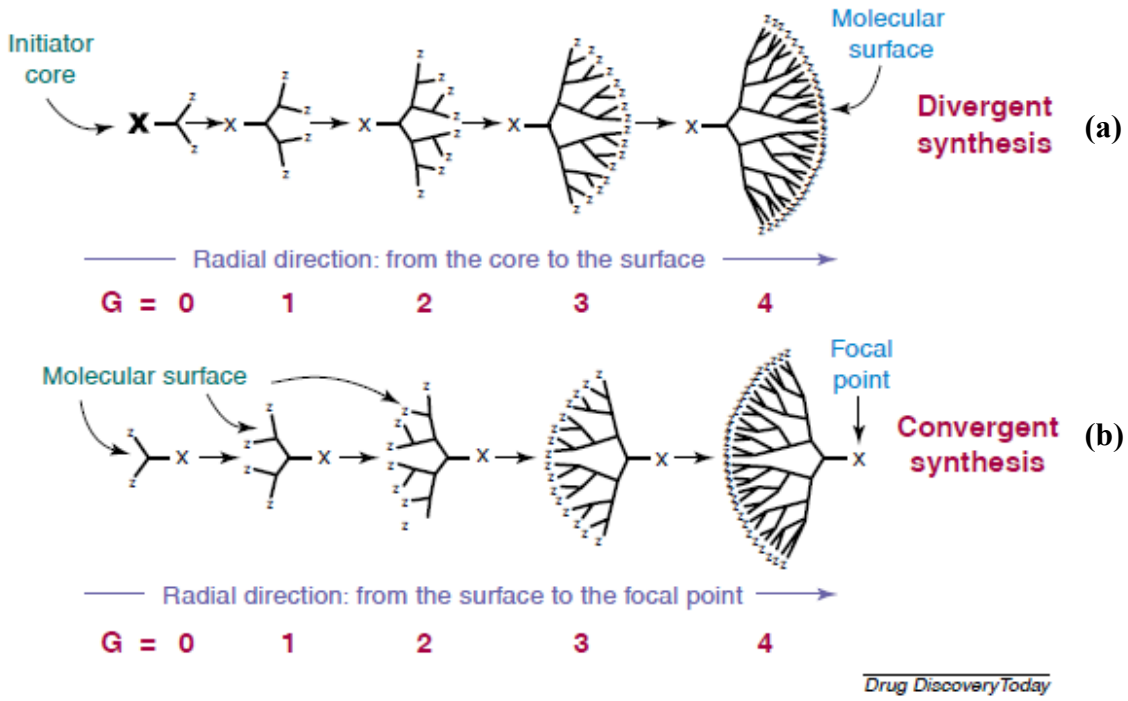

Figure 1.20: Two synthetic routes for dendritic macromolecules, **(a)** the divergent method and **(b)** the convergent method.[61]

Both synthetic routes have their advantages and disadvantages, but they complement each other in that the convergent approach has advantages at lower molecular weights while the divergent approach has advantages in its ability to reach much higher molecular weights.[62]

Both synthetic routes are used in the production of three main dendritic scaffolds, the poly(amido amine) (PAMAM), poly(propylenimine) (PPI) and poly(aryl ether) dendritic scaffolds.

1.6.2 Dendritic Scaffolds

1.6.2.1 PAMAM

PAMAM dendrimers consist of polyamide branches stemming from a central amine or diaminoalkane (diaminobutane) core (**Figure 1.21**).[63] They are synthesized via the divergent approach, irrelative of the fact that for higher generation dendrimers complete functionalization of the surface groups is difficult using this synthetic approach.[60,61] Synthesis

of these dendritic scaffolds involves repeating steps of double Michael addition of methyl acrylate to the terminal primary amines of the dendritic core followed by aminolysis of the terminal esters with ethylenediamine.[61]

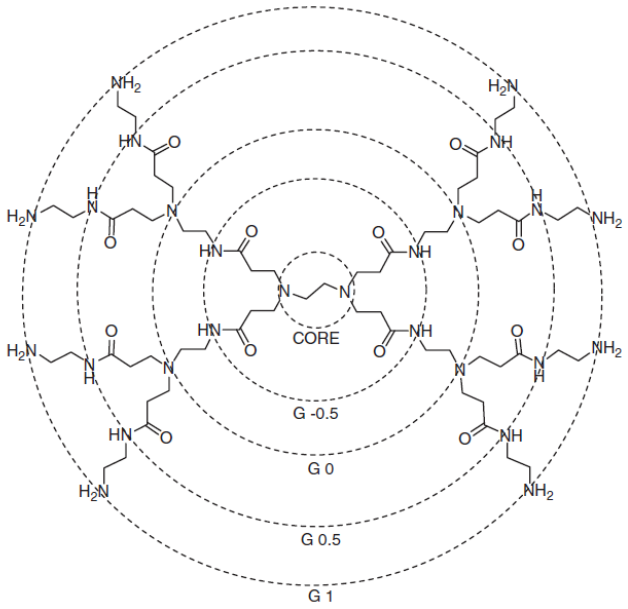

Figure 1.21: Schematic of a PAMAM dendritic scaffold.[64]

Tomalia *et al.*[59, 65] first synthesised these PAMAM dendrimers and they are the most widely used dendrimers for biological applications, i.e. as drug delivery vehicles.[64] This is due to properties such as good water solubility, low immunogenicity and their ability to mimic the properties of mammalian globular proteins.[64] In one particular study, PAMAM dendrimers did not elicit immune responses and exhibited low toxicity, especially when the periphery contained anionic or neutral groups, such as carboxylic or hydroxylic moieties.[62]

One limitation to PAMAM dendrimers is that molecules based on carbonyl-containing connecting groups are susceptible to reaction conditions such as reduction, hydrolysis and nucleophilic attack.

1.6.2.2 PPI

The first dendrimer, polypropyleneimine (PPI), was synthesized by Vögtle *et al.*[66] and is based on a diaminobutane (DAB) core, or any other primary or secondary amine core, with alkane branches that consist of amino groups as termini (**Figure 1.22**).[67] Synthesis of PPI dendrimers requires repeating steps of double Michael addition of acrylonitrile to the

dendritic core via the divergent synthetic approach and then followed by the hydrogenation of the nitriles.[67,68]

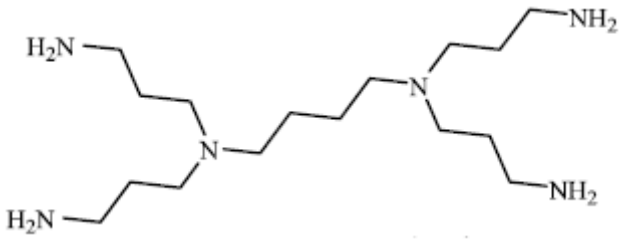

Figure 1.22: Figure of a PPI dendritic scaffold.

The PPI dendritic scaffold has been chosen for this study due to various reasons. For example, PPI dendrimers exhibit better general solubility compared to similar linear analogues.[57] This is advantageous as it can solubilise otherwise hydrophobic, non-soluble, anti-cancer drugs or moieties attached to the anti-cancer molecule.[68] The amine terminated surface of PPI dendrimers allows for the periphery to be easily modified in order to develop molecules that are ideal for cancer diagnosis and therapy.[64, 68] For example, the dendrimer can be functionalized with specific moieties to enhance access in physiological conditions.[64] This dendritic scaffold has also shown to be highly flexible with a homogenous density distribution.[69] These polyamines are therefore desirable as potential anticancer molecule scaffolds, especially since similar amine terminated molecules, such as spermidine found in ribosomes, are present within living cells. Therefore these macromolecules can be recognized by the cell without being rejected as foreign agents.

1.6.3 Properties of dendrimers

In order to develop dendrimers for biomedical applications, there are certain key aspects that need to be considered.

1.6.3.1 Charge and size

In one study, the retention time of the PAMAM dendrimers within the human body was evaluated. The cationic PAMAM dendrimers (amine terminated) were expelled quickly from circulation, meanwhile a prolonged circulation time was observed with their anionic counterparts (carboxylic acid terminated) (**Figure 1.23**).[70] This indicates that the charge on the dendrimers can affect the solubility and stability of dendrimers as potential anticancer drugs or drug delivery vehicles.[71] The anionic PAMAM dendrimers also showed clearance

rates that decreased with increasing size, hence the size also influences drug delivery efficacy.[70]

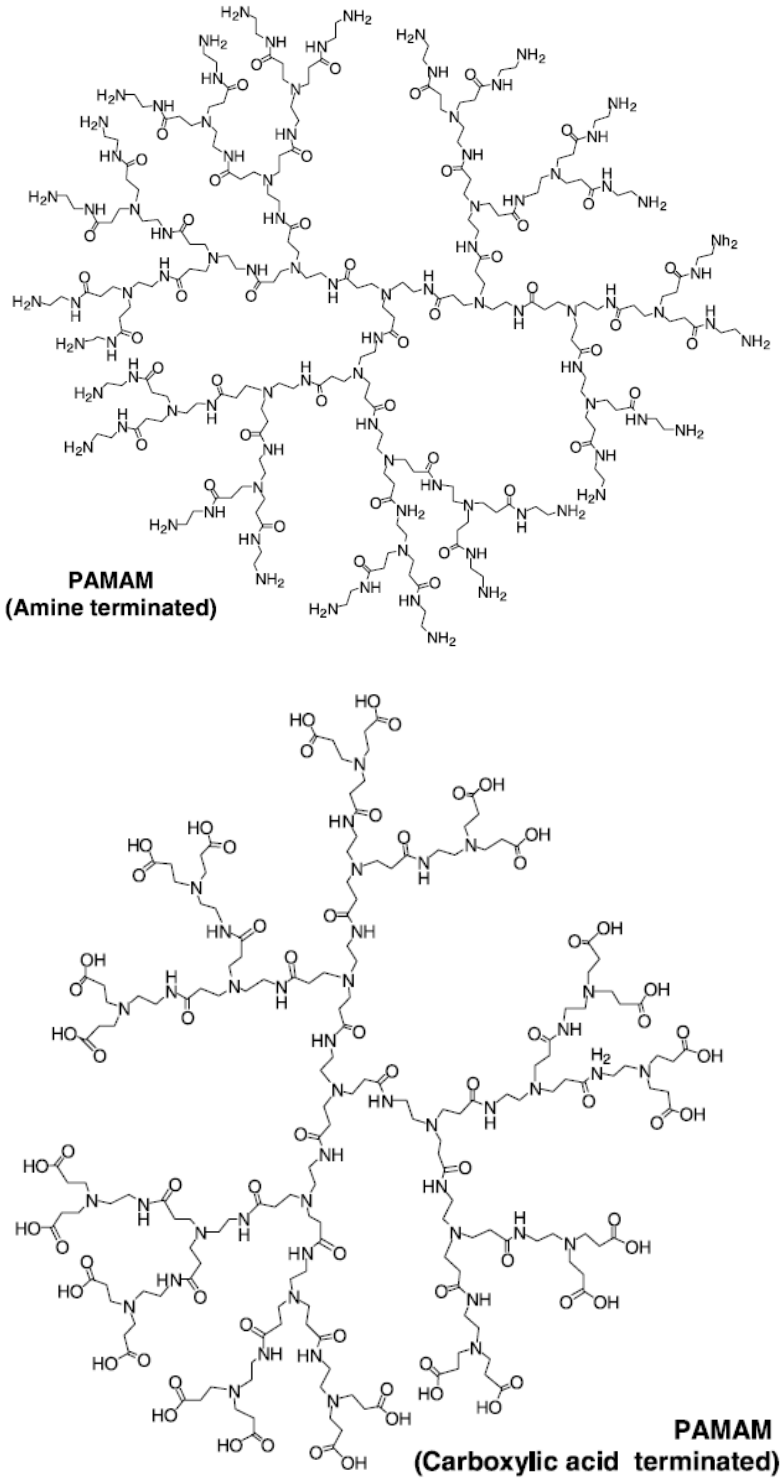

Figure 1.23: PAMAM cationic and anionic dendrimers.[56]

1.6.3.2 Functional groups

In the preparation of dendrimers, a suitable design of the ligand or end-group functionality has to be taken into consideration as it can determine properties such as water solubility and whether metal coordination is possible.[71] In this study, Schiff base ligands (**Figure 1.24**) with nitrogen and carbon donor atoms will be acting as end-group functionalities. This is due to their ability to readily form mono- or bidentate complexes with transition metals and exhibit interesting chemical and biological properties.[72] For example, the presence of the *C,N*-chelation has shown to induce strong nucleobase binding and high hydrophobicity.[72]

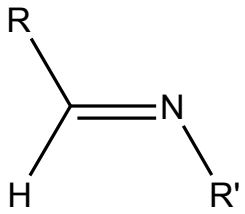

Figure 1.24: Schematic diagram of a Schiff base ligand.

1.6.3.3 EPR effect

Besides the fact that certain macromolecules and metal-based macromolecules can be taken up via endocytosis,[73-75] nanosized molecules are also able to exploit the Enhanced Permeability and Retention (EPR) effect (**Figure 1.25**).[57, 73, 76, 77] This effect is attributed to the fact that the blood vessels in tumours are irregular in shape, dilated, leaky and therefore more permeable.[20,77] The increased permeability of tumour cells allows larger molecules to enter the cancerous cells more effortlessly compared to non-cancerous cells, making them more selective.[73] The enhanced permeability can therefore be exploited by macromolecular drug delivery vehicles. The EPR effect also allows molecules to accumulate in the tumour site due to poor lymphatic drainage in the cancerous tissue.[73]

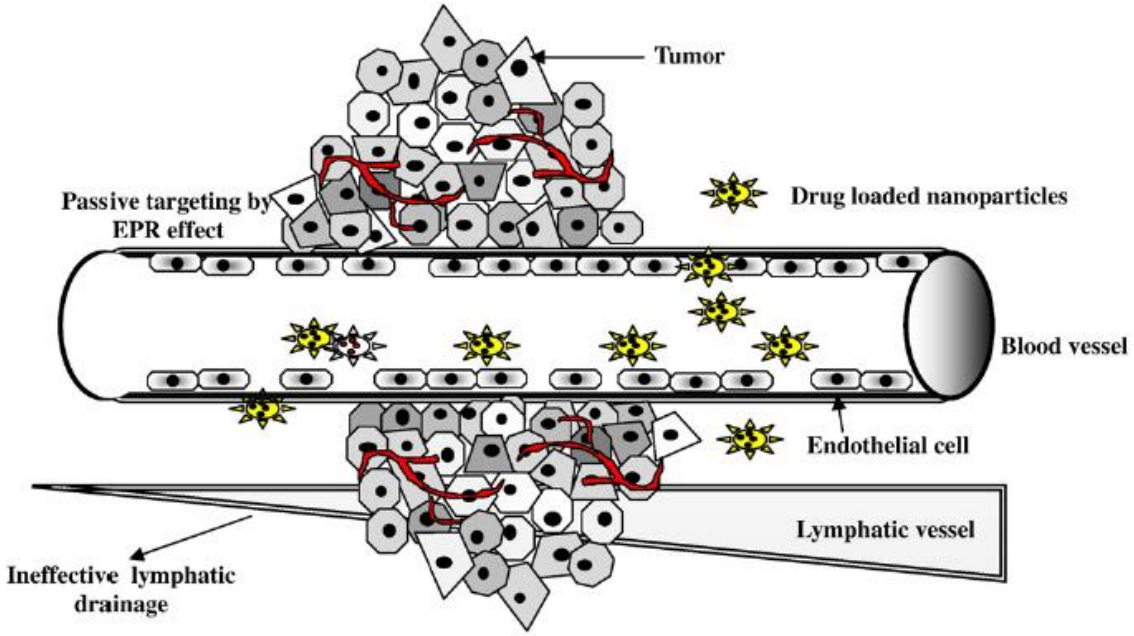

Figure 1.25: Schematic diagram of the EPR effect.[78]

1.6.3.4 Specificity

Once the molecule has reached the cancerous tissue, the rate and location of drug release needs to be controlled in order to avoid non-specific action of the molecule.[78] The drug is usually covalently bound to the drug delivery vehicle and is released via chemical or enzymatic cleavage of hydrolytically labile bonds.[56] Dendrimers have the low polydispersity which can ensure and monitor the drug release.[57] This provides reproducible pharmacokinetic behaviour[56] which means that the rates at which the drug action begins, the duration of the effect, the chemical changes of the substance in the body and the routes of excretion of the drug can all be determined with ease in contrast to that of linear polymers. [56,58]

1.6.3.5 Toxicity

As with most treatments of any disease worldwide, toxicity is one of the most important aspects to consider as any treatment that is too toxic is not worthwhile.[56,58, 79] The charge on metallodendrimers have been shown to play an important role in toxicity of drugs. Drug delivery vehicles that are positively charged generally show dose dependent toxicity while negatively charged or neutral dendrimers are less toxic and therefore more preferable.[70,80] But this is not always the case as it has been reported that cationic macromolecules are able to interfere with the cell membrane which is an advantage as it can therefore assist in the transport of the macromolecules into the cancerous cells.[80] Where there is an unfavourable

charge or a charge is required, it is possible to cap the molecules with counter-ions or neutral molecules to eliminate charge problems. For example, displacing a chloride counterion with a PF_6^- counterion to make a compound more stable or displace a chloride ligand coordinated to the metal centre with PTA to give a cationic versus a neutral complex.[70,81]

Other factors include cytotoxicity,[80] stability in solution[73] and intact release of the active drug component once the macromolecule has been released into the cell.[56] For example, the active agent needs to be soluble in physiological media in order to be able to reach the active site intact without decomposition.[56,79] Therefore, in order to develop and synthesize metallodendrimers, all the above features need to be considered.

1.7 Metallodendrimers as potential anticancer agents

In light of the benefits associated with dendrimers as potential anticancer agents, there is no doubt that these molecules show promising biological properties. These can also be enhanced with the incorporation of metal centres to give metallodendrimers.[43] Incorporating metal centres into these organic frameworks provides varied coordination and redox properties, as well as multinuclearity for biological recognition and improving the effectiveness of these potential chemotherapeutic drugs.[43] There are only a handful of biometallodendrimers that have been synthesized successfully and undergone anticancer *in vitro* and *in vivo* studies.

After the success of cisplatin, Jansen *et al*. synthesized the first tetranuclear platinum metallodendrimer based on the PPI dendritic scaffold, using the same general structure as cisplatin (**Figure 1.26**).[82] The tetranuclear complex behaved similarly to the trinuclear BBR3464 with respect to DNA binding and showed moderate *in vitro* activity with IC_{50} values ranging from 9-12 μM against a range of mouse leukaemia and human tumour cell lines.[82] The cytotoxicity of the complex can be attributed to the charge and the high branching of the metallodendrimer.[43, 82]

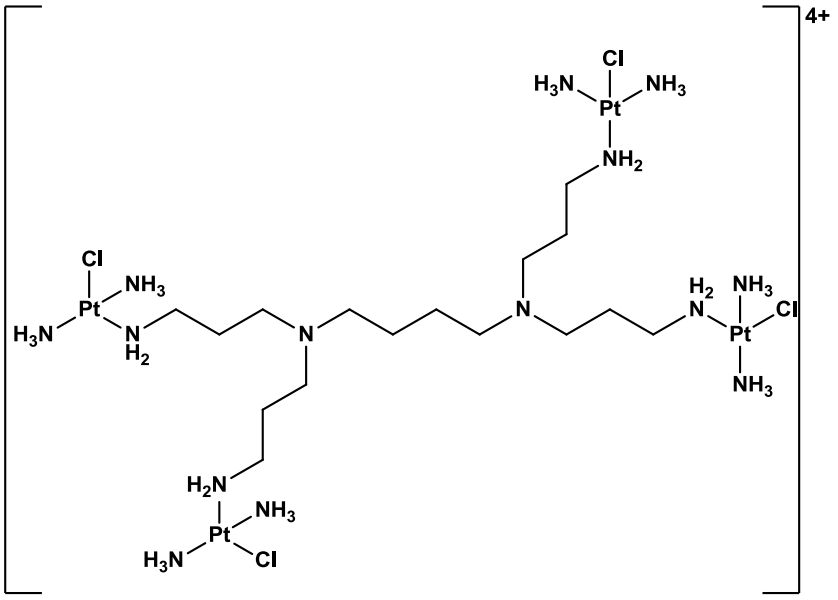

Figure 1.26: Tetranuclear PPI platinum metallodendrimer, based on cisplatin.[82]

Another tetranuclear platinum metallodendrimer was synthesized based on the PPI dendritic scaffold with a fluorophenyl(ethylenediamine) moiety to increase the selectivity of this compound for breast tumours (**Figure 1.27**).[43, 83] It showed an IC_{50} value of 5 μM comparable to that of cisplatin, 2 μM, in the MCF-7 breast cancer cell line.[43, 83]

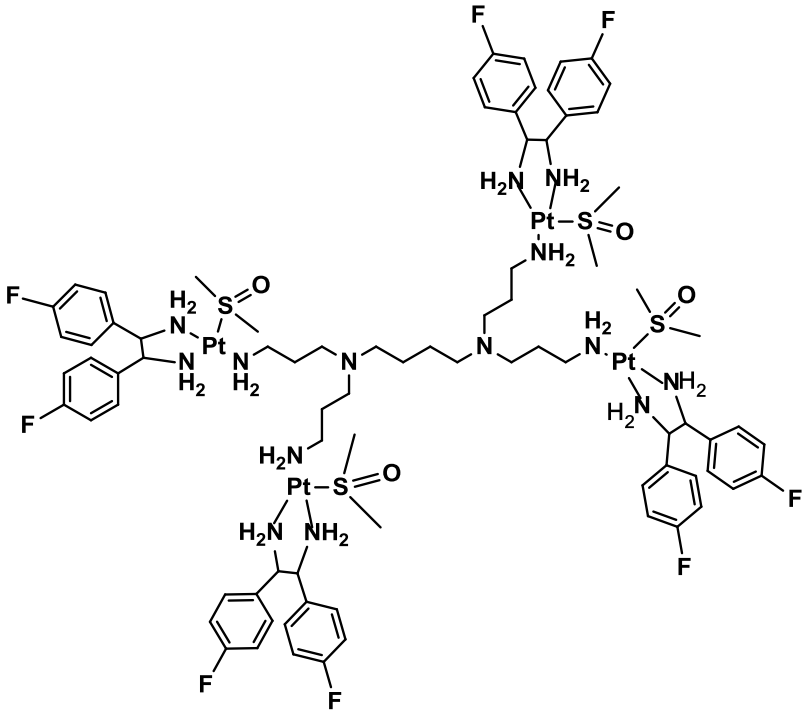

Figure 1.27: Tetranuclear PPI platinum metallodendrimer showing good cytotoxicity against the human breast cancer cell line MCF-7. [83]

Among the few non-platinum examples, a copper based PAMAM metallodendrimer showed *in vitro* cytotoxicity against leukaemia (MOLT-4), breast cancer (MCF-7) and Chang liver cell lines (**Figure 1.28**).[84] The *in vitro* activity for the tetranucelar complex was better than that of cisplatin, (**Figure 1.28**).[84]

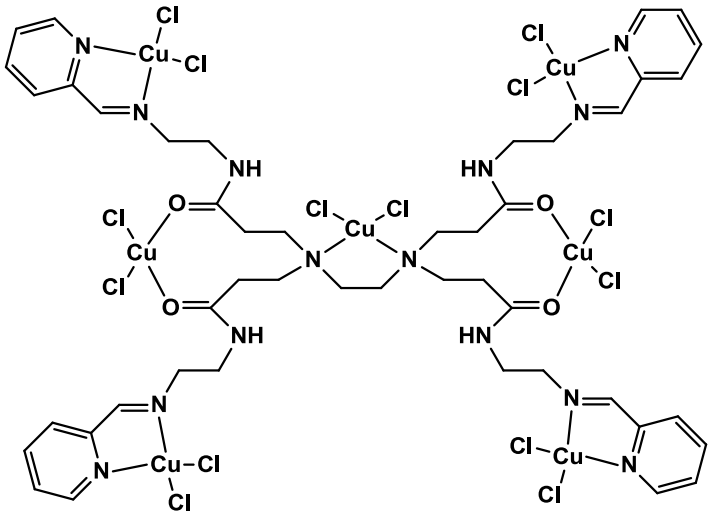

Cell line	IC_{50} (μM)	cisplatin IC_{50} (μM)
MOLT-4	11.1 ± 0.6	15.5 ± 4.2
MCF-7	10.2 ± 1.5	not detected
Chang liver	8.7 ± 0.7	73.5 ± 3

Figure 1.28: PAMAM heptanuclear copper metallodendrimer with the respective IC_{50} values.[84]

In another study Rodrigues *et al.*[81] prepared low-generation ruthenium metallodendrimers via the divergent approach based on a poly(alkylidenamine) dendritic scaffold (**Figure 1.29**). These poly(nitriles) are usually intermediates in the preparation of well-known PPI dendrimers, whereby repetitive steps of acrylonitrile is added to a diamine via a Michael reaction, followed by reduction to give the polyamine.[81] These were then functionalised on the periphery with $[Ru(\eta^5\text{-}C_5H_5)(PPh_3)_2]^+$ (**Figure 1.29**) or *cis*-$[RuCl(dppe)_2][PF_6]$.[81] A group of these metallodendrimers underwent degradation tests at 36°C in order to determine their stability in DMSO solution.[81] The metallodendrimers that contain the triphenyl phosphine (PPh_3) ligands showed instability which could indicate a release of the $[Ru(\eta^5\text{-}C_5H_5)(PPh_3)_2]^+$

metallofragments that can possibly enter and accumulate in the cancerous tissue.[81] This however would need to be confirmed by *in vitro* studies.

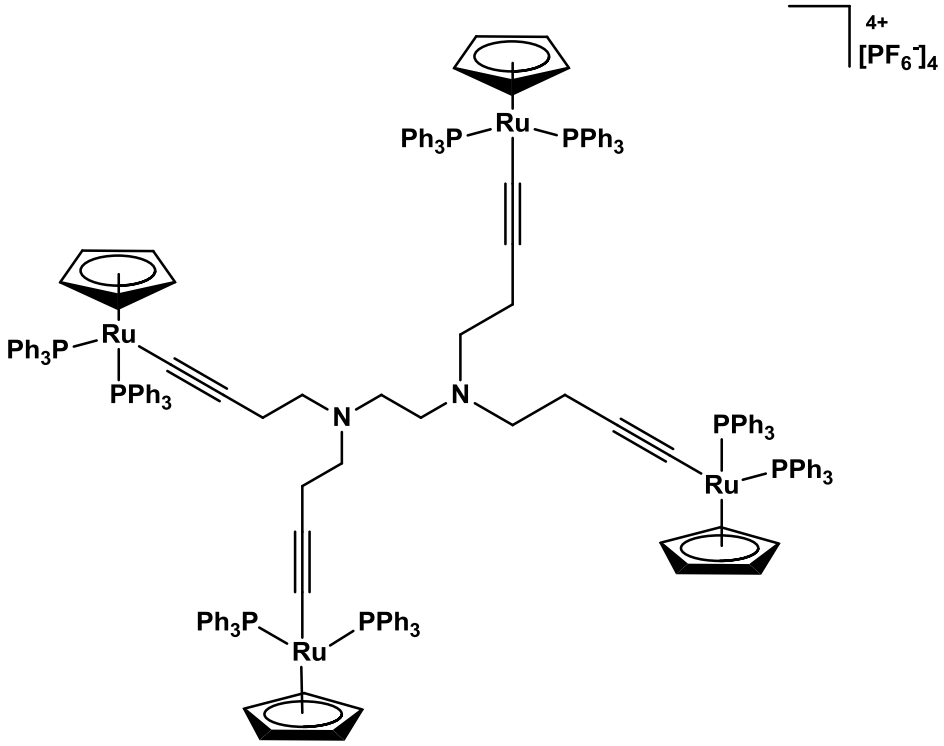

Figure 1.29: Poly(alkylidenamine) tetranuclear ruthenium metallodendrimer.[81]

Ruthenium(II)-arene metallodendrimers have exhibited *in vitro* cytotoxicity against A2780 and A2780cisR ovarian cancer cell lines (**Figure 1.30**).[13,81] Two PPI metallodendrimers, DAB-[Ru(η^6-C_6Me_6)Cl]$_8$ with a salicylaldimine or 2-pyridinecarboxaldimine surface ligand showed the best interactions with DNA and lower IC_{50} values *in vitro* in comparison to cisplatin.[13] The cationic fourth generation salicylaldimine ruthenium metallodendrimer, with the *p*-cymene arene moiety, displayed the best antiproliferative results, with an IC_{50} value of 0.8 ± 0.1 μM, compared to its neutral analogue which displayed a value of 2.9 ± 0.1 μM.[13, 85, 86] This could be due to the negative charge associated with the DNA backbone therefore making binding of cationic complexes more favourable than anionic or neutral complexes.[15] Besides the charge playing a key role in the activity, the results also concluded that there is a direct correlation between the increasing size of the metalldoendrimer and its DNA damage on interaction and cytotoxity.[13, 85, 86]

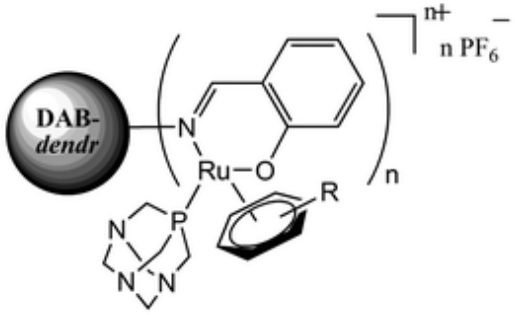

Figure 1.30: A series of PPI ruthenium metallodendrimers (n = 4-32; R = *p*-cymene or HMB).[85]

Lo *et al.* synthesized a series of iridium(III) metallodendrimers in order to further confirm that introducing metal complexes onto dendritic scaffolds can modify and even improve biological properties of these complexes.[43, 87] Tetranuclear iridium(III) polypyridine complexes (**Figure 1.31**) with one of two *C,N*-chelating ligands, phenylpyridine and phenylquinoline, were tested against the HeLa cancer cell line *in vitro*.[87] Both chelating ligands exhibited comparable IC_{50} values of 1.4-3.3 μM, which is better than their mononuclear analogues as well as cisplatin exhibiting values of and 26.4±2.0 μM, respectively.[87]

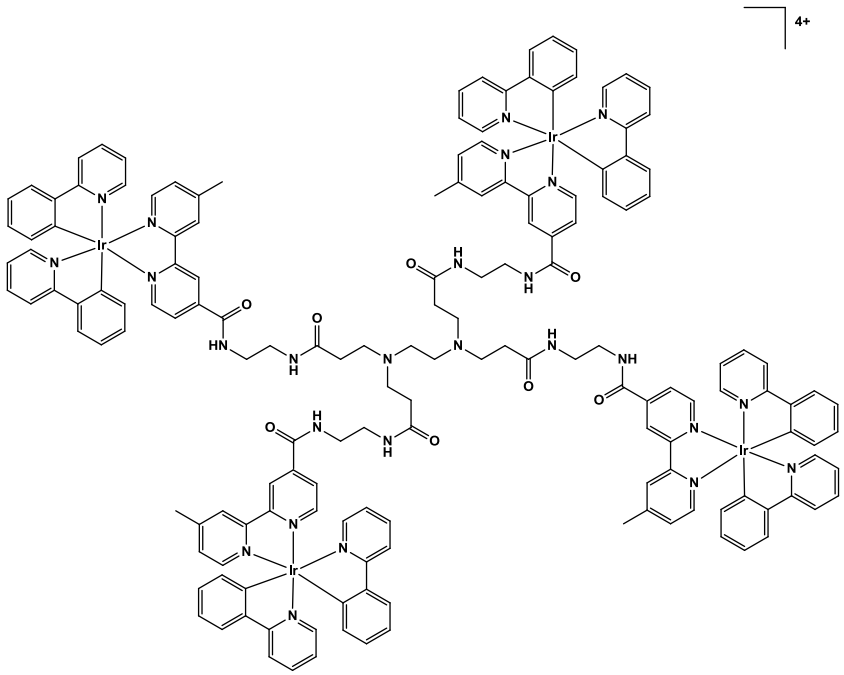

Figure 1.31: Representative iridium(III)-phenylpyridine metallodendrimer showing promising *in vitro* cytotoxicity (IC_{50} = 3.3±0.1 μM).[43]

The increased cytotoxicity compared to mononuclear derivatives, was attributed to an increase in metal centres on the periphery of the metallodendrimer and the increase in charge on the complex.[87,88] Besides showing good cytotoxicity, they were also able to demonstrate that the mononuclear and multinuclear complexes entered the cancerous cells via different pathways and that the multinuclear complexes bind to plasmid DNA in an electrostatic manner, whereas the mononuclear complexes did not.[87,88]

1.8 Concluding remarks

There have been limited biological investigations of metallodendrimers based on a variety of dendritic scaffolds, especially PAMAM and PPI scaffolds. With the known limitations associated with platinum-based compounds, there has been a shift in focus to ruthenium as well as rhodium and some iridium compounds. There is evidence that both neutral and cationic complexes based on the PPI scaffold have the ability to exhibit good biological activity. Within our research group there has also been investigations into cyclometalated rhodium(III) and iridium(III) complexes which show promising *in vitro* results and other investigations has shown that these complexes may be able to target different enzymatic pathways as anti-cancer agents.

1.9 Aims and Objectives

1.9.1 Aims

The aim of this project was to modify a PPI dendritic scaffold on the periphery with two Schiff base *C,N*-chelating moieties, allowing incorporation of different metal centres, ruthenium(II), rhodium(III) and iridium(III). This was to determine whether the aryl moiety and incorporation of different metal centres influences the cytotoxicity of these compounds and whether there is a correlation between size and cytotoxicity. A phosphorous moiety was incorporated in order to create a series of cationic analogues, as well as the incorporation of a ferrocenyl moiety to produce heterometallic complexes, therefore obtaining an effect of charge and heteronuclearity on cytotoxicity. The aim of the project was to determine whether the complexes show *in vitro* activity, further tests would need to be done in order to determine the drug-target and mode of action.

1.9.2 Objectives

1.9.2.1 Ligand synthesis

Naphthaldimine and benzaldimine *C,N*-chelating ligands (**Figure 1.32**) were synthesized and characterized. The synthesis was achieved by reacting propylamine or DAB-$(NH_2)_n$ (n=4 or 8) with naphthaldehyde and benzaldehyde via a Schiff-base condensation reaction. The ligands were characterized using a variety of spectroscopic and analytical techniques.

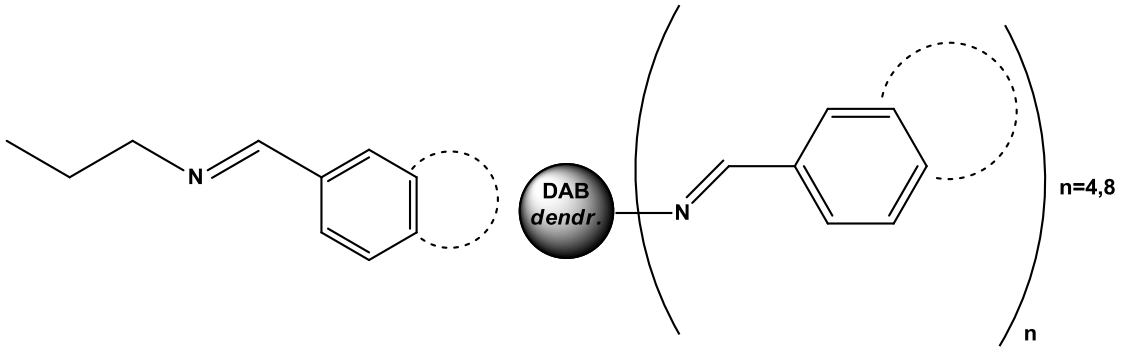

Figure 1.32: Naphthaldimine and benzaldimine monomeric and dendritic ligands.

1.9.2.2 Neutral metal complex synthesis

Ruthenium(II), rhodium(III) and iridium(III) metal complex analogues (**Figure 1.33**) of the above ligands were synthesized and characterized. The synthesis was achieved by metallation of the ligand with $[MCl_2(L)]_2$ (where M = Ru, Rh, Ir; L = *p*-cymene or Cp*). The metal complexes were characterized using a variety of spectroscopic and analytical techniques.

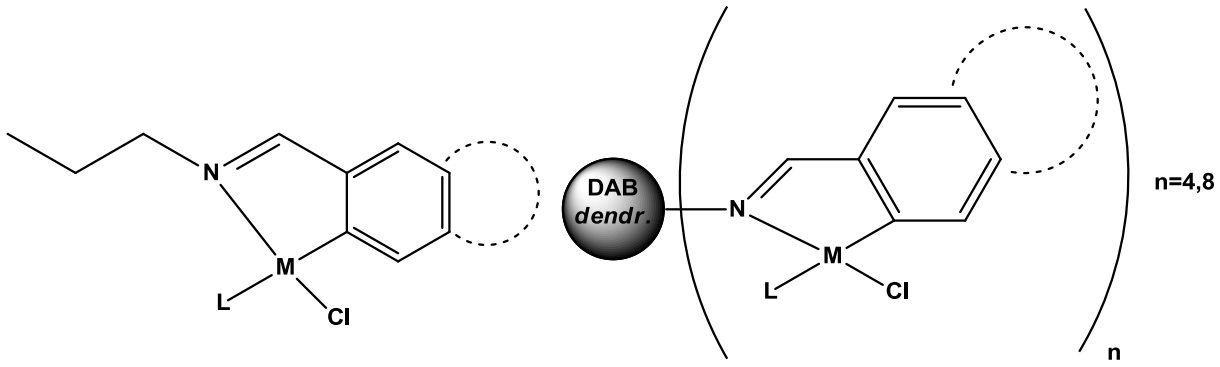

Figure 1.33: Neutral ruthenium, rhodium and iridium cyclometalated complexes.

1.9.2.3 Cationic and heterometallic complex synthesis

The synthesis of cationic derivatives (**Figure 1.34**) was achieved by displacement of the chloride with a phosphorous donor ligand, PTA. This was followed by salt metathesis with $NaPF_6$ to obtain a hexafluorophosphate counterion. The cationic metal complexes were characterized using a variety of spectroscopic and analytical techniques.

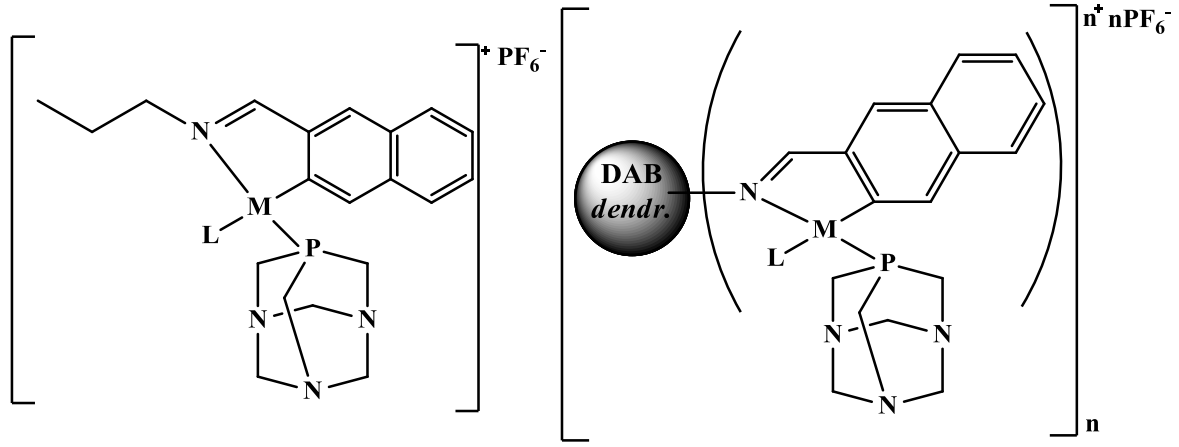

M = Ru, L = *p*-cymene
M = Rh/Ir, L = Cp*
n=4,8

Figure 1.34: Cationic ruthenium, rhodium and iridium cyclometalated complexes.

Heterometallic ferrocenyl - ruthenium(II), rhodium(III) and iridium(III) cationic analogues (**Figure 1.35**) were synthesized and charzterized. The synthesis was achieved by displacement of the chloride with a nitrogen-ferrocenyl ligand on the metal centre to obtain a cationic complex. This was followed by salt metathesis with $NaPF_6$ to obtain a hexafluorophosphate counterion. The cationic metal complexes were characterized using a variety of spectroscopic and analytical techniques.

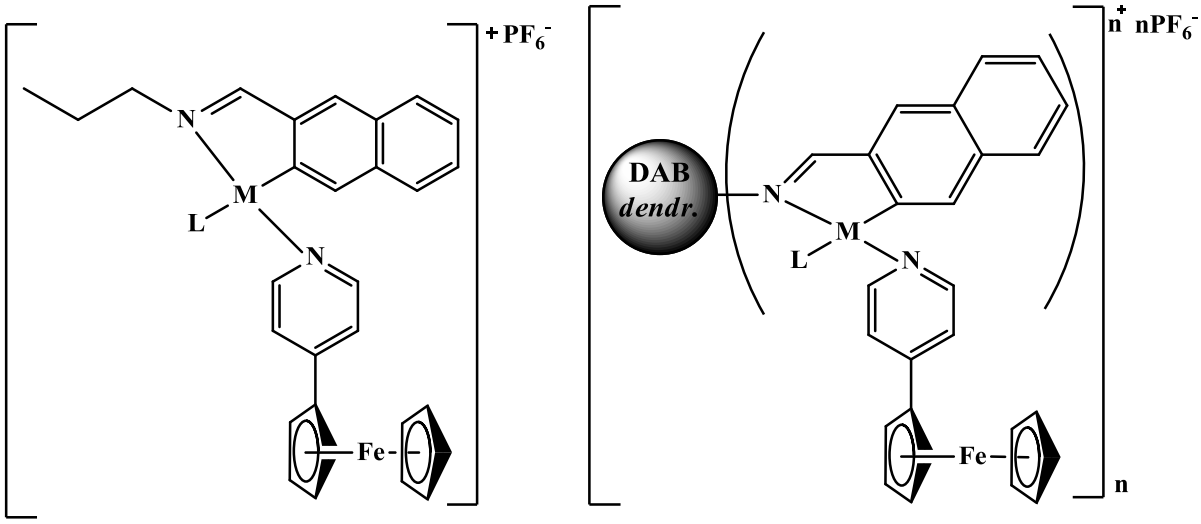

M = Rh/Ir, L = Cp*
n=4 or 8

Figure 1.35: Cationic heterometallic ferrocenyl-rhodium and iridium cyclometalated complexes.

1.9.2.4 Biological testing

The cytotoxicity studies of each ligand and metal complex was carried out by myself and collaborators at the Institut des Sciences et Ingénierie Chimiques, Ecole Polytechnique Fédérale de Lausanne (EPFL), Switzerland as well as at the University of the Western Cape (UWC). The cytotoxicity was studied against the human ovarian A2780 and A2780cisR cancer cell lines and the HEK or KMST-6 non-cancerous cell lines, to test for selectivity. A comparison between size of the complexes and the cytotoxicity was evaluated, as well as comparing the biological activity of the neutral versus the cationic complexes.

1.10 References

1. World Health Organization, *Cancer mortality and morbidity*, http://www.who.int/gho/ncd/mortality_morbidity/cancer/en/index.html, 27 February 2013.
2. A. Jemal, F. Bray, M. M. Center, J. Ferlay, E. Ward and D. Forman, *CA Cancer J. Clin.*, 2011, **61**, 69-90.

3. American Chemical Society, *Chemotherapy*, http://www.cancer.org/treatment/treatmentsandsideeffects/treatmenttypes/chemotherapy/index, 22 April 2013.
4. R. Sinha, G. J. Kim, S. Nie and D. M. Shin, *Mol. Cancer. Ther.*, 2006, **5**, 1909-1917.
5. N. Farrell, *Coord. Chem. Rev.*, 2002, **232**, 1-4.
6. B. Rosenberg, L. Van Camp, T. J.E. and V. H. Mansour, *Nature*, 1969, **222**, 385-.
7. B. Rosenberg, *Interdiscip. Sci. Rev.*, 1978, **3**, 134.
8. E. Rosenberg, F. Spada, K. Sugden, B. Martin, L. Milone, R. Gobetto, A. Viale and J. Fiedler, *J. Organomet. Chem.*, 2003, **668**, 51-58.
9. N. J. Wheate, S. Walker, G. E. Craig and R. Oun, *Dalton Trans.*, 2010, **39**, 8097-8340.
10. A. V. Klein and T. W. Hambley, *Chem. Rev.*, 2009, **109**, 4911-4920.
11. A. I. Minchinton and I. F. Tannock, *Nat. Rev. Cancer*, 2006, **6**, 583-592.
12. G. Sava, A. Bergamo and P. J. Dyson, *Dalton Trans.*, 2011, **40**, 9069-9075.
13. P. Govender, A. K. Renfrew, C. M. Clavel, P. J. Dyson, B. Therrien and G. S. Smith, *Dalton Trans.*, 2011, **40**, 1158-1167.
14. B. Therrien, W. H. Ang, F. Cherioux, L. Vieille-Petit, L. Juillerat-Jeanneret, G. Suss-Fink and P. J. Dyson, *J. Cluster Sci.*, 2007, **18**, 741-752.
15. A. Dorcier, W. H. Ang, S. Bolano, L. Gonsalvi, L. Juillerat-Jeannerat, G. Laurenczy, M. Peruzzini, A. D. Phillips, F. Zanobini and P. J. Dyson, *Organometallics*, 2006, **25**, 4090-4096.
16. P. J. Dyson and G. Sava, *Dalton Trans.*, 2006, **16**, 1929-1933.
17. C. G. Hartinger, S. Zorbas-Selfried, M. A. Jakupec, B. Kynast, H. Zorbas and B. K. Keppler, *J. Inorg. Biochem.*, 2006, **100**, 891-904.
18. M. Pongratz, P. Schluga, M. A. Jakupec, V. B. Arion, C. G. Hartinger, A. G. and B. K. Keppler, *J. Anal. At. Spectrom.*, 2004, **19**, 46-51.
19. G. Ludwig, G. N. Kaluderovic, T. Ruffer, M. Bette, M. Korb, M. Block, R. Paschke, H. Lang and D. Steinborn, *Dalton Trans.*, 2013, **42**, 3771-3774.
20. N. Cutillas, G. S. Yellol, C. de Haro, C. Vicente, V. Rodriguez and J. Ruiz, *Coord. Chem. Rev.*, 2013, **257**, 2784-2797.
21. C. S. Allardyce and P. J. Dyson, *J. Cluster Sci.*, 2001, **12**, 563-569.
22. A. Dorcier, P. J. Dyson, C. Gossens, U. Rothlisberger, S. R. and I. Tavernelli, *Organometallics*, 2005, **24**, 2114-2123.

23. P. Schluga, C. G. Hartinger, A. Egger, E. Reisner, M. Galanski, M. A. Jakupec and B. K. Keppler, *Dalton Trans.*, 2006, 1796-1802.
24. A. L. Noffke, A. Habtemariam, A. M. Pizarro and P. J. Sadler, *Chem. Commun.*, 2012, **48**, 5219-5246.
25. C. Scolaro, A. Bergamo, L. Brescacin, R. Delfino, M. Cocchietto, G. Laurenczy, T. J. Geldbach, G. Sava and P. J. Dyson, *J. Med. Chem.*, 2005, **48**, 4161-4171.
26. R. E. Morris, R. E. Aird, P. D. Murdoch, H. Chen, J. Cummings, N. D. Hughes, S. Parsons, A. Parkin, G. Boyd, D. I. Jodrell and P. J. Sadler, *J. Med. Chem.*, 2001, **44**, 3616-3621.
27. C. S. Allardyce, P. J. Dyson, D. J. Ellis and S. L. Heath, *Chem. Commun.*, 2001, **15**, 1396-1397.
28. C. S. Allardyce, P. J. Dyson, D. J. Ellis, P. A. Salter and R. Scopelliti, *J. Organomet. Chem.*, 2003, **668**, 35-42.
29. G. Marcon, A. Casini, P. Mura, L. Messori, A. Bergamo and P. Oriolo, *Metal-Based Drugs*, 2000, **7**, 195-200.
30. N. P. E. Barry and P. J. Sadler, *Chem. Soc. Rev.*, 2012, **41**, 3264-3279.
31. S. Mollin, S. Blanck, K. Harms and E. Meggers, *Inorg. Chim. Acta*, 2012, **393**, 261-268.
32. M. E. Reyland, *Biochem. Soc. Trans.*, 2007, **35**, 1001-1004.
33. C. H. Leung, H. J. Zhong, D. S. H. Chan and D. L. Ma, *Coord. Chem. Rev.*, 2013, **257**, 1764-1776.
34. J. S. Rawlings, K. M. Rosler and D. A. Harrison, *J. Cell Sci.*, 2004, **117**, 1281-1283.
35. C.-H. Leung, H. Yang, D. P.-Y. Ma, D. S.-H. Chan, H.-J. Zhong, Y.-W. Li, W.-F. Fong and D.-L. Ma, *Med. Chem. Comm.*, 2012, **3**, 696-698.
36. J. Ruiz, V. Rodriguez, N. Cutillas, K. G. Samper, M. Capdevila, O. Palacios and A. Espinosa, *Dalton Trans.*, 2012, **41**, 12847-12856.
37. M. J. Karkkainen and T. V. Petrova, *Oncogene*, 2000, **19**, 5598-5605.
38. A. Wilbuer, D. H. Vlecken, D. J. Schmitz, K. Kraling, K. Harms, C. P. Bagowski and E. Meggers, *Angew. Chem. Int. Ed.*, 2010, **49**, 3839-3942.
39. C.-H. Leung, H.-J. Zhong, H. Yang, Z. Cheng, D. S.-H. Chan, V. P.-Y. Ma, R. Abagyan, C.-Y. Wong and D.-L. Ma, *Angew. Chem. Int. Ed.*, 2012, **51**, 9010-9014.
40. H. Wajant, K. Pfizenmaier and P. Scheurich, *Cell Death Differ.*, 2003, **10**, 45-65.
41. Z. Liu, A. Habtemariam, A. M. Pizarro, G. J. Clarkson and P. J. Sadler, *Organometallics*, 2011, **30**, 4702-4710.

42. Z. Liu, L. Salassa, A. Habtemariam, A. M. Pizarro, G. J. Clarkson and P. J. Sadler, *J. Inorg. Chem.*, 2011, **50**, 5777-5783.
43. C. Billecke, S. Finniss, L. Tahash, C. Miller, T. Mikkelsen, N. P. Farrell and O. Bogler, *Neuro-Oncology*, 2006, **8**, 215-226.
44. P. Govender, B. Therrien and G. S. Smith, *Eur. J. Inorg. Chem.*, 2012, **2012**, 2853-2862 2012.
45. C. Bincoletto, I. L. S. Tersariol, C. R. Oliveira, S. Dreher, D. M. Fausto, M. A. Soufen, F. D. Nascimento and A. C. F. Caires, *Bioorg. Med. Chem.*, 2005, **13**, 3047-3055.
46. N. P. E. Barry, F. Edafe, P. J. Dyson and B. Therrien, *Dalton Trans.*, 2010, **39**, 2816-2820.
47. J. Mattsson, P. Govindaswamy, A. K. Renfrew, P. J. Dyson, P. Stepnicka, G. Suss-Fink and B. Therrien, *Organometallics*, 2009, **28**, 4350-4357.
48. A. Bergamo, G. Stocco, B. Gava, M. Cocchietto, E. Alessio, B. Serli, E. Iengo and G. Sava, *J. Pharmacol. Exp. Ther.*, 2003, **305**, 725-732.
49. G. Sava, K. Clerici, I. Capozzi, M. Cocchietto, R. Gagliardi, E. Alessio, G. Mestroni and A. Perbellini, *Anti-Cancer Drugs*, 1999, **10**, 129-139.
50. G. I. Pascu, A. C. G. Hotze, C. Sanchez-Cano, B. M. Kariuki and M. J. Hannon, *Angew. Chem. Int. Ed.*, 2007, **46**, 4374-4378.
51. J. Rajput, J. R. Moss, A. T. Hutton, D. T. Hendricks, C. E. Arendse and C. Imrie, *J. Organomet. Chem.*, 2004, **689**, 1553-1568.
52. S. Top, J. Tang, A. Vessieres, D. Carrez, P. C. and G. Jaouen, *Chem. Commun.*, 1996, 955-956.
53. P. Köpf-Maier, H. Köpf and E. W. Neuse, *Angew. Chem. Int. Ed. Engl.*, 1984, **23**, 456-457.
54. D. Osella, M. Ferrali, P. Zanello, F. Laschi, M. Fonatni, C. Nerri and G. Cavigiolio, *Inorg. Chim. Acta*, 2000, **306**, 42-48.
55. I. Cuadrado, M. Moran, C. M. Casado, B. Alonso and J. Losada, *Coord. Chem. Rev.*, 1999, **193-195**, 395-445.
56. F. Aulenta, W. Hayes and S. Rannard, *Eur. Polym. J.*, 2003, **39**, 1741-1771.
57. M. A. Mintzer and M. W. Grinstaff, *Chem. Soc. Rev.*, 2011, **40**, 173-190.
58. E. R. Gillies and J. M. J. Frechet, *Drug Discov. Today*, 2005, **10**, 35-43.
59. D. A. Tomalia, A. M. Naylor and W. A. Goddard, *Angew. Chem. Int. Ed. Engl.*, 1990, **29**, 138-175.

60. C. J. Hawker and J. M. J. Frechet, *J. Am. Chem. Soc.*, 1990, **112**, 7638-7647.
61. R. Esfand and D. A. Tomalia, *Drug Discov. Today*, 2001, **6**, 427-436.
62. J. C. Roberts, M. K. Bhalgat and R. T. Zera, *J. Biomed. Mater. Res.*, 1996, **30**, 53-65.
63. G. J. Kirkpatrick, J. A. Plumb, O. B. Sutcliffe, D. J. Flint and N. J. Wheate, *J. Inorg. Biochem.*, 2011, **105**, 1115-1122.
64. D. Q. McNerny, P. R. Leroueil and J. R. Baker, *Wiley Interdiscip. Rev. Nanomed. Nanobiotechnol.*, 2010, **2**, 249-259.
65. D. A. Tomalia, H. Baker, J. Dewald, M. Hall, G. Kallos, S. Martin, J. Roeck, J. Ryder and P. Smith, *Polym. J. (Tokyo)*, 1985, **17**, 117-132.
66. E. Buhleier, W. Wehner and F. Vogtle, *Synthesis*, 1978, **3**, 155-158.
67. E. M. M. de Brabander-van den Berg and E. W. Meijer, *Angew. Chem. Int. Ed. Engl.*, 1993, **32**, 1308-1311.
68. F. Wang, X. Cai, Y. Su, J. Hud, Q. Wu, H. Zhang, J. Xiao and Y. Cheng, *Acta Biomaterialia* 2012, **8**, 4304-4313.
69. A. W. Bosman, H. M. Janssen and E. W. Meijer, *Chem. Rev.*, 1999, **99**, 1665-1688.
70. N. Malik, R. Wiwattanapatapee, K. Lorenz, H. Frey, J. W. Weener, E. W. Meijer, P. W. and R. Duncan, *J. Control Rel.*, 2000, **65**, 133-148.
71. D. Astruc, E. Boisselier and C. Ornelas, *Chem. Rev.*, 2010, **110**, 1857-1959.
72. Z. Liu, L. Salassa, A. Habtemariam, A. M. Pizarro, G. J. Clarkson and P. J. Sadler, *Inorg. Chem.*, 2011, **50**, 5777-5783.
73. A. K. Iyer, G. Khaled, J. Fang and H. Maeda, *Drug Discov. Today*, 2006, **11**, 812-818.
74. H. Sun, H. Li and P. J. Sadler, *Chem. Rev.*, 1999, **99**, 2817-2842.
75. F. Kratz, M. Hartmann, B. Keppler and L. Messori, *J. Biol. Chem.*, 1994, **269**, 2581-2588.
76. T. Tanaka, S. Shiramoto, M. Miyashita, Y. Fujishima and Y. Kaneo, *Int. J. Pharm.*, 2004, **277**, 39-61.
77. M. J. Pisani, N. J. Wheate, F. R. Keene, J. R. Aldrich-Wright and J. G. Collins, *J. Inorg. Biochem.*, 2009, **103**, 373-380.
78. S. Acharya and S. K. Sahoo, *Drug Delivery Rev.*, 2011, **63**, 170-183.
79. S. El Kazzouli, N. El Brahmi, S. Mignani, M. Bousmina, M. Zablocka and J.-P. Majoral, *Curr. Med. Chem.*, 2012, **19**, 4995-5010.
80. J. B. Wolinsky and M. W. Grinstaff, *Adv. Rev.*, 2008, **60**, 1037-1055.

81. J. Rodrigues, M. G. Jardim, J. Figeira, M. Gouveia, H. Tomas and K. Rissanen, *New J. Chem.*, 2011, **35**, 1938-1943.

82. B. A. Jansen, J. v. d. Zwan, J. Reedijk, H. d. Dulk and J. Brouwer, *Eur. J. Inorg. Chem.*, 1999, **9**, 1429-1433.

83. T. Kapp, A. Dullin and R. Gust, *J. Med. Chem.*, 2006, **49**, 1182-1190.

84. X. Zhao, S. C. J. Loo, P. P.-F. Lee, T. T. Y. Tan and C. K. Chu, *J. Inorg. Biochem.*, 2010, **104**, 105-110.

85. P. Govender, L. C. Sudding, C. M. Clavel, P. J. Dyson, B. Therrien and G. S. Smith, *Dalton Trans.*, 2013, **42**, 1267-1277.

86. P. Govender, N. C. Antonels, J. Mattsson, A. K. Renfrew, P. J. Dyson, J. R. Moss, B. Therrien and G. S. Smith, *J. Organomet. Chem.*, 2009, **694**, 3470-3476.

87. K. Y. Zhang, H.-W. Liu, T. T.-H. Fong, X.-G. Chen and K. K.-W. Lo, *Inorg. Chem.*, 2010, **49**, 5432-5443.

88. R. Payne, P. Govender, B. Therrien, C.M. Clavel, P.J. Dyson and G.S. Smith, *J. Organomet. Chem.*, 2013, **729**, 20-27.

Chapter 2: Synthesis and Characterization of the Mono- and Polynuclear Neutral Ruthenium(II), Rhodium(III) and Iridium(III) Cyclometalated complexes based on Naphthaldimine and Benzaldimine Schiff Base Ligands

2.1 Introduction

Dendrimers, such as poly(propyleneimine) (PPI) (**Figure 2.1**) dendrimers are large macromolecules that can be constructed to a desired size.[1-5] They have been found to be useful in biological applications such as chemotherapeutics[6] due to their multivalency which means they are able to interact with multiple, specific receptors for biological recognition. This factor improves the selective activity of these molecules which could in turn reduce toxicity and side effects.[7]

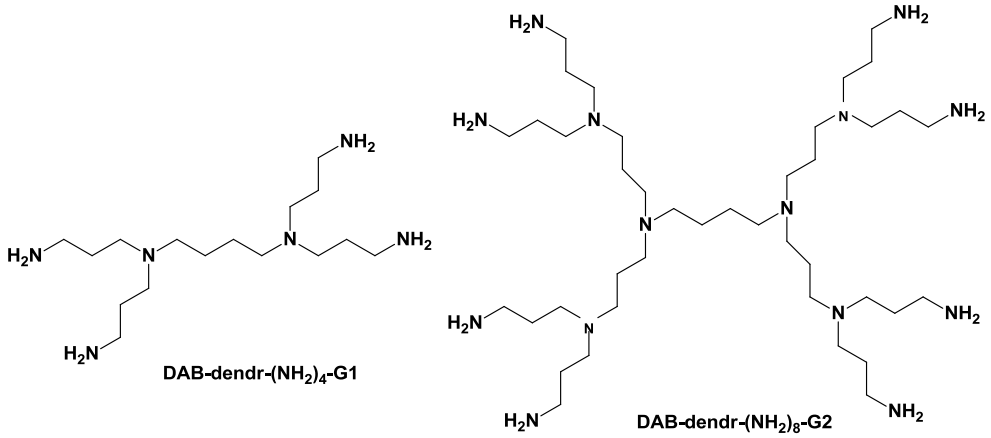

Figure 2.1: Structures of the first- and second-generation PPI dendritic scaffolds.

Since the discovery of cisplatin, the incorporation of metal centres has become of increasing biological interest.[8, 9] With the limitations associated with cisplatin, the use of platinum group metals, other than platinum, has become more prevalent. For example, ruthenium(II)[10], rhodium(III)[11, 12] and iridium(III) [3, 13, 14] complexes have displayed antitumour activity.

Ruthenium-arene complexes, for example, have shown an array of applications such as antiviral[15], antibacterial[16], antimalarial and anticancer agents.[10] There has also been investigation into nitrogen directed metallations[17,18] as potential DNA binding agents using palladium and platinum which showed IC_{50} values as low as 1.1 μmol/L.[19]

Our research group has focussed on ruthenium(II) PPI metallodendrimers therefore this project is an extension to previous work by focussing on the same dendritic scaffold but introducing new metals. There have been a few reports on rhodium(III) and iridium(III) cyclometalated complexes as potential kinase and protein inhibitors. For example one rhodium(III) cyclometalated complex showed an IC_{50} value as low as 30μM (**Figure 2.2a)**.[20] A well as an iridium(III) cyclometalated complex which showed promising tumour necrosis factor-α (TNF- α) inhibition, without the toxicity associated with other metallodrugs (**Figure 2.2b**).[21]

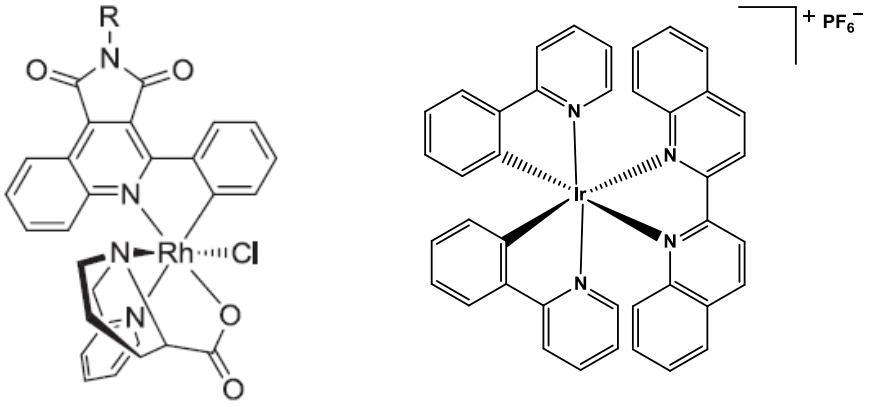

(a) **(b)**

Figure 2.2: Rhodium(III) (**a**) and iridium(III) (**b**) complexes as a protein kinase-C and TNF-α inhibitors, respectively. (where R = benzyl or H).[20, 22]

Multivalency is increased further by the presence of multiple metal centres. For example a series of tungsten-functionalized metallodendrimers were synthesized based on the diaminobutane (DAB) dendritic scaffold and studies showed that they were able to cleave DNA in com[arison to the mononuclear analogues, giving these multinuclear complexes good biological properties.[23]

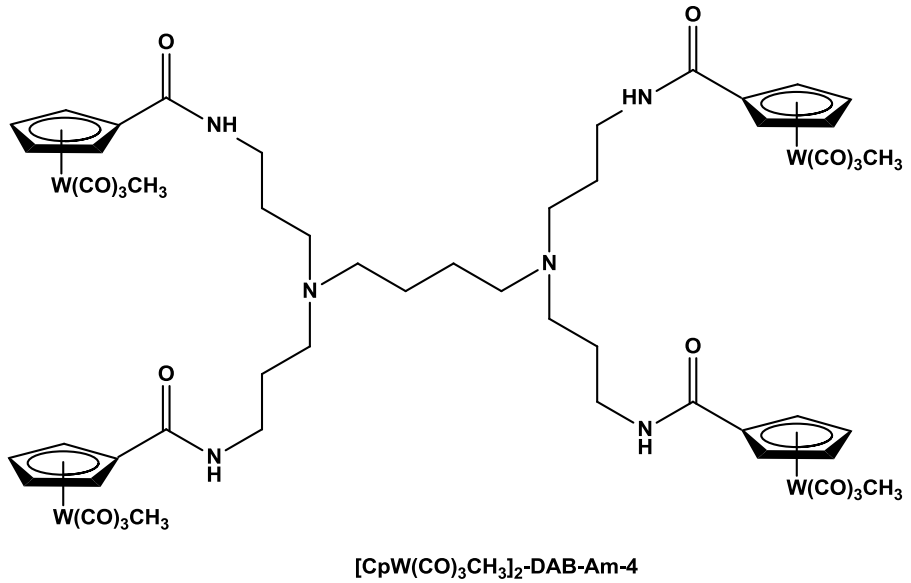

Figure 2.3: Multinuclear tungsten-functionalized metallodendrimer.[23]

With only very few examples of cyclometalated complexes as anticancer agents, we sought to develop a series of neutral cyclometalated multinuclear complexes as potential anti-cancer agents in order to incorporate multinuclearity as well as nitrogen-directed cyclometallation. Herein we discuss the synthesis and characterization of bidentate *C,N*-ligands, monomeric and dendritic, as well as the neutral ruthenium(II), rhodium(III) and iridium(III) mono- and polynuclear cyclometalated complexes based on these ligands.

2.2 Synthesis of the naphthaldimine and benzaldimine monomeric ligands 2.1 and 2.2

Two organic bidentate *C,N*-ligands (**2.1 & 2.2**) were synthesized by reacting propylamine with either naphthaldehyde or benzaldehyde, respectively, in a Schiff-base condensation reaction (**Scheme 2.1**) adapted from the work done by Mungwe *et al*.[24] The ligands differed from one another by the presence of a more extended phenyl group in the naphthaldehyde series of ligands compared to that of the benzaldehyde series. The extended phenyl group is incorporated as it can play a role in DNA intercalation[13] which could modify the anticancer activity of the naphthaldimine series of compounds versus the benzaldimine compounds.[13] Both ligands were stirred in ethanol at room temperature overnight. The naphthaldimine ligand (**2.1**) was obtained as a yellow-brown solid in a moderate yield of 62%, while the benzaldimine ligand (**2.2**) was obtained as a brown-red oil, in a good yield of 82%. Both ligands are soluble in most organic solvents, such as DCM, chloroform, acetone and ethanol.

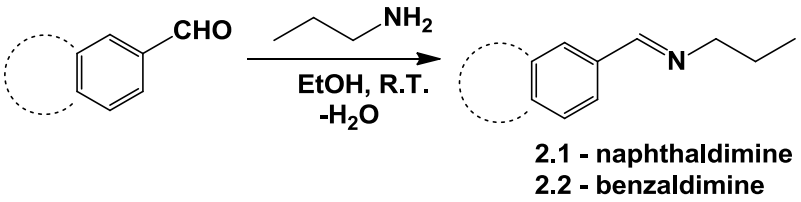

Scheme 2.1: Synthesis of naphthaldimine and benzaldimine monomeric ligands (**2.1 & 2.2**).

2.2.1 ^{1}H-NMR and ^{13}C{^{1}H}-NMR spectroscopy

Both ligands (**2.1 & 2.2**) were characterized by ^{1}H- and ^{13}C{^{1}H}-NMR spectroscopy. In the ^{1}H-NMR spectra of each ligand (**2.1 & 2.2)** that there is formation of the Schiff base. A doublet is observed at 8.43 and 8.28 ppm for **2.1** and **2.2**, respectively, corresponding to the imine proton due to long range coupling to the proton at position 5. The aromatic protons for the naphthaldimine and benzaldimine rings appear at typical chemical shifts associated with aromatic protons between 7.40 and 8.50 ppm (**Figure 2.4**). Another notable feature (**see Figure 2.4**) is the downfield positioning of the triplet corresponding to the protons at position 3, being adjacent to the electron-withdrawing imine nitrogen, seen at 3.65 and 3.60 ppm for each ligand (**2.1 & 2.2**), respectively. This is in comparison to the resonances of the protons at position 1 and 2, appearing further upfield between 0.98 and 1.78 ppm. This was also confirmed by using 2D-NMR techniques such as HSQC and COSY. As can be seen in **Figure 2.4**, the COSY shows the spin-spin coupling between the aliphatic protons at position 1,2 and 3, as well as long distance coupling of the imine proton at position 4 with the proton at position 3, also adjacent to the imine nitrogen. Hence the splitting observed for the imine doublet.

In the ^{13}C{^{1}H}-NMR spectra, the chemical shifts for the aliphatic carbons appear between 11.0-64.0 ppm, while the aromatic carbon atoms are further downfield, between 124.0-160.0 ppm. The imine carbon peak appears the furthest downfield at 160.0 ppm for the monomeric ligands (**2.1 & 2.2**) confirming the Schiff-base condensation reaction.

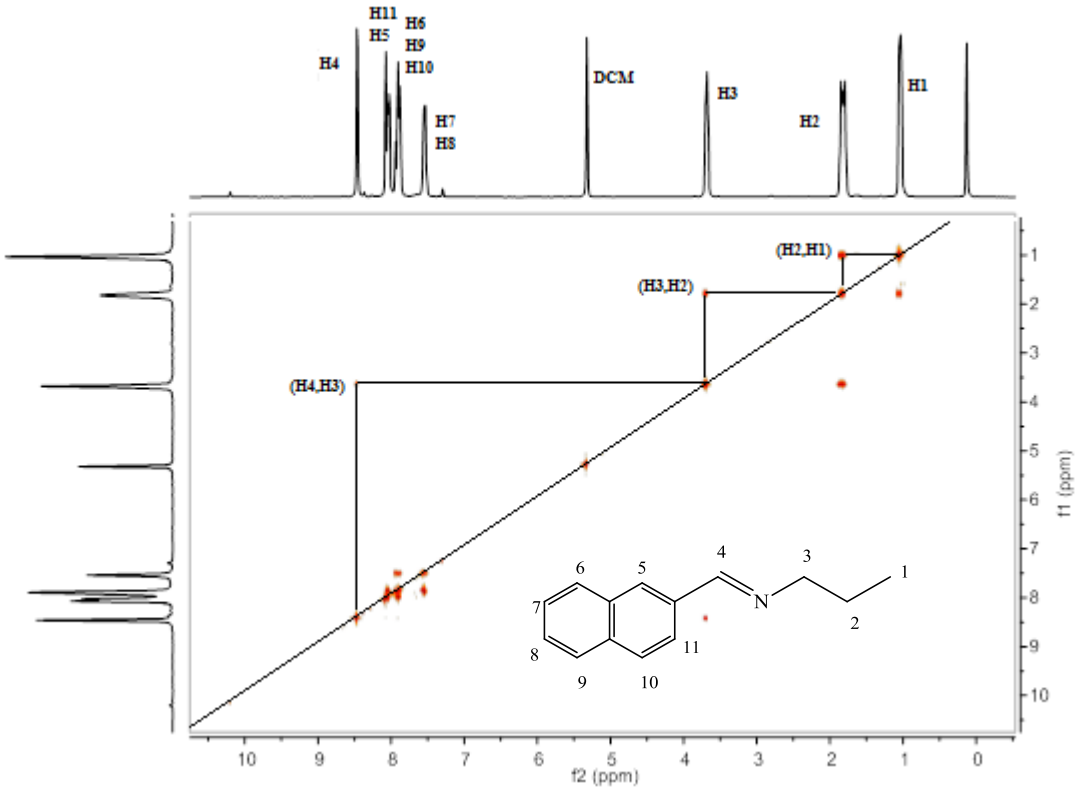

Figure 2.4: Representative COSY spectra of the naphthaldimine monomeric ligand (**2.1**).

2.2.2 Infrared (IR) spectroscopy

The IR spectra of each ligand was recorded as KBr pellets and shows the presence of an imine absorption band at 1640 and 1646 cm^{-1} for ligand **2.1 & 2.2**, respectively. This confirms the presence of an imine bond and in turn the formation of the Schiff base ligand.

2.2.3 Electron Ionization Mass Spectrometry (EI-MS)

The mass spectrum of the naphthaldimine ligand (**2.1**) has a fragmentation peak which corresponds to the loss of the propyl group and the nitrogen atom. In the mass spectrum of **2.2**, there is a molecular ion peak corresponding to the molecular mass of the desired product as well as a fragmentation peak corresponding to the loss of an ethyl group of the aliphatic chain (**Table 2.1**).

Table 2.1: Mass spectrometry data for monomeric ligands **2.1** and **2.2**.

Complex	Calculated M (g/mol)	Molecular fragment (*m/z*)	Assignment
2.1	197.28	141.01	$[M\text{-}C_3H_7N]^+$
2.2	147.22	147.08	$[M]^+$
	147.22	118.02	$[M\text{-}C_2H_5]^+$

2.3 Synthesis of the naphthaldimine and benzaldimine dendritic ligands 2.3-2.6

Following the synthesis of the monomeric ligands, a series of first- and second-generation PPI dendritic ligands were synthesized (**Scheme 2.2**) by reacting the appropriate aldehyde with the first- and second-generation poly(propylene amine) dendritic scaffold, DAB-dendr-$(NH_2)_4$-G1 or DAB-dendr-$(NH_2)_8$-G2, via a similar Schiff-base condensation reaction as the model monomeric ligand synthesis.[24] Through these reactions a series of poly(propyleneimine) dendritic ligands were obtained, with their spherical structure giving these molecules improved physical and chemical properties as potential anticancer-agents.[25] The dendritic ligands (**2.3-2.6**) were stirred in ethanol for 72-96 hours. To decrease the reaction time, a microwave reaction can also be performed in ethanol at 70°C for 30-45 minutes, yielding the desired product (**Scheme 2.2**).

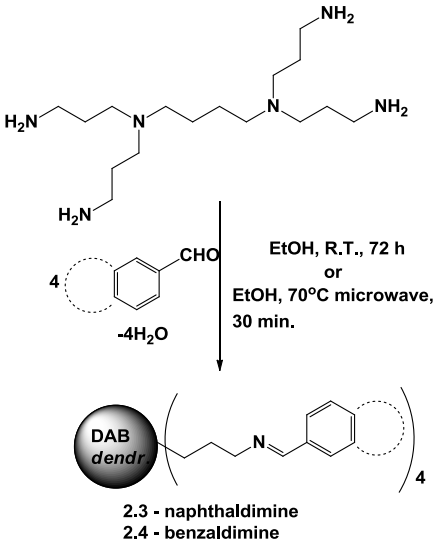

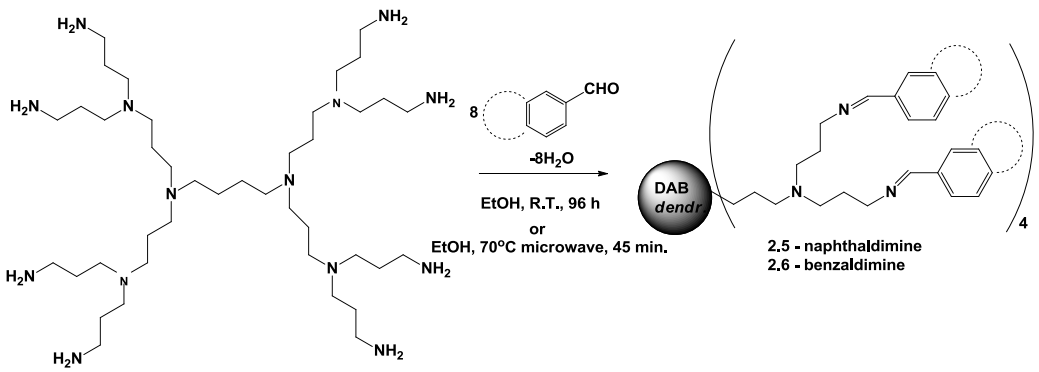

Scheme 2.2: Synthesis of the first- and second-generation *C,N*-chelating PPI dendritic ligands based on naphthaldimine (**2.3 & 2.5**) and benzaldimine (**2.4 & 2.6**).

The reactions proceeded over 72 and 96 hours, respectively for the first- (**2.3 & 2.4**) and second-generation (**2.5 & 2.6**) dendritic ligands, in order to ensure full functionalization of the periphery. For the first-generation dendritic ligands (**2.3 & 2.4**), the microwave reaction time was 30 minutes, while for the second-generation dendritic ligands (**2.5 & 2.6**) the microwave reaction took place over for 30-45 minutes. The first- and second-generation naphthaldimine dendritic ligands (**2.3 & 2.5**) were obtained as white solids, in moderate yields of 67 and 42%, respectively. The benzaldimine analogues (**2.4 & 2.6**) were obtained as yellow oils in moderate yields of 52% and 45%, respectively. All the dendritic ligands are soluble in DCM, chloroform, ethanol and acetone.

2.3.1 ^{1}H-NMR and ^{13}C{^{1}H}-NMR spectroscopy

All four dendritic ligands (**2.3-2.6**) were characterized by ^{1}H- and ^{13}C{^{1}H}-NMR spectroscopy. In the ^{1}H-NMR spectra of all four dendritic ligands (**2.3-2.6**) there is the presence of a doublet in each spectrum ranging between 8.25-8.40 ppm, corresponding to the imine proton and indicative of the formation of the Schiff base imine bond. The aromatic protons for the naphthaldimine and benzaldimine rings appear at typical chemical shifts associated with aromatic protons between 7.30 and 8.40 ppm (**Figure 2.5**).

The core protons at position 1 and 2 appear at different shifts in comparison to one another as the protons at position 2 are adjacent to the electron-withdrawing nitrogen atoms of the DAB-core. The protons at position 1 appear furthest upfield at 1.49, 1.43, 1.33 and 1.38 ppm for each dendritic ligand **2.3-2.6**, respectively. While the protons at position 2 are further downfield at 2.46, 2.41, 2.37 and 2.41 ppm, respectively (**Figure 2.5**). Another key feature in

the ^{1}H-NMR is the downfield position of the triplet corresponding to the protons on the carbon atom adjacent to the imine nitrogen (position 5 for G1 and position 8 for G2) appearing at 3.68, 3.62, 6.58 and 3.61 ppm for each dendritic ligand (**2.3-2.6**), respectively (**Figure 2.5**). This was also confirmed by using 2D-NMR techniques such as HSQC and COSY. The COSY of the dendritic ligands show similar trends found in the COSY of the monomeric ligands, whereby there is coupling between the aliphatic protons of the dendritic arms and between the core protons. There is also long distance coupling of the imine proton at position 9 with the proton at position 8, hence the splitting observed for the imine proton in the ^{1}H-NMR spectra.

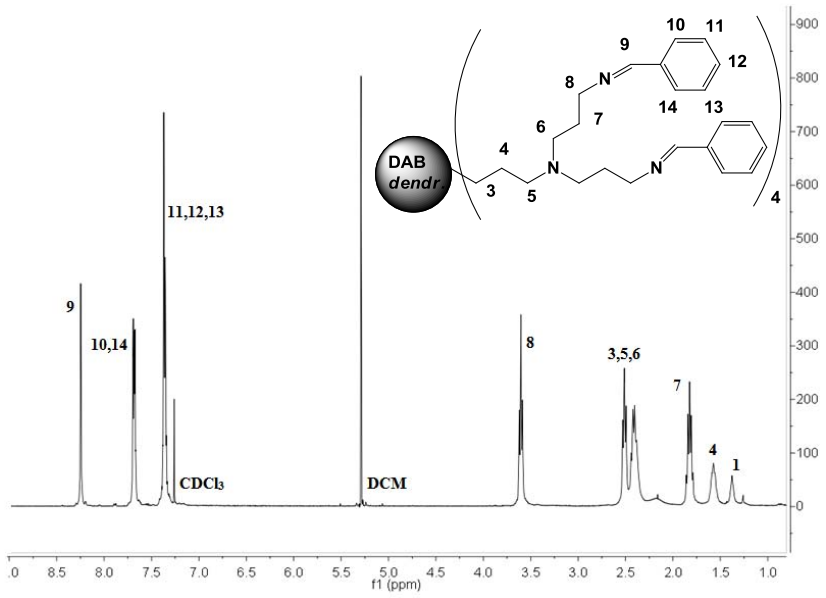

Figure 2.5: Representative ^{1}H-NMR spectrum of the benzaldimine G2 dendritic ligand (**2.6**).

In the ^{13}C{^{1}H}-NMR spectra of the dendritic ligands (**2.3-2.6**) the resonances for the aliphatic carbons appear between 24.0-60.0 ppm, while the aromatic carbon atoms were further downfield, between 124.0-160.0 ppm. The imine carbon peak appears the furthest downfield at 161.0 ppm for all the dendritic ligands (**2.3-2.6**) similar to the monomeric ligands (**2.1 & 2.2**), confirming Schiff-base formation.

2.3.2 Infrared (IR) spectroscopy

To further confirm that the Schiff-base condensation reaction occurred and that all the PPI peripheral arms were fully functionalised, IR spectroscopy was used. The IR spectra of all

four dendritic ligands (**2.3-2.6**) were recorded as KBr pellets and each spectrum shows the presence of an imine absorption band ranging between 1639 and 1646 cm^{-1}.

2.3.3 Low Resolution Electrospray Ionization Mass Spectrometry (ESI-MS)

All four dendritic ligands (**2.3-2.6**) exhibit base peaks in the mass spectra (**Table 2.2**). As can be seen in **Table 2.2**, dendritic ligands **2.3 2.5** and **2.6** form adducts with methanol, while ligand **2.4** forms an adduct with water and methanol (see **Table 2.2**).

Table 2.2: Mass spectrometry data for dendritic ligands **2.3-2.6**.

Complex	Calculated M (g/mol)	Molecular fragment (*m/z*)	Assignment
2.3	869.21	322.20	$[M+3H^{+}+3MeOH]^{3+}$
2.4	668.97	272.20	$[M+3H_3O^{+}+MeOH]^{3+}$
2.5	1878.64	408.20	$[M+5H^{+}+MeOH]^{5+}$
2.6	1478.16	773.80	$[M+2H^{+}+2MeOH]^{2+}$

2.4 Synthesis of the mononuclear cyclometalated naphthaldimine and benzaldimine complexes 2.7-2.12

Before synthesizing the half sandwich ruthenium(II), rhodium(III) and iridium(III) complexes, the appropriate metal dimer precursors were synthesized by reacting the appropriate metal salt ($MCl_2.nH_2O$) with α-phellandrene in the case of ruthenium or pentamethylcyclopentadiene in the case of rhodium and iridium **(Scheme 2.3**).[25, 26]

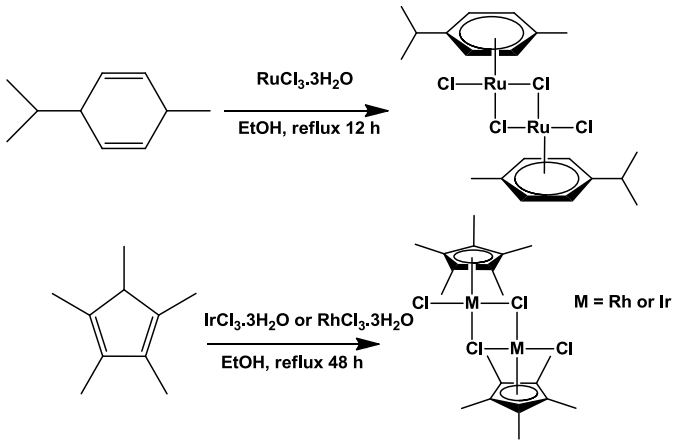

Scheme 2.3: Synthesis of the ruthenium(II), rhodium(III) and iridium(III) metal precursors.

The monomeric ligands (**2.1 & 2.2**) were cyclometalated using one of three metallic dimers, $[Ru(p\text{-cymene})Cl_2]_2$, $[Rh(\eta^5\text{-}C_5Me_5)Cl_2]_2$ or $[Ir(\eta^5\text{-}C_5Me_5)Cl_2]$, in methanol or ethanol (**Scheme 2.5**) for two hours to produce a series of mononuclear complexes (**2.7-2.12**). The synthetic method followed was a similar method used by Govender *et al.*[27] Sodium acetate was used for the selective C-H activation of the ortho-proton as previously reported results[28] show that acetate can stimulate the cyclometallation of imines with ruthenium, rhodium or iridium metal salts at room temperature.[28] Ortho CH-activation can be attributed to the directing effect of the imine bond on the metal centre. The proposed mechanism of the reaction is shown in **Scheme 2.4**. It is suggested that NaOAc acts as an intramolecular base and facilitates the break-up of the dimer and exchange of the chloride ligand (**Scheme 2.4**).[28] There are two likely mechanisms for the C–H activation step to occur; oxidative addition of the aryl C–H bond followed by reductive elimination (**Scheme 2.4** - via D^1).[28] The alternative route is said to first involve the electrophilic attack of the metal on the arene (**Scheme 2.4** - via D^2) followed by loss of a proton.[28]

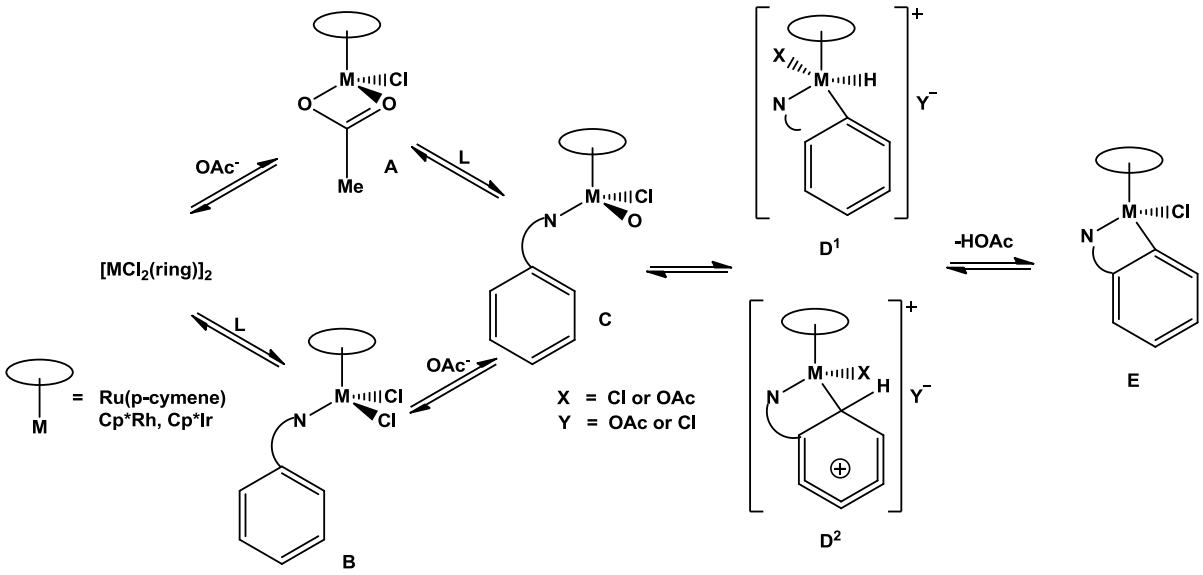

Scheme 2.4: Proposed mechanism of reaction for the cyclometallation of imines.[28]

The ruthenium(II) naphthaldimine (**2.7**) and benzaldimine (**2.10**) complexes were obtained as golden-brown solids in moderate to poor yields of 65 and 25%, respectively. The ruthenium(II) naphthaldimine (2.7) and benzaldimine (2.10) complexes were obtained as golden-brown solids in moderate to poor yields of 65 and 25%, respectively. In general, the ruthenium dimer showed a poor reactivity with the benzaldimine ligands and often produced unstable compounds. The rhodium(III) (**2.8 & 2.11**) and iridium(III) (**2.9 & 2.12**) complexes

were obtained as orange solids in moderate yields ranging between 51-71%. All the mononuclear complexes are soluble in methanol, ethanol, DCM and chloroform. The iridium(III) complexes (**2.9 & 2.12**) tend to be less soluble or sparingly soluble compared to the ruthenium(II) and rhodium(III) complexes.

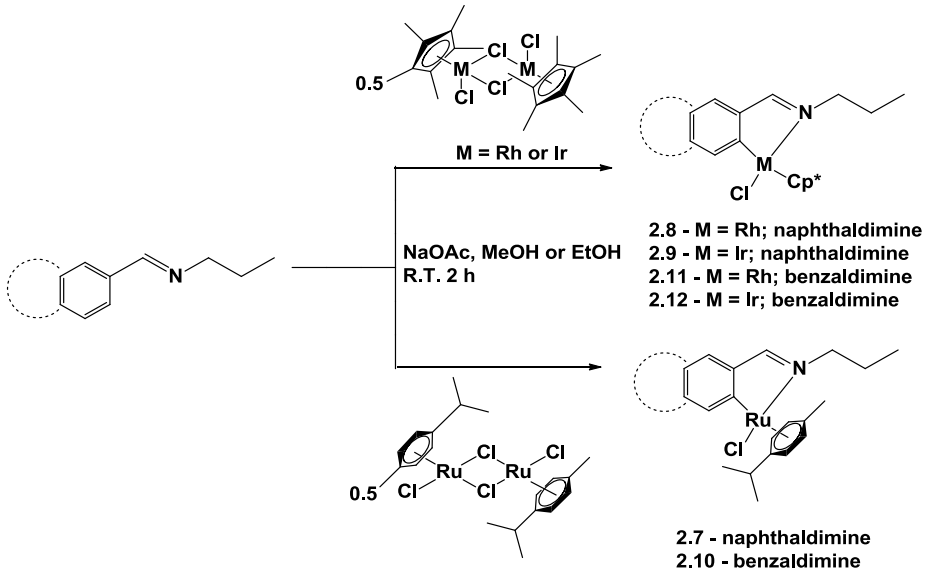

Scheme 2.5: Synthesis of the ruthenium(II), rhodium(III) and iridium(III) *C,N*–chelating naphthaldimine and benzaldimine mononuclear complexes (**2.7-2.12**).

2.4.1 ^{1}H-NMR and ^{13}C{^{1}H}-NMR spectroscopy

All the mononuclear complexes were characterized by ^{1}H- and ^{13}C{^{1}H}-NMR spectroscopy. The ^{1}H-NMR spectra of all six complexes (**2.7-2.12**) have a characteristic imine singlet between 7.99 and 8.96 ppm, indicating the imine bond is still intact. There is also a shift of the imine singlet in each metal complex when compared to imine resonance observed in the naphthaldimine (**2.1**) and benzaldimine (**2.2**) metal-free ligands. This confirms the coordination of the metal centre to the imine nitrogen. As expected, the aromatic protons for the phenyl rings appear between 7.00 and 8.44 ppm, which are typical chemical shifts for aromatic protons (**Figure 2.6a & b**). In the ^{1}H-NMR spectra of the ruthenium complexes (**2.7 & 2.10**) there is a loss of two-fold symmetry of the *p*-cymene moiety which results in the methyl protons of the isopropyl group exhibiting two doublets in the range of 0.81-1.10 ppm (**Figure 2.6b**). A septet is also observed at 2.49 ppm assigned to the single proton of the isopropyl group (**Figure 2.6b**). The aromatic protons of the *p*-cymene moiety display four separate doublets in the range 4.84-5.70 ppm, as opposed to two doublets in the free metal-dimer (**Figure 2.6b**). This is because the *p*-cymene moiety now has less freedom of rotation

and therefore all four aromatic protons appear in different environments. In some cases two of the signals overlap and seem to appear as one peak. Complexes **2.8**, **2.9**, **2.11** and **2.12** exhibit a singlet at about 1.70 ppm corresponding to the methyl protons of the pentamethylcyclopentadienyl (Cp*) moiety. In all six complexes (**2.7-2.12**), two sets of resonances are observed for each $–CH_2$ group of the propyl chain. This can be attributed to the diastereotopic nature of the protons induced by the chiral metal centre, now coordinated in a *C,N*-bidentate fashion to the naphthaldimine and benzaldimine ligands. In order to confirm the assignments made from the ^{1}H- and ^{13}C{^{1}H}-NMR, 2D-NMR techniques were used such as HSQC and COSY.

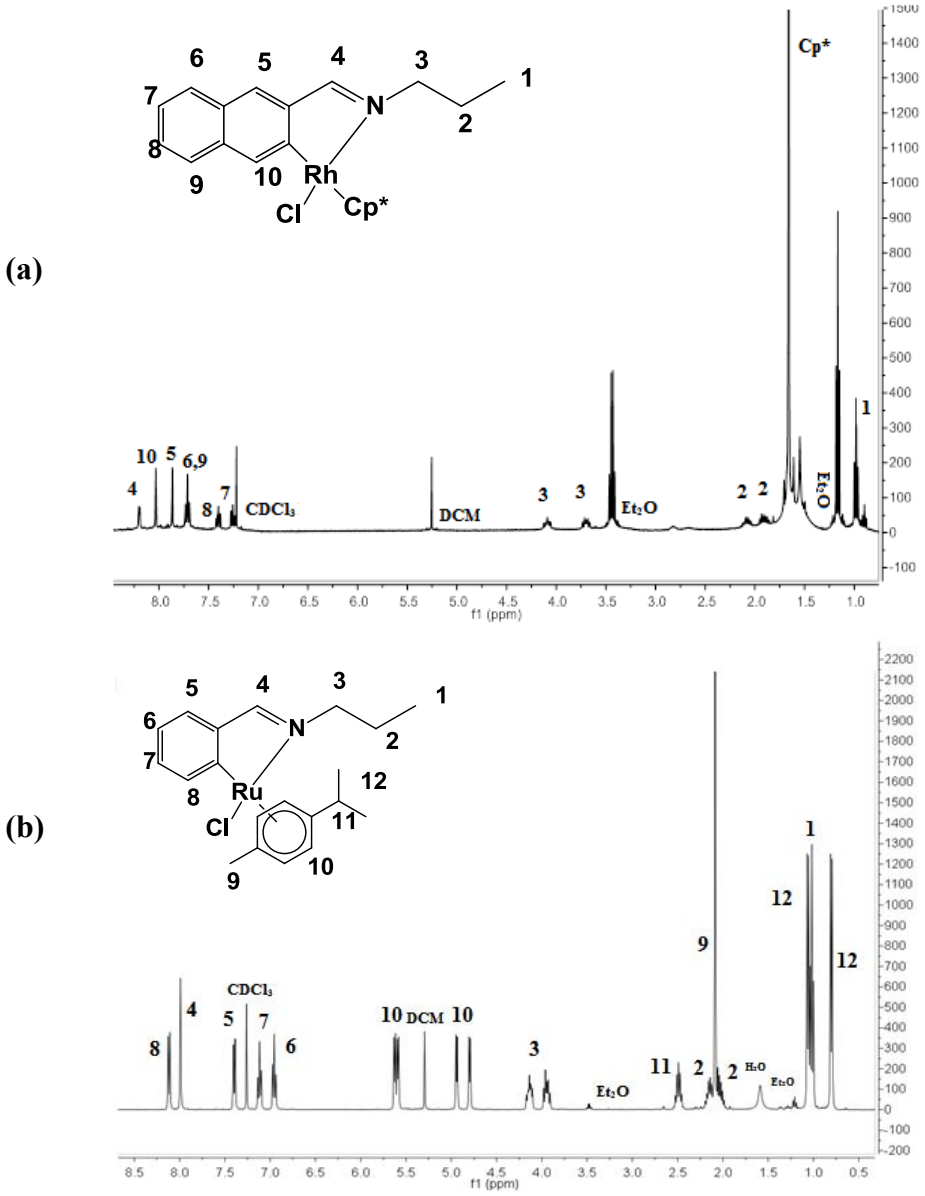

Figure 2.6: Representative ^{1}H-NMR spectrum of the rhodium(III) naphthaldimine (**2.8**) and ruthenium(II) benzaldimine (**2.10**) mononuclear complexes.

$^{13}C\{^{1}H\}$-NMR spectroscopy shows characteristic imine carbon peaks for each metal complex (**2.7-2.12**) at about 145.0 ppm, further upfield when compared to the imine carbon shift in the metal-free ligands (**2.1 & 2.2**) which appears at about 160.0 ppm. This is expected as the imine nitrogen is now coordinated to a metal centre. There is back donation occurring between the imine nitrogen and metal centre, therefore more electron density lies on the imine functional group (see **Figure 2.7**). The chemical shifts for the aliphatic carbon atoms appear between 11.0-68.0 ppm, while the aromatic carbon atoms appeared furthest downfield, between 101.0-178.0 ppm. The aromatic carbons on the *p*-cymene ligand appear between ~70.0-100.0 ppm in the ruthenium complexes (**2.7 & 2.10**), while the CH_3 substituents on the Cp* moiety in complexes **2.8 2.9 2.11** and **2.12**, appear at ~9.00 ppm.

2.4.2 Infrared (IR) spectroscopy

IR spectroscopy was used to determine whether the imine bond was still intact and to confirm the coordination of the metal centre to the imine nitrogen atom of the ligands (**2.1 & 2.2**). The IR spectra of all six complexes (**2.7-2.12**) were recorded as KBr pellets and show the presence of an imine absorption band ranging between 1602 and 1614 cm^{-1}. These values indicate a shift in the imine absorption band in each metal complex (**2.7-2.12**) to a lower frequency, when compared to the imine absorption bands for the metal-free ligands (**2.1 & 2.2**) with values of 1640 and 1646 cm^{-1}, respectively. This shift is expected and it confirms the coordination of the metal centre to the imine nitrogen as there is back donation from the metal centre's filled d-orbital into the empty π^*-antibonding orbital of the imine nitrogen. This increases the electron density on the nitrogen and in turn increases the electron density on the carbon-nitrogen imine bond and hence the imine absorption bands occur at lower frequencies in the complexes. This is known as the synergistic effect (**Figure 2.7**).[29]

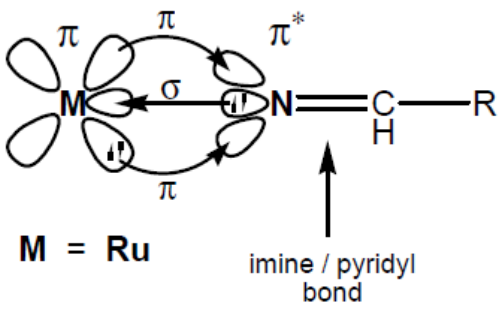

Figure 2.7: Molecular orbital diagram illustrating the synergistic effect.[29]

2.4.3 Electron Ionization Mass Spectrometry (EI-MS)

The mass spectrum of the each complex (**2.7-2.12**) show base peaks corresponding to the molecular ion without the chloride ion, $[M\text{-}Cl]^+$.

2.4.4 X-ray crystallography

The structures of complexes **2.7**, **2.8**, **2.11** and **2.12** were confirmed by single-crystal X-ray diffraction whereby single crystals of each complex was grown from a methanol/hexane mixture[30] (**Figure 2.8**). This characterization technique confirms the characteristic pseudo-tetrahedral "piano-stool" geometry with a η^5-coordination of the Cp* to the rhodium (**2.8 & 2.11**) and iridium (**2.12**) metal centres and a η^6-coordination of the *p*-cymene arene-ring to the ruthenium centre (**2.7**). This coordination forms the 'seat' of the piano stool and the other two ligands form the 'legs' of the stool (**Figure 2.8**).

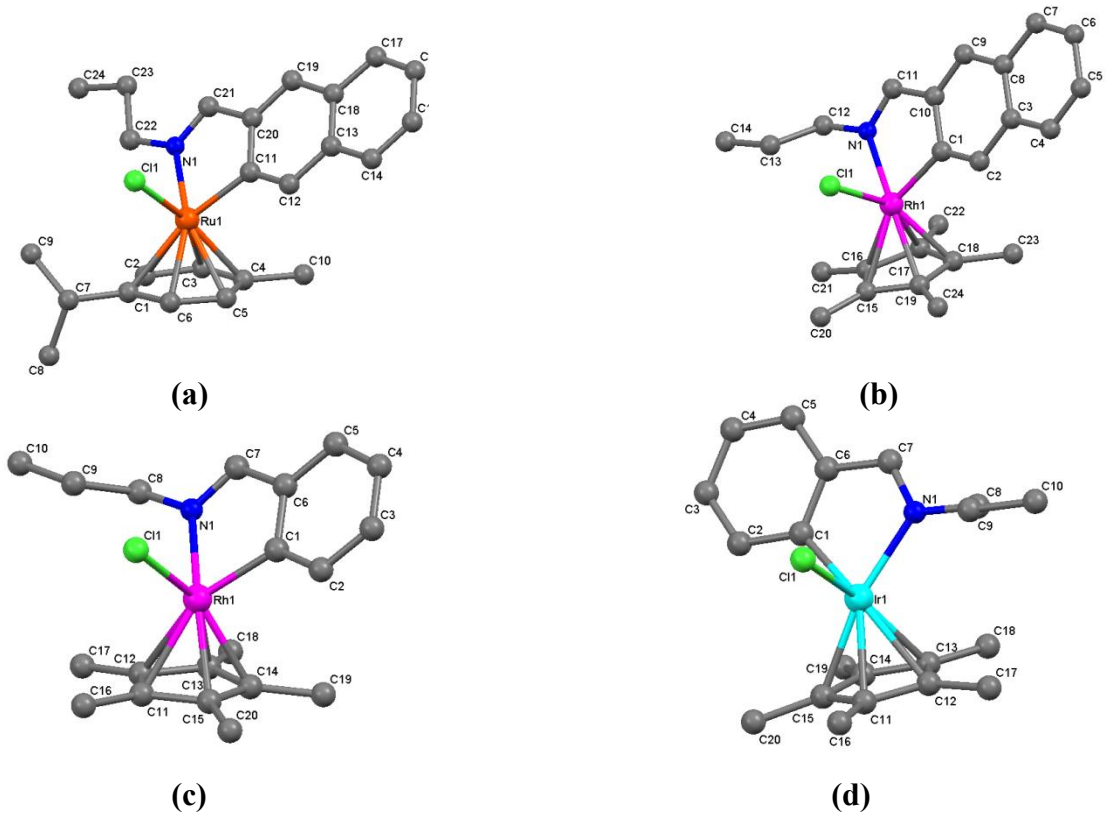

Figure 2.8: X-ray molecular structure of **(a)** ruthenium(III) (**2.7**); (**b):** rhodium(III) (**2.8**) naphthaldimine and **(c)** rhodium(III) (**2.11**) and **(d)** iridium(III) (**2.12**) benzaldimine complexes.

Complexes **2.8**, **2.11** and **2.12** crystallize with the monoclinic space group $P2_1/n$. The distances between the metal centres and the aromatic carbon atoms range between 2.15 and 2.27 Å. The bond lengths between the metal centres and the chloride ligands are similar for both rhodium(III) complexes (**2.8 & 2.11**) with values of 2.39 and 2.40 Å, respectively. The iridium(III) complex (**2.12**) has a metal-Cl bond length of 2.40 Å. The distance between the metal centres and the carbon coordinated to the metal centre, are between 2.03 Å and 2.04 Å, which are considerably shorter than the metal-N bond lengths, ranging between 2.09 and 2.10 Å. In all three complexes **2.8**, **2.11** and **2.12**, the angle around the metal centre from the carbon coordinated to the metal centre to the nitrogen atom lies between 78.25° and 78.96° (**Table 2.3**). The rhodium(III) (**2.8 & 2.11**) and iridium(III) (**2.12**) complexes showed similar geometric parameters to each other and to similar related mononuclear iridium complexes reported in the literature.[14] The ruthenium(II) naphthaldimine complex (**2.7**) is also comparable to other related Ru(arene)Cl complexes.[31, 32]

Table 2.3: Crystallographic parameters with selected bond lengths and bond angles for the ruthenium(II) (**2.7**) and rhodium(III) naphthaldimine and rhodium (**2.11**) and iridium (**2.12**) benzaldimine mononuclear complexes.

Chemical formula	**$C_{24}H_{27}ClNRu$**	**$C_{24}H_{29}ClNRh$**	**$C_{20}H_{27}ClNRh$**	**$C_{20}H_{27}ClIrN$**
Formula weight (g/mol)	466.01	469.86	419.79	509.11
Crystal system	Monoclinic	Monoclinic	Monoclinic	Monoclinic
Space group	*P*21/c	*P*21/n	*P*21/n	*P*21/n
a (Å)	13.776	8.4123(4)	8.2170(3)	8.2604(3)
b (Å)	7.796	12.7708(5)	17.1415(9)	17.0360(6)
c (Å)	20.725	26.8982(12)	13.1453(6)	13.0692(4)
α (°)	90.00	90.00	90.00	90.00
ß (°)	116.78	94.9730(10)	90.306(3)	90.0180(10)
ɣ (°)	90.00	90.00	90.00	90.00
V (Å^3)	1987.1	2878.8(2)	1851.51(15)	1839.15(11)
Z	4	4	4	4
T (K)	293(2)	173(2)	173(2)	173(2)
Bond	**Distances (Å)**			
M(1)-C(11) or Ru(1)-C(1)	2.279(2)	2.256(3)	2.243(2)	2.239(2)
M(1)-C(12) or Ru(1)-(C2)	2.257(2)	2.275(3)	2.279(2)	2.277(2)
M(1)-C(13) or Ru(1)-C(3)	2.163(2)	2.166(3)	2.174(2)	2.174(2)
M(1)-C(14) or Ru(1)-C(4)	2.168(2)	2.167(3)	2.157(2)	2.151(3)
M(1)-C(15) or Ru(1)-C(5)	2.161(2)	2.159(3)	2.159(2)	2.167(3)
M(1)-Cl(1) or Ru(1)-Cl(1)	2.4027(6)	2.3984(8)	2.3943(6)	2.4047(6)
M(1)-N(1) or Ru(1)-N(1)	2.0692(18)	2.097(3)	2.091(2)	2.086(2)
M(1)-C(1) or Ru(1)-C(6)	2.176(2)	2.030(3)	2.032(2)	2.038(2)
Ru(1)-C(11)	2.036(2)			
Bond	**Angles(°)**			
C(1)-M(1)-N(1)	78.20(8)	78.96(12)	78.93(9)	78.25(9)
C(1)-M(1)-Cl(1)	84.98(6)	86.01(8)	86.37(7)	85.82(7)

The ruthenium(II) naphthaldimine complex (**2.7**) crystallizes with the monoclinic space group $P2_1/c$, with the distances between the ruthenium centre and the arene aromatic carbons ranging between 2.16 and 2.28 Å. The bond length between the ruthenium metal centre and the chloride ligand is 2.40 Å. The distance between the ruthenium and the carbon atom coordinated to the metal centre is 2.04 Å, which is considerably shorter than the ruthenium-N bond length of 2.07 Å. The angle around the metal centre from the carbon atom coordinated to the metal centre to the nitrogen atom lies at 78.20° (**Table 2.3**).

2.5 Synthesis of the cyclometalated naphthaldimine and benzaldimine G1 & G2-metallodendrimers 2.13-2.24

The first- and second-generation dendritic ligands (**2.3-2.6**) were reacted with either the $[Ru(p\text{-cymene})Cl_2]_2$, $[Rh(\eta^5\text{-}C_5Me_5)Cl_2]_2$ or $[Ir(\eta^5\text{-}C_5Me_5)Cl_2]_2$ dimer in a 1:2 ratio for the first-generation metallodendrimers (**2.13-2.16**) or 1:4 ratio for the second-generation metallodendrimers (**2.19-2.24**). The cyclometalation was done in the presence of sodium acetate (**Schemes 2.6 & 2.7**). A similar general synthetic method was used for the metallation of the monomeric ligands[27], except the metallation of the dendritic ligands required stirring in ethanol or methanol for 24-48 hours.

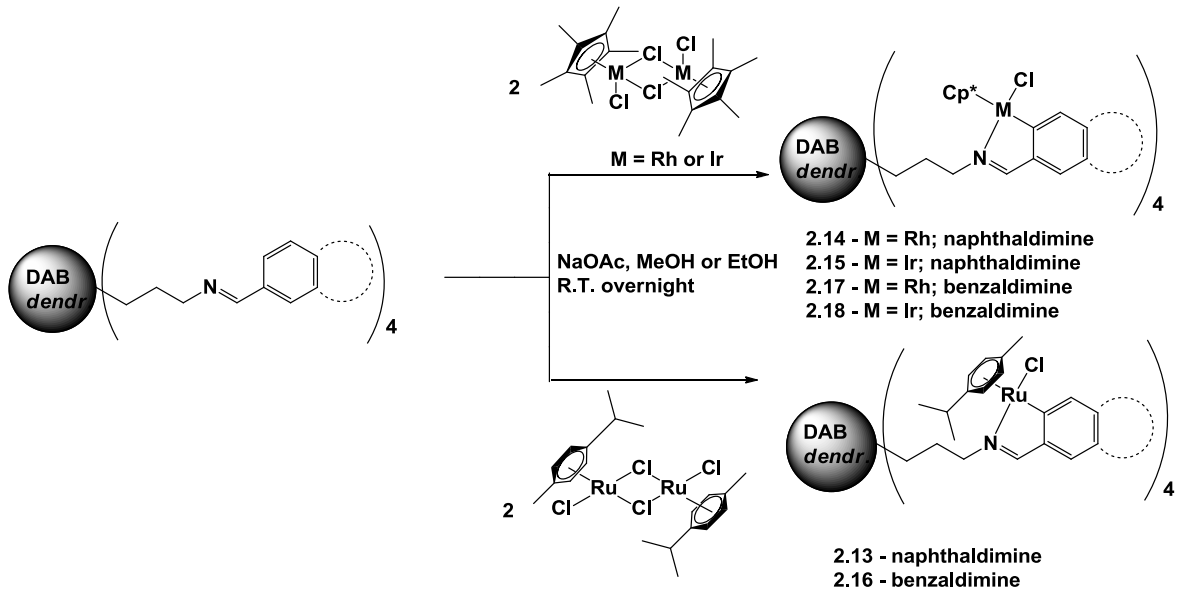

Scheme 2.6: Synthesis of ruthenium(II), rhodium(III) and iridium(III) tetranuclear *C,N*-chelating naphthaldimine (**2.13-2.15**) and benzaldimine (**2.16-2.18**) metallodendrimers.

The ruthenium(II) naphthaldimine and benzaldimine metallodendrimers (**2.13**, **2.16**, **2.19 & 2.22**) were obtained as green-brown solids. The first-generation ruthenium(II) metallodendrimers (**2.13 & 2.16**) were obtained in moderate to good yields of 99 and 65%, respectively, while the second-generation ruthenium metallodendrimers (**2.19 & 2.22**) were obtained in poor yields of about 32%. The rhodium(III) (**2.14, 2.17, 2.20 & 2.23**) and iridium(III) (**2.15, 2.18, 2.21 & 2.24**) metallodendrimers were obtained as orange solids in yields ranging between 29 and 80%. All the metallodendrimers (**2.13-2.24**) are soluble in methanol, ethanol, DCM and chloroform. The low yields of the second generation complexes can be attributed to functionalization of 8 arms therefore a longer period of time was required but due to results obtained in the early synthesis attempts, the reaction could not proceed for too long without decomposition of the products.

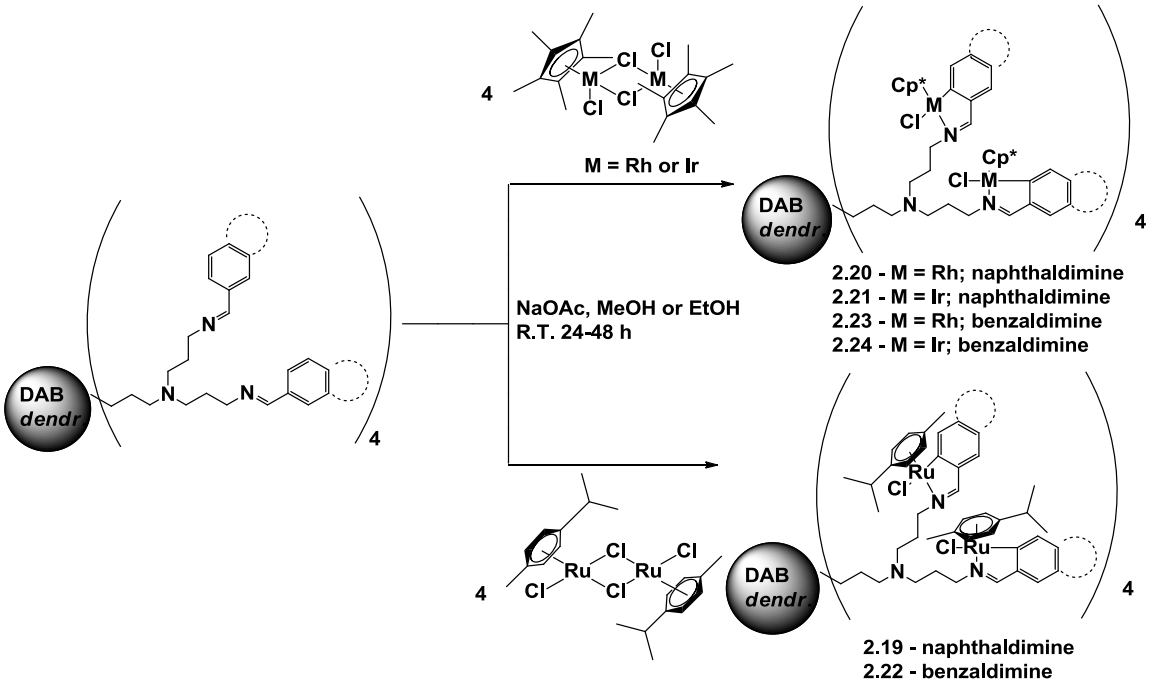

Scheme 2.7: Synthesis of ruthenium(II), rhodium(III), and iridium(III) octanuclear *C,N*-chelating naphthaldimine (**2.19-2.21**) and benzaldimine (**2.22-2.24**)

metallodendrimers.

2.5.1 ^{1}H-NMR and ^{13}C{^{1}H}-NMR spectroscopy

In the ^{1}H-NMR spectra of all the metallodendrimers (**2.13-2.24**) there is a shift of the imine singlet compared to the resonance observed in the ^{1}H-NMR spectra of the metal-free dendritic ligands (**2.3-2.6**). This result confirms that the imine bond is still intact and that

there is coordination of the metal centre to the imine nitrogen. The imine proton is observed furthest downfield in the ^{1}H-NMR spectra between 8.00-8.45 ppm (**Figures 2.9 & 2.10**). IR spectroscopy was used to further confirm coordination of the metal centre to the dendritic ligands (**2.3-2.6**).

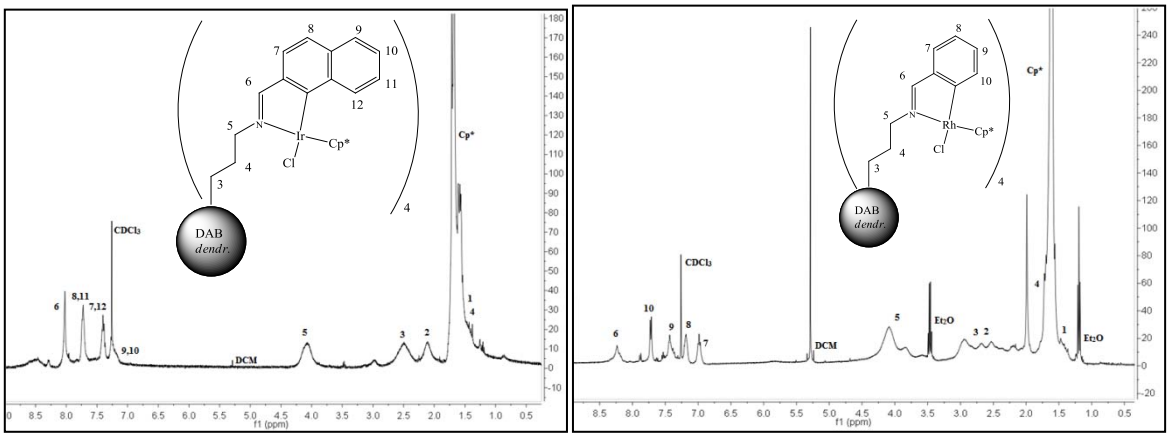

Figure 2.9: Representative ^{1}H-NMR spectra of the iridium(III) naphthaldimine (**2.15**) and rhodium(III) benzaldimine (**2.17**) G1 metallodendrimers.

The aromatic protons for the naphthaldimine and benzaldimine phenyl rings of metallodendrimers **2.13-2.24** appear between 7.00 and 8.45 ppm, in the expected region for aromatic protons. The ruthenium complexes (**2.13**, **2.16**, **2.19 & 2.22**) exhibit a loss of two-fold symmetry of the *p*-cymene moiety in the ^{1}H-NMR spectra, which results in the methyl protons of the isopropyl group exhibiting two broad peaks between 1.20 and 1.75 ppm. There is an additional broad peak observed between 1.80 and 2.80 ppm assigned to the single proton of the isopropyl group. The aromatic protons of the *p*-cymene moiety display four separate peaks in the range 4.60-5.80 ppm, as opposed to two peaks in the metal-free dimer. This is because the *p*-cymene moiety now has less freedom of rotation and therefore all four aromatic protons appear in different environments, but in some cases two of the signals overlap and seem to appear as one peak, especially with the broadening of the peaks in the metallodendrimers. The rhodium(III) (**2.14, 2.17, 2.20, 2.23**) and iridium(III) (**2.15, 2.18, 2.21 & 2.24**) metallodendrimers exhibit a broad singlet between 1.56 and 1.68 ppm corresponding to the methyl protons of the pentamethylcyclopentadienyl (Cp*) moiety (**Figures 2.9 & 2.10**).

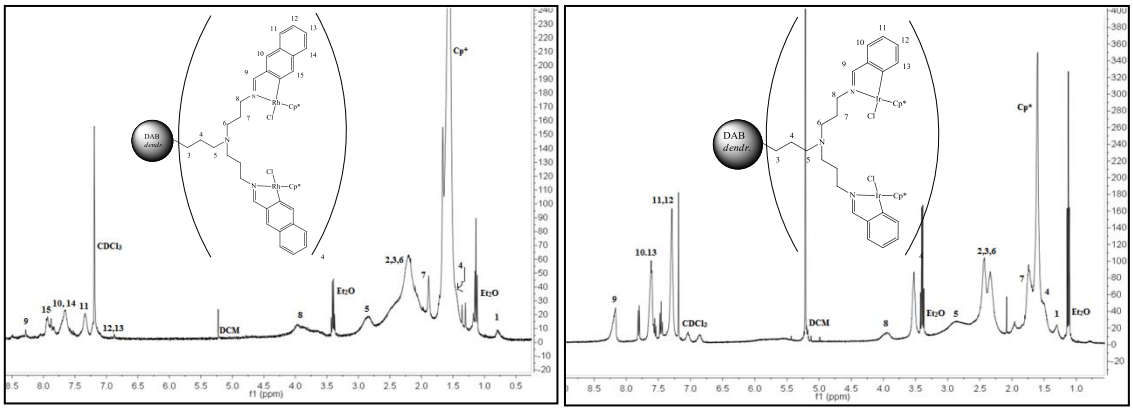

Figure 2.10: Representative ^{1}H-NMR spectra of the rhodium(III) naphthaldimine (**2.20**) and iridium(III) benzaldimine (**2.24**) G2 metallodendrimers.

In all the metallodendrimers (**2.13-2.24**), two broad peaks are observed at about 3.89-4.20 ppm corresponding to the $–CH_2$ group adjacent to the imine nitrogen. This can be attributed to the diastereotopic nature of the protons induced by the chiral metal centre, now coordinated in a *C,N*-bidentate fashion to the dendritic ligands. In the rhodium(III) complexes (**2.14**, **2.17**, **2.20 & 2.23**) the peak appears as two broad signals which are expected as these two protons are in different environments due to diastereotopicity. If one proton is replaced with another functional group it would generate a set of diastereomers, being adjacent to the chiral metal centre. This can also be due to the fact that rhodium(III) is NMR active. Whereas in the ruthenium(II) (**2.13, 2.15, 2.19 & 2.22**) and iridium(III) (**2.15, 2.17, 2.21 & 2.24**) complexes the peaks overlap to appear as one broad peak.

The peaks observed in the ^{1}H-NMR spectra of all the metallodendrimers appear as broadened peaks. The broadening of the peaks is due to the fact that each peak represents four times as many protons for each one of the four metallodendritic arms and therefore on the NMR-time scale the peaks average out to a broadened peak. These assignments were made in conjunction with 2D-NMR techniques such as HSQC and COSY.

The ^{13}C{^{1}H}-NMR spectra exhibit imine carbon peaks downfield in each spectra ranging between 142.1 and 147.0 ppm for all 12 metallodendrimers (**2.13-2.24**). The chemical shifts for the aliphatic carbons of each metallodendrimer (**2.13-2.24**) appear between 9.00-60.0 ppm, while the aromatic carbon atoms appear furthest downfield between 123.0-176.0 ppm. The aromatic carbons on the *p*-cymene ligand appear between ~70.0-100.0 ppm in complexes

2.13 2.16 2.19 and **2.22**, while the carbons on the Cp* ligand in complexes **2.14**, **2.15**, **2.17**, **2.18**, **2.20**, **2.21**, **2.23** and **2.24** appear at ~9.00 ppm.

2.5.2 Infrared (IR) spectroscopy

IR spectroscopy was used to determine whether the imine bond was still intact and to confirm the coordination of the metal centre to the imine nitrogen atom of the dendritic ligands (**2.3-2.6**). The IR spectra of all twelve metallodendrimers (**2.13-2.24**) were recorded as KBr pellets and each complex exhibited a shifted imine absorption band to a lower frequency ranging between 1600-1610 cm^{-1}, compared to the metal-free dendritic ligands (**2.3-2.6**) with imine absorption bands at 1639, 1643, 1639 and 1646 cm^{-1}, respectively.

2.5.3 High Resolution Electrospray Ionization Mass Spectrometry (ESI-MS)

The MS spectra of the ruthenium(II) (**2.13**) and rhodium(III) (**2.14**) naphthaldimine G1 metallodendrimers show base peaks corresponding to the loss of chloride ligands as well as exhibiting molecular ion peaks (**Table 2.4**). The rhodium(III) benzaldimine (**2.17**) G1 metallodendrimer exhibits a molecular ion peak only in the mass spectrum, while the MS of the G1 metallodendrimers **2.15** & **2.16**, show base peaks corresponding to the loss of the chloride ligands (**Table 2.4**). Metallodendrimer **2.18** exhibits a base peak in the mass spectrum corresponding to an adduct with two protons (**Table 2.4**).

Table 2.4: Mass spectrometry data for G1 metallodendrimers (**2.13-2.18**).

Complex	Calculated M (g/mol)	Molecular fragment (*m/z*)	Assignment
2.13	1948.15	613.8303	$[M\text{-}3Cl^-]^{3+}$
		1948.4221	$[M]^+$
2.14	1959.52	1923.4847	$[M\text{-}Cl^-]^+$
		1959.4465	$[M]^+$
2.15	2316.78	1122.4001	$[M\text{-}2Cl^-]^{2+}$
2.16	1474.91	407.1664	$[M\text{-}4Cl^-]^{4+}$
		544.2101	$[M\text{-}3Cl^-]^{3+}$
		842.1741	$[M\text{-}2Cl^-]^{2+}$
2.17	1759.30	1759.4011	$[M]^+$
2.18	2116.54	1059.3232	$[M+2H^+]^{2+}$

The mass spectra of each G2 metallodendrimer (**2.19-2.24**) exhibit base peaks corresponding to the loss of the chloride ligands (**Table 2.5**).

Table 2.5: Mass spectrometry data for G2 metallodendrimers (**2.19-2.24**).

Complex	Calculated M (g/mol)	Molecular fragment (*m/z*)	Assignment
2.19	4036.53	466.15	$[M\text{-}8Cl^-]^{8+}$
		974.24	$[M\text{-}4Cl^-]^{4+}$
2.20	4059.27	640.93	$[M\text{-}6Cl^-]^{6+}$
2.21	4773.79	761.74	$[M\text{-}6Cl^-]^{6+}$
		1152.39	$[M\text{-}4Cl^-]^{4+}$
2.22	3636.05	569.01	$[M\text{-}6Cl^-]^{6+}$
		873.22	$[M\text{-}4Cl^-]^{4+}$
2.23	3658.83	574.22	$[M\text{-}6Cl^-]^{6+}$
		696.23	$[M\text{-}5Cl^-]^{5+}$
2.24	4373.31	589.23	$[M\text{-}7Cl^-]^{7+}$
		693.31	$[M\text{-}6Cl^-]^{6+}$

2.6 Conclusion

A series of new naphthaldimine and benzaldimine *C,N*-bidentate chelating ligands (**2.1-2.6**) were synthesized in good yields. New ruthenium(II), rhodium(III) and iridium(III) mononuclear (**2.7-2.12**), tetranuclear (**2.13-2.18**) and octanuclear (**2.19-2.24**) complexes were synthesized by reacting the ligands with the appropriate metal dimer precursor, $[Ru(p\text{-cymene})Cl_2]_2$, $[Rh(\eta^5\text{-}C_5Me_5)Cl_2]_2$ or $[Ir(\eta^5\text{-}C_5Me_5)Cl_2]_2$ and obtaining the desired products in a variety of yields, decreasing with the increase in metallodendrimer generation. The rhodium(III) and iridium(III) complexes tended to be easier to synthesize and purify, as well as being generally more stable than the ruthenium(II) complexes. All the ligands and complexes were successfully characterized by ^{1}H-NMR, $^{13}C\{^1H\}$-NMR and IR spectroscopy, as well as mass spectrometry. Four of the mononuclear metal complexes were also characterized using X-ray crystallography.

2.7 References

1. N. Malik, R. Wiwattanapatapee, K. Lorenz, H. Frey, J. W. Weener, E. W. Meijer, P. W. and R. Duncan, *J. Control Rel.*, 2000, **65**, 133-148.
2. D. Astruc, E. Boisselier and C. Ornelas, *Chem. Rev.*, 2010, **110**, 1857-1959.
3. Z. Liu, L. Salassa, A. Habtemariam, A. M. Pizarro, G. J. Clarkson and P. J. Sadler, *J. Inorg. Chem.*, 2011, **50**, 5777-5783.
4. A. K. Iyer, G. Khaled, J. Fang and H. Maeda, *Drug Discov. Today*, 2006, **11**, 812-818.
5. S. El Kazzouli, N. El Brahmi, S. Mignani, M. Bousmina, M. Zablocka and J.-P. Majoral, *Curr. Med. Chem.*, 2012, **19**, 4995-5010.
6. E. R. Gillies and J. M. J. Frechet, *Drug Discov. Today*, 2005, **10**, 35-43.
7. P. Govender, B. Therrien and G. S. Smith, *Eur. J. Inorg. Chem.*, 2012.
8. N. J. Wheate, S. Walker, G. E. Craig and R. Oun, *Dalton Trans.*, 2010, **39**, 8097-8340.
9. B. Rosenberg, *Interdiscip. Sci. Rev.*, 1978, **3**, 134.
10. G. Süss-Fink, *Dalton Trans.*, 2010, **39**, 1673-1688.
11. B. Therrien, W. H. Ang, F. Cherioux, L. Vieille-Petit, L. Juillerat-Jeanneret, G. Suss-Fink and P. J. Dyson, *J. Cluster Sci.*, 2007, **18**, 741-752.
12. E. Rosenberg, F. Spada, K. Sugden, B. Martin, L. Milone, R. Gobetto, A. Viale and J. Fiedler, *J. Organomet. Chem.*, 2003, **668**, 51-58.
13. Z. Liu, A. Habtemariam, A. M. Pizarro, G. J. Clarkson and P. J. Sadler, *Organometallics*, 2011, **30**, 4702-4710.
14. Z. Liu, A. Habtemariam, A. M. Pizarro, S. A. Fletcher, A. Kisova, O. Vrana, L. Salassa, P. C. A. Bruijnincx, G. J. Clarkson, V. Brabec and P. J. Sadler, *J. Med. Chem.*, 2011, **54**, 3011-3026.

15. C. S. Allardyce, P. J. Dyson, D. J. Ellis, P. A. Salter and R. Scopelliti, *J. Organomet. Chem.*, 2003, **668**, 35-42.

16. M. Melchart and P. J. Sadler, *in Bioorganometallics*, Ed. G. Jaouen, Wiley-VCH, Weinheim, 1st Edn., 2006, vol. 1, ch. 2, pp. 39-62.

17. D. S. Black, G. B. Deacon and G. L. Edwards, *Aust. J. Chem.*, 1994, **47**, 217-227.

18. D. S. Black, G. B. Deacon, G. L. Edwards and B. M. Gatehouse, *Aust. J. Chem.*, **46**, 1326-1336.

19. G. L. Edwards, D. S. Black, G. B. Deacon and L. P. G. Wakelin, *Can. J. Chem.*, 2005, **83**, 980-989.

20. S. Mollin, S. Blanck, K. Harms and E. Meggers, *Inorg. Chim. Acta*, 2012, **393**, 261-268.

21. C.-H. Leung, H.-J. Zhong, H. Yang, Z. Cheng, D. S.-H. Chan, V. P.-Y. Ma, R. Abagyan, C.-Y. Wong and D.-L. Ma, *Angew. Chem. Int. Ed.*, 2012, **51**, 9010-9014.

22. C. H. Leung, H. J. Zhong, D. S. H. Chan and D. L. Ma, *Coord. Chem. Rev.*, 2013, **257**, 1764-1776.

23. A. L. Hurley and D. L. Mohler, *Org. Lett.*, 2000, **2**, 2745-2748.

24. N. Mungwe, A. J. Swarts, S. F. Mapolie and G. Westman, *J. Organomet. Chem.*, 2011, **696**, 3527-3535.

25. M. A. Mintzer and M.W. Grinstaff, *Chem. Soc. Rev.*, 2011, **40**, 173-190.

26. C. White, A. Yates, P. M. Maitlis and D. M. Heinekey, *Inorg. Synth.*, 2007, **29**, 228-234.

27. P. Govender, A. K. Renfrew, C. M. Clavel, P. J. Dyson, B. Therrien and G. S. Smith, *Dalton Trans.*, 2011, **40**, 1158-1167.

28. D. L. Davies, O. Al-Duaij, J. Fawcett, M. Giardiello, S. T. Hilton and D. R. Russell, *Dalton Trans.*, 2003, 4132-4138.

29. E. C. and A. Salzer, *in Organometallics*, VCH Publishers Inc., New York, 2nd Edn. 1992, chapter 1, pp. 1.

30. B. Spingler, S. Schnidrig, T. Todorova and F. Wild, *Cryst. Eng. Comm.*, 2012, **14**, 751-757.

31. Q. Zhou, P. Li, R. Lu, Q. Qian, X. Lei, Q. Xiao, S. Huang, L. Liu, C. Huang and W. Su, *Z. Anorg. Allg. Chem.*, 2013, **639**, 943-946.

32. B. Therrien, C. Saïd-Mohamed and G. Süss-Fink, *Inorg. Chim. Acta.*, 2008, **361**, 2601-2608.

Chapter 3: Synthesis and Characterization of Mono- and Polynuclear Cationic Homometallic and Heterometallic Cyclometalated Complexes

3.1 Introduction

One of the main classes of bioorganometallic compounds that has been developed is the RAPTA series of complexes, with the general formula Ru(η^6-arene)(PTA)Cl_2 containing the phosphaadamantane ligand, 1,3,5-triaza-7-phosphatricyclo[3.3.1.1]decane (PTA).[1-7] These RAPTA compounds, specifically RAPTA-C (**Figure 3.1**), have shown poor *in vitro* cytotoxicity, but were shown to exhibit antitumour[8] and antimetastatic[2] behaviour *in vivo*. PTA is an amphiphilic ligand which is soluble in water and other organic solvents. It is proposed that this ligand can provide easy transport of macromolecules within the body and across lipophilic cell membranes.[9]

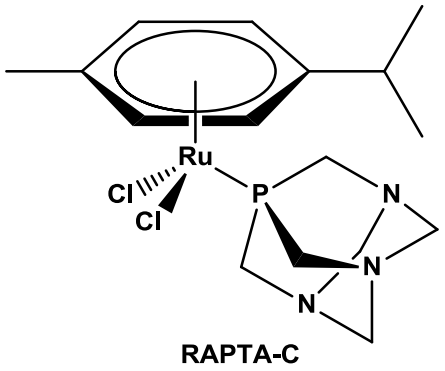

Figure 3.1: Structure of the anticancer ruthenium(II) complex: RAPTA-C.

For RAPTA complexes there is a synergistic effect between the mechanism of action of both the organic unit and the inorganic unit.[9] The ruthenium(II)-arene subunit has the potential to coordinate to biomolecules within the body and there is evidence that it binds to proteins such as histones versus the DNA back-bone itself.[10] Dyson *et al.* synthesized a series of napthalimide-tagged ruthenium(II) arene complexes and tested the *in vitro* anti-cancer activity of these complexes.[9] Three complexes (**Figure 3.2**) showed good activity against the A2780 and A2780*cis*R cancer cell lines, exhibiting IC_{50} values ranging between 2.31-8.53 μM for the cisplatin-sensitive strain, A2780, and 2.28-9.09 μM for the cisplatin-resistant strain, A2780*cis*R.[9]

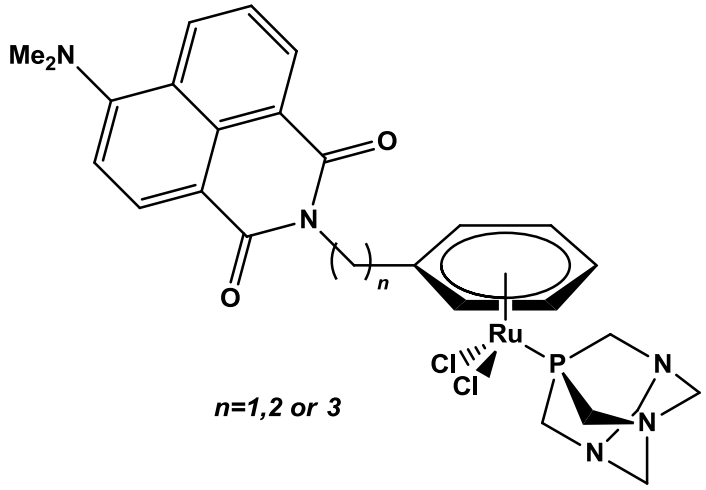

Figure 3.2: Structure of the naphthalimide-tagged RAPTA-type complexes.[9]

Therefore by incorporating an organic subunit, such as the naphthaldimine moiety, this could act as a DNA-intercalator.[9] With the binding abilities of the inorganic ruthenium(II)-arene sub-unit to nucleosome histones and the possible intercalation of the naphthaldimine organic moiety, the cytotoxic effect of the compound could be enhanced compared to cisplatin which intercalates with DNA only.[9] Hence the motivation to incorporate PTA into ruthenium(II), rhodium(III) and iridium(III) naphthaldimine complexes in this project is to improve the ampiphilic character and due to the fact that these target metastatic tumors.

Incorporating ferrocene into organometallic compounds has also attracted much interest in bioorganometallic chemistry, for application as anti-cancer drugs.[11, 12] This can be attributed to its lipophilicity, stability toward air and moisture, non-toxicity, small size, aromaticity and its redox behaviour.[12-14] As has been discussed previously, the biological activity of the ferrocene moiety can be attributed to its ability to generate free radical metabolites which then induces oxidative DNA damage.[15] The low formal potential of ferrocene in water renders it vulnerable to biological oxidation-reduction processes, and it is the oxidised analogue of ferrocene that is said to act as the antitumour agent.[14, 15]

Therefore incorporating ferrocene into organometallic frameworks could improve the biological activity of these compounds.[12] Ferrocifen[16, 17] (**Figure 3.3**) is one such example which is a ferrocenyl derivative of the well-known anticancer drug tamoxifen, and has shown higher anticancer activity compared to its precursor compounds.[12]

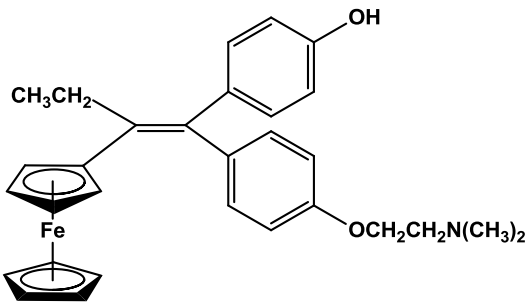

Figure 3.3: Ferrocifen, the ferrocenyl derivative of the known anticancer drug, tamoxifen.[11]

Since the success of cationic complexes which have shown improved anti-cancer activity, compared to their neutral analogues, there is an increasing interest in developing cationic complexes as potential anti-cancer agents.

3.2 Reactions with PTA

3.2.1 Synthesis of the cationic naphthaldimine mononuclear complexes 3.1-3.3

The synthesis of the cationic complexes followed a similar method to the synthesis of the neutral complexes, adopting a method used by Govender *et al.*[18], whereby the naphthaldimine ligand (**2.1**) was metallated with one of the metallic dimeric precursors in the presence of sodium acetate for the selective C-H activation of the alpha proton in order for cyclometalation to occur.[19] The cationic series of complexes was synthesized only with the naphthaldimine ligand (**2.1**) due to the fact that the benzaldimine complexes were less stable and exhibited decomposition over time and in solution. In this case, the neutral precursors were not isolated. The reaction mixture was filtered through Celite followed by the addition of PTA, which was stirred for a further 30-60 minutes, in order to replace the chloride ligand with the more water-soluble PTA phosphorous-donor ligand. This, in turn,, generates the corresponding cationic complexes (**Scheme 3.1**). Hexafluorophosphate was finally added at 0^{o}C in order to replace the chloride counterion with a more stable counterion (**Scheme 3.1**).[20]

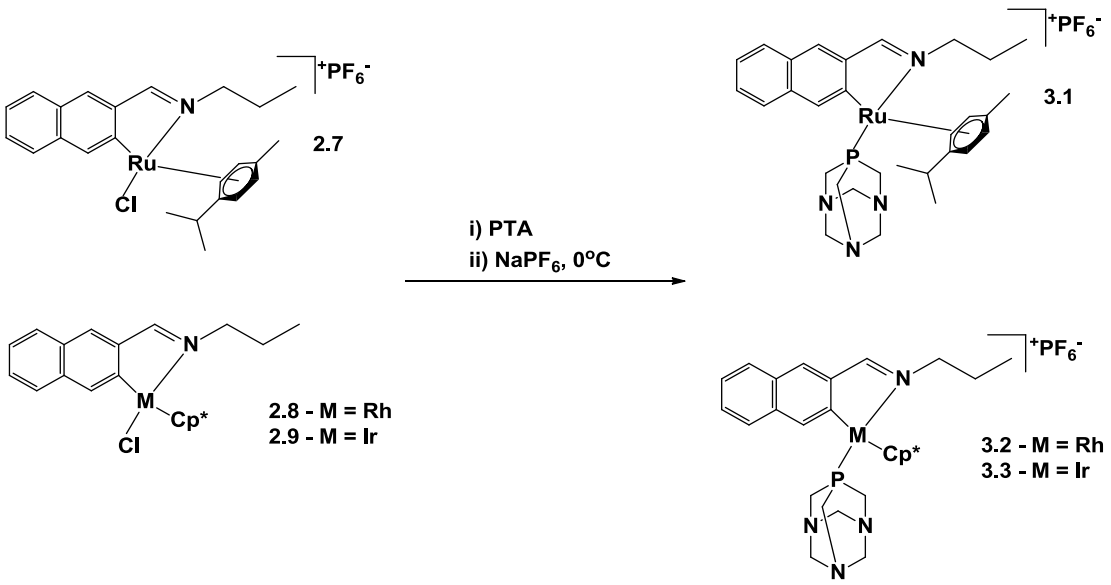

Scheme 3.1: Synthesis of the cationic ruthenium(II), rhodium(III) and iridium(III) *C,N*–chelating naphthaldimine mononuclear complexes (**3.1-3.3**).

The ruthenium(II) naphthaldimine cationic complex (**3.1**) was obtained as a red-brown solid in a poor yield of 15%, while the rhodium(III) and iridium(III) naphthaldimine complexes (**3.2 & 3.3**) were obtained as yellow-orange solids in moderate yields ranging between 34 and 47%. All the mononuclear complexes are soluble in acetone, methanol, ethanol, DCM, chloroform and only sparingly soluble in water. All the cationic mononuclear complexes (**3.1-3.3**) were characterized using ^{1}H-, ^{13}C- and ^{31}P{^{1}H}-NMR spectroscopy.

3.2.1.1 ^{1}H-, ^{13}C{^{1}H}- and ^{31}P{^{1}H}-NMR spectroscopy

The ^{1}H-NMR spectrum of each complex (**3.1-3.3**) displays a characteristic imine singlet upfield at 8.61, 8.73 and 8.85 ppm, respectively, indicating that the imine bond is still intact. The aromatic protons for the naphthaldimine ring appear at typical aromatic chemical shifts between 7.44 and 8.40 ppm (**Figure 3.4**). The PTA protons appear between 3.64 and 4.36 ppm in the ^{1}H-NMR spectra of each cationic complex (**3.1-3.3**).

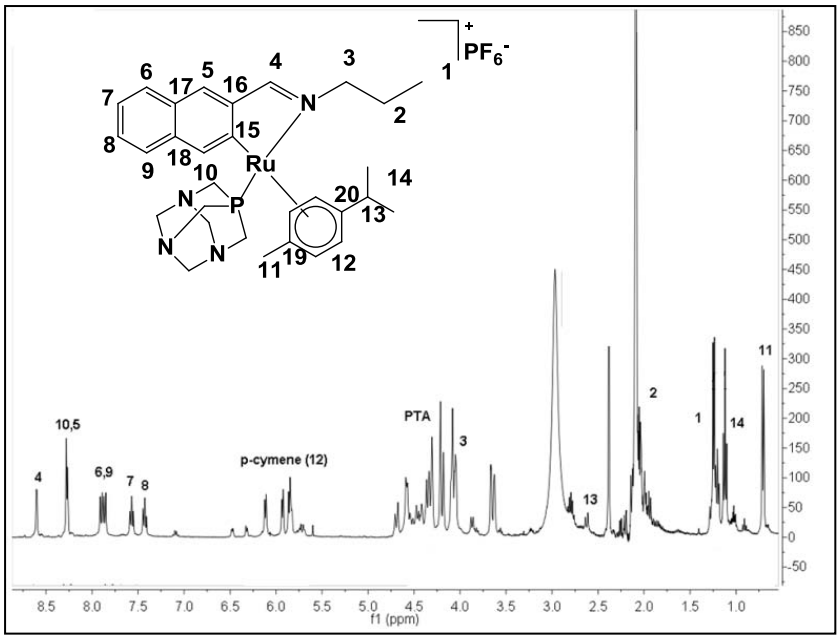

Figure 3.4: Representative ^{1}H-NMR spectrum of the ruthenium(II) naphthaldimine cationic mononuclear complex (**3.1**).

In the ^{1}H-NMR spectrum of the cationic ruthenium(II) complex (**3.1**), there is a loss of two-fold symmetry of the *p*-cymene moiety which results in the methyl protons of the isopropyl group exhibiting two sets of doublets at 1.07 and 1.26 ppm (**Figure 3.4**). There is also evidence of a septet observed at 2.51 ppm assigned to the single proton of the isopropyl group. The aromatic protons of the *p*-cymene moiety display four separate doublets in the range 5.86-6.10 ppm, as opposed to two doublets in the ruthenium(III)-dimer. This can be attributed to the *p*-cymene moiety having less freedom of rotation or that the ruthenium(II) centre is chiral and therefore all four aromatic protons appear in different environments. In some cases two of the signals overlap and appear as a broad doublet.

Complexes **3.2** and **3.3** exhibit a singlet at 1.91 and 2.00 ppm, respectively, in the ^{1}H-NMR, corresponding to the methyl protons of the pentamethylcyclopentadienyl (Cp*) moiety (**Figure 3.5**). In all three complexes (**3.1-3.3**), two sets of resonances are observed for each –CH_2 group of the propyl chain at about ~4.00 ppm. This can be attributed to the diasterotopic nature of the protons induced by the chiral metal centre.

These assignments were made and confirmed using 2D-NMR techniques such as HSQC and COSY, whereby the COSY shows the spin-spin coupling between proton 1 and 2, as well as between 2 and 3 of the propyl chain as well as between the PTA protons (**Figure 3.5**).

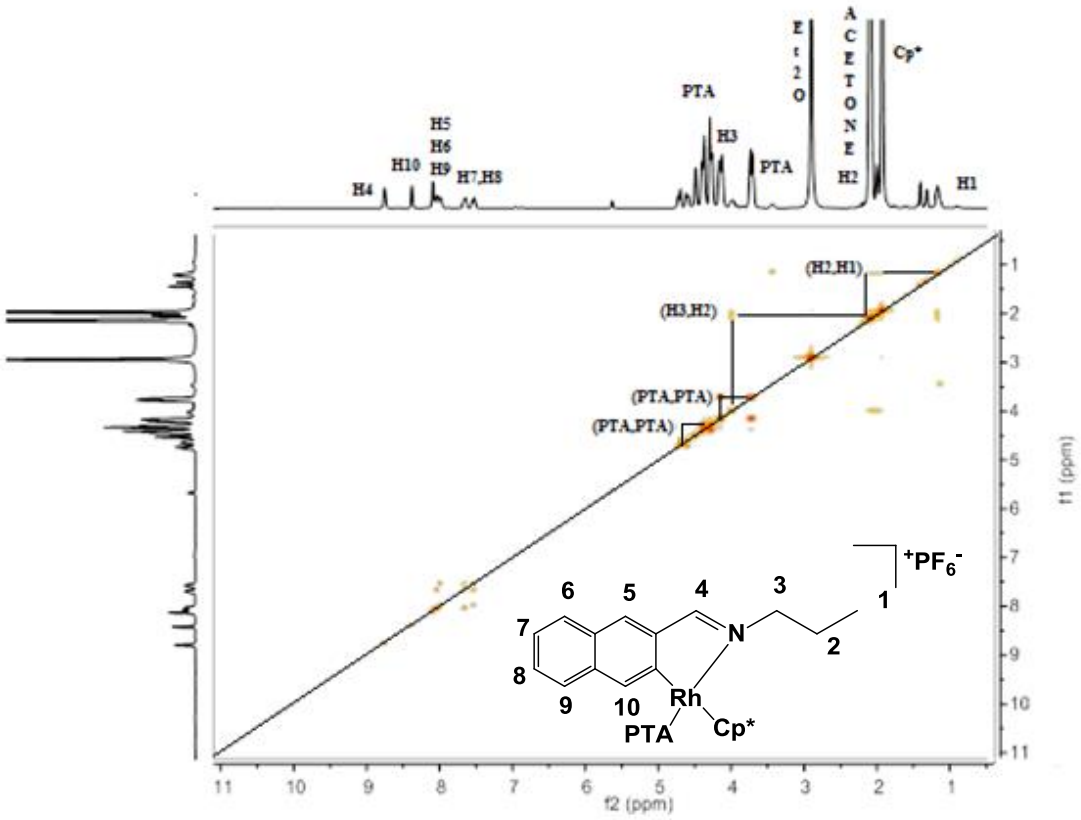

Figure 3.5: Representative COSY spectrum of the rhodium(III) naphthaldimine cationic mononuclear complexes (**3.2**).

In the $^{13}C\{^{1}H\}$-NMR spectra the imine carbon resonances appear downfield at about ~175.0 ppm for each metal complex (**3.1-3.3**). The chemical shifts for the aliphatic carbons appear between 10.4-72.5 ppm, while the aromatic carbon atoms appear furthest downfield, between 119.9 and 147.1 ppm. The aromatic carbons on the *p*-cymene ligand of the ruthenium complex (**3.1**) appear between 86.3 and 92.6 ppm, while the carbons on the Cp* moiety in complexes **3.2** and **3.3**, appear at 9.01 and 8.71 ppm, respectively.

In the $^{31}P\{^{1}H\}$-NMR spectrum of each complex (**3.1-3.3**), a septet is observed at -144.0 ppm which corresponds to the hexafluorophosphate counterion. This septet is observed due to the coupling of the phosphorous to all six fluorine atoms. The spectra of the ruthenium(II) and iridium(III) complexes (**3.1 & 3.3**), display a singlet at -39.9 and -79.5 ppm, respectively, which corresponds to the PTA coordinated to the metal centre. A doublet is observed in the spectrum of the rhodium(III) complex (**3.2**) at -44.9 ppm, with a coupling constant of -45 Hz, as rhodium is NMR-active and confirms that there is coupling between the rhodium(III) metal centre and the P-donor ligand of the PTA moiety.

3.2.1.2 Infrared (IR) spectroscopy

The IR spectra of all three complexes (**3.1-3.3**) were recorded as KBr pellets and show the presence of imine absorption bands ranging between 1602 and 1607 cm^{-1}. These values indicate a shift in the imine absorption band from 1640 cm^{-1} for the metal-free ligand (**2.1**) to lower frequencies for each cationic metal complex (**3.1-3.3**). This shift is expected as it confirms the coordination of the metal centres to the imine nitrogen due to metal-nitrogen back donation, as previously discussed.

Table 3.1: IR spectroscopy data for the cationic mononuclear complexes (**3.1-3.3**) versus the data obtained for the corresponding neutral analogues (**2.7-2.9**).

Complex	Cationic complex (cm^{-1})	Neutral complex (cm^{-1})
Ru(II)	1602 **(3.1)**	1611 **(2.7)**
Rh(III)	1607 **(3.2)**	1610 **(2.8)**
Ir(III)	1602 **(3.3)**	1603 **(2.9)**

The imine absorption band in the IR spectra of each cationic complex (**3.1-3.3**) is consistent with that of the neutral complexes (**2.7-2.9**) (**Table 3.1**).

3.2.1.3 Electron Ionization Mass Spectrometry (EI-MS)

The mass spectra of each complex (**3.1-3.3**) show fragmentation peaks corresponding to the loss of a hexafluorophosphate counterion as well as the PTA moiety corresponding to the molecular ion $[M-(PF_6+PTA)]^+$.

3.2.2 Synthesis of the cationic naphthaldimine G1 & G2 metallodendrimers 3.4-3.9

The synthesis of the G1 and G2 cationic metallodendrimers was similar to the synthesis of the cationic mononuclear complexes (**3.1-3.3**),[18] whereby PTA was added to the reaction mixture after cyclometalation and finally sodium hexafluorophosphate was added at 0^oC in order to replace the chloride ligand (**Scheme 3.2 & 3.3**).[20]

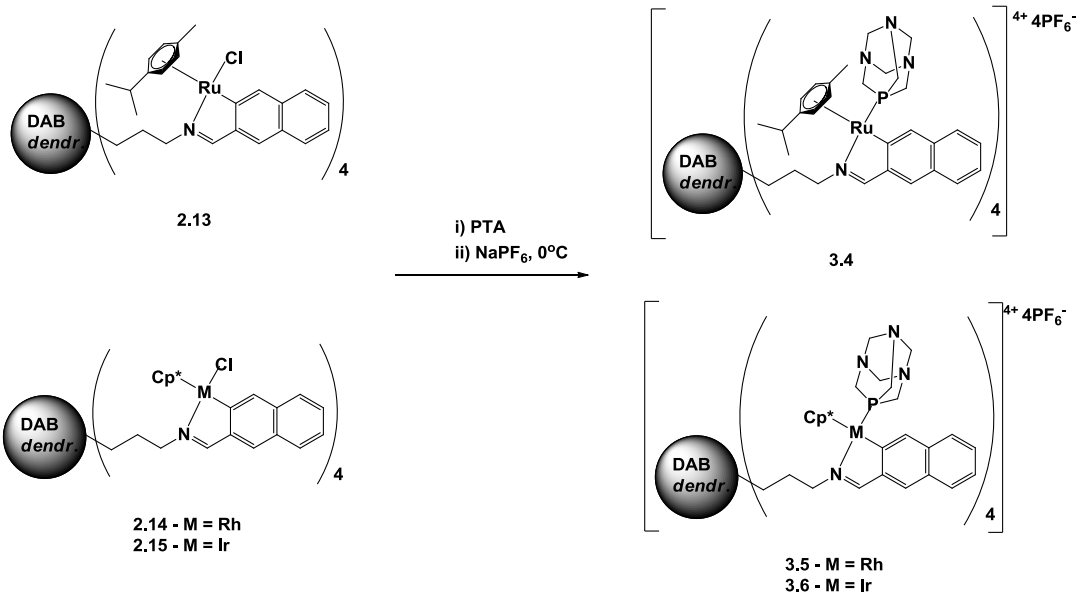

Scheme 3.2: Synthesis of the cationic ruthenium(II), rhodium(III) and iridium(III) *C,N*–chelating G1 naphthaldimine metallodendrimers (**3.4-3.6**).

The ruthenium(II) naphthaldimine G1 and G2 cationic complexes (**3.4 & 3.7**) were obtained as yellow-brown solids in moderate yields of approximately 40%, while the rhodium(III) (**3.5 & 3.6**) and iridium(III) (**3.8 & 3.9**) metallodendrimers were obtained as yellow-orange solids in poor to moderate yields. All the cationic metallodendrimers (**3.4-3.9**) are soluble in acetone, methanol, ethanol, DCM and chloroform and sparingly soluble in water.

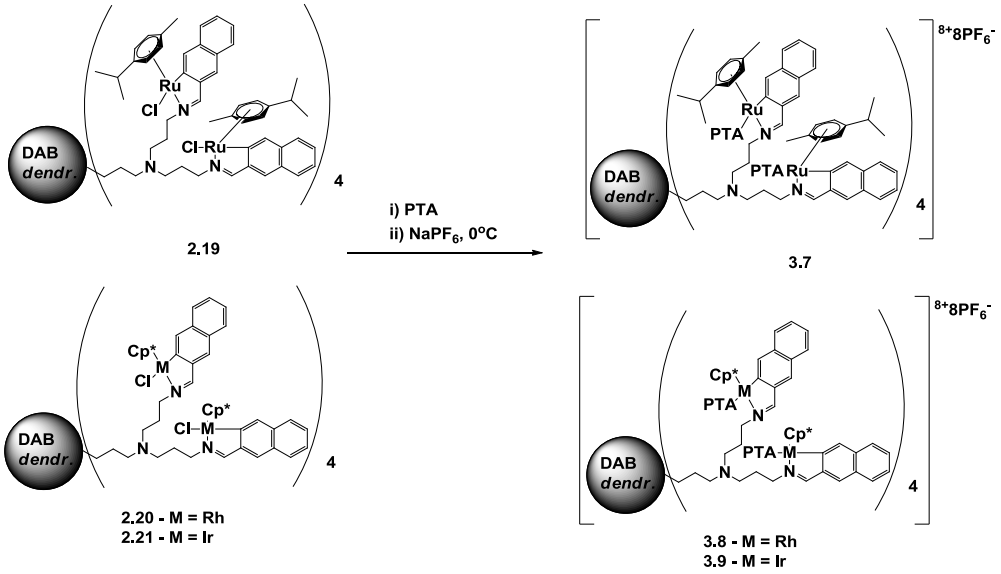

Scheme 3.3: Synthesis of the cationic ruthenium(II), rhodium(III) and iridium(III) *C,N*–chelating G2 naphthaldimine metallodendrimers (**3.7-3.9**).

3.2.2.1 ^{1}H-, ^{13}C{^{1}H}- and ^{31}P{^{1}H}-NMR spectroscopy

The imine singlet in both the first- and second-generation metallodendrimers (**3.4-3.9**) is observed upfield in each ^{1}H-NMR spectrum between 8.57 and 8.84 ppm. This result confirms that the imine bond is still intact (**Figures 3.6 & 3.7**).

The core protons of the metallodendrimers appear in similar ranges far upfield, with the ruthenium(II) complexes (**3.4 & 3.7**) having their core protons generally more upfield than the rhodium(III) (**3.5 & 3.6**) and iridium(III) (**3.8 & 3.9**) complexes. The core protons of the ruthenium(II) G1 (**3.4**) and G2 (**3.7**) metallodendrimers appear between 0.71 and 2.44 ppm, while the core protons of the rhodium(III) (**3.5 & 3.8**) and iridium(III) (**3.6 & 3.9**) metallodendrimers appear slightly more downfield between 1.30-3.66 ppm.

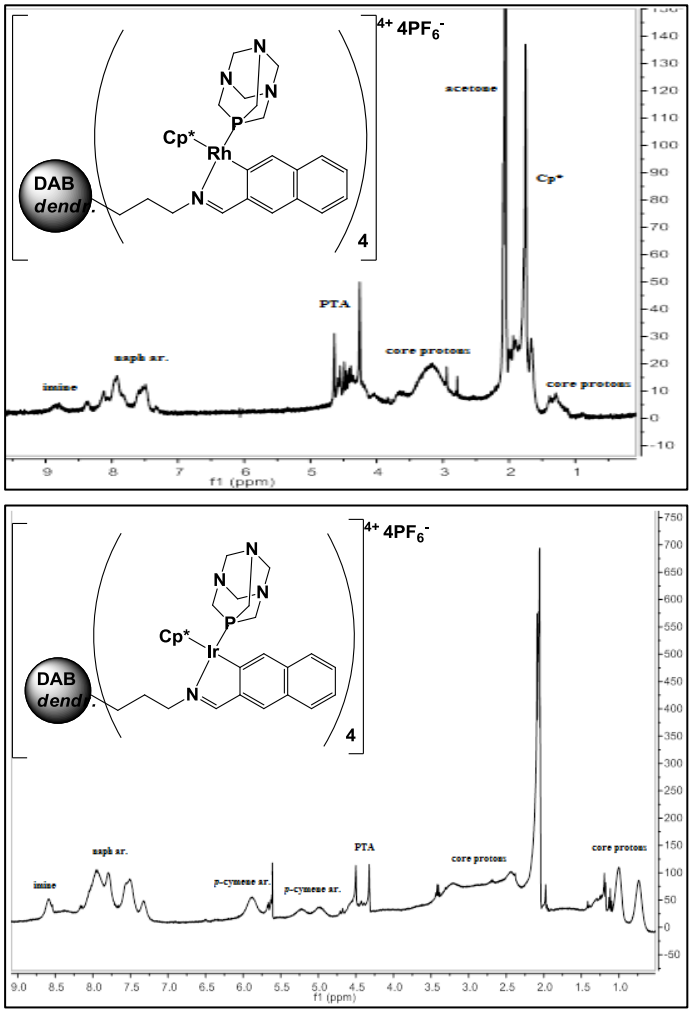

Figure 3.6: Representative ^{1}H-NMR spectra of the cationic rhodium(III) (**3.5**) and iridium(III) (**3.6**) naphthaldimine G1 metallodendrimers.

For all six metallodendrimers (**3.4.-3.9**), the aromatic protons for the naphthaldimine phenyl ring appear between 7.29 and 8.58 ppm, which is the expected region for aromatic protons. The cationic ruthenium complexes (**3.4 & 3.7**) exhibit a loss of two-fold symmetry of the *p*-cymene moiety as well as the aromatic protons of the *p*-cymene moiety in each ruthenium complex displaying four separate peaks in the ^{1}H-NMR spectra between 4.95 and 5.86 ppm. These trends are observed in the model cationic mononuclear complex (**3.1**) due to diastereotopicity and loss freedom of rotation of the *p*-cymene moiety. However in the metallodendrimers two of the *p*–cymene resonances overlap and appear as one peak due to broadening of the peaks. The Cp* methyl protons in the rhodium(III) (**3.5 & 3.8**) and iridium(III) (**3.6 & 3.9**) metallodendrimers, appear as a broad singlet at about ~1.70 ppm.

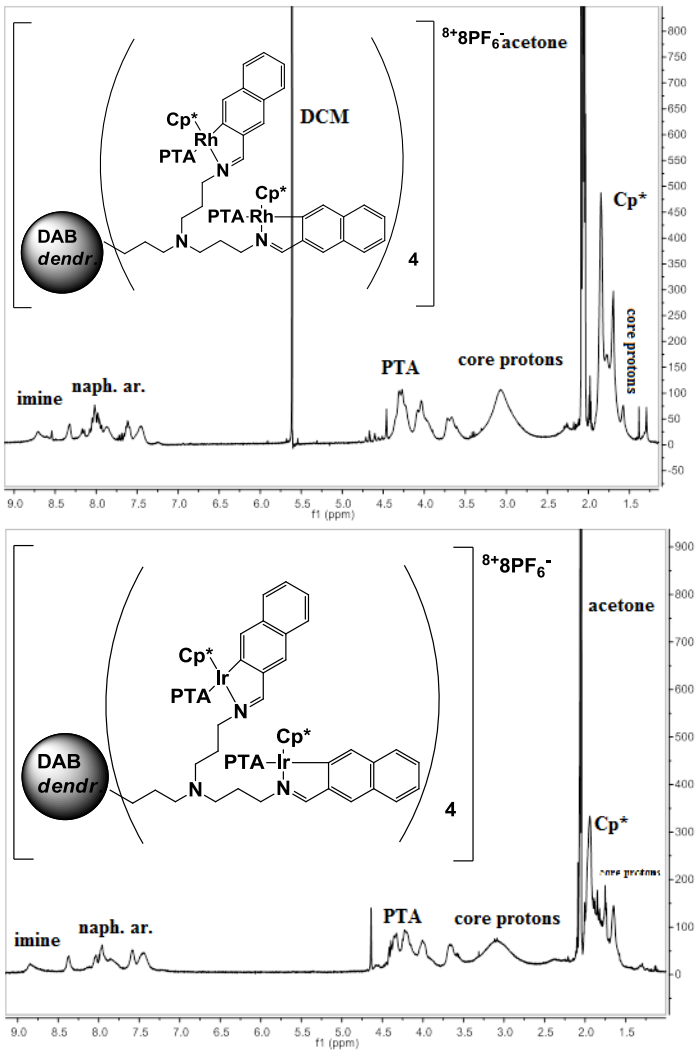

Figure 3.7: Representative ^{1}H-NMR spectra of the cationic rhodium(III) (**3.8**) and iridium(III) (**3.9**) naphthaldimine G2 metallodendrimers.

In the spectra of all six metallodendrimers (**3.4-3.9**), two sets of broad resonances are observed between 3.91 and 4.13 ppm corresponding to the $–CH_2$ group adjacent to the imine nitrogen, which can be attributed to the diasterotopicity of the protons induced by the now chiral metal centre. The proton signals associated with the PTA moiety appear in the region 3.58-4.64 ppm for all six metallodendrimers (**3.4-3.9**).

The spectra obtained from $^{13}C\{^1H\}$-NMR spectroscopy exhibit imine carbon resonances downfield between 174.70 and 177.50 ppm for each cationic G1 and G2 metallodendrimer (**3.4-3.9**). The aliphatic carbon atoms resonate at chemical shifts between 9.32 and 62.35 ppm for the rhodium(III) (**3.5 & 3.8**) and iridium(III) (**3.6 & 3.9**) metallodendrimers, while for the ruthenium(II) metallodendrimers (**3.4 & 3.7**) the aliphatics range further downfield between 18.21 and 72.86 ppm. The aromatic carbons of the *p*-cymene moiety appear between 79.73 and 94.72 ppm, while the carbons of the Cp* moiety in the rhodium(III) (**3.5 & 3.8**) and iridium(III) (**3.6 & 3.9**) metallodendrimers, appear at about ~9.00 ppm. The carbon atoms associated with the PTA moiety in each metallodendrimer (**3.4-3.9**) appear between 49.79 and 72.00 ppm. All the NMR spectroscopy assignments were made using 2D-NMR techniques such as HSQC and COSY whereby similar trends were found for the metallodendrimers as the model cationic mononuclear complexes, except for the presence of the core protons.

In the $^{31}P\{^1H\}$-NMR spectrum of each metallodendrimer (**3.4-3.9**), a septet is observed at -144.0 ppm which corresponds to the hexafluorophosphate counterion. The spectra of the ruthenium(II) (**3.4 & 3.7**) and iridium(III) (**3.6 & 3.9**) complexes displays a singlet at about -30.0 and -79.1 ppm, respectively, while a doublet is observed in the spectra of the rhodium(III) (**3.5 & 3.8**) complexes at about -44.0 ppm. These resonances correspond to the coupling of the metal centre to the PTA moiety, and further attest to only one phosphorous containing compound.

3.2.2.2 Infrared (IR) spectroscopy

In the IR spectra of each cationic metallodendrimer (**3.4-3.9**), there has been a shift of the imine absorption band to a lower frequency compared to that of the metal-free ligands (**2.3 & 2.5**), which have imine absorption bands at 1639 cm^{-1} which confirms the coordination of the metal centres to the dendritic ligands in a *C,N*-bidentate fashion.

Table 3.2: IR spectroscopy data for the cationic metallodendrimers (**3.4.-3.9**) versus the data obtained for the corresponding neutral analogues (**2.13-2.15**) and (**2.19-2.21**).

Complex	Cationic complex (cm^{-1})	Neutral complex (cm^{-1})
Ru(II)-G1	1600 **(3.4)**	1604 **(2.13)**
Rh(III)-G1	1613 **(3.5)**	1609 **(2.14)**
Ir(III)-G1	1604 **(3.6)**	1602 **(2.15)**
Ru(II)-G2	1603 **(3.7)**	1602 **(2.19)**
Rh(III)-G2	1609 **(3.8)**	1610 **(2.20)**
Ir(III)-G2	1602 **(3.9)**	1600 **(2.21)**

As with the model mononuclear complexes, the IR imine absorption band of each cationic complex corresponds to the analogous neutral complexes. (**Table 3.2**)

3.2.2.3 High Resolution Electrospray Ionization Mass Spectrometry (ESI-MS)

All six metallodendrimers (**3.4-3.9**) show base peaks without several or all of the PF_6 counterions and PTA moieties. The ruthenium G1 metallodendrimer (**3.4**) shows a base peak corresponding to the loss of the PF_6 counterions as well as forming an adduct with water. The rest of the metallodendrimers (**3.5-3.9**) exhibit base peaks corresponding to the loss of all or a few of the PF_6 counterions and PTA moiety (**Table 3.3**).

Table 3.3: Mass spectrometry data for the cationic metallodendrimers (**3.4.-3.9**).

Complex	Calculated M (g/mol)	Molecular fragment (*m/z*)	Assignment
3.4	3014.81	626.1612	$[M\text{-}4PF_6\text{+}4H_2O]^{4+}$
3.5	3026.20	533.2226	$[M\text{-}4PF_6\text{-}2PTA]^{4+}$
3.6	3383.44	1391.4447	$[M\text{-}2PF_6\text{-}2PTA]^{2+}$
3.7	6169.85	585.1436	$[M\text{-}8PF_6\text{-}2PTA)]^{8+}$
3.8	6192.63	587.1556	$[M\text{-}8PF_6\text{-}2PTA]^{8+}$
3.9	6907.11	1215.4901	$[M\text{-}4PF_6\text{-}PTA)]^{4+}$

3.3 Reactions with ferrocenyl-pyridine

3.3.1 Synthesis of the cationic heterometallic-ferrocenyl mononuclear complexes 3.10 & 3.11

An additional series of cationic compounds were synthesized by incorporating a ferrocenyl moiety in order to obtain a series of heterometallic complexes. The chloride ligand coordinated to the metal centre was displaced by a ferrocenyl-pyridine nitrogen-donor ligand, making these complexes cationic. The ferrocenyl moiety used was 4-ferrocenyl-pyridine, with the pyridine-nitrogen acting as the nitrogen donor ligand to be coordinated to the rhodium(III) or iridium(III) metal centre. The synthesis used followed the procedure outlined by Imrie *et al.*[11] whereby bromoferrocene was reacted with magnesium, in the presence of 1,2-dibromoethane acting as a catalyst, to form a Grignard reagent.[11] This was then reacted with 4-bromopyridine in the presence of a nickel catalyst (**Scheme 3.4**).[11]

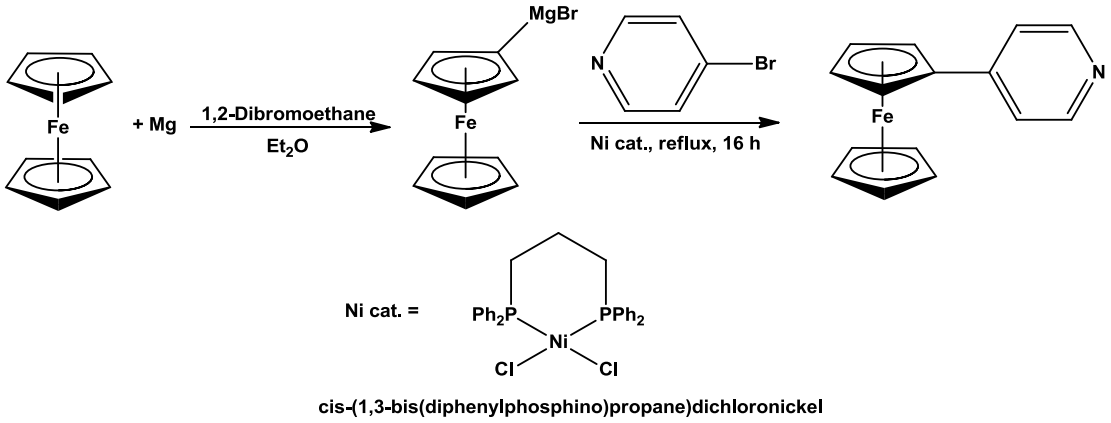

Scheme 3.4: Synthetic procedure for 4-ferrocenyl-pyridine.[11]

The cyclometalation of the naphthaldimine monomeric ligand **2.1** followed the same procedure used throughout this project using only the rhodium(III) and iridium(III)-Cp* dimeric precursors.[19] The ruthenium(II) *p*-cymene analogues were attempted but were obtained as impure solids, with the ^{1}H-NMR spectra exhibiting a mixture of products. This could be attributed to the incomplete cyclometalation occuring. After cyclometalation, the reaction mixture was filtered through Celite followed by the addition of the ferrocenyl-pyridine, which was stirred for a further 30-60 minutes. Sodium hexafluorophosphate was finally added at 0^{o}C in order to replace the chloride counterion with a more stable counterion (**Scheme 3.5**).[20]

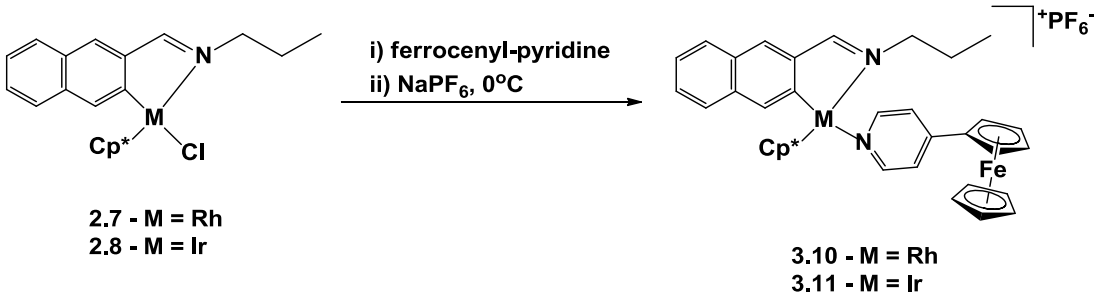

Scheme 3.5: Synthesis of the heterometallic rhodium(III) and iridium(III) *C,N*–chelating mononuclear complexes (**3.10 & 3.11**).

The heterometallic mononuclear complexes (**3.10 & 3.11**) were obtained as dark red solids in moderate yields ranging between 28 and 38%. All the mononuclear complexes are soluble in acetone, methanol, ethanol, DCM and chloroform.

3.3.1.1 ^{1}H-NMR and ^{13}C{^{1}H}-NMR spectroscopy

In the ^{1}H-NMR spectra of each complex (**3.10 & 3.11**), the imine singlet appears downfield between 8.74 and 8.91 ppm. This is an indication that the imine bond is still intact. The ferrocenyl protons on the substituted and unsubstituted Cp rings appear in similar regions, further upfield between 3.98 and 4.89 ppm while the naphthaldimine aromatic protons appear between 7.43-8.47 ppm (**Figure 3.8**).

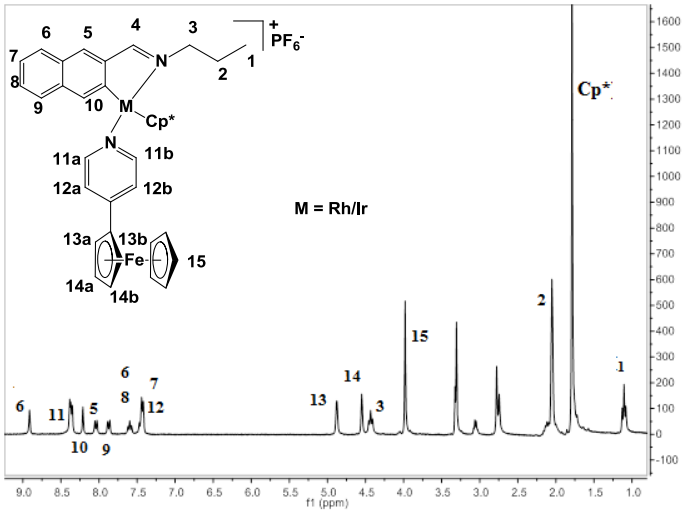

Figure 3.8: Representative ^{1}H-NMR spectrum of the heterometallic rhodium(III) naphthaldimine mononuclear complex (**3.10**).

In the ^{1}H-NMR spectra, a singlet is observed for the protons of the Cp* moiety and a triplet for the –CH_2 group adjacent to the imine nitrogen, at similar resonances found in the neutral (**2.8 & 2.9**) and cationic (**3.2 & 3.3**) analogues. These assignments were made and confirmed using 2D-NMR techniques such as HSQC and COSY. As can be seen in **Figure 3.9**, the COSY of the iridium(III) heterometallic complex (**3.11**) shows the spin-spin coupling between the protons 1 and, as well as 2 and 3 of the propyl chain, coupling between the ferrocenyl protons (protons 13 & 14) and coupling of the aromatic protons to each other.

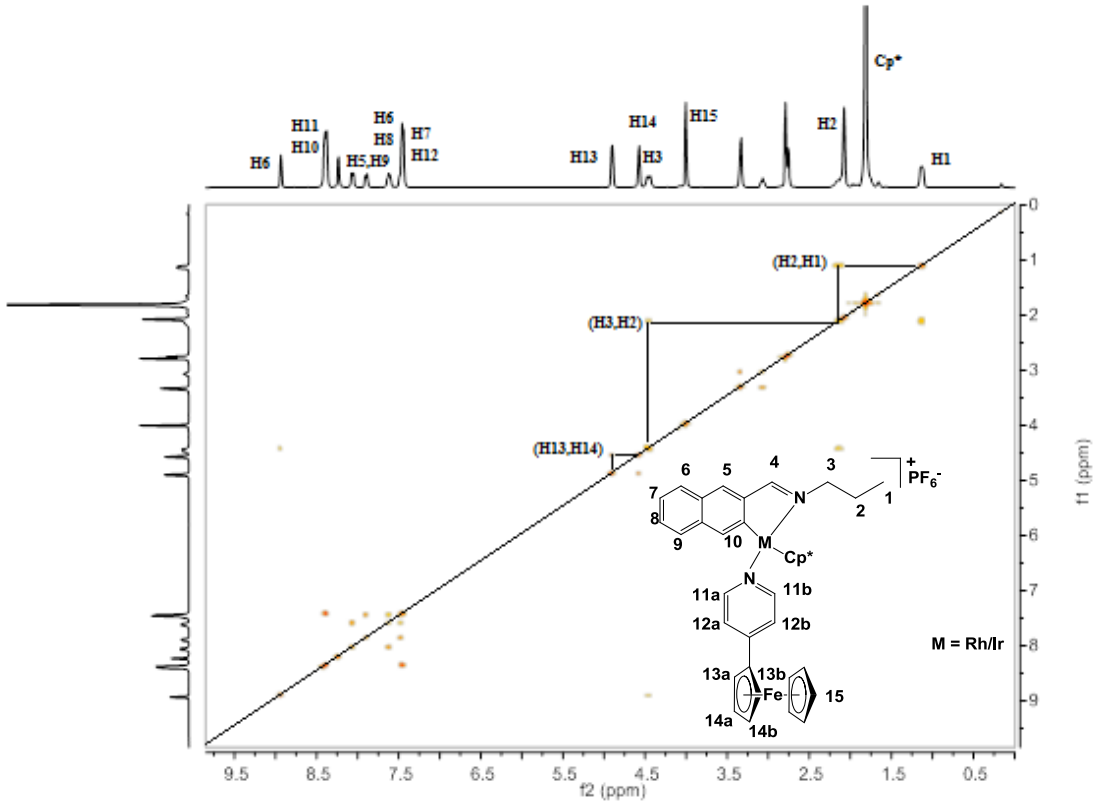

Figure 3.9: Representative COSY spectrum of the heterometallic iridium(III) naphthaldimine mononuclear complex (**3.11**).

The ^{13}C{^{1}H}-NMR spectra display resonances corresponding to the imine carbon peaks downfield at about ~175.0 ppm for each metal complex (**3.10 & 3.11**). The resonances for the aliphatic, aromatic and Cp* moiety carbons appear at similar resonances to that of the neutral (**2.8 & 2.9**) and cationic (**3.2 & 3.3**) analogues. In between these resonances, the ferrocenyl aromatic protons appear between 67.4 and 71.7 ppm.

3.3.1.2 Infrared (IR) spectroscopy

The IR spectra of both complexes (**3.10 & 3.11**) were recorded as KBr pellets and show the presence of imine absorption bands at 1611 cm^{-1}. These values indicate a shift in the imine absorption band from 1640 cm^{-1} for the metal-free ligand (**2.1**) to lower frequencies for each heterometallic complex (**3.10 & 3.11**). This shift is expected as it confirms the coordination of the metal centres to the imine nitrogen due to metal-nitrogen back donation, as previously discussed.

Table 3.4: IR spectroscopy data for the heterometallic complexes (**3.10 & 3.11**) versus the data obtained for the corresponding neutral analogues (**2.8 & 2.9**).

Complex	Cationic complex (cm^{-1})	Neutral complex (cm^{-1})
Rh(III)	1611 **(3.10)**	1610 **(2.8)**
Ir(III)	1611 **(3.11)**	1602 **(2.9)**

As can be seen in **Table 3.4**), the neutral and heterometallic complexes have similar imine absorption band values.

3.3.1.3 Electron Ionization Mass Spectrometry (EI-MS)

The mass spectra of each mononuclear complex (**3.10 & 3.11**) show fragmentation peaks without the hexafluorophosphate counterions and ferrocenyl-pyridine ligand. The rhodium(III) complex (**3.10**) also shows the loss of the Cp*moiety (**Table 3.5**).

Table 3.5: Mass spectrometry data for the heterometallic mononuclear complexes (**3.10** & **3.11**).

Complex	Calculated M (g/mol)	Molecular fragment (*m/z*)	Assignment
3.10	842.49	295.05	$[M\text{-}PF_6\text{-}(Fc\text{-}py)\text{-}Cp^*]^{2+}$
3.11	931.80	519.10	$[M\text{-}PF_6\text{-}(Fc\text{-}py)]^{+}$.

3.3.2 Synthesis of the cationic heterometallic-ferrocenyl G1 and G2 metallodendrimers 3.12-3.15

Once the model mononuclear complexes (**3.10 & 3.11**) had been synthesized, the first- and second-generation metallodendrimers (**3.12-3.15**) were then synthesized to obtain a series of polynuclear-heterometallic complexes. The same reaction protocol was using cyclometalation and chloride displacement was followed as for the mononuclear analogues (**3.1-3.3**) (**Scheme 3.6 & 3.7**).[19]

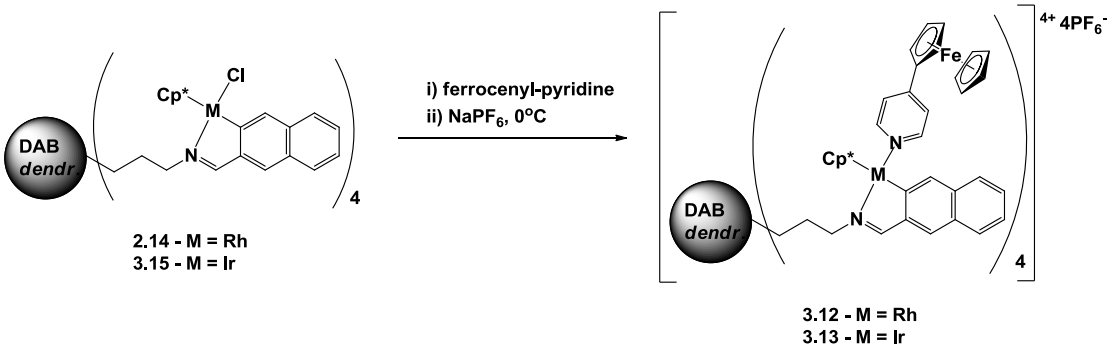

Scheme 3.6: Synthesis of the heterometallic rhodium(III) and iridium(III) *C,N*–chelating G1 naphthaldimine metallodendrimers (**3.12 & 3.13**).

All four poly-heterometallic complexes (**3.12-3.15**) were obtained as red-orange solids in moderate yields between 24 and 51%, and are soluble in acetone, methanol, ethanol, DCM and chloroform.

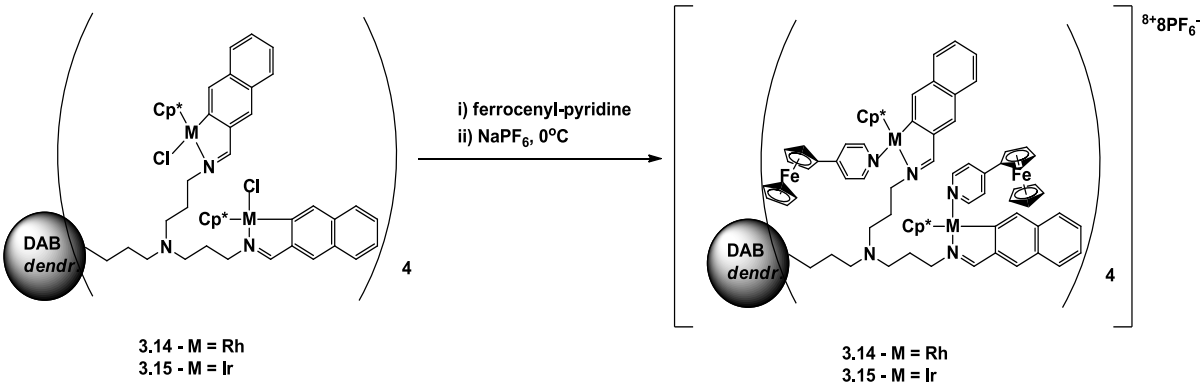

Scheme 3.7: Synthesis of the heterometallic rhodium(III) and iridium(III) *C,N*–chelating G2 naphthaldimine metallodendrimers (**3.14 & 3.15**).

3.3.2.1 ^{1}H-NMR and ^{13}C{^{1}H}-NMR spectroscopy

The resonances observed in the ^{1}H-NMR spectra of the poly-heterometallic complexes appear as broadened signals due to chemical equivalence of the polymeric compounds on the NMR timescale. In the ^{1}H-NMR spectra of the heterometallic metallodendrimers (**3.12-3.15**) the imine resonance appears downfield between 8.49 and 8.74 ppm. This result confirms that the imine bond is still intact (**Figure 3.10**). The naphthaldimine aromatic protons of the metallodendrimers appear in similar ranges downfield between 7.18 and 8.29 ppm, while the ferrocenyl protons for each heterometallic metallodendrimer (**3.12-3.15**) appear between 3.94 and 4.83 ppm.

In the ^{1}H-NMR spectra of the heterometallic metallodendrimers (**3.12-3.15**), a singlet is observed at ~1.70 ppm for the Cp* moiety and a broad singlet between 3.87 and 4.46 ppm for the $–CH_2$ group adjacent to the imine nitrogen, similarly to the model mononuclear complexes (**3.10 & 3.11**). All the NMR spectroscopy assignments were made using 2D-NMR techniques such as HSQC and COSY, whereby the aliphatic protons, including the core protons, showed spin-spin coupling. The same is observed for the aromatic protons and the ferrocenyl moiety.

The ^{13}C{^{1}H}-NMR spectra exhibit imine carbon peaks downfield between 174.96 and 177.18 ppm for each heterometallic first- and second-generation metallodendrimer (**3.12-3.15**). The chemical shifts for the aliphatic carbons appear between 7.91 and 71.9 ppm, while the aromatic carbons appear further downfield between 121.5 and 158.8 ppm. The carbons on the Cp* moiety appear at about ~8.30 ppm. The carbon atoms associated with the ferrocenyl-pyridine moiety appear between 67.8 and 72.0 ppm.

3.3.2.2 Infrared (IR) spectroscopy

It is evident in the IR spectra of each heterometallic complex (**3.12-3.15**) that the imine absorption bands are at lower frequencies compared to the metal-free dendritic ligands (**2.3 & 2.5**) with an imine absorption band at 1639cm^{-1}, which confirms the coordination of the metal centres to the dendritic ligands. (**Table 3.6**)

Table 3.6: IR spectroscopy data for the heterometallic metallodendrimers (**3.12-3.15**) versus the data obtained for the corresponding neutral analogues (**2.14, 2.15, 2.20 & 2.21**).

Complex	Heterometallic complex (cm^{-1})	Neutral complex (cm^{-1})
Rh(III)-G1	1610 **(3.12)**	1609 **(2.14)**
Ir(III)-G1	1610 **(3.13)**	1602 **(2.15)**
Rh(III)-G2	1608 **(3.14)**	1600 **(2.20)**
Ir(III)-G2	1610 **(3.15)**	1600 **(2.21)**

For certain cases, such as the rhodium(III) G1 metallodendrimer (**3.12**), the cationic and neutral complexes exhibit almost identical imine absorption bands.

3.3.2.3 High Resolution Electrospray Ionization Mass Spectrometry (ESI-MS)

All four metallodendrimers (**3.12-3.15**) exhibit the presence of base peaks in the mass spectra. The base peaks present in the mass spectra of complexes **3.12** and **3.15** correspond to the loss of all or several PF_6 counterions as well as the loss of the ferrocenyl-pyridine moiety (**Table 3.9**). The base peaks correspond to complexes **3.13** and **3.14** form adducts with methanol and formic acid, respectively, as well as the loss of the PF_6 counterions (**Table 3.7**).

Table 3.7: Mass spectrometry data for the heterometallic metallodendrimers (**3.12-3.15**).

Complex	Calculated M (g/mol)	Molecular fragment (*m/z*)	Assignment
3.12	3450.06	653.8500	$[M\text{-}4PF_6\text{-}(Fc\text{-}py)]^{4+}$
3.13	3807.30	1058.3701	$[M\text{-}3PF6+MeOH]^{3+}$
3.14	7040.32	782.2932	$[M\text{-}8PF6+HCO_2H]^{8+}$
3.15	7754.82	1058.3744	$[M\text{-}6PF6\text{-}2(Fc\text{-}py)]^{6+}$

3.4 Conclusions

A series of cationic mononuclear and polynuclear dendritic ruthenium(II), rhodium(III) and iridium(III) complexes were obtained through reactivity studies with PTA, which presented a succession of air-stable chelating, bidentate *C,N*-donor ruthenium(II), rhodium(III) and iridium(III) metallodendrimers. These new complexes were fully characterized using

spectroscopic and analytical techniques, i.e. ^{1}H-NMR, ^{13}C{^{1}H}-NMR, IR spectroscopy and mass spectrometry.

Furthermore a series of cationic heterometallic complexes were also succesfully synthesized by incorporating a ferrocenyl-pyridine moeity. Only the rhodium(III) and iridium(III) analogues were synthesized for this series of compounds. This was the case as cyclometalation involves the intramolecular C-H activation via a process involving attack of an electrophilic metal centre on the C-H bond of the desired ligand, in this case the naphthaldimine ligand.[21] Therefore the arene ligand attached to the ruthenium centre needs to be less π–electron donating, while the ligand needs to be more electron rich, in order for successful cyclometalation to occur. It has been shown previously that [Ru(HMB)Cl_2]$_2$ lends itself more to cyclometalation than [Ru(*p*-cymene)Cl_2]$_2$ as the benzene ring is a weaker π-electron donor, compared to the *p*-cymene ligand.[22, 23] However the rhodium(III) and iridium(III)-ferrocenyl heterometallic complexes were synthesized successfully and fully characterized using spectroscopic and analytical techniques.

3.5 References

1. C. G. Hartinger and P. J. Dyson, *Chem. Soc. Rev.*, 2009, **38**, 391-401.

2. C. Scolaro, A. Bergamo, L. Brescacin, R. Delfino, M. Cocchietto, G. Laurenczy, T. J. Geldbach, G. Sava and P. J. Dyson, *J. Med. Chem.*, 2005, **48**, 4161-4171.

3. C. Scolaro, T. J. Geldbach, S. Rochat, A. Dorcier, C. Gossens, A. Bergamo, M. Cocchietto, I. Tavernelli, G. Sava, U. Rothlisberger and P. J. Dyson, *Organometallics*, 2006, **25**, 756-765.

4. P. J. Dyson, *Chimia*, 2007, **61**, 698-703.

5. A. K. Renfrew, A. D. Phillips, E. Tapavicza, R. Scopelliti, U. Rothlisberger and P. J. Dyson, *Organometallics*, 2009, **28**, 5061-5071.

6. C. S. Allardyce, P. J. Dyson, D. J. Ellis and S. L. Heath, *Chem. Commun.*, 2001, **15**, 1396-1397.

7. P. Govender, L. C. Sudding, C. M. Clavel, P. J. Dyson, B. Therrien and G. S. Smith, *Dalton Trans.*, 2013, **42**, 1267-1277.

8. S. Chatterjee, S. Kundu, A. Bhattacharyya, C. G. Hartinger and P. J. Dyson, *J. Biol. Inorg. Chem.*, 2008, **13**, 1149-1155.

9. K. J. Kilpin, C. M. Clavel, F. Edafe and P. J. Dyson, *Organometallics*, 2012, **31**, 7031-7039.

10. B. Wu, M. S. Ong, M. Groessl, Z. Adhireksan, C. G. Hartinger, P. J. Dyson and D. C.A., *Chem. Eur. J.*, 2011, **17**, 3562-3566.

11. J. Rajput, J. R. Moss, A. T. Hutton, D. T. Hendricks, C. E. Arendse and C. Imrie, *J. Organomet. Chem.*, 2004, **689**, 1553-1568.

12. A. Esparza-Ruiz, C. Herrmann, J. Chen, B. O. Patrick, E. Polishchuk and C. Orvig, *Inorg. Chim. Acta*, 2012, **393**, 276-283.

13. C. Biot, W. Daher, C. M. Ndiaye, P. Melnyk, B. Pradines, N. Chavain, A. Pellet, L. Fraisse, L. Pelinski, C. Jarry, J. Brocard, J. Khalife, I. Forfar-Bares and D. Dive, *J. Med. Chem.*, 2006, **49**, 4707-4714.

14. C. Biot, G. Glorian, L. A. Maciejewski and J. S. Brocard, *J. Med. Chem.*, 1997, **40**, 3715-3718.

15. E. W. Neuse, M. G. Meirim and N. F. Blom, *Organometallics*, 1988, **7**, 2562-2565.

16. S. Top, A. Vessieres, C. Cabestaing, I. Laios, G. Leclercq, C. Provot and G. Jaouen, *J. Organomet. Chem.*, 2001, **637**, 500-506.

17. P. Pigeon, S. Top, A. Vessières, M. Huchè, M. Görmen, M. E. Arbi, M. A. Plamont, M. J. McGlinchey and G. Jaouen, *New J. Chem.*, 2011, **35**, 2212-2218.

18. P. Govender, A. K. Renfrew, C. M. Clavel, P. J. Dyson, B. Therrien and G. S. Smith, *Dalton Trans.*, 2011, **40**, 1158-1167.

19. D. L. Davies, O. Al-Duaij, J. Fawcett, M. Giardiello, S. T. Hilton and D. R. Russell, *Dalton Trans.*, 2003, 4132-4138.

20. Z. Liu, L. Salassa, A. Habtemariam, A. M. Pizarro, G. J. Clarkson and P. J. Sadler, *Inorg. Chem.*, 2011, **50**, 5777-5783.

21. H. C. L. Abbenhuis, M. Pfeffer, J. P. Sutter, A. Decian, J. Fischer, J. H.L. and J. H. Nelson, *Organometallics*, 1993, **12**, 4464-4472.

22. H. C. Brown and J. D. Brady, *J. Am. Chem. Soc.*, 1952, **74**, 3570-3582.

23. S. P. Nolan, K. L. Martin, E. D. Stevens and P. J. Fagan, *Organometallics*, 1992, **11**, 3947-3953.

Chapter 4: *In Vitro* Antitumour Evaluation of Multinuclear Ruthenium(II), Rhodium(III)and Iridium(III) Metallodendrimers

4.1 Introduction

Ruthenium-based compounds currently in clinical trials are NAMI-A and KP1019 (**Figure 4.1**).[1, 2] It is proposed that ruthenium is more active in the +2 oxidation state and it is understood that ruthenium(III) is reduced to ruthenium(II) *in vivo*.[2] Therefore there has been a shift in focus from ruthenium(III) to ruthenium(II)-arene compounds, with the π-coordinated arene-rings stabilizing ruthenium in its +2 oxidation state.

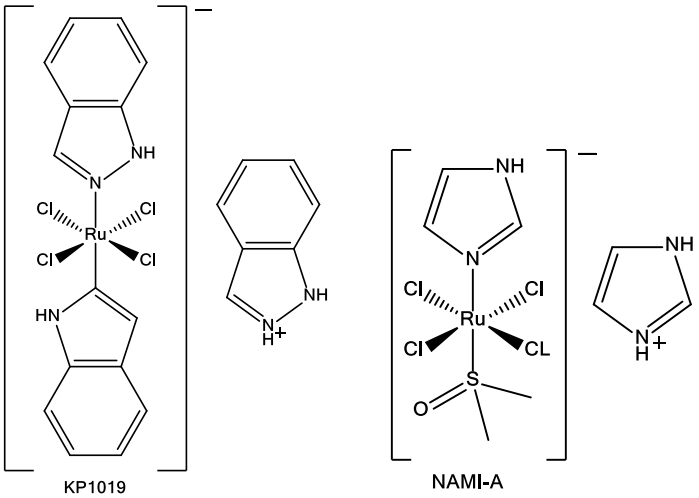

Figure 4.1: Structure of ruthenium(III) anti-tumour drugs KP1019 and NAMI-A.[3]

The ruthenium-arene unit has desirable amphiphilic properties such as the hydrophobic nature of the arene ligand with the hydrophilic nature of the ruthenium metal centre. The halide ligand is very labile and undergoes hydrolysis in an aqueous environment.[4] It has also been proposed that ruthenium(II)-arene complexes undergo aquation *in vivo* leading to reactive cationic species (**Figure 4.2**).[5] Aquation is believed to be the key aspect in the biological activity of certain ruthenium-arene and cyclometalated complexes as it has been proposed that the aquated cationic complex could bind covalently to DNA acting as DNA binding agents or DNA-intercalators of the planar moiety into the DNA double helix. [4]

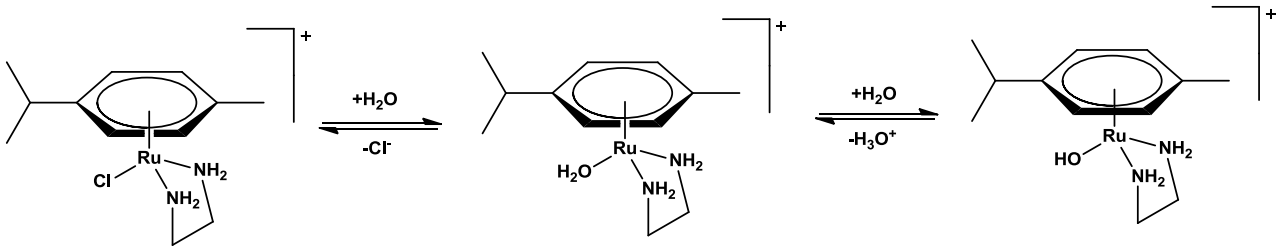

Figure 4.2: Schematic of the proposed aquation that occurs *in vivo*.[5]

There are only a handful of examples of rhodium(III) and iridium(III) complexes showing promising anticancer activity. Sadler *et al*.[6] synthesized a series of mononuclear cyclometalated iridium complexes and evaluated their cytotoxicity against the A2780 ovarian cancer cell line.[6] The complexes (**Figure 4.3**) exhibited IC_{50} values of 2.14 ± 0.50μM and 0.70 ± 0.04μM, respectively, compared to cisplatin with an IC_{50} value of 1.19 ± 0.12μM.[6, 7] They proposed, besides the possibility of DNA intercalation, the presence of the *C,N*-chelating ligand switches on biological activity.[6]

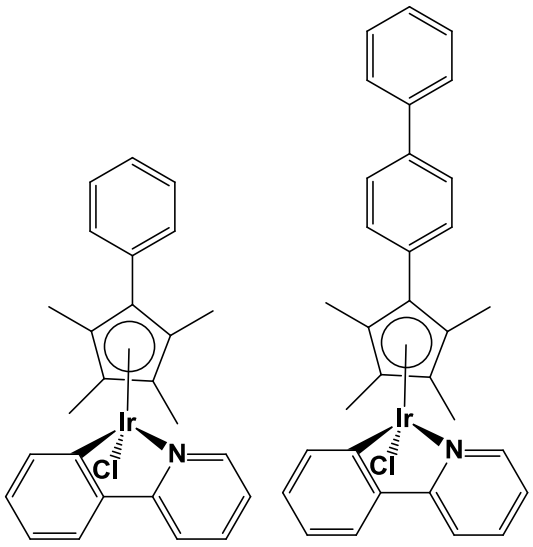

Figure 4.3: Iridium cyclometalated complexes showing good *in vitro* activity.[6]

Ruthenium RAPTA-type compounds show *in vivo* anticancer activity and rhodium derivatives have also been synthesized.[8, 9] The rhodium analogues showed comparable *in vitro* activity to the related ruthenium(II) compounds, against the T47D breast carcinoma, A549 lung carcinoma and HT29 colon carcinoma cell lines.[10] Therefore there is promising evidence that rhodium and iridium complexes can be used in biological applications, such as anticancer treatment.[6, 7]

Multinuclearity is said to improve biological recognition and cytotoxicity of potential chemotherapeutic drugs.[11] There are only a handful of ruthenium(II) biometallodendrimers, and even fewer containing rhodium(III) and iridium(III) that have been synthesized and undergone anticancer *in vitro* and *in vivo* studies.[12]

Jansen *et al*.[13] synthesized the first tetranuclear platinum metallodendrimer by incorporating the cisplatin moiety onto the PPI dendritic scaffold (**Figure 4.4**).[13] The tetranuclear complex showed moderate *in vitro* activity with IC_{50} values ranging from 9-12 μM against a range of mouse leukaemia and human tumour cell lines.[13] The cytotoxicity of the complex can be attributed to the charge and the polynuclearity of the metallodendrimer.[11, 13]

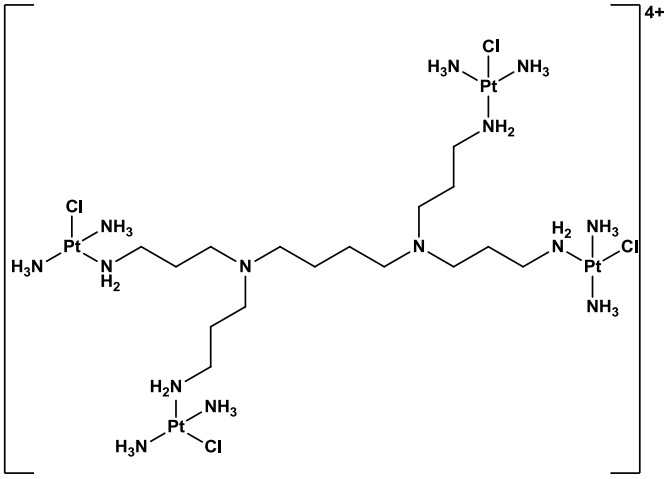

Figure 4.4: Tetranuclear PPI platinum metallodendrimer showing moderate *in vitro* activity.[13]

A supramolecular assembly with ruthenium(II) arene corners linked by polypyridyl spacers were synthesized. Their anticancer activity was evaluated against human ovarian cancer cells and the complexes displayed activities similar to cisplatin (**Figure 4.5**) .[14, 15]

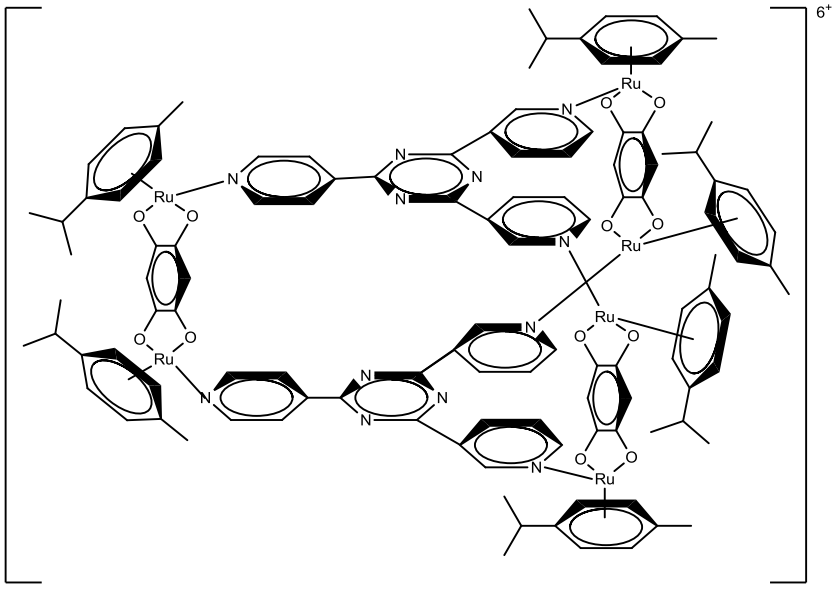

Figure 4.5: Ruthenium-arene molecular assembly tested for anti-cancer activity.[14]

Multinuclearity[13] has shown to improve cytotoxicity of biorganometallic complexes, as well as the incorporation of ruthenium(II)-arene[16, 17] and cyclometalated[6, 7, 18-20] moieties. Therefore this study focusses on combining cyclometalated ruthenium(II)-arene, rhodium(III) and iridium(III) complexes with multinuclear scaffolds, namely metallodendrimers.

This chapter describes the *in vitro* biological activity of the synthesized ligands (**2.1-2.6**), as well as the ruthenium(II), rhodium(III) and iridium(III) neutral (**2.7-2.24**) and cationic (**3.1-3.9**) complexes (**Figure 4.6**). These complexes were tested against the cisplatin-sensitive (A2780) and cisplatin-resistant (A2780*cisR*) human ovarian cancer cell lines, as well as the non-tumorous HEK or KMST-6 cell line.

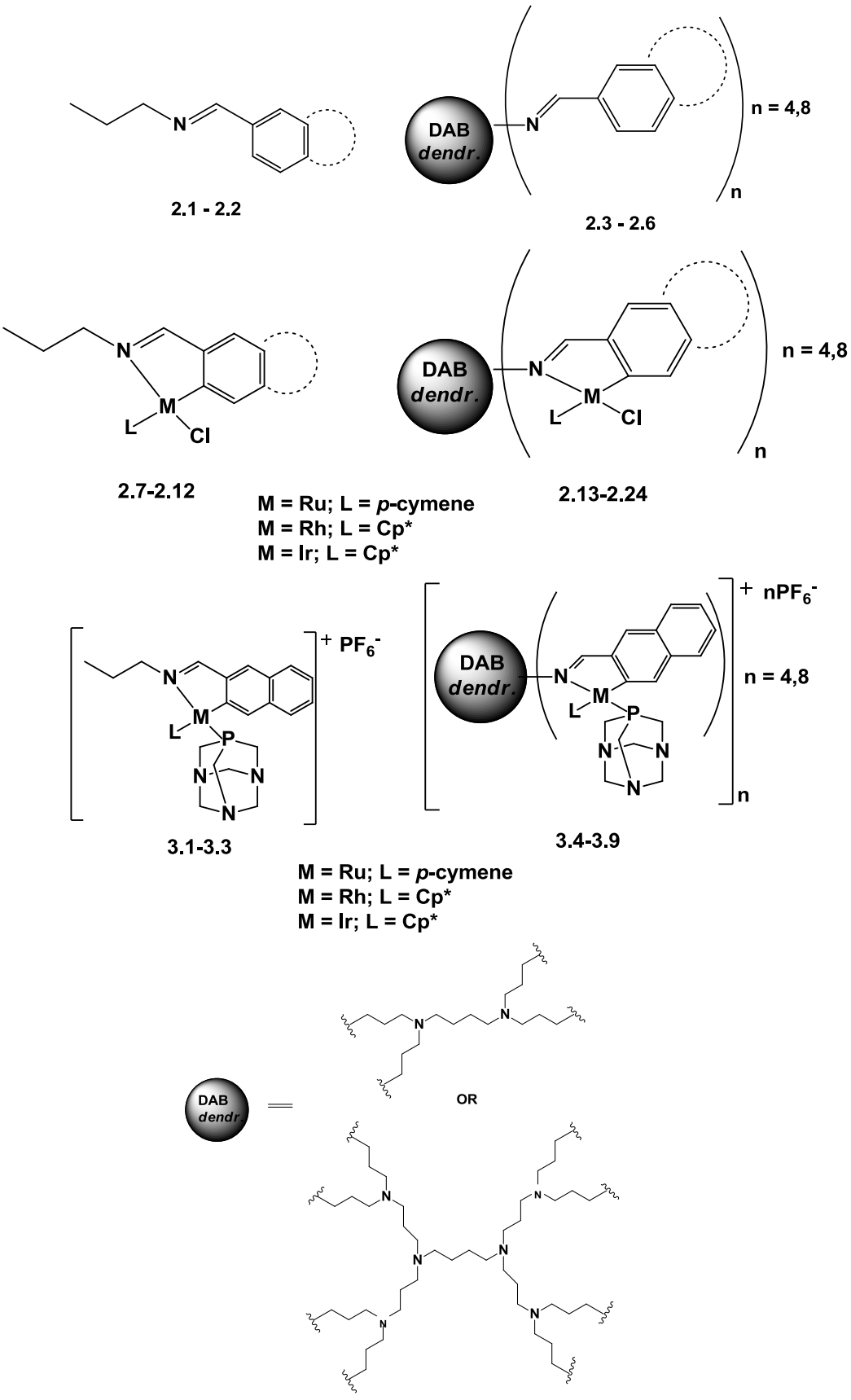

Figure 4.6: Monomeric and dendritic ligands **2.1-2.6**, neutral **2.7-2.24** and cationic **3.1-3.9** ruthenium(II), rhodium(III) and iridium(III) complexes which were tested for anticancer activity.

4.2 Ligands versus complexes

The ligands and complexes were compared following their biological evaluation in the cisplatin-sensitive and cisplatin-resistant human ovarian cancer cell line, as well as the non-cancerous KMST-6 human skin tissue or HEK human embryonic kidney cell line. The naphthaldimine and benzaldimine ligands were tested against the respective cells (**Table 4.1 & Figure 4.7**). The ligands showed moderate activity with no specificity towards the cancerous versus non-cancerous cells. This indicates that these will be toxic as anticancer agents, whereas the metal complexes show more specificity towards cancerous versus non-cancerous cells. Therefore the incorporation of metal centres into these organic frameworks may increase the specificity and antiproliferative activity.

Table 4.1: IC_{50} values of the naphthaldimine & benzaldimine ligands (**2.1-2.6**).

Compound ref.	IC50 A2780 (µM)	IC50 A2780cisR (µM)	IC50 HEK (µM)
2.1	68.4±1.8	79.3	78.8±1.7
2.2	18.0±2.0	10.5	18.4±2.4
2.3	5.5±0.5	NA	4.2±0.5
2.4	60.0±4.4	40.0	75.4±3.4
2.5	17.3±11.3	NA	11.7±8.9
2.6	30.5±0.5	5.80	14.3±4.1

Figure 4.7: Graph illustrating the IC_{50} values of the naphthaldimine & benzaldimine ligands (**2.1-2.6**).

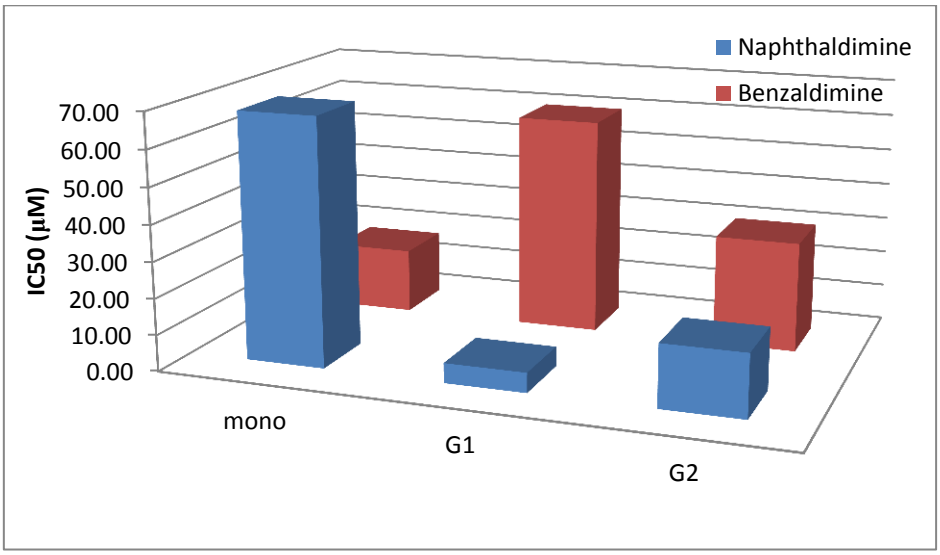

4.3 Influence of the number of metal centres (n = 4,8)

There is sufficient evidence that ruthenium, rhodium and iridium complexes have shown potential *in vitro* anticancer activity.[12] Therefore as a preliminary study, the synthesized complexes were also tested *in vitro* to see whether they do show potential anticancer activity. Table **4.1** shows the IC_{50} values for the mononuclear (**2.7-2.9**), first- (**2.13-2.15**) and second-generation (**2.19-2.21**) naphthaldimine complexes. Comparison of their biological activity based on the number of metal moieties shows that with an increase in generation size there is an increase in cytotoxicity in most cases.

Table 4.2: IC_{50} values of the neutral naphthaldimine complexes, comparing size and cytotoxicity.

Naphthaldimine compound	No. of metals	A2780	A2780cisR	HEK
Ruthenium(II)		(IC_{50} μM)	(IC_{50} μM)	(IC_{50} μM)
2.7	1	9.9 ± 1.3	8.2 ± 2.5	NA
2.13	4	19.6 ± 1.2	18.97 ± 1.3	NA
2.19	8	8.1 ± 0.8	<1.56	5.2 ± 1.1
Rhodium(III)				
2.8	1	13.4 ± 2.4	19.0 ± 1.2	52.9 ± 67.9
2.14	4	104.4 ± 15.0	105.4 ± 8.2	126.5 ± 178.9
2.20	8	8.0 ± 0.5	3.11	4.5 ± 0.5
Iridium(III)				
2.9	1	20.1 ± 13.6	19.0 ± 8.5	72.4 ± 91.1
2.15	4	29.7 ± 0.1	28.1 ± 2.0	NA
2.21	8	13.7 ± 0.1	3.0	5.0 ± 1.2
cisplatin	1	1.5	25	

The second-generation complexes (**2.19-2.21**) with 8 metal centres each, show the best activity with IC_{50} values ranging between 8.0 and 13.7 μM, compared to their analogous mononuclear and first-generation complexes (**Table 4.2**). An unusual trend is noticed when comparing the mononuclear (**2.7-2.9**) and first-generation (**2.13-2.15**) complexes, there is a decrease in activity on going from the mononuclear complex to the first-generation complex. Without certainty, it may be attributed to back-folding of some of the repeat units in the first-

generation metallodendrimers, compared to the mononuclear and second-generation complexes due to greater steric bulk at the periphery which reduces 'back folding'.[21] Therefore it can be proposed that the metal centres situated on the periphery of the first-generation metallodendrimers are not able to perform their respective biological activity due to this supposed 'back folding'. Further work needs to be done, for example synthesizing and testing third- and fourth-generation metallodendrimers, in order to confirm this hypothesis.

However, the second generation complexes, with the most metal centres (n=8), still show the best activity therefore confirming that with an increase in size and number of metals, there is an increase in cytotoxicity, which correlates with previously published work.[22]

Another key feature observed is that the mononuclear and first-generation complexes show selectivity towards cancer cells over healthy cells, having lower IC_{50} values against the cancerous cells versus the non-cancerous HEK cells. However further biological tests would need to be performed in order to confirm this hypothesis as the error values obtained for the first-generation complexes are very large. This is not the case for the second-generation complexes, but the complexes do seem to be more selective for the cisplatin-resistant cell line versus the healthy HEK cells (**Table 4.2**).

The rhodium(III) (**2.20**) and ruthenium(II) (**2.19**) second-generation metallodendrimers showed the best activity with IC_{50} values of 8.0 and 8.1 μM, respectively (**Table 4.2**). These values are approximately 5 times lower when compared to cisplatin (1.5μM) against the cisplatin-sensitive human ovarian cancer cell line, A2780. When comparing the IC_{50} values of the second-generation complexes (**2.19-2.21**) against the cisplatin-resistant ovarian cancer cell line, A2780*cisR*, the second generation complexes are far more active than cisplatin (25μM) with IC_{50} values as low as 1.56-3.00 μM. This could be attributed to these new complexes acting via a different mechanism of action compared to cisplatin and are therefore able to overcome cisplatin-resistant mechanisms.

4.4 Influence of the metal centre – ruthenium(II) vs. rhodium(III) vs. iridium(III)

The ruthenium centre has a *p*-cymene arene ligand, whereas the rhodium(III) and iridium(III) metal centres have a pentamethylcyclopentadienyl ligand. Bearing this is mind the ruthenium(II) (**2.19**) and rhodium(III) (**2.20**) second-generation complexes show comparable activity with the lowest IC_{50} values (**Table 4.2 & Figure 4.8**). When comparing the

rhodium(III) and iridium(III) complexes, in general, the rhodium(III) complexes show greater activity, with the exception of the rhodium(III) first-generation (**2.14**) complex (**Table 4.2 & Figure 4.8**).

Figure 4.8: Graph illustrating the effect of the metal centre on the cytotoxicity of each neutral naphthaldimine complex **2.7-2.9**, **2.13-2.15 & 2.19-2.21**.

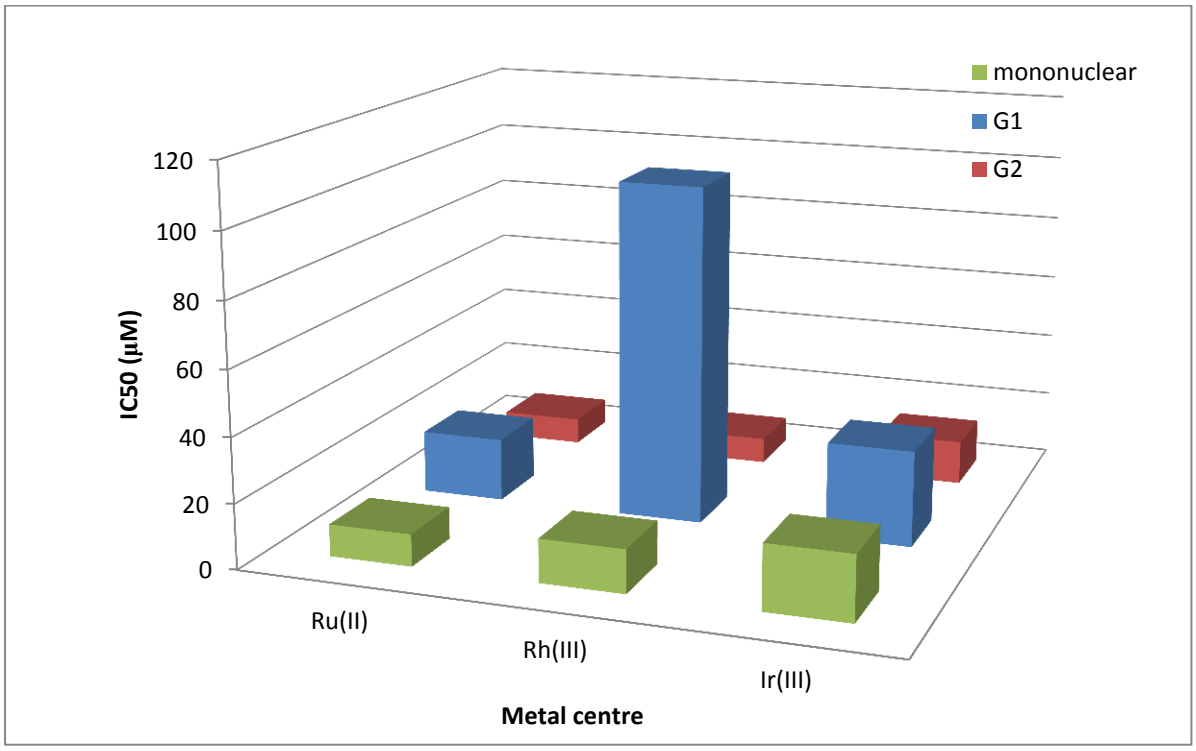

4.5 Influence of the naphthaldimine versus the benzaldimine *C,N*-ligand

The mononuclear (**2.10-2.12**), first- (**2.16-2.18**) and second- (**2.22-2.24**) generation benzaldimine complexes were compared following their biological evaluation in the cisplatin-resistant human ovarian cancer cell line and the non-cancerous KMST-6 human skin tissue cell line. This was due to contamination issues associated with the cisplatin-sensitive cell line, which could not be grown in order for accurate testing to occur.

The ruthenium(II) benzaldimine complexes were the only complexes to show that an increase in generation size and number of metals lead to an increase in activity, indicated by a decrease in IC_{50} value from 22.3 to 15.5 µM (**Table 4.3 & Figure 4.9**). The rhodium(III) and iridium(III) benzaldimine series showed the opposite effect, whereby the biological activity decreased with an increase in size and number of metal atoms on the complex.

Another key feature observed is that the benzaldimine complexes show selectivity towards cancerous cells versus healthy cells, exhibiting high IC_{50} values against the non-cancerous cells (KMST-6) with values as high as 130.00 μM (**Table 4.3**).

Table 4.3: IC_{50} values of the neutral benzaldimine series of complexes (**2.10-2.12, 2.16-2.18 & 2.22-2.24**).

Benzaldimine compound	No of metals	A2780cisR	KMST-6
Ruthenium(II)		(IC_{50} μM)	(IC_{50} μM)
2.10	1	22.3 ± 1.0	62.9 ± 41.2
2.16	4	17.5 ± 6.0	28.5 ± 0.8
2.22	8	15.5 ± 1.2	54.0 ± 1.2
Rhodium(III)			
2.11	1	16.5 ± 3.5	58.1 ± 81.59
2.17	4	76.0 ± 12.0	110.0 ± 0.3
2.23	8	30.0 ± 2.0	130.5 ± 4.00
Iridium(III)			
2.12	1	8.5 ± 0.8	41.5 ± 57.3
2.18	4	67.0 ± 1.6	112.0 ± 1.3
2.24	8	18.5 ± 0.45	96.0 ± 0.8

Although the ruthenium(II) benzaldimine complexes showed an increase in activity with an increase in size, the second-generation ruthenium(II) metallodendrimer (**2.22**) still did not show the best activity. The iridium(III) mononuclear complex (**2.12**) showed the best antiproliferative activity within the benzaldimine series with an IC_{50} value of 8.5 μM (**Table 4.3 & Figure 4.9**).

Figure 4.9: Graph illustrating the effect of the Schiff base ligand on the cytotoxicity of each neutral complex.

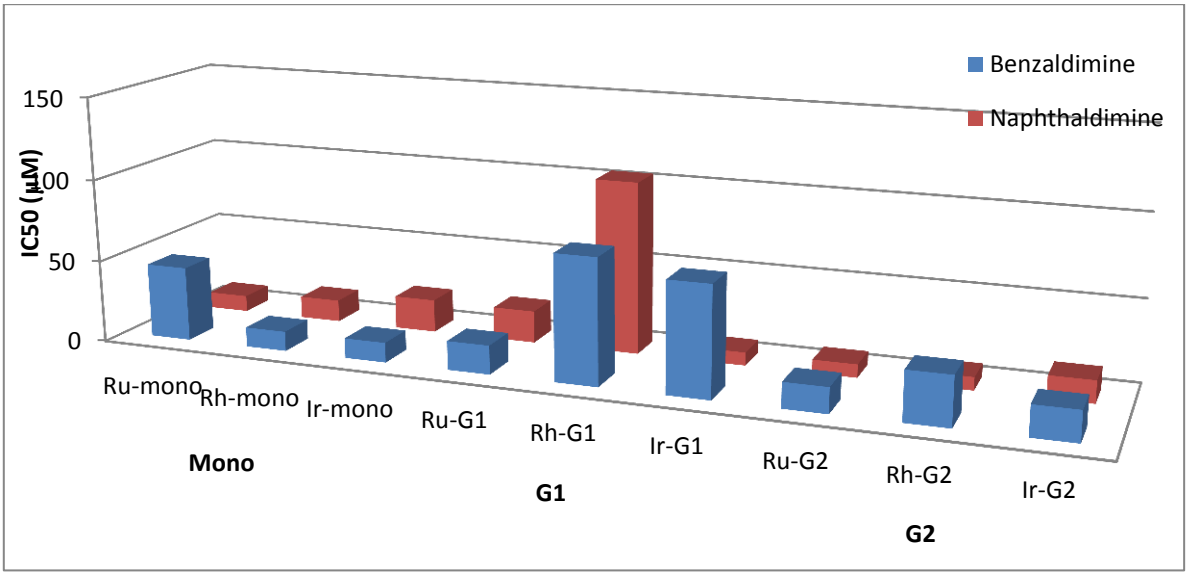

When comparing the activity of the neutral naphthaldimine versus the benzaldimine complexes, the activities of the mononuclear and first-generation complexes are comparable. The naphthaldimine second-generation complexes show better activity versus the second-generation benzaldimine complexes (**Table 4.3 & Graph 4.9**). The naphthaldimine series also shows a direct correlation between size and cytotoxicity, whereas the activities of the benzaldimine complexes do not show any obvious trend (**Table 4.3**).

4.6 Influence of the charge – neutral versus cationic complexes

There is precedence in the literature that cationic complexes[22] and complexes containing PTA[8, 9], such as the RAPTA type complexes, show improved cytotoxicity. This is ascribed to the fact that PTA has shown to enhance the water solubility of organometallic complexes. As can be seen in **Table 4.4** there is a direct correlation between size of the metallodendrimer, number of metal atoms and cytotoxicity. Going from the mononuclear complexes (**3.1-3.3**) to the first- (**3.4-3.6**) and then second-generation (**3.7-3.9**) complexes there is an increase in activity. The only exception being the first-generation rhodium(III) complex (**3.5**) which shows a decrease in activity going from the mononuclear (**3.2**) to the first-generation (**3.5**) complex, a similar trend observed for the neutral complexes.

Table 4.4: IC_{50} values of the cationic naphthaldimine complexes comparing charge and cytotoxicity.

Naphthaldimine compound	No of metals	A2780	A2780cisR	HEK
Ruthenium(II)		(IC_{50} μM)	(IC_{50} μM)	(IC_{50} μM)
3.1	1	27.7 ± 0.6	NA	10.3 ± 1.1
3.4	4	4.03 ± 1.13	5.48	5.00 ± 1.2
3.7	8	1.35 ± 0.14	2.34	4.2 ± 0.5
Rhodium(III)				
3.2	1	1.52 ± 0.05	1.49 ± 0.03	75.4 ± 3.4
3.5	4	9.26 ± 0.72	4.90	18.4 ± 2.4
3.8	8	2.10 ± 0.09	1.78 ± 0.56	4.5 ± 0.5
Iridium(III)				
3.3	1	28.8 ± 2.2	45.6	14.3 ± 4.1
3.6	4	3.59 ± 0.25	3.83	78.8 ± 1.7
3.9	8	2.75 ± 0.01	1.61 ± 0.02	5.2 ± 1.1

All three second-generation complexes (**3.7-3.9**) with 8 metal centres display the best cytotoxicity among the PTA-derivatives with IC_{50} values comparable to cisplatin, ranging between 1.35-2.75 μM. The first-generation complexes exhibited values of about ~5.00 μM while the mononuclear complexes varied from ~28.00 μM, with the exception of the rhodium(III) mononuclear cationic complex (**3.2**).

Figure 4.10: IC_{50} values of the neutral versus cationic naphthaldimine series of complexes.

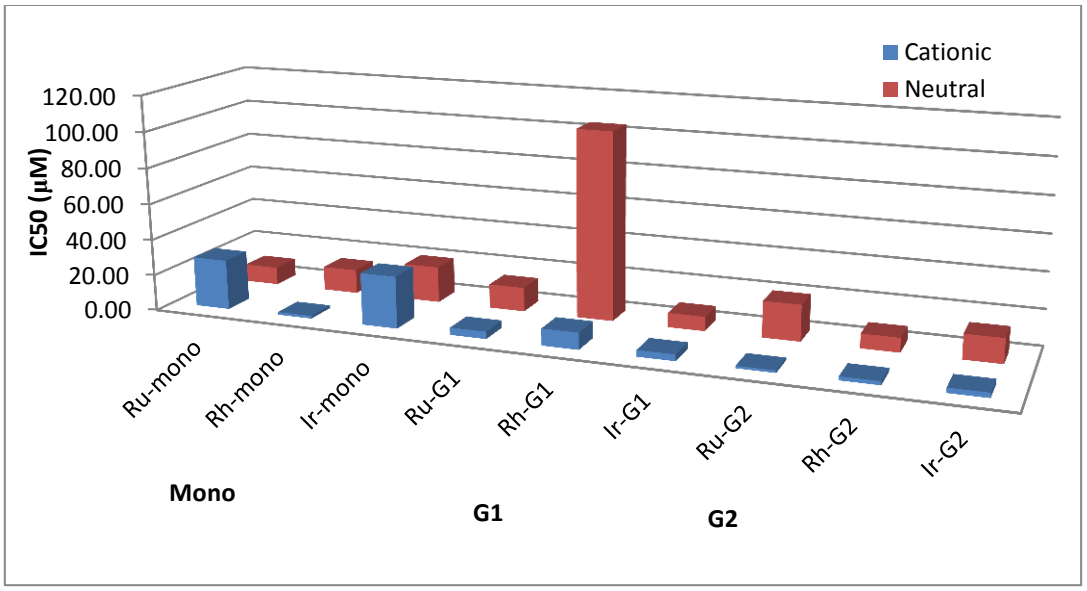

The IC_{50} values of the neutral ruthenium(II), rhodium(III) and iridium(III) complexes were compared to the cationic PTA-derivatives (**Table 4.4 & Figure 4.10**). In general, all the cationic complexes (**3.1-3.9**) show better *in vitro* activity compared to their neutral analogues. For the second-generation cationic complexes there has been between a 4-10 fold increase in activity compared to the neutral complexes. This correlates with studies that state that the presence of a charge on a molecule can increase cytotoxicity, either by interaction with negatively charged DNA backbone or an increase in macromolecular uptake.[10,11,14]

4.7 Conclusions

Following the synthesis of a series of new neutral and cationic dendritic ruthenium(II), rhodium(III) and iridium(III) multinuclear complexes based on a naphthaldimine and benzaldimine Schiff base ligand (**2.7-2.24 & 3.1-3.9**), their cytotoxicities against the cisplatin sensitive A2780 and cisplatin resistant A2780cisR human ovarian cancer cell lines, as well as the non-cancerous HEK and KMST-6 calls, were evaluated.

A ruthenium(II), second-generation cationic cyclometalated *C,N*-chelating bidentate naphthaldimine octanuclear complex **3.7** showed the best antiproliferative activity with an IC_{50} of 1.35±0.14 µM, with the rhodium(III) analogue showing comparable activity.

All the naphthaldimine complexes, neutral and cationic, showed better activity against the cisplatin resistant A2780cisR cell line, when compared to cisplatin. This was the case for all complexes except the cationic ruthenium(II) mononuclear and neutral rhodium first-generation complexes. This is a promising result as it indicates that these complexes could act via a different mechanism of action to cisplatin and therefore overcome cisplatin-resistant mechanisms.

The cationic naphthaldimine series of complexes showed greater activity than the neutral naphthaldimine series. This is expected as an increase in charge could allow for better uptake of the anticancer drug, as well as interact with molecules within the cell, facilitating in its biological anticancer activity.

The naphthaldimine complexes show better and expected results versus the benzaldimine series, which could be due to the extended aromatic moiety in the naphthaldimine complexes which could play some sort of role in the anti-cancer activity of these complexes.

In general the *in vitro* biological studies that were performed show preliminary results which need to be taken further in order to determine the full potential of these complexes as anticancer agents. Studies such as DNA-binding studies could be performed in order to determine the target of these complexes and whether they function via a different mode of action to cisplatin.

4.8 References

1. C. G. Hartinger, S. Zorbas-Selfried, M. A. Jakupec, B. Kynast, H. Zorbas and B. K. Keppler, *J. Inorg. Biochem.*, 2006, **100**, 891-904.

2. M. J. Clarke, S. Bitler, D. Rennert, B. M. and A. D. Kelman, *J. Inorg. Biochem.*, 1980, **12**, 79-87.

3. B. Therrien, W. H. Ang, F. Cherioux, L. Vieille-Petit, L. Juillerat-Jeanneret, G. Suss-Fink and P. J. Dyson, *J. Cluster Sci.*, 2007, **18**, 741-752.

4. R. E. Morris, R. E. Aird, P. Del Socorro Murdoch, H. Chen, J. Cummings, N. D. Hughes, S. Parsons, A. Parkin, G. Boyd, D. I. Jodrell and P. J. Sadler, *J. Med. Chem.*, 2001, **44**, 3616-3621.

5. G. L. Edwards, D. S. Black, G. B. Deacon and L. P. G. Wakelin, *Can. J. Chem.*, 2005, **83**, 980-989.

6. Z. Liu, A. Habtemariam, A. M. Pizarro, G. J. Clarkson and P. J. Sadler, *Organometallics*, 2011, **30**, 4702-4710.

7. Z. Liu, L. Salassa, A. Habtemariam, A. M. Pizarro, G. J. Clarkson and P. J. Sadler, *J. Inorg. Chem.*, 2011, **50**, 5777-5783.

8. C. Scolaro, A. Bergamo, L. Brescacin, R. Delfino, M. Cocchietto, G. Laurenczy, T. J. Geldbach, G. Sava and P. J. Dyson, *J. Med. Chem.*, 2005, **48**, 4161-4171.

9. S. Chatterjee, S. Kundu, A. Bhattacharyya, C. G. Hartinger and P. J. Dyson, *J. Biol. Inorg. Chem.*, 2008, **13**, 1149-1155.

10. A. Dorcier, W. H. Ang, S. Bolano, L. Gonsalvi, L. Juillerat-Jeannerat, G. Laurenczy, M. Peruzzini, A. D. Phillips, F. Zanobini and P. J. Dyson, *Organometallics*, 2006, **25**, 4090-4096.

11. P. Govender, B. Therrien and G. S. Smith, Eur. J. Inorg. Chem., 2012, **2012**, 2853-2862.

12. R. Payne, P. Govender, B. Therrien, C.M. Clavel, P.J. Dyson and G.S. Smith, J. Organomet. Chem., 2013, 729, 20-27.

13. B. A. Jansen, J. v. d. Zwan, J. Reedijk, H. d. Dulk and J. Brouwer, *Eur. J. Inorg. Chem.*, 1999, **9**, 1429-1433.

14. B. Therrien, G. Suss-Fink, P. Govindaswamy, A. K. Renfrew and P. J. Dyson, *Angew. Chem. Int. Ed.*, 2008, **47**, 3773.

15. J. Mattsson, P. Govindaswamy, A. K. Renfrew, P. J. Dyson, P. Stepnicka, G. Suss-Fink and B. Therrien, *Organometallics*, 2009, **28**, 4350-4357.

16. M. Melchart and P. J. Sadler, *in Bioorganometallics*, Ed. G. Jaouen, Wiley-VCH, Weinheim, 1st Edn., 2006, vol. 1, ch. 2, pp. 39-62.

17. W. H. Ang and P. J. Dyson, *Eur. J. Inorg. Chem.*, 2006, 4003-4018.

18. S. Mollin, S. Blanck, K. Harms and E. Meggers, *Inorg. Chim. Acta*, 2012, **393**, 261268.

19. C. H. Leung, H. J. Zhong, D. S. H. Chan and D. L. Ma, *Coord. Chem. Rev.*, 2013, **257**, 1764-1776.

20. C.-H. Leung, H. Yang, D. P.-Y. Ma, D. S.-H. Chan, H.-J. Zhong, Y.-W. Li, W.-F. Fong and D.-L. Ma, *Med. Chem. Comm.*, 2012, **3**.

21. C. B. Gorman and J. C. Smith, *Polymer*, 2000, **41**, 675-683.

22. P. Govender, A. K. Renfrew, C. M. Clavel, P. J. Dyson, B. Therrien and G. S. Smith, *Dalton Trans.*, 2011, **40**, 1158-1167.

Chapter 5: Experimental Details

General

All reaction solvents were dried over Molecular Sieve Dehydrate Fluka with indicator and all samples were dried under vacuum. Naphthaldehyde, benzaldehyde, *n*-propylamine and 1,4-diaminobutane poly(propyleneimine) tetraamine (DAB-*dendr*-$(NH_2)_4$-**G1**) were purchased from Aldrich; α-Phellandrene was purchased from Fluka; 1,4-diaminobutane poly(propyleneimine) octaamine (DAB-*dendr*-$(NH_2)_8$-**G2**) was purchased from SyMO Chem and used without further purification. Ruthenium(III), rhodium(III) and iridium(III) trichloride trihydrate was obtained as a generous donation from Johnson Matthey/Anglo Platinum. $[Ru(p\text{-cymene})Cl_2)]_2$[1], $[Rh(\eta^5\text{-}C_5Me_5)Cl_2]_2$[2] and $[Ir(\eta^5\text{-}C_5Me_5)Cl_2]_2$[2] were prepared according to literature methods.

Deuterated solvents were purchased from Aldrich. Nuclear magnetic resonance (NMR) spectra were recorded on a Varian Unity XR400 spectrometer (^{1}H: 399.95 MHz, $^{13}C\{^1H\}$: 100.58 MHz) or Varian Mercury XR300 spectrometer (^{1}H: 300.08 MHz, $^{13}C\{^1H\}$: 75.46 MHz) or Bruker Ultrashield 400 Plus spectrometer (^{1}H: 400.20 MHz, $^{13}C\{^1H\}$: 100.60 MHz) at 30 ^oC with tetramethylsilane as an internal standard. Infrared (IR) absorptions were measured on a Perkin-Elmer Spectrum One FT-IR spectrometer as KBr pellets. Microanalysis for carbon, hydrogen and nitrogen were carried out using a Fisions EA 1108 CHNS elemental analyser. For certain metallodendrimers, the analyses are outside acceptable limits, and are ascribed to the encapsulation of solvent molecules and other inorganic salts by dendritic compounds. Melting points were determined using a Büchi Melting Point (B-540) instrument and are corrected. Mass spectrometry was carried out at the University of Stellenbosch on a Waters API Quattro Micro triple quadrupole mass spectrometer. Data were recorded using low and high resolution Electrospray Ionisation (ESI) mass spectrometry in the positive-ion mode.

5.1 Synthesis of monomeric and dendritic ligands

*5.1.1 General synthesis of the naphthaldimine and benzaldimine Schiff-base monomeric ligands **2.1** & **2.2***[3]

Propylamine (**2.1:** 1.00 mL, 12.2 mmol; **2.2:** 1.00 mL, 12.2 mmol) was dissolved in ethanol (15.0 mL) followed by the dropwise addition of naphthaldehyde (**2.1:** 1.90 g, 12.2 mmol) or benzaldehyde (**2.2:** 1.23 mL, 12.2 mmol). The reaction mixture was allowed to stir for 24 hours after which the solvent was removed on the rotary evaporator. The residue was dissolved in DCM (20.0 mL) and washed with water (15 x 10.0 mL). The organic layer was collected, dried over anhydrous $MgSO_4$ and then filtered by gravity. The solvent was removed on the rotary evaporator to yield the desired products as a yellow-brown solid (**2.1**) or brown-red oil. (**2.2**)

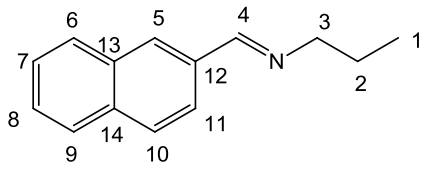

2.1: Yellow-brown solid. Yield = 1.48 g (62%). **IR** (KBr) ν(C=N) 1640 cm^{-1}. **^{1}H NMR** (400 MHz, $CDCl_3$) δ (ppm) = 1.00 (t, 3H, **H_1**); 1.78 (m, 2H, **H_2**); 3.65 (t, 2H, **H_3**); 7.51 (t, 2H, **H_7**, **H_8**); 7.86 (m, 3H, **H_6**, **H_9**, **H_{10}**); 7.99 (m, 1H, **H_5**); 8.04 (m, 1H, **H_{11}**); 8.43 (d, 1H, **H_4**).

^{13}C{^{1}H}-NMR (100 MHz, $CDCl_3$) δ (ppm) = 11.89 (**C_1**); 24.15 (**C_2**); 63.64 (**C_3**); 123.96 (**C_5**); 126.40 (**C_8**); 127.00 (**C_7**); 127.86 (**C_9**); 128.42 (**C_{10}**); 128.57 (**C_6**);); 129.61 (**C_{11}**); 133.19 (**C_{14}**); 134.11 (**C_{13}**); 134.67 (**C_{12}**); 160.86 (**C_4**). Melting point: 44-47°C.

Elemental Analysis (%): Calc. For $C_{14}H_{15}N$ (197.28): C, 85.24; H, 7.66; N, 7.10; Found: C, 84.49; H, 7.39; N, 7.06. **MS** (ESI, m/z): 141.01 $[M\text{-}C_3H_7N]^+$.

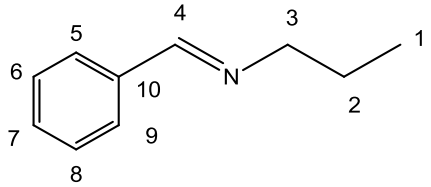

2.2: Brown-red oil. Yield = 1.48 g (82%). **IR** (KBr) ν(C=N) 1646 cm^{-1}. **^{1}H NMR** (400 MHz, $CDCl_3$) δ (ppm) =0.98 (t, 3H, **H_1**); 1.76 (m, 2H, **H_2**); 3.60 (t, 2H, **H_3**); 7.41 (t, 3H, **H_6**, **H_7**, **H_8**); 7.75 (d, 2H, **H_5**, **H_9**); 8.28 (d, 1H, **H_4**).

$^{13}C\{^1H\}$-NMR (100 MHz, $CDCl_3$) δ (ppm) = 11.82 (**C_1**); 24.07 (**C_2**); 63.51 (**C_3**); 128.04 (**C_5, C_9**); 128.56 (**C_6, C_7**); 130.42 (**C_8**); 136.42 (**C_{10}**); 160.79 (**C_4**).

Elemental Analysis (%): Calc. For $C_{10}H_{13}N$ (147.22): C, 81.59; H, 8.90; N, 9.51; Found: C, 81.94; H, 8.39; N, 4.85. **MS** (ESI, m/z): 118.02 $[M\text{-}C_2H_5]^+$. 147.08 $[M]^+$.

*5.1.2 General synthesis of the naphthaldimine and benzaldimine G1 (**2.3** & **2.4**) and G2 (**2.5** & **2.6**) Schiff-base dendritic ligands*

The PPI G1 (**2.3:** 0.120 mL, 0.373 mmol; **2.4:** 0.196 g, 0.62 mmol) or G2 (**2.5:** 0.526 g, 0.680 mmol; **2.6:** 0.249 g, 0.322 mmol) dendritic scaffold was dissolved in ethanol (**2.3:** 10.0 mL; **2.4:** 15.0 mL; **2.5:** 50.0 mL; **2.6:** 25.0 mL) followed by the addition of naphthaldehyde (**2.3;** 0.237 g, 1.52 mmol; **2.5;** 0.853 g, 5.46 mmol) or benzaldehyde (**2.4:** 0.260 mL, 2.55 mmol; **2.6:** 0.260 mL, 2.55 mmol). The reaction mixture was allowed to stir for 72-96 hours after which the solvent was removed on a rotary evaporator and the residue was dissolved in DCM (30.0 mL) and washed with a 7:3 water-brine mixture (15 x 30.0 mL). The organic layer was collected, dried over anhydrous $MgSO_4$ and then filtered by gravity. The solvent was removed on a rotary evaporator to yield the desired products as white solids (**2.3 & 2.5**) or yellow oils (**2.4 & 2.6**).

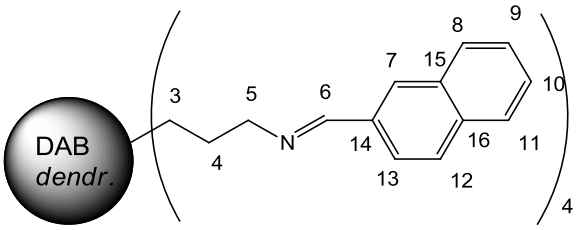

2.3: White solid. Yield = 0.216 g (67%). **IR** (KBr) ν(C=N) 1639 cm^{-1}. **^1H NMR** (400 MHz, $CDCl_3$) δ (ppm) = 1.49 (sep, 4H, **H_{core}**); 1.89 (sep, 8H, **H_4**); 2.46 (t, 4H, **H_{core}**); 2.57 (t, 8H, **H_3**); 3.68 (t, 8H, **H_5**); 7.47 (m, 8H, **H_9, H_{10}**); 7.81 (t, 12H, **H_8, H_{11}, H_{12}**); 7.95 (m, 8H, **H_7, H_{13}**); 8.40 (d, 4H, **H_6**). Melting point: 104-108°C.

$^{13}C\{^1H\}$-NMR (100 MHz, $CDCl_3$) δ (ppm) = 25.25 (**C_{core}**); 28.40 (**C_4**); 51.74 (**C_3**); 54.11 (**C_{core}**); 59.74 (**C_5**); 123.88 (**C_{13}**); 126.36 (**C_{10}**); 126.97 (**C_9**); 127.83 (**C_{11}**); 128.41 (**C_8**); 128.57 (**C_{12}**); 129.66 (**C_7**); 133.14 (**C_{16}**); 134.05 (**C_{15}**); 134.64 (**C_{14}**); 161.06 (**C_6**).

Elemental Analysis (%): Calc. For $C_{60}H_{64}N_6$ (869.21): C, 82.91; H, 7.42; N, 9.67; Found: C, 80.44; H, 6.78; N, 9.43. **MS** (ESI LR, m/z): 322.20 $[M+3H^+ +3MeOH]^{3+}$.

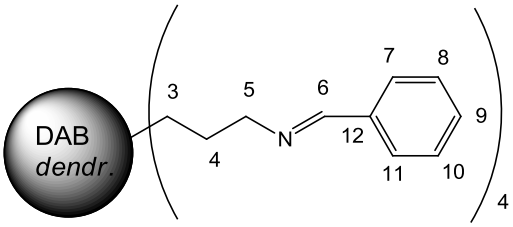

2.4: Yellow oil. Yield = 0.314 g (76%). **IR** (KBr) ν(C=N) 1643 cm^{-1}. **^{1}H NMR** (400 MHz, $CDCl_3$) δ (ppm) = 1.43 (p, 4H, $\mathbf{H_{core}}$); 1.83 (p, 8H, $\mathbf{H_4}$); 2.41 (t, 4H, $\mathbf{H_{core}}$); 2.51 (t, 8H, $\mathbf{H_3}$); 3.62 (t, 8H, $\mathbf{H_5}$); 7.38 (m, 12H, $\mathbf{H_8, H_9, H_{10}}$); 7.70 (dd, 8H, $\mathbf{H_7, H_{11}}$); 8.26 (d, 4H, $\mathbf{H_6}$).

^{13}C{^{1}H}-NMR (100 MHz, $CDCl_3$) δ (ppm) = 25.26 ($\mathbf{C_{core}}$); 28.42 ($\mathbf{C_4}$); 51.73 ($\mathbf{C_{core}}$); 54.11 ($\mathbf{C_3}$); 59.71 ($\mathbf{C_5}$); 127.37 ($\mathbf{C_7}$); 127.67 ($\mathbf{C_{11}}$); 128.02 ($\mathbf{C_{10}}$); 128.55 ($\mathbf{C_9}$); 130.42 ($\mathbf{C_8}$); 136..67 ($\mathbf{C_{12}}$); 160.96 ($\mathbf{C_6}$). Melting point: 134-137°C.

Elemental Analysis (%): Calc. For $C_{44}H_{56}N_6$ (668.97): C, 79.00; H, 8.44; N, 12.56; Found: C, 77.40; H, 7.70; N, 12.30. **MS** (ESI LR, m/z): 272.20 $[M+3H_3O^+ +MeOH]^{3+}$.

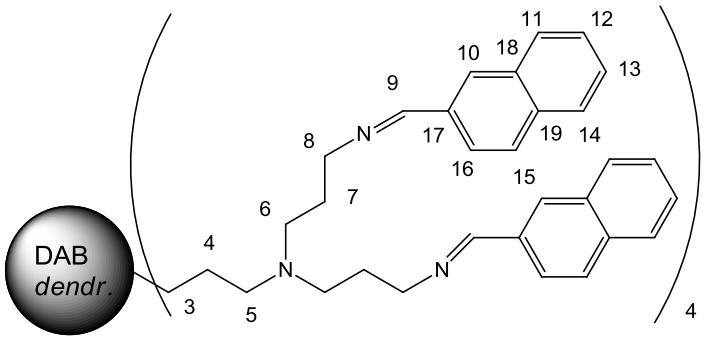

2.5: White solid. Yield = 0.842 g (66%). **IR** (KBr) ν(C=N) 1639 cm^{-1}. **^{1}H NMR** (400 MHz, $CDCl_3$) δ (ppm) = 1.33 (m, 4H, $\mathbf{H_{core}}$); 1.53 (m, 8H, $\mathbf{H_4}$); 1.80 (sep, 16H, $\mathbf{H_7}$); 2.37 (m, 20H, $\mathbf{H_{core}, H_3, H_5}$); 2.47 (t, 16H, $\mathbf{H_6}$); 3.58 (t, 16H, $\mathbf{H_8}$); 7.37 (m, 16H, $\mathbf{H_{12}, H_{13}}$); 7.70 (m, 24H, $\mathbf{H_{11}, H_{14}, H_{15}}$); 7.86 (m, 16H, $\mathbf{H_{10}, H_{16}}$); 8.36 (d, 8H, $\mathbf{H_9}$).

^{13}C{^{1}H}-NMR (100 MHz, $CDCl_3$) δ (ppm) = 24.75 ($\mathbf{C_4}$); 25.20 ($\mathbf{C_{core}}$); 28.48 ($\mathbf{C_7}$); 51.77 ($\mathbf{C_6}$); 52.37 ($\mathbf{C_5}$); 53.40 ($\mathbf{C_3}$); 54.26 ($\mathbf{C_{core}}$); 59.79 ($\mathbf{C_8}$); 123.88 ($\mathbf{C_{10}}$); 126.34 ($\mathbf{C_{13}}$); 126.95 ($\mathbf{C_{12}}$); 127.82 ($\mathbf{C_{14}}$); 128.39 ($\mathbf{C_{11}}$); 128.56 ($\mathbf{C_{15}}$); 129.67 ($\mathbf{C_{16}}$); 133.13 ($\mathbf{C_{19}}$); 134.05 ($\mathbf{C_{18}}$); 134.62 ($\mathbf{C_{17}}$); 160.99 ($\mathbf{C_9}$). Melting point: 64-67°C.

Elemental Analysis (%): Calc. For $C_{128}H_{144}N_{14}$ (1878.64): C, 81.84; H, 7.73; N, 10.44; Found: C, 78.54; H, 7.54; N, 10.37. **MS** (ESI LR, m/z): 408.20 $[M+5H^+ +MeOH]^{5+}$.

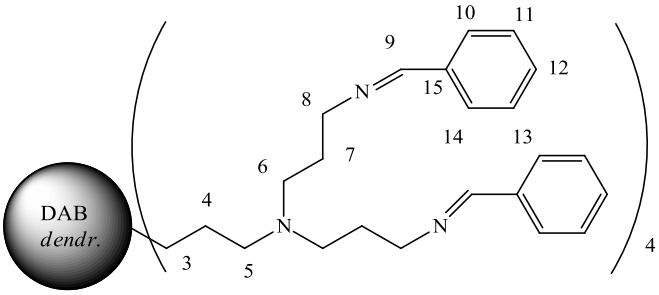

2.6: Yellow oil. Yield = 0.214 g (45%). **IR** (DCM) ν(C=N) 1646 cm^{-1}. **^{1}H NMR** (400 MHz, $CDCl_3$) δ (ppm) = 1.38 (m, 4H, $\mathbf{H_{core}}$); 1.57 (br sep, 8H, $\mathbf{H_4}$); 1.82 (sep, 16H, $\mathbf{H_7}$); 2.41 (m, 20H, $\mathbf{H_{core}}$, $\mathbf{H_3}$, $\mathbf{H_5}$); 2.51 (t, 16H, $\mathbf{H_6}$); 3.61 (t, 16H, $\mathbf{H_8}$); 7.37 (m, 24H, $\mathbf{H_{11}}$, $\mathbf{H_{12}}$, $\mathbf{H_{13}}$); 7.69 (dd, 8H, $\mathbf{H_{10}}$, $\mathbf{H_{14}}$); 8.25 (d, 8H, $\mathbf{H_9}$).

^{13}C{^{1}H}-NMR (100 MHz, $CDCl_3$) δ (ppm) = 24.68 ($\mathbf{C_4}$); 25.16 ($\mathbf{C_{core}}$); 28.42 ($\mathbf{C_7}$); 51.76 ($\mathbf{C_6}$); 52.29 ($\mathbf{C_3}$); 52.37 ($\mathbf{C_5}$); 54.26 ($\mathbf{C_{core}}$); 59.72 ($\mathbf{C_8}$); 128.04 ($\mathbf{C_{10}}$, $\mathbf{C_{14}}$); 128.54 ($\mathbf{C_{11}}$, $\mathbf{C_{12}}$); 130.42 ($\mathbf{C_{13}}$); 136.38 ($\mathbf{C_{15}}$); 160.93 ($\mathbf{C_9}$).

Elemental Analysis (%): Calc. For $C_{96}H_{128}N_{14}$ (1478.16): C, 78.00; H, 8.73; N, 13.27; Found: C, 74.44; H, 7.27; N, 13.12. **MS** (ESI LR, m/z): 773.80 $[M+2H^+ +2MeOH]^{2+}$.

5.2 Synthesis of the neutral mononuclear and dendritic cyclometalated complexes:

5.2.1 *General synthesis of the cyclometalated ruthenium(II), rhodium(III) and iridium(III) naphthaldimine mononuclear complexes **2.7, 2.8 & 2.9**.*

The naphthaldimine ligand (**2.7:** 0.0530 g, 0.269 mmol; **2.8:** 0.0409 g, 0.207 mmol; **2.9:** 0.0408 g, 0.207 mmol), sodium acetate (**2.7:** 0.0443 g, 0.540 mmol; **2.8:** 0.0339 g, 0.413 mmol; **2.9:** 0.0343 g, 0.418 mmol) and the $[Ru(p\text{-cymene})Cl_2)]_2$ (0.0822 g, 0.134 mmol), $[Rh(\eta^5\text{-}C_5Me_5)Cl_2]_2$ (0.0634 g, 0.102 mmol) or $[Ir(\eta^5\text{-}C_5Me_5)Cl_2]_2$ (0.0810 g, 0.102 mmol) dimer were stirred together in DCM or methanol (20.0 mL) for 2 hours at room temperature. The reaction mixture was filtered through Celite, washing with DCM or methanol. The solvent was removed to obtain the crude product. This was then washed with diethyl ether to obtain the desired product as a golden brown (**2.7**), orange-red (**2.8**) or orange-brown (**2.9**) solid. The ruthenium(II) complex (**2.7)** was recrystallized from DCM, whereas the rhodium(III) (**2.8**) and iridium(III) (**2.9**) complexes were recrystallized from methanol and hexane by slow evaporation.

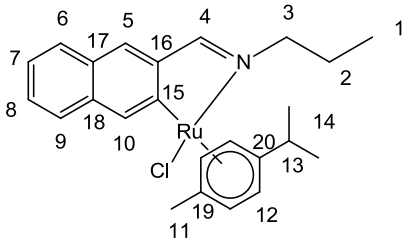

2.7: Golden brown solid. Yield = 0.0790 g (63%). **IR** (KBr) ν(C=N) 1611 cm^{-1}. **^{1}H NMR** (400 MHz, $CDCl_3$) δ (ppm) = 0.81 (d, 3H, **H_{14}**); 1.10 (m, 6H, **H_1** & **H_{14}**); 2.11 (m, 1H, **H_2**); 2.16 (s, 3H, **H_{11}**); 2.24 (m, 1H, **H_2**); 2.49 (sept, 1H, **H_{13}**); 4.00 (m, 1H, **H_3**); 4.21 (m, 1H, **H_3**); 4.84 (d, 1H, **H_{12}**); 4.96 (d, 1H, **H_{12}**); 5.64 (d, 1H, **H_{12}**); 5.70 (d, 1H, **H_{12}**); 7.27 (t, 1H, **H_7**); 7.44 (t, 1H, **H_8**); 7.73 (t, 2H, **H_6 & H_9**); 7.90 (s, 1H, **H_5**); 8.15 (s, 1H, **H_{10}**); 8.45 (s, 1H, **H_4**).
^{13}C{^{1}H}-NMR (100 MHz, $CDCl_3$) δ (ppm) = 11.94 (**C_{11}**); 18.90 (**C_1**); 23.34 (**C_{14}**); 30.80 (**C_{14}**); 68.20 (**C_1**); 77.30 (**C_{18}**); 79.43 (**C_{12}**); 80.55 (**C_{12}**); 89.93 (**C_{12}**); 91.32 (**C_{12}**); 101.20 (**C_{19}, C_{20}**); 103.14 (**C_{13}**); 123.61 (**C_{16}, C_{17}**); 126.51 (**C_6**); 127.11 (**C_{15}**); 128.7 (**C_5**); 130.47 (**C_7**); 134.93 (**C_8**); 136.21 (**C_9**); 145.28 (**C_4**); 171.72 (**C_3**); 178.01 (**C_{10}**). Melting point: 148-150^{o}C.
Elemental Analysis (%): Calc. For $C_{24}H_{28}ClNRu$ (467.01): C, 61.72; H, 6.04; N, 3.00; Found: C, 61.76; H, 6.16; N, 2.99. **MS** (ESI, m/z): 432.3 $[M\text{-}Cl]^+$.

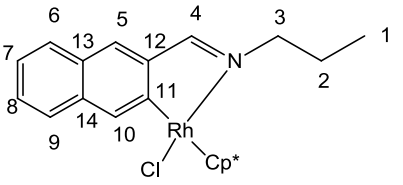

2.8: Orange-red solid. Yield = 0.048 g (50%). **IR** (KBr) ν(C=N) 1610 cm^{-1}. **^{1}H NMR** (400 MHz, $CDCl_3$) δ (ppm) = 1.01 (t, 3H, **H_1**); 1.69 (s, 15H, **Cp***); 1.93 (m, 1H, **H_2**); 2.11 (m, 1H, **H_2**); 3.72 (m, 1H, **H_3**); 4.12 (m, 1H, **H_3**); 7.29 (t, 1H, **H_7**); 7.44 (t, 1H, **H_8**); 7.74 (t, 2H, **H_6 & H_9**); 7.90 (s, 1H, **H_5**); 8.06 (s, 1H, **H_{10}**); 8.23 (s, 1H, **H_4**).

^{13}C{^{1}H}-NMR (100 MHz, $CDCl_3$) δ (ppm) = 11.75 (**C_2**); 63.98 (**C_1**); 95.70 (**Cp***); 123.84 (**C_6**); 126.60 (**C_{13}**); 127.06 (**C_7**); 128.70 (**C_{14}**); 129.16 (**C_9**); 129.57 (**C_8**); 130.50 (**C_{10}**); 134.63 (**C_{12}**); 135.68 (**C_5**); 145.21 (**C_4**); 171.69 (**C_3**); 192.35 (**C_{11}**). Melting point: 168-170^{o}C.

Elemental Analysis (%): Calc. For $C_{24}H_{29}ClNRh$ (469.86): C, 61.35; H, 6.22; N, 2.98; Found: C, 58.81; H, 6.16; N, 2.58. **MS** (ESI, m/z): 434.23 $[M\text{-}Cl]^+$.

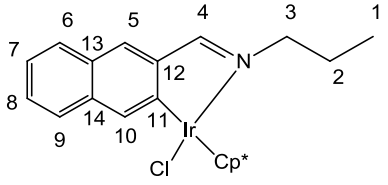

2.9: Orange-brown solid. Yield = 0.08 g (71%). **IR** (KBr) ν(C=N) 1603 cm^{-1}. **^{1}H NMR** (400 MHz, $CDCl_3$) δ (ppm) = 1.03 (t, 3H, **H_1**); 1.80 (s, 15H, **Cp***); 1.98 (m, 1H, **H_2**); 2.12 (m, 1H, **H_2**); 3.93 (m, 1H, **H_3**); 4.11 (m, 1H, **H_3**); 7.27 (t, 1H, **H_7**); 7.42 (t, 1H, **H_8**); 7.74 (t, 2H, **H_6 & H_9**); 8.01 (s, 1H, **H_5**); 8.06 (s, 1H, **H_{10}**); 8.44 (s, 1H, **H_4**).

^{13}C{^{1}H}-NMR (100 MHz, $CDCl_3$) δ (ppm) = 22.77 (**C_1**); 65.23 (**C_2**); 88.51 (**Cp***); 123.50 (**C_6**); 126.57 (**C_{13}, C_{14}**); 127.07 (**C_7**); 128.37 (**C_9**); 128.83 (**C_8**); 130.10 (**C_5**); 132.06 (**C_{10}**); 136.60 (**C_{12}**); 145.21 (**C_4**); 171.69 (**C_{11}**); 192.35 (**C_3**). Melting point: 206-208^{o}C.

Elemental Analysis (%): Calc. For $C_{24}H_{29}ClIrN$ (559.17): C, 51.55; H, 5.23; N, 2.50; Found: C, 50.83; H, 5.35; N, 2.63. **MS** (ESI, m/z): 524.4 $[M\text{-}Cl]^+$.

*5.2.2 General synthesis of the cyclometalated ruthenium(II), rhodium(III) and iridium(III) naphthaldimine G1 metallodendrimers **2.13, 2.14 & 2.15**.*

The naphthaldimine G1 dendritic ligand (**2.13:** 0.0439 g, 0.0505 mmol; **2.14:** (0.0492 g, 0.0566 mmol; **2.15:** 0.0205 g, 0.0236 mmol), sodium acetate (**2.13:** 0.0169 g, 0.206 mmol; **2.14:** 0.0186 g, 0.227 mmol; **2.15:** 0.0081 g, 0.0987 mmol) and the $[Ru(p\text{-cymene})Cl_2]_2$ (0.0613 g, 0.100 mmol), $[Rh(\eta\text{-}C_5Me_5)Cl_2]_2$ (0.0700 g, 0.113 mmol) or $[Ir(\eta\text{-}C_5Me_5)Cl_2]_2$ (0.0376 g, 0.0472 mmol) dimer were stirred together in DCM or methanol (20.0 mL) overnight at room temperature. The ruthenium complex (**2.13**) was synthesized under argon. After which the reaction mixture was filtered through Celite and washed with DCM or methanol. The solvent was removed on a rotary evaporator to obtain the crude product. The solid was dissolved in a minimum amount of DCM and diethyl ether was slowly added to the solution down the side of the flask. A solid started to precipitate out and the suspension was placed in the fridge overnight. The solid was filtered under vacuum yielding the desired product as a green-brown (**2.13**), light yellow-orange (**2.14**) or light yellow-orange (**2.15**) solid.

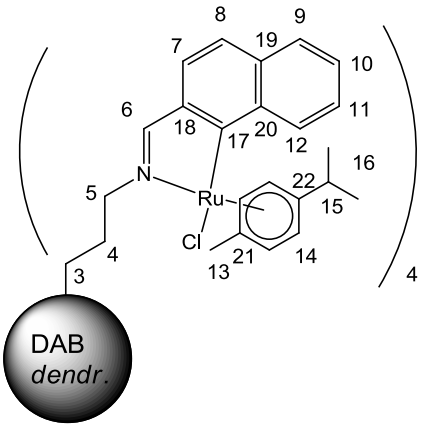

2.13: Green-brown solid. Yield = 0.0800 g (81%). **IR** (KBr) ν(C=N) 1604 cm^{-1}. **^{1}H NMR** (400 MHz, $CDCl_3$) δ (ppm) = 0.72 (m, 8H, **H_4**); 1.10 (m, 4H, **H_{core}**); 1.49 (m, 24H, **H_{16}**); 1.66 (s, 12H, **H_{13}**); 2.48 (m, 4H, **H_{core}**); 2.50 (m, 8H, **H_3**); 2.32 (m, 4H, **H_{15}**); 3.47 (t, 8H, **H_5**); 5.40 (d, 8H, **H_{14}**); 5.62 (d, 8H, **H_{14}**); 7.39 (m, 8H, **H_9, H_{10}**); 7.58 (m, 4H, **H_8**); 7.65 (m, 4H, **H_{11}**); 7.80 (m, 8H, **H_7, H_{12}**); 8.32 (s, 4H, **H_6**).

^{13}C{^{1}H}-NMR (100 MHz, $CDCl_3$) δ (ppm) = 22.00 (**C_{16}**); 22.27 (**C_{core}**); 25.04 (**C_{13}**); 28.10 (**C_4**); 51.61 (**C_{15}**); 53.01 (**C_3**); 53.96 (**C_{core}**); 59.68 (**C_5**); 81.16-81.51; (**C_{14}**); 122.97 (**C_{19}**); 123.85 (**C_7**); 126.82 (**C_{21},C_{22}**); 127.09 (**C_9**); 127.83 (**C_{10}**); 128.56 (**C_8**); 129.10 (**C_{11}**); 129.69 (**C_{12}**); 133.45 (**C_{20}**); 133.97 (**C_{18}**); 135.00 (**C_{17}**); 142.12 (**C_6**). Melting point: 124-128^{o}C.

Elemental Analysis (%): Calc. For $C_{100}H_{116}Cl_4N_6Ru_4$ (1948.15): C, 61.65; H, 6.00; N, 4.31; Found: C, 57.95; H, 6.51; N, 6.50. **MS** (ESI HR, m/z): 613.83 $[M\text{-}3Cl]^{3+}$; 1948.42 $[M]^+$.

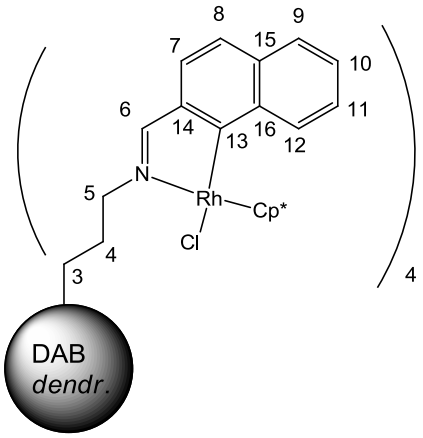

2.14: Yellow-orange solid. Yield = 0.0605 g (52%). **IR** (KBr) ν(C=N) 1609 cm^{-1}. **^{1}H NMR** (400 MHz, $CDCl_3$) δ (ppm) = 1.57 (m, 4H, **H_{core}**); 1.61 (s, 60H, **Cp***); 1.70 (m, 8H, **H_4**); 2.20 (br t, 8H, **H_3**); 2.92 (m, 4H, **H_{core}**); 3.96 (splitting of br m, 8H, **H_5**); 7.30 (m, 8H, **H_8,H_9**); 7.43 (m, 8H, **H_{10},H_{11}**); 7.74 (m, 8H, **H_7,H_{12}**); 8.03 (s, 4H, **H_6**).

$^{13}C\{^1H\}$-NMR (100 MHz, $CDCl_3$) δ (ppm) = 9.35 (**Cp***); 23.56 (**C_4**); 24.64 (**C_{core}**); 26.25 (**C_3**); 51.57 (**C_{core}**); 59.72 (**C_5**); 123.68 (**C_{10}**); 123.74 (**C_{15}**); 126.50 (**C_7**); 126.93 (**C_9**); 128.30 (**C_8**); 128.77 (**C_{12}**); 130.48 (**C_{11}**); 133.37 (**C_{16}**); 135.60 (**C_{14}**); 135.64 (**C_{13}**); 145.66 (**C_6**). Melting point: 220-224°C.

Elemental Analysis (%): Calc. For $C_{100}H_{120}Cl_4N_6Rh_4$ (1959.54): C, 61.29; H, 6.17; N, 4.29; Found: C, 63.17; H, 6.02; N, 4.93. **MS** (ESI HR, m/z): 1923.48 $[M\text{-}Cl]^+$, 1959.44 $[M]^+$.

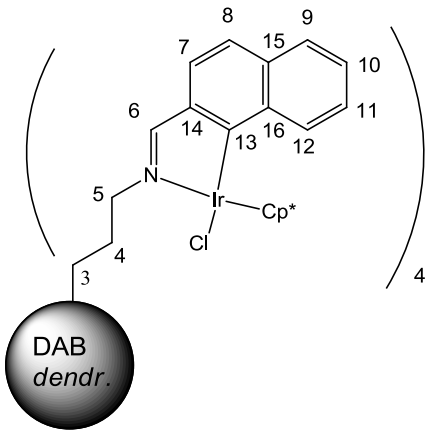

2.15: Yellow-orange solid. Yield = 0.0230 g (42%). **IR** (KBr) ν(C=N) 1602 cm^{-1}. **^1H NMR** (400 MHz, $CDCl_3$) δ (ppm) = 1.50 (m, 8H, **H_4**); 1.75 (m, 8H, **H_{core}**); 1.65 (s, 60H, **Cp***); 2.11 (m, 4H, **H_{core}**); 2.49 (br m, 8H, **H_3**); 4.12 (m, 8H, **H_5**); 7.26 (t, 8H, **H_{10}**); 7.39 (t, 8H, **H_9**); 7.73 (t, 8H, **H_8 & H_{11}**); 8.02 (t, 8H, **H_7 & H_{12}**); 8.29 (br s, 4H, **H_6**).

$^{13}C\{^1H\}$-NMR (100 MHz, $CDCl_3$) δ (ppm) = 9.15 (**Cp***); 25.64 (**C_4**); 26.35 (**C_{core}**); 28.16 (**C_{core}**); 51.60 (**C_3**); 60.96 (**C_5**); 122.87 (**C_{15}**); 123.40 (**C_{10}**); 126.47 (**C_8**); 126.98 (**C_9**); 128.88 (**C_{11}**); 130.09 (**C_{12}**); 131.87 (**C_7**); 136.60 (**C_{13}**); 141.18 (**C_{16}**); 141.37 (**C_{14}**); 146.27 (**C_6**). Melting point: 226-232°C.

Elemental Analysis (%): Calc. for $C_{100}H_{120}Cl_4Ir_4N_6$ (2316.78): C, 51.84; H, 5.22; N, 3.63; Found: C, 49.00; H, 5.31; N, 3.16. **MS** (ESI HR, m/z): 1122.40 $[M\text{-}2Cl]^{2+}$.

*5.2.3 General synthesis of the cyclometalated ruthenium, rhodium and iridium naphthaldimine G2 metallodendrimers **2.19, 2.20 & 2.21***

The naphthaldimine G2 dendritic ligand (**2.19:** 0.120 g, 0.0639 mmol; **2.20:** 0.109 g, 0.0579 mmol; **2.21:** 0.121 g, 0.0645 mmol), sodium acetate (**2.19:** 0.0424 g, 0.517 mmol; **2.20:** 0.0386 g, 0.470 mmol; **2.21:** 0.0432 g, 0.527 mmol) and $[Ru(p\text{-cymene})Cl_2]_2$ (0.158 g, 0.258 mmol), $[Rh(\eta^5\text{-}C_5Me_5)Cl_2]_2$ (0.144 g, 0.232 mmol) or $[Ir(\eta^5\text{-}C_5Me_5)Cl_2]_2$ (0.205 g, 0.258 mmol) dimer were stirred together in DCM or methanol (30.0 mL) for 24-48 hours at room

temperature. After which the reaction mixture was filtered through Celite and washed with DCM or methanol. The solvent was removed on a rotary evaporator to obtain the crude product which was then dissolved in a minimum amount of DCM and diethyl ether was slowly added to the solution down the side of the flask until a solid starts precipitating out. The solid was filtered under vacuum yielding the desired product as a green-brown (**2.19**), red-orange solid (**2.20**) or red-orange (**2.21**) solid.

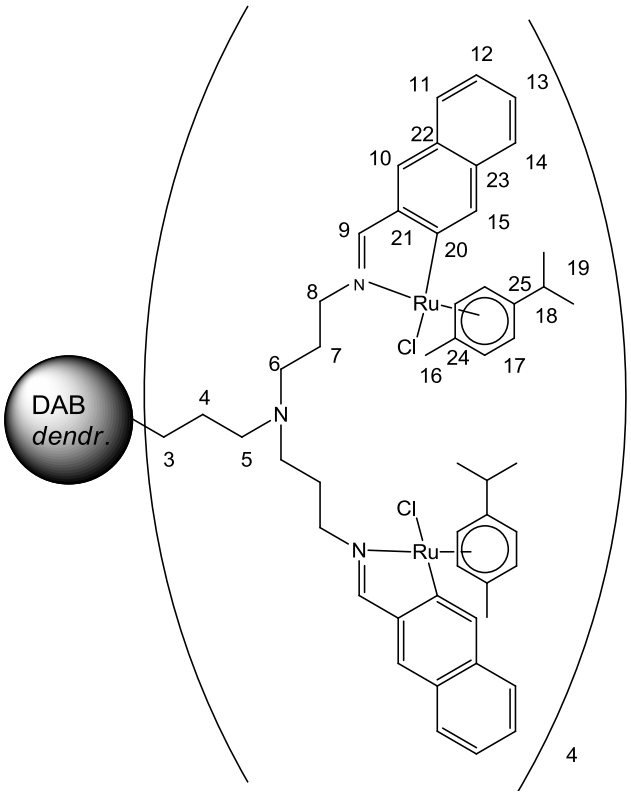

2.19: Green-brown solid. Yield = 0.0602 g (23%). **IR** (KBr) ν(C=N) 1602 cm^{-1}. **^{1}H NMR** (400 MHz, $CDCl_3$) δ (ppm) = 0.66 (m, 4H, **H_{core}**); 0.94 (m, 8H, **H_4**); 1.17-1.19 (br m, 88H, **H_7, H_{16}, H_{19}**); 1.80 (br m, 8H, **H_{18}**); 2.24-2.85 (m, 36H, **H_{core}, H_3, H_5, H_6**); 4.10 (br m; 16H, **H_8**); 5.20-5.55 (m, 32H, **H_{17}**); 7.17 (m, 8H, **H_{12}, H_{13}**); 7.36 (t, 4H, **H_{14}**); 7.64 (t, 8H, **H_{10}, H_{11}**); 7.94 (m, 4H, **H_{15}**); 8.35 (s, 4H, **H_9**).

^{13}C{^{1}H}-NMR (100 MHz, $CDCl_3$) δ (ppm) = 18.79 (**C_{16}**); 21.00 (**C_1**); 22.31 (**C_4**); 23.37 (**C_{19}**); 23.95 (**C_7**); 30.70 (**C_{18}**); 51.49-58.88 (**C_2**, **C_3**, **C_5**, **C_6**).; 63.70 (**C_8**); 79.46, 81.10, 89.75, 91.84 (**C_{17}**); 122.69 (**C_{12}**, **C_{13}**, **C_{24}**).; 126.14 (**C_{11}**); 127.07 (**C_{14}**); 127.66 (**C_{10}**); 128.76 (**C_{15}**); 130.23 (**C_{25}**); 133.05 (**C_{22}**); 133.96 (**C_{21}**); 134.63 (**C_{23}**); 135.98 (**C_{20}**); 145.37 (**C_9**). Melting point: 103-105^{o}C.

Elemental Analysis (%): Calc. for $C_{208}H_{248}Cl_8N_{14}Ru_8$ (4036.53 g/mol): C, 61.89; H, 6.19; N, 4.86; Found: C, 56.04; H, 6.00; N, 4.52. **MS** (ESI HR, m/z): 407.16 $[M\text{-}4Cl]^{4+}$; 544.21 $[M\text{-}3Cl]^{3+}$; 842.17 $[M\text{-}2Cl]^{2+}$.

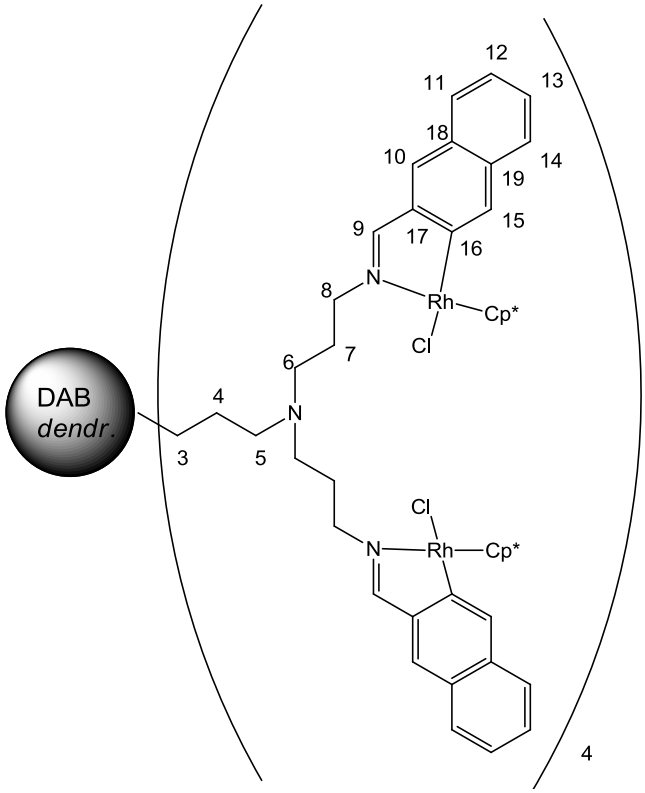

2.20: Orange-yellow solid. Yield = 0.240 g (80%). **IR** (KBr) ν(C=N) 1610 cm^{-1}. **^{1}H NMR** (400 MHz, $CDCl_3$) δ (ppm) = 0.8 (m, 4H, **H_{core}**); 1.18 (m, 8H, **H_4**); 1.56 (s, 120H, **Cp***); 1.89 (br m, 16H, **H_7**); 2.20 (br m, 36H, **H_{core}, H_3, H_5, H_6**): 3.97 (splitting, 16H, **H_8**); 7.20 (m, 16H, **H_{12}, H_{13}**); 7.34 (m, 8H, **H_{11}**); 7.65 (m, 16H, **H_{10}, H_{14}**); 7.88 (m, 8H, **H_{15}**); 7.93 (br s, 8H, **H_9**). Melting point: 178-180°C.

^{13}C{^{1}H}-NMR (100 MHz, $CDCl_3$) δ (ppm) = 9.41 (**Cp***); 10.70 (**C_{core}**); 12.80 (**C_4**); 26.00 (**C_7**); 45.88 (**C_3**); 51.83 (**C_{core}**); 52.97 (**C_5**); 54.16 (**C_6**); 59.90 (**C_8**); 93.20 (**C_{18}**); 95.70 (**C_{19}**); 123.73 (**C_{12}**); 125.0 (**C_{13}**); 126.43 (**C_{10}**); 126.91 (**C_{11}**); 128.22 (**C_{14}**); 128.83 (**C_{15}**); 130.48 (**C_{17}**); 135.52 (**C_{16}**); 143.36 (**C_9**). Melting point: 183-188°C.

Elemental Analysis (%): Calc. for $C_{208}H_{256}Cl_8N_{14}Rh_8$ (4059.27 g/mol): C, 61.54; H, 6.36; N, 4.83; Found: C, 53.76; H, 6.36; N, 3.45. **MS** (ESI HR, m/z): 640.93 $[M\text{-}6Cl]^{6+}$.

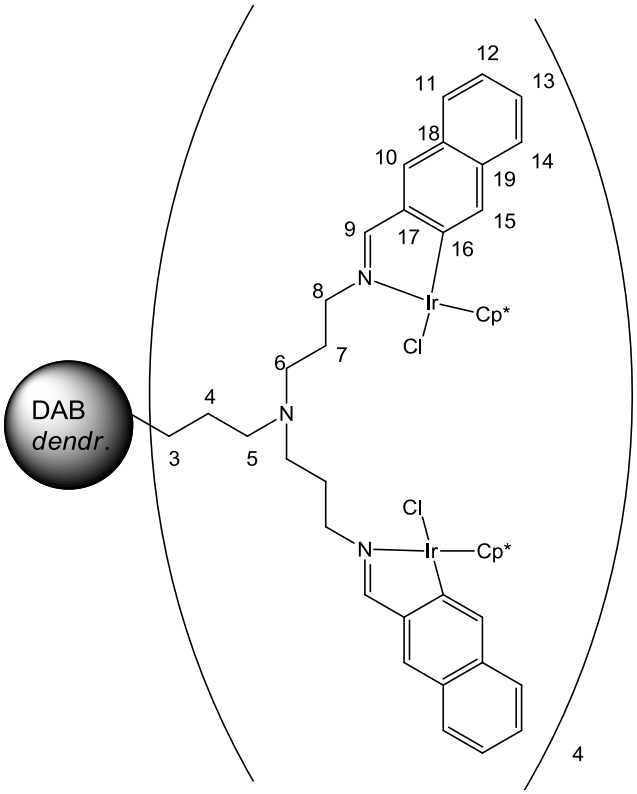

2.21: Red-orange solid. Yield = 0.243 g (79%). **IR** (KBr) ν(C=N) 1600 cm^{-1}. **^{1}H NMR** (400 MHz, $CDCl_3$) δ (ppm) = 1.40 (m, 4H, **H_{core}**); 1.48 (m, 8H, **H_4**); 1.60 (s, 120H, **Cp***); 1.86 (br m, 16H, **H_7**); 1.94 (br m, 36H, **H_{core}**, **H_3**, **H_5**) 2.50 (br m, 16H, **H_6**): 4.00 (br m, 16H, **H_8**); 7.32 (m, 16H, **H_{12}**, **H_{13}**); 7.65 (m, 8H, **H_{11}**, **H_{14}**); 7.93 (m, 16H, **H_{10}**, **H_{15}**); 8.45 (br s, 8H, **H_9**). Melting point: 180-182°C.

^{13}C{^{1}H}-NMR (100 MHz, $CDCl_3$) δ (ppm) = 9.17 (**Cp***); 20.97 (**C_{core}**); 24.33 (**C_4**); 29.15 (**C_7**); 51.11-53.19 (**C_{core}**, **C_3**, **C_5**, **C_6**); 60.86 (**C_8**); 126.43 (**C_{12}**); 127.08 (**C_{11}**); 127.65 (**C_{13}**); 128.99 (**C_{10}**); 130.04 (**C_{14}**); 131.9 (**C_{15}**); 134.86 (**C_{17}**); 136.55 (**C_{16}**); 146.98 (**C_9**). Melting point: 106-108°C.

Elemental Analysis (%): Calc. for $C_{208}H_{256}Cl_8Ir_8N_{14}$ (4773.79 g/mol): C, 52.33; H, 5.40; N, 4.11; Found: C, 49.00; H, 5.27; N, 3.54. **MS** (ESI HR, m/z): 761.74 $[M\text{-}6Cl]^{6+}$; 1152.39 $[M\text{-}4Cl]^{4+}$.

*5.2.4 General synthesis of the cyclometalated ruthenium(II), rhodium(III) and iridium(III) benzaldimine mononuclear complexes **2.10, 2.11 & 2.12**.*

The benzaldimine ligand (**2.10:** 0.0798 g, 0.542 mmol; **2.11:** 0.0286 g, 0.194 mmol; **2.12:** 0.101 g, 0.688 mmol), sodium acetate (**2.10:** 0.0907 g, 1.12 mmol; **2.11:** 0.0322 g, 0.392 mmol; **2.12:** 0.0590 g, 0.719 mmol) and the $[Ru(p\text{-cymene})Cl_2]_2$ (0.155 g, 0.253 mmol), $[Rh(\eta\text{-}C_5Me_5)Cl_2]_2$ (0.0603 g, 0.0976 mmol) or $[Ir(\eta\text{-}C_5Me_5)Cl_2]_2$ (0.271 g, 0.340 mmol) dimer were stirred together in DCM or methanol (50.0 mL) for 2 hours at room temperature. The ruthenium complex (**2.10**) was synthesized under argon. After which the reaction mixture was filtered through Celite and washed with DCM or methanol. The solvent was removed on a rotary evaporator to obtain the crude product. The solid was washed with diethyl ether and placed in the freezer. A solid precipitated out, which was filtered under vacuum washing with cold diethyl ether to yield the desired product as an orange-gold (**2.10**), red-orange (**2.11**) or orange (**2.12**) solid. The rhodium(III) (**2.11**) and iridium(III) (**2.12**) complexes were recrystallized from methanol and hexane by slow evaporation.

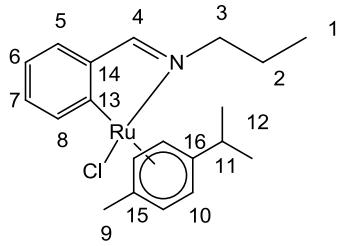

2.10: Orange-gold solid. Yield = 0.0525 g (25%). **IR** (KBr) ν(C=N) 1602 cm^{-1}. **^{1}H NMR** (400 MHz, $CDCl_3$) δ (ppm) = 0.8 (d, 3H, **H_{12}**); 1.02 (t, 3H, **H_1**); 1.06 (d, 3H, **H_{12}**); 2.05 (m, 1H, **H_2**); 2.08 (s, 3H, **H_{11}**); 2.15 (m, 1H, **H_2**); 2.49 (m, 1H, **H_{11}**); 3.94 (m, 1H, **H_3**); 4.14 (m, 1H, **H_3**); 4.80 (d, 1H, **H_{10}**); 4.94 (d, 1H, **H_{10}**); 5.59 (d, 1H, **H_{10}**); 5.63 (d, 1H, **H_{10}**); 6.95 (t, 1H, **H_6**); 7.12 (t, 1H, **H_7**); 7.40 (d, 1H, **H_5**); 7.99 (s, 1H, **H_4**); 8.12 (d, 2H, H_8).

^{13}C{^{1}H}-NMR (100 MHz, $CDCl_3$) δ (ppm) = 18.89 (**C_9**); 21.25 (**C_{10}**); 22.96 (**C_1**); 30.92 (**C_9**); 67.92 (**C_2**); 79.72 (**C_{11}**); 80.87 (**C_{11}**); 89.79 (**C_{11}**); 91.20 (**C_{11}**); 101.44 (**C_{16}**); 102.77 (**C_{15}**); 120.00 (**C_8**); 122.20 (**C_5, C_{14}**); 128.44 (**C_7**); 129.46 (**C_{13}**); 138.96 (**C_6**); 145.21 (**C_4**); 171.62 (**C_3**). Melting point: 108-111^{o}C.

Elemental Analysis (%): Calc. For $C_{20}H_{26}ClNRu$ (416.95): C, 57.61; H, 6.28; N, 3.36; Found: C, 56.99; H, 6.26; N, 3.39. **MS** (ESI, m/z): 382.2 $[M\text{-}Cl]^+$.

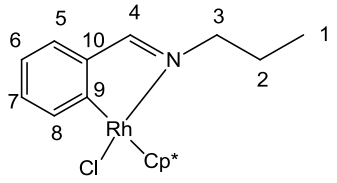

2.11: Red-orange solid. Yield = 0.0550 g (68%). **IR** (KBr) ν(C=N) 1614 cm^{-1}. **^{1}H NMR** (400 MHz, $CDCl_3$) δ (ppm) = 0.99 (t, 3H, **H_1**); 1.66 (s, 15H, **Cp***); 1.89 (m, 1H, **H_2**); 2.07 (m, 1H, **H_2**); 3.66 (m, 1H, **H_3**); 4.07 (m, 1H, **H_3**); 7.00 (t, 1H, **H_6**); 7.21 (t, 1H, **H_7**); 7.40 (d, 1H, **H_5**); 7.76 (d, 1H, **H_8**); 8.10 (d, 1H, **H_4**).

^{13}C{^{1}H}-NMR (100 MHz, $CDCl_3$) δ (ppm) = 11.73 (**Cp^***); 22.94 (**C_1**); 63.71 (**C_2**); 95.8 (**C_{10}**); 122.45 (**C_8**); 127.88 (**C_7**); 130.62 (**C_9**); 135.87 (**C_6**); 145.25 (**C_5**); 145.69 (**C_4**); 171.80 (**C_3**). Melting point: 171-173^{o}C.

Elemental Analysis (%): Calc. For $C_{20}H_{27}ClNRh$ (419.80): C, 57.22; H, 6.48; N, 3.34; Found: C, 56.96; H, 6.71; N, 2.80. **MS** (ESI, m/z): 384.2 $[M\text{-}Cl]^+$.

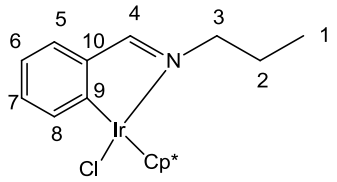

2.12: Orange solid. Yield = 0.0550 g (16%). **IR** (KBr) ν(C=N) 1605 cm^{-1}. **^{1}H NMR** (400 MHz, $CDCl_3$) δ (ppm) = 1.00 (t, 3H, **H_1**); 1.72 (s, 15H, **Cp***); 1.88 (m, 1H, **H_2**); 2.01 (m, 1H, **H_2**); 3.86 (m, 1H, **H_3**); 4.03 (m, 1H, **H_3**); 6.97 (t, 1H, **H_6**); 7.15 (t, 1H, **H_7**); 7.50 (d, 1H, **H_5**); 7.75 (d, 1H, **H_8**); 8.30 (S, 1H, **H_4**).

^{13}C{^{1}H}-NMR (100 MHz, $CDCl_3$) δ (ppm) = 22.67 (**C_1**); 64.78 (**C_2**); 88.72 (**Cp***); 121.82 (**C_8**); 127.98 (**C_7**); 131.42 (**C_9**); 134.62 (**C_6**); 146.25 (**C_4**); 168.19 (**C_5, C_{10}**); 174.34 (**C_3**). Melting point: 178-181^{o}C.

Elemental Analysis (%): Calc. For $C_{20}H_{27}ClIrN$ (509.11): C, 47.18; H, 5.35; N, 2.75; Found: C, 46.85; H, 5.50; N, 2.25. **MS** (ESI, m/z): 474.3 $[M\text{-}Cl]^+$.

*5.2.5 General synthesis of the cyclometalated ruthenium(II), rhodium(III) and iridium(III) benzaldimine G1 metallodendrimers **2.16, 2.17 & 2.18***

The benzaldimine G1 dendritic ligand (**2.16:** 0.107 g, 0.160 mmol; **2.17:** 0.10 g, 0.15 mmol; **2.18:** 0.10 g, 0.16 mmol), sodium acetate (**2.16:** 0.0525 g, 0.640 mmol; **2.17:** 0.05 g, 0.61 mmol; **2.18:** 0.05 g, 0.64 mmol) and [Ru(*p*-cymene)Cl_2]$_2$ (0.196 g, 0.319 mmol), [Rh(η^5–C_5Me_5)Cl_2]$_2$ (0.19 g, 0.31 mmol) or [Ir(η^5-C_5Me_5)Cl_2]$_2$ (0.25 g, 0.31 mmol) dimer were stirred together in DCM or methanol (62.0 mL) for 24 hours at room temperature. After which the reaction mixture was filtered through Celite, washing with DCM or methanol. The solvent was removed on a rotary evaporator to obtain the crude product. The solid was dissolved in a minimum amount of DCM and diethyl ether was slowly added to the solution down the side of the flask. A solid started to precipitate out and the suspension was placed in the fridge overnight. The solid was filtered under vacuum yielding a green-brown (**2.16**) or red-orange (**2.17**, **2.18**) solid.

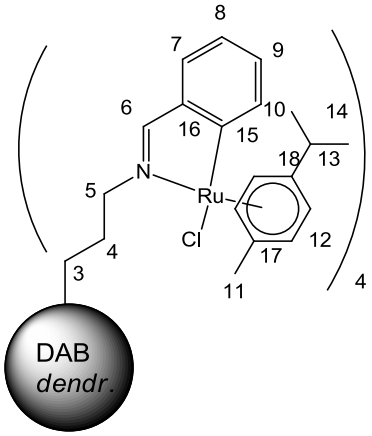

2.16: Green-brown solid. Yield = 0.180 g (64%). **IR** (KBr) ν(C=N) 1602 cm^{-1}. **^{1}H NMR** (400 MHz, $CDCl_3$) δ (ppm) = 0.80 (m, 4H, **H_{core}**); 1.05 (m, 8H, **H_4**); 1.28 (m, 36H, **H_{11}, H_{14}**); 2.43 (m, 12H, **H_{core},H_3**); 2.83 (m, 4H, **H_{13}**); 4.07 (br m, 8H, **H_5**); 4.85, 4.99, 5.63 (br m, 16H, **H_{12}**); 6.96 (br m, 4H, **H_8**); 7.13 (br m, 4H, **H_9**); 7.39 (br m, 8H, **H_7, H_{10}**); 8.12 (br s, 4H, **H_6**).

^{13}C{^{1}H}-NMR (100 MHz, $CDCl_3$) δ (ppm) = 18.82 (**C_{core}**); 20.95, 21.16 (**C_{11},C_{14}**); 23.27 (**C_4**); 30.82 (**C_{core},**); 30.95 (**C_3**); 51.59 (**C_{13}**); 64.04 (**C_5**); 83.47, 83.75, 89.67 (**C_{12}**); 127.37 (**C_{17}**); 128.04 (**C_7**); 128.44 (**C_{18}**); 128.59 (**C_8**); 128.79 (**C_9**); 129.49 (**C_{10}**); 129.74 (**C_{16}**); 129.97 (**C_{15}**); 143.99 (**C_6**).

Elemental Analysis (%): Calc. For $C_{84}H_{108}Cl_4N_6Ru_4$ (1747.91): C, 57.72; H, 6.23; N, 4.81; Found: C, 56.06; H, 7.41; N, 7.88. **MS** (ESI-HR, m/z): 842.17 $[M-2Cl]^{2+}$, 544.21 $[M-3Cl]^{3+}$, 407.16 $[M-4Cl]^{4+}$

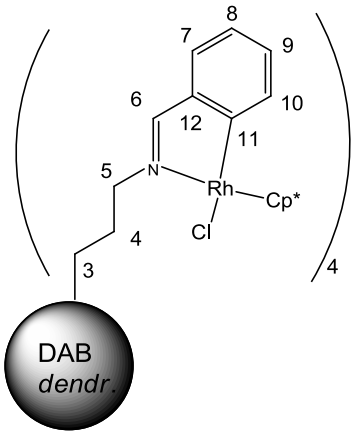

2.17: Red-orange solid. Yield = 0.21 g (79%). **IR** (KBr) ν(C=N) 1607cm^{-1}. **^{1}H NMR** (400 MHz, $CDCl_3$) δ (ppm) = 1.60 (m, 4H, **H_{core}**); 1.63 (s, 60H, **Cp***); 2.20 (br m, 8H, **H_4**); 2.68 (br m, 4H, **H_{core}**); 2.80 (br m, 8H, **H_3**): 4.09 (splitting, 8H, **H_5**); 6.98 (t, 4H, **H_9**); 7.18 (t, 4H, **H_8**); 7.43 (t, 4H, **H_{10}**); 7.72 (d, 4H, **H_7**); 8.23 (s, 4H, **H_6**).

^{13}C{^{1}H}-NMR (100 MHz, $CDCl_3$) δ (ppm) = 9.31 (**Cp***); 23.09 (**C_{core}**); 25.64 (**C_4**); 51.49 (**C_3**); 53.41 (**C_{core}**); 59.46 (**C_5**); 122.43 (**C_9**); 128.05 (**C_{12}**); 128.24 (**C_{10}**); 130.55 (**C_8**); 131.00 (**C_{11}**); 135.84 (**C_7**); 145.29 (**C_6**). Melting point: 84-88^{o}C.

Elemental Analysis (%): Calc. for $C_{84}H_{112}Cl_4N_6Rh_4$ (1759.30): C, 57.35; H, 6.42; N, 4.78; Found: C, 52.81; H, 7.02; N, 4.40. **MS** (ESI, m/z): 1759.40 $[M]^+$.

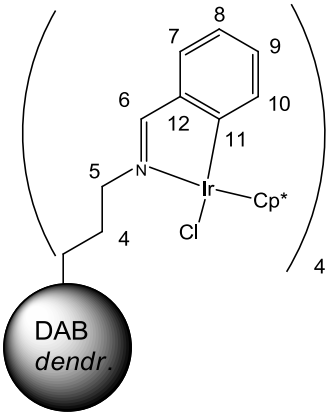

2.18: Red-orange solid. Yield = 0.17 g (50%). **IR** (KBr) ν(C=N) 1600 cm^{-1}. **^{1}H NMR** (400 MHz, $CDCl_3$) δ (ppm) = 1.56 (m, 4H, **H_{core}**); 1.62 (s, 60H, **Cp***); 2.21 (br m, 8H, **H_4**); 2.60

(br m, 4H, $\mathbf{H_{core}}$); 2.72 (br m, 8H, $\mathbf{H_3}$); 3.97 (br s, 8H, $\mathbf{H_5}$); 6.90 (t, 4H, $\mathbf{H_9}$); 7.07 (t, 4H, $\mathbf{H_8}$); 7.46 (m, 4H, $\mathbf{H_{10}}$); 7.66 (d, 4H, $\mathbf{H_7}$); 8.30 (s, 4H, $\mathbf{H_6}$).

$^{13}C\{^1H\}$-NMR (100 MHz, $CDCl_3$) δ (ppm) = 9.12 (**Cp***); 25.77 ($\mathbf{C_{core}}$); 27.90 ($\mathbf{C_4}$); 51.29 ($\mathbf{C_3}$); 53.53 ($\mathbf{C_{core}}$); 60.66 ($\mathbf{C_5}$); 121.73 ($\mathbf{C_9}$); 128.02 ($\mathbf{C_{10}}$); 130.27 ($\mathbf{C_{11}}$); 130.65 ($\mathbf{C_{12}}$); 131.34 ($\mathbf{C_8}$); 134.57 ($\mathbf{C_7}$); 146.39 ($\mathbf{C_6}$). Melting point: 200-202^{o}C.

Elemental Analysis (%): Calc. for $C_{84}H_{112}Cl_4Ir_4N_6$ (2116.54): C, 47.67; H, 5.33; N, 3.97; Found: C, 47.36; H, 5.27; N, 4.17. **MS** (ESI, m/z): 1059.32 $[M+2H^+]^{2+}$.

*5.2.6 General synthesis of the cyclometalated ruthenium(II), rhodium(III) and iridium(III) benzaldimine G2 metallodendrimers **2.22, 2.23 & 2.24**.*

The G2 benzaldimine dendritic ligand (**2.22:** 0.0649 g, 0.0440 mmol; **2.23:** 0.0379 g, 0.026 mmol; **2.24:** 0.0355 g, 0.0240 mmol), sodium acetate (**2.22:** 0.0577 g, 0.703 mmol; **2.23:** 0.0167 g, 0.200 mmol; **2.24:** 0.0158 g, 0.193 mmol) and the $[Ru(p\text{-cymene})Cl_2]_2$ (0.108 g, 0.176 mmol), $[Rh(\eta^5\text{-}C_5Me_5)Cl_2]_2$ (0.0617 g, 0.100 mmol) or $[Ir(\eta^5\text{-}C_5Me_5)Cl_2]_2$ (0.0762 g, 0.0956 mmol) dimer were stirred together in methanol (20.0 mL) for 24-48 hours at room temperature. After which the reaction mixture was filtered through Celite, and washed with methanol. The crude ruthenium(II) complex (**2.22**) was dissolved in acetone and filtered by gravity. This was repeated with DCM, the solvent was removed on the rotary evaporator and the solid was washed with diethyl ether to give the desired product as a golden-brown solid (**2.22**). The crude rhodium(III) (**2.23**) and iridium(III) (**2.24**) complexes were dissolved in a minimum amount of DCM followed by an excess of diethyl ether whereby a solid precipitated out of solution. The solid was filtered under vacuum to give the desired products as a yellow (**2.23**) or orange-yellow (**2.24**) solid.

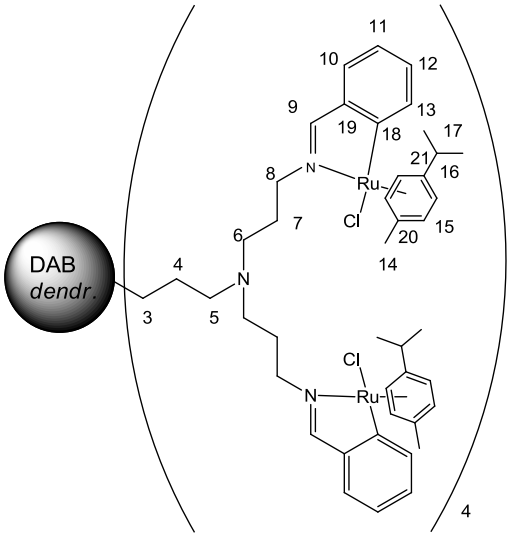

2.22: Golden-brown solid. Yield = 0.140 g (88%). **IR** (KBr) ν(C=N) 1600 cm^{-1}. **^{1}H NMR** (400 MHz, $CDCl_3$) δ (ppm) = 0.74 (br m, 4H, **H_{core}**); 0.99 (br m, 8H, **H_4**); 1.22 (br m, 72H, **H_{14},H_{17}**); 1.59 (br m, 16H, **H_7**); 1.96 (br m, 8H, **H_{16}**); 2.40 (br m, 28H, **H_{core}, H_3, H_6**); 3.74 (br m, 8H, **H_5**); 4.01-4.11 (br m, 16H, **H_8**); 4.75, 4.90, 5.32, 5.43 (br m, 32H, **H_{15}**); 6.87 (br m, 8H, **H_{10}**); 7.04 (br m, 8H, **H_{11}**); 7.32 (br m, 16H, **H_{12},H_{13}**); 8.05 (br s, 8H, **H_9**).

^{13}C{^{1}H}-NMR (100 MHz, $CDCl_3$) δ (ppm) = 18.86 (**C_{16}**); 21.16 (**C_{core}**); 22.22 (**C_{14}**); 22.44 (**C_{17}**); 23.28 (**C_4**); 30.92-31.48 (**C_{core},C_3,C_6**); 51.65 (**C_5**); 64.07 (**C_8**); 79.67, 81.45, 89.64, 91.64 (**C_{15}**); 100.81 (**C_{21}**); 102.97 (**C_{20}**); 122.09 (**C_{10}**); 127.56 (**C_{11}**); 128.46 (**C_{12}**); 128.95 (**C_{13}**); 129.26 (**C_{18}**); 138.98 (**C_{19}**); 145.31 (**C_9**). Melting point: 110-113°C.

Elemental Analysis (%): Calc. For $C_{176}H_{232}Cl_8N_{14}Ru_8$ (3636.05): C, 58.14; H, 6.43; N, 5.39; Found: C, 56.79; H, 6.16; N, 4.88. **MS** (ESI-HR, m/z): 569.01 $[M-6Cl]^+$, 873.22 $[M-4Cl]^+$.

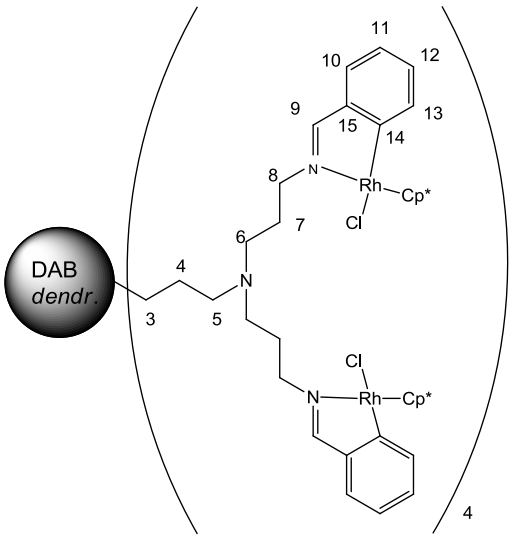

2.23: Yellow solid. Yield = 0.0800 g (58%). **IR** (KBr) ν(C=N) 1609 cm^{-1}. **^{1}H NMR** (400 MHz, $CDCl_3$) δ (ppm) = 1.37 (m, 4H, **H_{core}**); 1.57 (m, 8H, **H_4**); 1.63 (s, 120H, **Cp***); 1.81 (br m, 16H, **H_7**); 2.41-2.50 (br m, 20H, **H_{core}, H_3, H_5**); 2.94 (br m, 16H, **H_6**); 3.90-4.01 (splitting of br m, 16H, **H_8**); 7.38 (br m, 16H, **H_{11}, H_{12}**); 7.69 (br m, 16H, **H_{10},H_{13}**); 8.26 (s, 8H, **H_9**).

^{13}C{^{1}H}-NMR (100 MHz, $CDCl_3$) δ (ppm) = 9.34 (**Cp***); 24.79 (**C_{core}**); 28.47 (**C_7**); 29.69 (**C_{core}**); 30.34 (**C_4**); 51.8-52.19 (**$C_{3,5,6}$**); 59.72 (**C_8**); 126.95 (**C_{10}**); 128.04 (**C_{11}**); 128.57 (**C_{12}**); 129.48 (**C_{13}**); 130.48 (**C_{14}**); 136.39 (**C_{15}**); 146.49 (**C_9**). Melting point: 115-119^{o}C.

Elemental Analysis (%): Calc. for $C_{176}H_{240}Cl_8N_{14}Rh_8$ (3658.83 g/mol): C, 57.78; H, 6.61; N, 5.36; Found: C, 52.48; H, 6.30; N, 4.84. **MS** (ESI-HR, m/z): 574.22 $[M\text{-}6Cl]^{6+}$, 696.23 $[M\text{-}5Cl]^{5+}$.

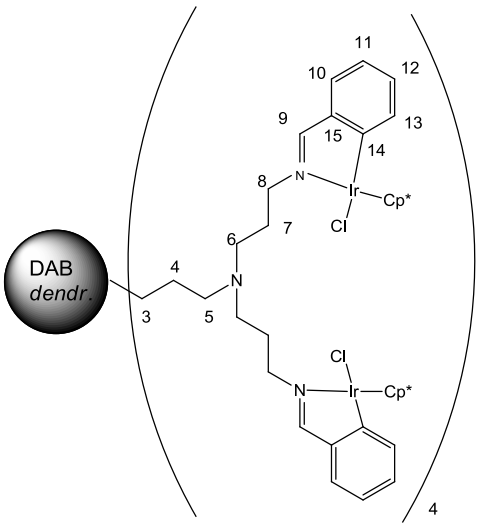

2.24: Orange-yellow solid. Yield = 0.0500 g (48%). **IR** (KBr) ν(C=N) 1600 cm^{-1}. **^{1}H NMR** (400 MHz, $CDCl_3$) δ (ppm) = 1.43 (m, 4H, **H_{core}**); 1.61 (m, 8H, **H_4**); 1.68 (s, 120H, **Cp***); 1.83 (br m, 16H, **H_7**); 2.42 (br m, 20H, **H_{core}, H_3, H_5**); 2.50 (br m, 16H, **H_6**); 4.02 (br m, 16H, **H_8**); 7.37 (t, 16H, **H_{11}, H_{12}**); 7.69 (d, 16H, **H_{10},H_{13}**); 8.26 (s, 8H, **H_9**).

^{13}C{^{1}H}-NMR (100 MHz, $CDCl_3$) δ (ppm) = 9.10 (**Cp***); 24.62 (**C_{core}**); 26.55 (**C_7**); 28.39 (**C_{core}**); 29.68 (**C_4**); 51.50-52.35 (**$C_{3,5,6}$**); 59.70 (**C_8**); 128.04 (**C_{10}**); 128.56 (**C_{11}**); 130.43 (**C_{12}**); 131.29 (**C_{14}**); 134.60 (**C_{13}**); 136.36 (**C_{15}**); 145.96 (**C_9**). Melting point: 121-123^{o}C

Elemental Analysis (%): Calc. For $C_{176}H_{240}Cl_8Ir_8N_{14}$ (4373.31): C, 48.30; H, 5.53; N, 4.48; Found: C, 45.29; H, 6.25; N, 4.40. **MS** (ESI-HR, m/z): 589.23 $[M-7Cl]^{7+}$, 693.31 $[M-6Cl]^{6+}$.

5.3 Synthesis of the cationic mononuclear and dendritic cyclometalated complexes containing PTA

*5.3.1 General synthesis of the cationic ruthenium(II), rhodium(III) and iridium(III) naphthaldimine mononuclear complexes **3.1, 3.2 & 3.3**.*

The naphthaldimine monomeric ligand (**3.1:** 0.115 g, 0.581 mmol; **3.2:** 0.0733 g, 0.372 mmol; **3.3:** 0.0739 g, 0.375 mmol) and sodium acetate (**3.1:** 0.0485 g, 0.591 mmol; **3.2:** 0.0301 g, 0.367 mmol; **3.3:** 0.0309 g, 0.377 mmol) was suspended in DCM or methanol (15.0 mL) followed by the addition of the $[Ru(p\text{-cymene})Cl_2]_2$ (0.178 g, 0.291 mmol), $[Rh(\eta\text{-}C_5Me_5)Cl_2]_2$ (0.114 g, 0.185 mmol) or $[Ir(\eta\text{-}C_5Me_5)Cl_2]_2$ (0.147 g, 0.185 mmol) dimer. The reaction mixture was allowed to stir for a couple of hours after which it was filtered through Celite. PTA (**3.1:** 0.0937 g, 0.596 mmol; **3.2:** 0.0573 g, 0.365 mmol; **3.3:** 0.0599 g, 0.381 mmol) was added to the reaction mixture and allowed to stir for a further 30-40 minutes. The solvent was removed on a rotary evaporator; the residue was dissolved in a minimum amount of acetone and filtered through Celite. A minimum amount of methanol was added followed by the addition of the $NaPF_6$ (**3.1:** 0.102 g, 0.604 mmol; **3.2:** 0.0616 g, 0.367 mmol; **3.3:** 0.0642 g, 0.382 mmol). This was stirred at 0^{o}C for about 30-40 minutes whereby a solid precipitated out of solution, which was then filtered under vacuum, washing with cold methanol and diethyl ether, to yield a orange-yellow (**3.2**) or light yellow (**3.3**) solid. The ruthenium(II) complex (**3.1**) did not precipitate out of solution therefore the solvent was removed on a rotary evaporator and the residue was dissolved in a minimum amount of DCM

followed by the addition of an excess amount of diethyl ether, whereby a solid precipitated out of solution. This was filtered under vacuum to yield a red-brown (**3.1**) solid.

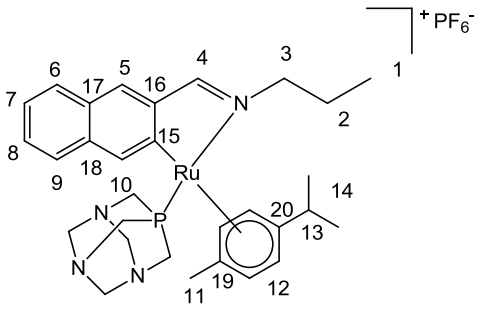

3.1: Red-brown solid. Yield = 0.0651 g (15%). **IR:** (KBr pellets), ν/cm^{-1}: 1602 (C=N), 801 (s, P–F). **^{1}H NMR** (400 MHz, acetone-d$_6$) δ (ppm) = 0.72 (d, 3H, **H$_{11}$**); 1.07 (d, 3H, **H$_{14}$**); 1.12 (t, 3H, **H$_1$**); 1.26 (m, 6H, **H$_{14}$**); 1.98, 2.16 (m, 2H, **H$_2$**); 2.51 (sep, 1H, **H$_{13}$**); 3.64 (d, 3H **PTA**); 4.05 (m, 2H, **H$_3$**); 4.08, 4.20, 4.30 (d, 9H **, PTA**); 5.86 (m, 2H, **H$_{12}$**); 5.92, 6.10 (d, 2H, **H$_{12}$**); 7.44 (t, 1H, **H$_8$**); 7.58 (t, 1H, **H$_8$**); 7.85, (d, 1H, **H$_9$**); 7.91 (d, 1H, **H$_6$**); 8.26 (s, 1H, **H$_5$**) 8.28 (s, 1H, **H$_{10}$**); 8.61 (s, 1H, **H$_4$**).

^{13}C{^{1}H}-NMR (100 MHz, acetone-d$_6$) δ (ppm) = 10.68 (**C$_1$**); 18.85 (**C$_{11}$**); 20.83, 22.70 (**C$_{14}$**); 24.09 (**C$_2$**); 31.21 (**C$_{13}$**); 51.51, 51.68 (**PTA**); 52.09-52.27 (**C$_3$**); 68.81, 72.32, 72.39 (**PTA**); 86.34,87.03,87.59, 92.55 (**C$_{12}$**); 119.91 (**C$_{20}$**); 121.83 (**C$_{19}$**); 123.14 (**C$_{17}$**); 124.72 (**C$_7$**); 125.97 (**C$_9$**); 128.20 (**C$_8$**); 129.02 (**C$_6$**); 129.90 (**C$_5$**); 130.74 (**C$_{15}$**); 134.91 (**C$_{18}$**); 138.16 (**C$_{10}$**); 146.02 (**C$_{16}$**); 174.47 (**C$_4$**). Melting point: 164-168^{o}C.

^{31}P{^{1}H}-NMR (MHz, acetone-d$_6$) δ (ppm) = singlet; -39.96 (**PTA**); septet; -144.19 (**PF$_6$**).

Elemental Analysis (%): Calc. For $C_{30}H_{40}F_6N_4P_2Ru$ (733.68): C, 49.11; H, 5.50; N, 7.64; Found: C, 47.96; H, 6.03; N, 5.41. **MS** (EI, m/z): 429.05 $[M-(PF_6+PTA)]^+$.

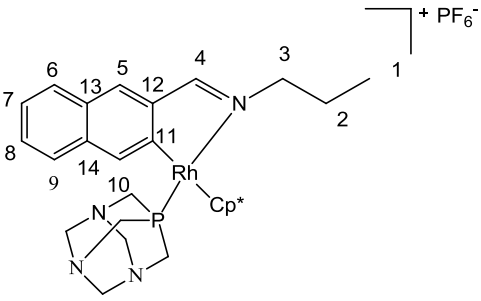

3.2: Orange-yellow solid. Yield = 0.122 g (47%). **IR:** (KBr pellets), ν/cm^{-1}: 1607 (C=N), 843 (s, P–F). **^{1}H NMR** (400 MHz, acetone-d$_6$) δ (ppm) = 1.15 (t, 3H, **H$_1$**); 1.91 (s, 15H, **Cp***);

1.98 (m, 2H, **H_2**); 3.97 (t, 2H **H_3**) 3.68, 4.11, 4.27, 4.34 (d ,12H, **PTA**); 7.51, 7.63 (t, 2H, **H_7**,**H_8**); 8.01, 8.03 (d, 2H, **H_6**,**H_9**); 8.07 (s, 1H, **H_5**); 8.36 (s, 1H, **H_{10}**); 8.73 (s, 1H, **H_4**).

$^{13}C\{^1H\}$-NMR (100 MHz, acetone-d_6) δ (ppm) = 9.01 (**Cp***); 10.66 (**C_1**); 23.73 (**C_2**); 49.77, 49.92 (**PTA**); 63.95 (**C_3**); 72.30, 72.36 (**PTA**); 125.34 (**C_7**); 126.44 (**C_9**); 128.47 (**C_8**); 129.08 (**C_6**); 130.93 (**C_{11}**); 131.07 (**C_{13}**); 134.64 (**C_{14}**); 134.68 (**C_5**); 134.97 (**C_{12}**); 135.54 (**C_{10}**); 174.59 (**C_4**). Melting point: 240-242^{o}C.

$^{31}P\{^1H\}$-NMR (MHz, acetone-d_6) δ (ppm) = doublet; -44.97 (**PTA**); septet; -144.24 (**PF_6**).

Elemental Analysis (%): Calc. For $C_{30}H_{41}F_6N_4P_2Rh$ (736.53): C, 48.92; H, 5.61; N, 7.61; Found: C, 48.25; H, 6.58; N, 7.16. **MS** (EI, m/z): 434.12 $[M-(PF_6+PTA)]^+$.

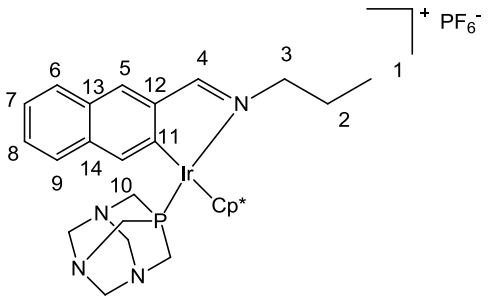

3.3: Light yellow solid. Yield = 0.102 g (34%). **IR:** (KBr pellets), ν/cm^{-1}: 1602 (C=N), 842 (s, P–F). **^1H NMR** (400 MHz, acetone-d_6) δ (ppm) = 1.16 (t, 3H, **H_1**); 2.00 (s, 15H, **Cp***); 2.05 (sex, 2H, **H_2**); 3.65 (d, 3H **PTA**); 4.04 (m, 2H, **H_3**); 4.08, 4.22, 4.36 (d, 9H, **PTA**); 7.49, 7.60 (t, 2H, **H_7**,**H_8**); 7.95, 7.98 (d, 2H, **H_6**,**H_9**); 8.08 (s, 1H, **H_5**); 8.40 (s, 1H, **H_{10}**); 8.85 (s, 1H, **H_4**).

$^{13}C\{^1H\}$-NMR (100 MHz, acetone-d_6) δ (ppm) = 8.71 (**Cp***); 10.45 (**C_1**); 23.76 (**C_2**); 48.60, 48.82 (**PTA**); 65.94 (**C_3**); 72.40, 72.47 (**PTA**); 124.93 (**C_7**); 126.38 (**C_9**); 128.52 (**C_8**); 129.22 (**C_6**); 130.98 (**C_{10}**); 130.61 (**C_{11}**); 133.65 (**C_{14}**); 133.68 (**C_5**); 136.29 (**C_{13}**); 147.10 (**C_{12}**); 177.44 (**C_4**). Melting point: 186-188^{o}C .

$^{31}P\{^1H\}$-NMR (MHz, acetone-d_6) δ (ppm) = singlet; -79.47 (**PTA**); septet; -144.22 (**PF_6**).

Elemental Analysis (%): Calc. For $C_{30}H_{41}F_6N_4IrP_2$ (825.84): C, 43.63; H, 5.00; N, 6.78; Found: C, 42.90; H, 5.26; N, 5.96. **MS** (EI, m/z): 524.19 $[M-(PF_6+PTA)]^+$.

*5.3.2 General synthesis of the cationic ruthenium(II), rhodium(III) and iridium(III) naphthaldimine G1 metallodendrimers **3.4, 3.5 & 3.6**.*

The G1 naphthaldimine dendritic ligand (**3.4:** 0.101 g, 0.116 mmol; **3.5:** 0.0693 g, 0.0797 mmol; **3.6:** 0.0145 g, 0.0167 mmol) and sodium acetate (**3.4:** 0.0394 g, 0.480 mmol; **3.5:** 0.0260 g, 0.317 mmol; **3.6:** 0.0056 g, 0.0683 mmol) was suspended in methanol or ethanol (20.0 mL) followed by the addition of the $[Ru(p\text{-cymene})Cl_2]_2$ (0.143 g, 0.233 mmol), $[Rh(\eta\text{-}C_5Me_5)Cl_2]_2$ (0.0990 g, 0.160 mmol) or $[Ir(\eta\text{-}C_5Me_5)Cl_2]_2$ (0.0266 g, 0.0334 mmol) dimer. The reaction mixture was allowed to stir overnight after which it was filtered through Celite. The PTA (**3.4:** 0.0761 g, 0.484 mmol; **3.5:** 0.0489 g, 0.311 mmol; **3.6:** 0.0110 g, 0.0700 mmol) was added to the reaction mixture and allowed to stir for a further 30-40 minutes. The solvent was removed and the residue was dissolved in acetone and filtered through Celite. The solvent was removed again and a minimum amount of methanol was added followed by the addition of the $NaPF_6$ (**3.4:** 0.0818 g, 0.487 mmol; **3.5:** 0.0534 g, 0.318 mmol; **3.6:** 0.0119 g, 0.0708 mmol). This was stirred at 0°C for about 30-40 minutes, whereby a solid precipitated out, which was then filtered under vacuum, washing with cold ethanol and diethyl ether. The crude product was dissolved in acetone, filtered through Celite and repeated with DCM. The DCM was reduced and an excess of diethyl ether was added whereby a solid precipitated out of solution and filtered by gravity to give the desired product as a golden-brown (**3.4**), orange-yellow (**3.5**) or orange (**3.6**) solid.

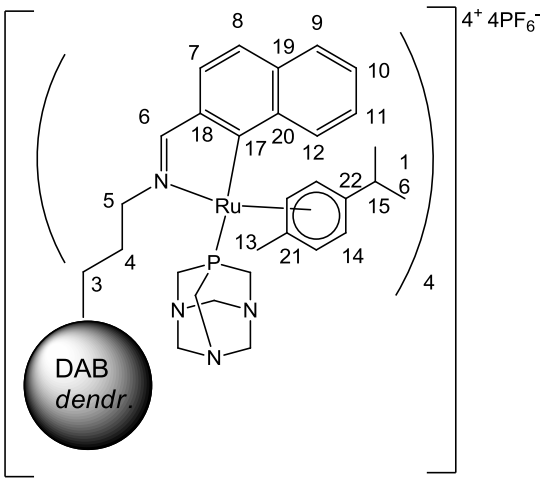

3.4: Golden-brown solid. Yield = 0.144 g (40%). **IR:** (KBr pellets), ν/cm^{-1}: 1600 (C=N), 841 (s, P–F). **^{1}H NMR** (400 MHz, acetone-d_6) δ (ppm) = 0.74 (s, 12H, $\mathbf{H_{13}}$); 0.97 (t, 4H, $\mathbf{H_{core}}$); 1.18 (d, 24H, $\mathbf{H_{16}}$); 2.42 (br m, 20H, $\mathbf{H_{core}}$,$\mathbf{H_3}$,$\mathbf{H_4}$); 2.70 (sep, 4H, $\mathbf{H_{15}}$); 3.91 (br m, 8H, $\mathbf{H_5}$); 4.32, 4.50 (d, 48H **, PTA**); 5.01 (br m, 4H, $\mathbf{H_{14}}$); 5.17 (br m, 4H, $\mathbf{H_{14}}$); 5.85 (br m, 8H, $\mathbf{H_{14}}$);

7.29 (br m, 4H, **H_9**); 7.46 (br t, 4H, **H_{10}**); 8.07 (br m, 8H, **H_8,H_{11}**); 7.99 (br m, 4H, **H_7**) 8.37 (br m, 4H, **H_{12}**); 8.72 (br s, 4H, **H_6**).

$^{13}C\{^1H\}$-NMR (100 MHz, acetone-d_6) δ (ppm) = 18.21 (**C_{13}**); 20.40 (**C_{16}**); 22.86 (**C_{core}**); 30.15-31.00 (**C_{core},C_3,C_4**); 33.50 (**C_{15}**); 51.50, 52.32 (**PTA**); 63.10 (**C_5**); 72.33, 72.90 (**PTA**); 79.73, 82.02, 88.36, 90.13 (**C_{14}**); 123.66 (**C_9**); 124.56 (**C_{20}**); 126.18 (**C_8**); 127.33 (**C_{11}**); 128.83 (**C_{10}**); 129.17 (**C_7**); 129.56 (**C_{12}**); 130.45 (**C_{17}**); 134.89 (**C_{19}**); 137.05 (**C_{18}**); 175.14 (**C_6**).

$^{31}P\{^1H\}$-NMR (MHz, acetone-d_6) δ (ppm) = singlet; -30.45 (**PTA**); septet; -144.14 (**PF_6**).

Elemental Analysis (%): Calc. For $C_{124}H_{164}F_{24}N_{18}P_8Ru_4$ (3014.81): C, 49.40; H, 5.48; N, 8.36; Found: C, 47.29; H, 5.76; N, 5.36. **MS** (HR-ESI, m/z): 626.16 $[M\text{-}4PF_6\text{+}4H_2O]^{4+}$.

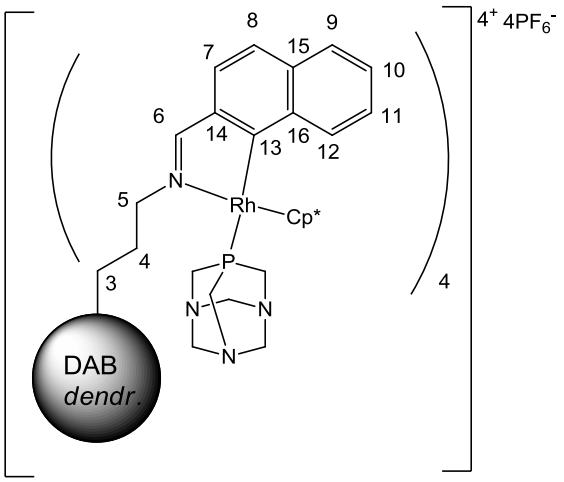

3.5: Orange-yellow solid. Yield = 0.0138 g (7%). **IR:** (KBr pellets), ν/cm^{-1}: 1613 (C=N), 844 (s, P–F). **^1H NMR** (400 MHz, acetone-d_6) δ (ppm) = 1.60 (m, 4H, **H_{core}**); 1.72 (s, 60H, **Cp***); 2.30 (br m, 8H, **H_4**) 3.20 (br m, 12H, **H_{core},H_3**); 3.66-3.70 (m, 12H, **PTA**); 3.96 (br m, 8H, **H_5**); 4.03-4.31 (m, 36H, **PTA**); 7.49 (br m, 4H, **H_{11}**); 7.62 (br m, 4H, **H_9**); 7.94-8.14 (br m, 8H, **H_7,H_8**); 8.33 (br m, 4H, **H_{10}**); 8.58 (br m, 4H, **H_{12}**); 8.71 (br s, 4H, **H_6**).

$^{13}C\{^1H\}$-NMR (100 MHz, acetone-d_6) δ (ppm) = 9.09 (**Cp***); 9.60 (**C_{core}**); 24.01 (**C_4**); 49.79,49.95 (**PTA**); 50.81-51.23 (**C_{core},C_3**); 59.22 (**C_5**); 72.33 (**PTA**); 123.92 (**C_{11}**); 125.31 (**C_{14}**); 126.43 (**C_8**); 127.28 (**C_9**); 128.47 (**C_{15}**); 128.80 (**C_{16}**); 129.14 (**C_7**); 130.54 (**C_{13}**); 131.06 (**C_{12}**); 133.76 (**C_{10}**); 174.85 (**C_6**). Melting point: 201-204°C.

$^{31}P\{^1H\}$-NMR (MHz, acetone-d_6) δ (ppm) = doublet; -44.32 (**PTA**); septet; -144.14 (**PF_6**).

Elemental Analysis (%): Calc. For $C_{124}H_{168}F_{24}N_{18}P_8Rh_4$ (3026.20): C, 49.22; H, 5.60; N, 8.33; Found: C, 47.23; H, 6.70; N, 5.94. **MS** (HR-ESI, m/z): 533.22 $[M\text{-}4PF_6\text{-}2PTA)]^{4+}$.

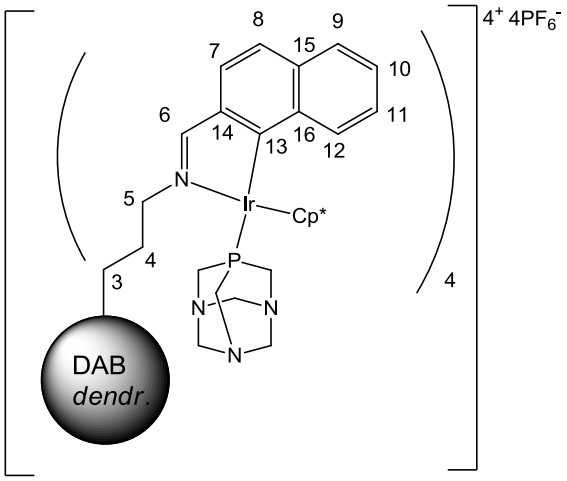

Orange solid. Yield = 0.0300 g (53%). **IR:** (KBr pellets), ν/cm^{-1}: 1604 (C=N), 843 (s, P–F). **^{1}H NMR** (400 MHz, acetone-d_6) δ (ppm) = 1.30 (m, 4H, **H_{core}**); 1.75 (s, 60H, **Cp***); 2.20 (br m, 8H, **H_4**); 3.66 (br m, 12H, **H_{core},H_3**); 4.04 (br m, 8H, **H_5**); 4.25, 4.49, 4.64 (d, 48H, **PTA**); 7.51 (br m, 4H, **H_8**); 7.61 (br m, 4H, **H_7**); 7.92 (br m, 8H, **H_9,H_{10}**); 8.13 (br m, 8H, **H_{11}**); 8.38 (br m, 4H, **H_{12}**); 8.81 (br s, 4H, **H_6**).

^{13}C{^{1}H}-NMR (100 MHz, acetone-d_6) δ (ppm) = 8.81 (**Cp***); 9.32 (**C_{core}**); 28.01 (**C_4**); 48.88, 49.28 (**C_{core},C_3**); 50.91 (**C_5**); 51.47 (**PTA**); 72.40 (**PTA**); 124.93 (**C_8**); 122.34 (**C_{16}**); 126.38 (**C_{11}**); 127.73 (**C_{15}**); 128.55 (**C_7**); 129.27 (**C_{10}**); 129.55 (**C_9**); 131.09 (**C_{13}**); 133.66 (**C_{12}**); 136.27 (**C_{14}**); 177.50 (**C_6**). Melting point: 233-235^{o}C.

^{31}P{^{1}H}-NMR (MHz, acetone-d6) δ (ppm) = singlet; -79.09 (**PTA**); septet; -144.12 (**PF_6**).

Elemental Analysis (%): Calc. For $C_{124}H_{168}F_{24}Ir_4N_{18}P_8$ (3383.44): C, 44.02; H, 5.00; N, 7.45; Found: C, 41.38; H, 5.61; N, 5.84. **MS** (HR-ESI, m/z): 1391.44 $[M\text{-}2PF_6\text{-}2PTA)]^{4+}$.

*5.3.3 General synthesis of the cationic ruthenium(II), rhodium(III) and iridium(III) naphthaldimine G2 metallodendrimers **3.7, 3.8 & 3.9**.*

The G2 naphthaldimine dendritic ligand (**3.7:** 0.0773 g, 0.0412 mmol; **3.8:** 0.103 g, 0.0550 mmol; **3.9:** 0.110 g, 0.0584 mmol) and sodium acetate (**3.7:** 0.0271 g, 0.330 mmol; **3.8:** 0.0371 g, 0.452 mmol; **3.9:** 0.0385 g, 0.469 mmol) was suspended in methanol or ethanol

(20.0 mL) followed by the addition of the $[Ru(p\text{-cymene})Cl_2]_2$ (0.101 g, 0.165 mmol), $[Rh(\eta\text{-}C_5Me_5)Cl_2]_2$ (0.135 g, 0.219 mmol) or $[Ir(\eta\text{-}C_5Me_5)Cl_2]_2$ (0.186 g, 0.234 mmol) dimer. The reaction mixture was allowed to stir for 24-48 hours after which it was filtered through Celite. PTA (**3.7:** 0.0518 g, 0.330 mmol; **3.8:** 0.0716 g, 0.456 mmol; **3.9:** 0.0739 g, 0.470 mmol) was added to the reaction mixture and allowed to stir for a further 30-40 minutes. The solvent was removed, the residue dissolved in a minimum amount of acetone and filtered through Celite. The solvent was removed once again, a minimum amount of methanol was added followed by the addition of $NaPF_6$ (**3.7:** 0.0554 g, 0.330 mmol; **3.8:** 0.0775 g, 0.461 mmol; **3.9:** 0.0792 g, 0.472 mmol). This was stirred at 0^oC for about 30-40 minutes, whereby a solid precipitated out, which was then filtered under vacuum, washing with cold methanol and diethyl ether. The crude product was dissolved in acetone, filtered through Celite and repeated with DCM. The DCM was then reduced and an excess of diethyl ether was added whereby a solid precipitated out and filtered under vacuum to yield a golden brown (**3.7**), orange-yellow (**3.8**) or yellow (**3.9**) solid.

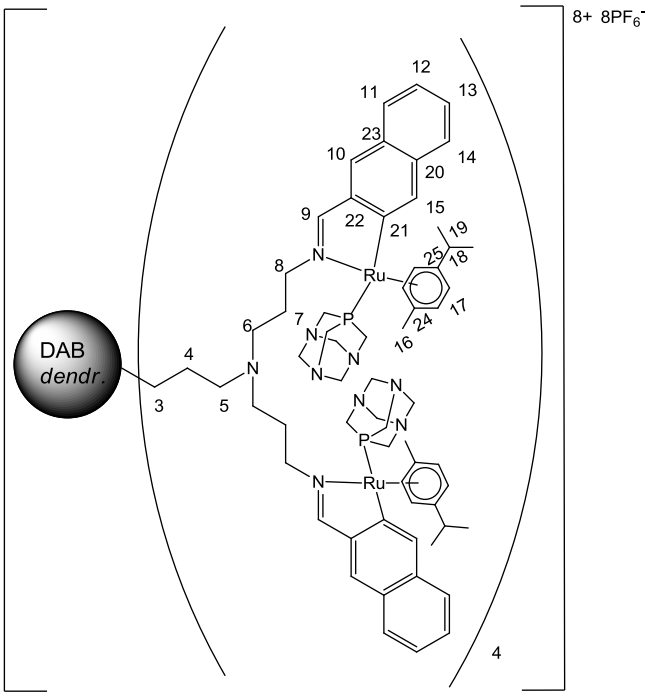

3.7: Golden brown solid. Yield = 0.100 g (39%). **IR:** (KBr pellets), ν/cm^{-1}: 1603 (C=N), 835 (s, P–F). **^{1}H NMR** (400 MHz, acetone-d_6) δ (ppm) = 0.71 (br m, 4H, $\mathbf{H_{core}}$); 0.99 (br m, 32H, $\mathbf{H_4}$,$\mathbf{H_{16}}$); 1.46 (br m, 48H, $\mathbf{H_{19}}$); 1.84 (br m, 16H, $\mathbf{H_7}$); 2.10 (br m, 8H, $\mathbf{H_{18}}$); 2.44 (br m, 32H, $\mathbf{H_{core}}$,$\mathbf{H_3}$, $\mathbf{H_5}$, $\mathbf{H_6}$); 4.13 (br m, 16H, $\mathbf{H_8}$); 4.32, 4.43, 4.57 (d, 96H, **PTA**); 4.95 (br m, 8H, $\mathbf{H_{17}}$); 5.19 (br m, 8H, $\mathbf{H_{17}}$); 5.86 (br m, 16H, $\mathbf{H_{17}}$); 7.54 (br m, 8H, $\mathbf{H_{12}}$,$\mathbf{H_{13}}$); 7.78 (br m, 4H, $\mathbf{H_{14}}$); 7.94 (br m, 8H, $\mathbf{H_{10}}$,$\mathbf{H_{11}}$); 8.32 (br m, 4H, $\mathbf{H_{15}}$); 8.57 (br s, 8H, $\mathbf{H_9}$).

$^{13}C\{^1H\}$-NMR (100 MHz, acetone-d_6) δ (ppm) = 18.42 (**C_{16}**); 20.42 (**C_{core}**); 21.38 (**C_{19}**); 22.88 (**C_4**); 30.78 (**C_7**); 42.17 (**C_{18}**); 51.42 (**C_{core}**); 51.89 (**C_3**); 52.19 (**C_5**); 52.72 (**C_6**); 58.60-72.86 (**PTA, C_8**); 90.12, 92.03, 94.72 (**C_{17}**); 123.60 (**C_{12}**); 123.75 (**C_{13}**); 126.21 (**C_{14}**); 126.34 (**C_{25}**); 127.26 (**C_{10}**); 127.73 (**C_{11}**); 128.84 (**C_{15}**); 124.80 (**C_{23}**); 130.38 (**C_{21}**); 133.67 (**C_{22}**); 134.75 (**C_{20}**); 136.51 (**C_{24}**); 175.90 (**C_9**). Melting point: 190-193^oC.

$^{31}P\{^1H\}$-NMR (MHz, acetone-d6) δ (ppm) = singlet; -36.68 (**PTA**); septet; -144.11 (**PF_6**).

Elemental Analysis (%): Calc. For $C_{256}H_{344}F_{48}N_{38}P_{16}Ru_8$ (6169.85): C, 49.84; H, 5.62; N, 8.63; Found: C, 51.96; H, 6.46; N, 8.58. **MS** (HR-ESI, m/z): 585.14 $[M\text{-}8PF_6\text{-}2PTA]^{8+}$.

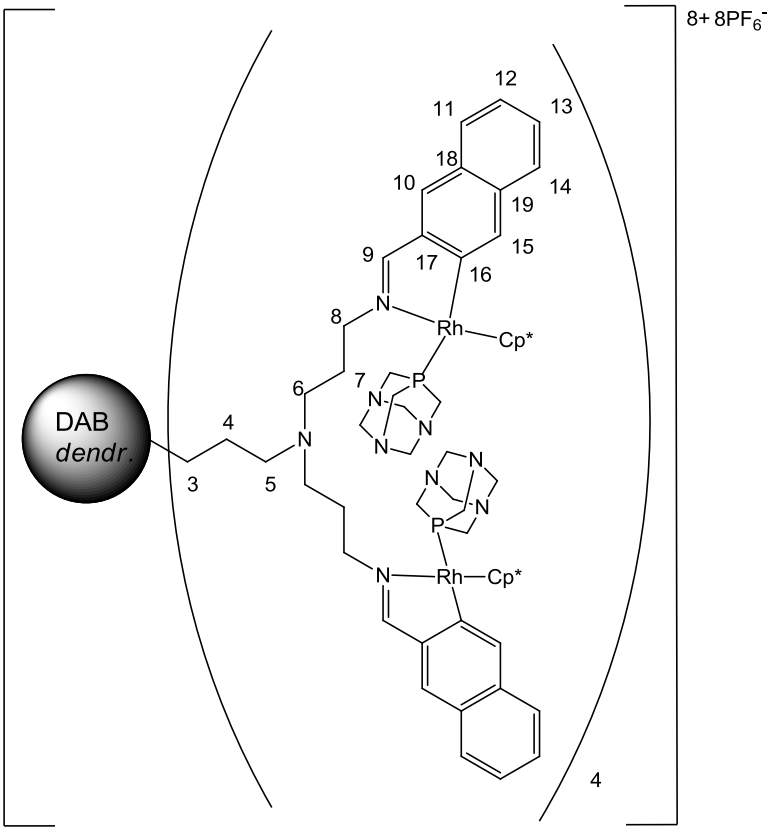

3.8: Orange-yellow solid. Yield = 0.158 g (50%). **IR:** (KBr pellets), ν/cm^{-1}: 1609 (C=N), 843 (s, P–F). **^1H NMR** (400 MHz, acetone-d_6) δ (ppm) = 1.58 (br m, 4H, **H_{core}**); 1.70 (s, 120H, **Cp***); 2.10 (br m, 24H, **H_4,H_7**); 3.00 (br m, 28H, **H_{core},H_3,H_6**); 3.66 (br d, 32H, **PTA**); 3.72 (br m, 8H, **H_5**); 4.03 (br m, 16H, **H_8**); 4.10, 4.28, 4.31 (d, 64H, **PTA**); 7.45 (br m, 8H, **H_{12}**); 7.61 (br m, 8H, **H_{13}**); 7.88 (br m, 8H, **H_{11}**); 7.98 (m, 8H, **H_{14}**); 8.02 (br m, 8H, **H_{10}**); 8.33 (br m, 8H, **H_{15}**); 8.71 (br s, 8H, **H_9**).

$^{13}C\{^1H\}$-NMR (100 MHz, acetone-d_6) δ (ppm) = 8.66 (**C_{core}**); 9.12 (**Cp***); 27.29-27.63 (**C_4,C_7**); 49.83, 49.92 (**PTA**); 50.69 (**C_5**); 52.35 (**C_{core}**); 54.03 (**C_3**); 60.21 (**C_8**); 72.33 (**PTA**);

123.24 (**C_{15}**); 125.30 (**C_{13}**); 126.44 (**C_{14}**); 127.17 (**C_{18}**); 128.04 (**C_{19}**); 128.47 (**C_{12}**); 129.12 (**C_{11}**); 131.01 (**C_{16}**); 135.49 (**C_{17}**); 174.70 (**C_9**). Melting point: 211-214°C.

$^{31}P\{^1H\}$-NMR (MHz, acetone-d_6) δ (ppm) = doublet; -44.34 (**PTA**); septet; -144.15 (**PF_6**).

Elemental Analysis (%): Calc. For $C_{256}H_{352}F_{48}N_{38}P_{16}Rh_8$ (6192.63): C, 49.65; H, 5.73; N, 8.60; Found: C, 48.70; H, 6.56.; N, 6.45. **MS** (HR-ESI, m/z): 587.15 $[M\text{-}8PF_6\text{-}2PTA]^{8+}$.

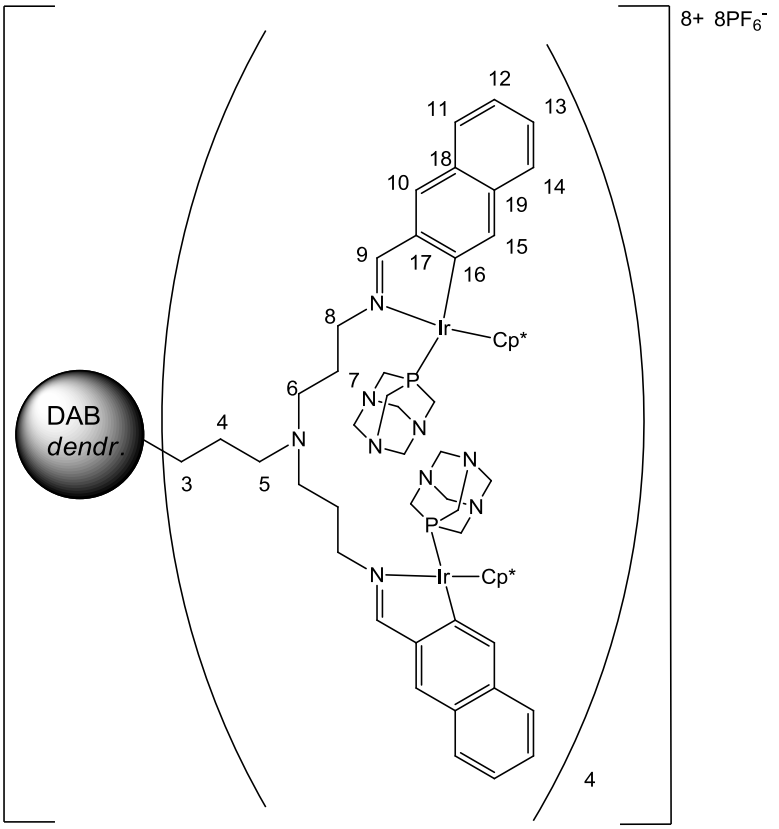

3.9: Yellow solid. Yield = 0.117 g (30%). **IR:** (KBr pellets), ν/cm^{-1}: 1602 (C=N), 843 (s, P–F). **^1H NMR** (400 MHz, acetone-d_6) δ (ppm) = 1.64 (m, 4H, **H_{core}**); 1.96 (s, 120H, **Cp***); 2.39 (br m, 20H, **H_{core},H_3,H_4**); 3.09 (br m, 32H, **H_6,H_7**); 3.58 (br m, 24H, **PTA**); 3.66 (br m, 8H, **H_5**); 4.01 (br m, 16H, **H_8**); 4.33, 4.40 (br m, 72H, **PTA**); 7.45 (br m, 8H, **H_{14}**); 7.58 (br m, 8H, **H_{11}**); 7.86 (br m, 8H, **H_{13}**); 7.96 (br m, 8H, **H_{12}**); 8.03 (br m, 8H, **H_{10}**); 8.37 (br m, 8H, **H_{15}**); 8.84 (br s, 8H, **H_9**).

$^{13}C\{^1H\}$-NMR (100 MHz, acetone-d_6) δ (ppm) = 8.81 (**Cp***); 9.32 (**C_{core}**); 22.64 (**C_{core}**); 23.86 (**C_3**); 25.61 (**C_4**); 48.64, 48.84 (**PTA**); 50.37 (**C_5**); 51.36 (**C_6**); 51.47 (**C_7**); 62.35 (**C_8**); 72.36 (**PTA**); 124.91 (**C_{14}**); 126.38 (**C_{12}**); 128.53 (**C_{11}**); 129.26 (**C_{13}**); 130.43 (**C_{16}**); 131.17 (**C_{15}**); 133.69 (**C_{10}**); 137.25 (**C_{17}**); 177.45 (**C_9**). Melting point: 247-250°C.

$^{31}P\{^{1}H\}$-NMR (MHz, acetone-d_6) δ (ppm) = singlet; -79.09 (**PTA**); septet; -144.09 (**PF_6**).

Elemental Analysis (%): Calc. For $C_{256}H_{352}F_{48}Ir_8N_{38}P_{16}$ (6907.11): C, 44.52; H, 5.14; N, 7.71; Found: C, 41.81; H, 5.22; N, 5.85. **MS** (HR-ESI, m/z): 1215.49 $[M\text{-}4PF_6\text{-}PTA]^{4+}$.

5.4 Synthesis of the cationic ferrocenyl-pyridine heteronuclear complexes

*5.4.1 General synthesis of the cationic rhodium(III) & iridium(III)-ferrocenyl naphthaldimine mononuclear complexes **3.10 & 3.11**.*

The naphthaldimine monomeric ligand (**3.10:** 0.0224 g, 0.114 mmol; **3.11:** 0.0259 g, 0.131 mmol) and sodium acetate (**3.10:** 0.0095 g, 0.116 mmol; **3.11:** 0.0110 g, 0.134 mmol) were suspended in methanol (15.0 mL) followed by the addition of the $[Rh(\eta\text{-}C_5Me_5)Cl_2]_2$ (0.0359 g, 0.0581 mmol) or $[Ir(\eta\text{-}C_5Me_5)Cl_2]_2$ (0.0525 g, 0.0659 mmol) dimer. The reaction mixture was allowed to stir for 2 hours, after which it was filtered through Celite. The 4-ferrocenylpyridine (**3.10:** 0.0306 g, 0.116 mmol; **3.11:** 0.0347 g, 0.132 mmol) was added to the reaction mixture and allowed to stir for a further 30 minutes. The solvent was removed, the residue dissolved in acetone and filtered through Celite. The solvent was once again removed and the residue dissolved in a minimum amount of methanol, followed by the addition of the $NaPF_6$ (**3.10:** 0.0197 g, 0.117 mmol; **3.11:** 0.0229 g, 0.136 mmol). This was stirred at 0°C for about 30-60 minutes, whereby a solid precipitated out, which was then filtered under vacuum, washing with cold methanol and diethyl ether to yield the desired product as dark red solids.

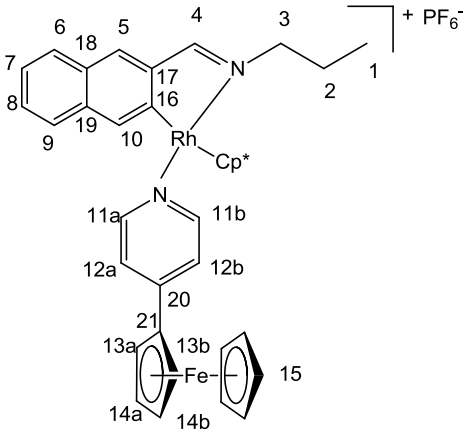

3.10: Dark red solid. Yield = 0.0273 g (28%). **IR:** (KBr pellets), ν/cm^{-1}: 1611 (C=N), 841 (s, P–F). **^{1}H NMR** (400 MHz, acetone-d$_6$) δ (ppm) = 1.11 (t, 3H, **H$_1$**); 1.77 (s, 15H, **Cp***); 2.07 (m, 2H, **H$_2$**); 4.00 (s, 5H, **H$_{15}$**); 4.36 (t, 2H, **H$_3$**); 4.55 (m, 2H, **H$_{14}$**); 4.89 (m, 2H, **H$_{13}$**); 7.49 (t, 1H, **H$_7$**); 7.52 (d, 2H, **H$_{12}$**); 7.64 (t, 1H, **H$_8$**); 7.92 (d, 1H, **H$_6$**); 8.09 (d, 1H, **H$_9$**); 8.17 (s, 1H, **H$_5$**); 8.36 (d, 2H, **H$_{11}$**); 8.47 (s, 1H, **H$_{10}$**); 8.74 (s, 1H, **H$_6$**).

^{13}C{^{1}H}-NMR (100 MHz, acetone-d$_6$) δ (ppm) = 8.44 (**Cp***); 10.49 (**C$_1$**); 23.00 (**C$_2$**); 61.35 (**C$_3$**); 67.35, 67.61 (**C$_{13}$**); 70.15 (**C$_{15}$**); 71.54 (**C$_{14}$**); 122.53 (**C$_{12}$**); 124.95 (**C$_7$**); 125.10 (**C$_{11}$**); 126.79 (**C$_9$**); 127.98 (**C$_8$**); 129.02 (**C$_6$**); 129.44 (**C$_5$**); 131.06 (**C$_{16}$**); 133.00 (**C$_{10}$**); 136.29 (**C$_{17}$**); 147.30 (**C$_{19}$**); 148.23 (**C$_{18}$**); 152.04 (**C$_{20}$**); 152.81 (**C$_{21}$**); 175.30 (**C$_4$**). Melting point: 239-243^{o}C.

Elemental Analysis (%): Calc. For $C_{39}H_{42}F_6FeN_2PRh$ (842.49): C, 55.60; H, 5.02; N, 3.33; Found: C, 55.00; H, 5.96; N, 2.72. **MS** (EI, m/z): 295.05 [M-PF$_6$-(Fc-py)-Cp*]$^{2+}$.

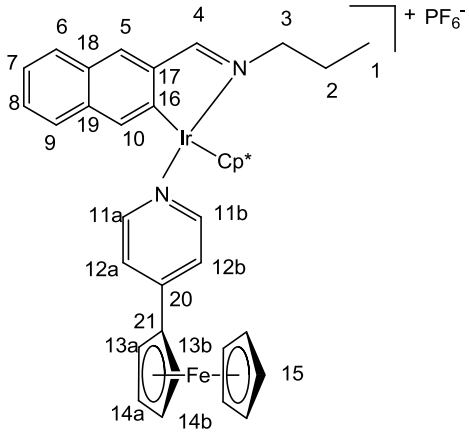

3.11: Dark red solid. Yield = 0.0455 g (38%). **IR:** (KBr pellets), ν/cm^{-1}: 1611 (C=N), 841 (s, P–F). **^{1}H NMR** (400 MHz, acetone-d$_6$) δ (ppm) = 1.11 (t, 3H, **H$_1$**); 1.79 (s, 15H, **Cp***); 2.05 (m, 2H, **H$_2$**); 3.98 (s, 5H, **H$_{15}$**); 4.43 (t, 2H, **H$_3$**); 4.55 (s, 2H, **H$_{14}$**); 4.88 (s, 2H, **H$_{13}$**); 7.43 (d, 2H, **H$_{12}$**); 7.47 (t, 1H, **H$_7$**); 7.60 (t, 1H, **H$_8$**); 7.88 (d, 1H, **H$_6$**); 8.04 (d, 1H, **H$_9$**); 8.21 (s, 1H, **H$_5$**); 8.35 (s, 1H, **H$_{10}$**); 8.38 (d, 2H, **H$_{11}$**); 8.91 (s, 1H, **H$_6$**).

^{13}C NMR (100 MHz, acetone-d$_6$) δ (ppm) = 8.16 (**Cp***); 10.38 (**C$_1$**); 23.01 (**C$_2$**); 62.79 (**C$_3$**); 67.38, 67.68 (**C$_{13}$**); 70.20 (**C$_{15}$**); 71.70, 71.73 (**C$_{14}$**); 122.88 (**C$_{12}$**); 124.66 (**C$_7$**); 125.00 (**C$_{11}$**); 126.72 (**C$_9$**); 128.08 (**C$_8$**); 129.13 (**C$_6$**); 129.75 (**C$_5$**); 130.71 (**C$_{16}$**); 131.95 (**C$_{10}$**); 137.06 (**C$_{17}$**); 147.88 (**C$_{19}$**); 149.00 (**C$_{18}$**); 152.94 (**C$_4$**); 153.54 (**C$_{20}$**); 177.46 (**C$_{21}$**). Melting point: 267-268^{o}C.

Elemental Analysis (%): Calc. for $C_{39}H_{42}F_6FeIrN_2P$ (931.80 g/mol): C, 50.27; H, 4.54; N, 3.01; Found: C, 50.00; H, 4.59; N, 2.65. **MS** (EI, m/z): 519.10 $[M\text{-}PF_6\text{-}(Fc\text{-}py)]^+$.

*5.4.2 General synthesis of the cationic rhodium(III) and iridium(III)-ferrocenyl naphthaldimine G1 metallodendrimers **3.12 & 3.13***

The naphthaldimine G1 dendritic ligand (**3.12:** 0.0106 g, 0.0122 mmol; **3.13:** 0.0137 g, 0.0158 mmol) and sodium acetate (**3.12:** 0.0044 g, 0.0536 mmol; **3.13:** 0.0052 g, 0.0634 mmol) were suspended in methanol (10.0 mL) followed by the addition of the $[Rh(\eta\text{-}C_5Me_5)Cl_2]_2$ (0.0155 g, 0.0251 mmol) or $[Ir(\eta\text{-}C_5Me_5)Cl_2]_2$ (0.0253 g, 0.0318 mmol). The reaction mixture was allowed to stir overnight, after which it was filtered through Celite. The 4-ferrocenylpyridine (**3.12:** 0.0130 g, 0.0494 mmol; **3.13:** 0.0165 g, 0.0627 mmol) was added to the reaction mixture and allowed to stir for a further 30-60 minutes. The solvent was removed, the residue dissolved in acetone and filtered through Celite. The solvent was once again removed and the residue dissolved in a minimum amount of methanol, followed by the addition of the $NaPF_6$ (**3.12:** 0.00840 g, 0.0500 mmol; **3.13:** 0.0112 g, 0.0667 mmol). This was stirred at 0°C for about 1 hour, whereby a solid precipitated out, which was then filtered under vacuum, washing with cold methanol and diethyl ether to yield the desired products as orange-red solids.

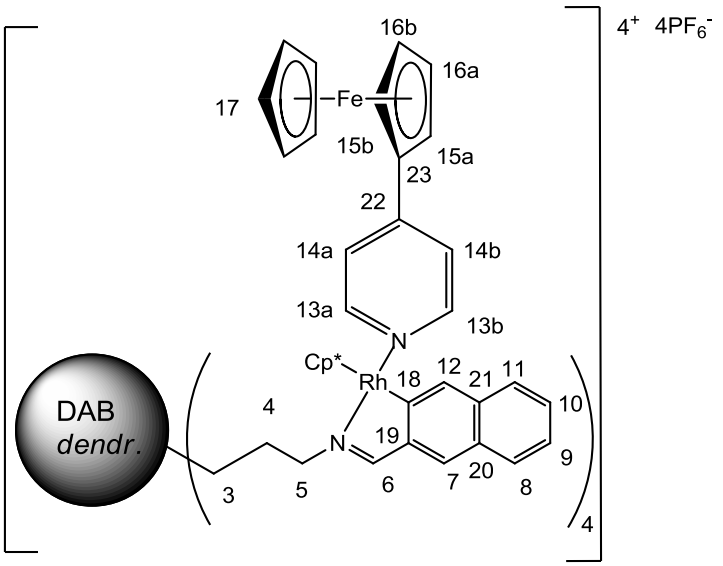

3.12: Orange-red solid. Yield = 0.0100 g (24%). **IR:** (KBr pellets), ν/cm^{-1}: 1608 (C=N), 831 (s, P–F). **^{1}H NMR** (400 MHz, acetone-d_6) δ (ppm) = 1.11 (m, 4H, $\mathbf{H_{core}}$); 1.68 (s, 60H, **Cp***); 1.82 (m, 8H, $\mathbf{H_4}$); 3.77, 3.85 (m, 12H, $\mathbf{H_{core}}$,$\mathbf{H_3}$); 3.94 (m, 20H, $\mathbf{H_{17}}$); 4.46 (m, 16H, $\mathbf{H_5}$,$\mathbf{H_{16}}$);

4.80 (m, 8H, **H_{15}**); 7.40 (m, 12H, **H_9,H_{14}**); 7.57 (m, 4H, **H_{10}**); 7.76 (m, 8H, **H_8,H_{11}**); 8.02 (m, 8H, **H_7,H_{12}**); 8.29 (m, 8H, **H_{13}**); 8.74 (br s, 4H, **H_6**).

$^{13}C\{^1H\}$-NMR (100 MHz, acetone-d_6) δ (ppm) = 8.42 (**Cp***); 8.84 (**C_{core}**); 25.60 (**C_4**); 51.26 (**C_{core}**); 52.57 (**C_3**); 67.82 (**C_{15}**); 70.46 (**C_{17}**); 71.78 (**C_{16}**); 71.94 (**C_5**); 122.30-124.02 (**C_{20}, C_{21}, C_{22} C_{23}**); 125.09 (**C_9**); 126.92 (**C_{14}**); 127.95 (**C_7**); 128.15 (**C_{10}**); 129.20 (**C_{12}**); 129.58 (**C_{11}**); 129.85 (**C_8**); 131.18 (**C_{18}**); 133.06 (**C_{13}**); 136.40 (**C_{19}**); 174.99 (**C_6**). Melting point: 204-206°C.

Elemental Analysis (%): Calc. For $C_{160}H_{172}F_{24}Fe_4N_{10}P_4Rh_4$ (3450.06): C, 55.70; H, 5.02; N, 4.06; Found: C, 53.40; H, 5.89; N, 3.56. **MS** (ESI-HR, m/z): 653.85 $[M\text{-}4PF_6\text{-}(Fc\text{-}py)]^{4+}$.

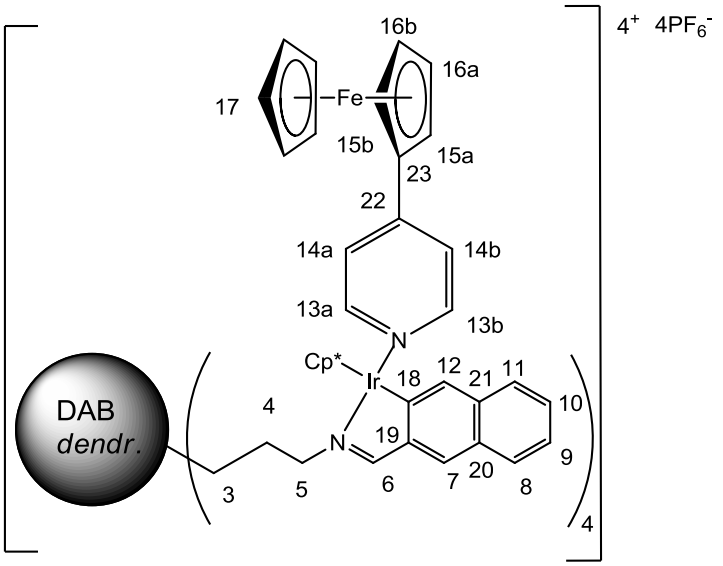

3.13: Orange-red solid. Yield = 0.0266 g (44%). **IR:** (KBr pellets), ν/cm^{-1}: 1610 (C=N), 835 (s, P–F). **^1H NMR** (400 MHz, acetone-d_6) δ (ppm) = 1.46 (m, 4H, **H_{core}**); 1.68 (s, 60H, **Cp***); 2.25 (m, 8H, **H_4**); 3.80, 3.86 (m, 12H, **H_{core},H_3**); 3.97 (m, 20H, **H_{17}**); 4.44, 4.53 (m, 16H, **H_5,H_{16}**); 4.83 (m, 8H, **H_{15}**); 7.47 (m, 12H, **H_9,H_{14}**); 7.62 (m, 4H, **H_{10}**); 7.80, 7.88 (m, 8H, **H_8,H_{11}**); 8.07 (m, 8H, **H_7,H_{12}**); 8.28 (m, 8H, **H_{13}**); 8.55 (br s, 4H, **H_6**).

$^{13}C\{^1H\}$-NMR (100 MHz, acetone-d_6) δ (ppm) = 8.30 (**Cp***); 8.81 (**C_{core}**); 25.57 (**C_4**); 51.28 (**C_{core}**); 51.41 (**C_3**); 67.30 (**C_{15}**); 71.03 (**C_{17}**); 71.54 (**C_{16}**); 71.80 (**C_5**); 121.48-122.78 (**C_{20}, C_{21}, C_{22} C_{23}**); 123.23 (**C_9**); 124.41 (**C_{14}**); 126.08 (**C_{10}**); 126.51 (**C_{12}**); 127.98 (**C_{11}**); 128.72 (**C_8**); 129.08 (**C_7**); 129.914 (**C_{13}**); 132.14 (**C_{18}**); 152.65 (**C_6**); 177.18 (**C_{19}**). Melting point: 215-217°C.

Elemental Analysis (%): Calc. For $C_{160}H_{172}F_{24}Fe_4Ir_4N_{10}P_4$ (3807.30): C, 50.48; H, 4.55; N, 3.68; Found: C, 47.28; H, 5.31; N, 3.02. **MS** (ESI-HR, m/z): 1058.37 $[M\text{-}3PF_6\text{+}MeOH]^{3+}$.

5.4.3 General synthesis of the cationic rhodium(III) and iridium(III)-ferrocenyl naphthaldimine G2 metallodendrimers ***3.14 & 3.15****.*

The naphthaldimine G2 dendritic ligand (**3.14:** 0.0250 g, 0.0133 mmol; **3.15:** 0.0466 g, 0.0248 mmol) and sodium acetate (**3.14:** 0.0090 g, 0.110 mmol; **3.15:** 0.0165 g, 0.201 mmol) was suspended in methanol (20.0 mL) followed by the addition of the $[Rh(\eta\text{-}C_5Me_5)Cl_2]_2$ (0.0333 g, 0.0539 mmol) or $[Ir(\eta\text{-}C_5Me_5)Cl_2]_2$ (0.0798 g, 0.0100 mmol) dimer. The reaction mixture was allowed to stir for 24-48 hours, after which it was filtered through Celite. The 4-ferrocenylpyridine (**3.14:** 0.0280 g, 0.106 mmol; **3.15:** 0.0532 g, 0.0202 mmol) was added to the reaction mixture and allowed to stir for a further 30-60 minutes. The solvent was removed, the residue dissolved in acetone and filtered by gravity. The solvent was once again removed and the residue dissolved in a minimum amount of methanol, followed by the addition of the $NaPF_6$ (**3.14:** 0.0186 g, 0.111 mmol; **3.15:** 0.0343 g, 0.204 mmol). This was stirred at 0^oC for about 1 hour, whereby a solid precipitated out, which was then filtered under vacuum, washing with cold methanol and diethyl ether to yield the desired products as dark orange solids.

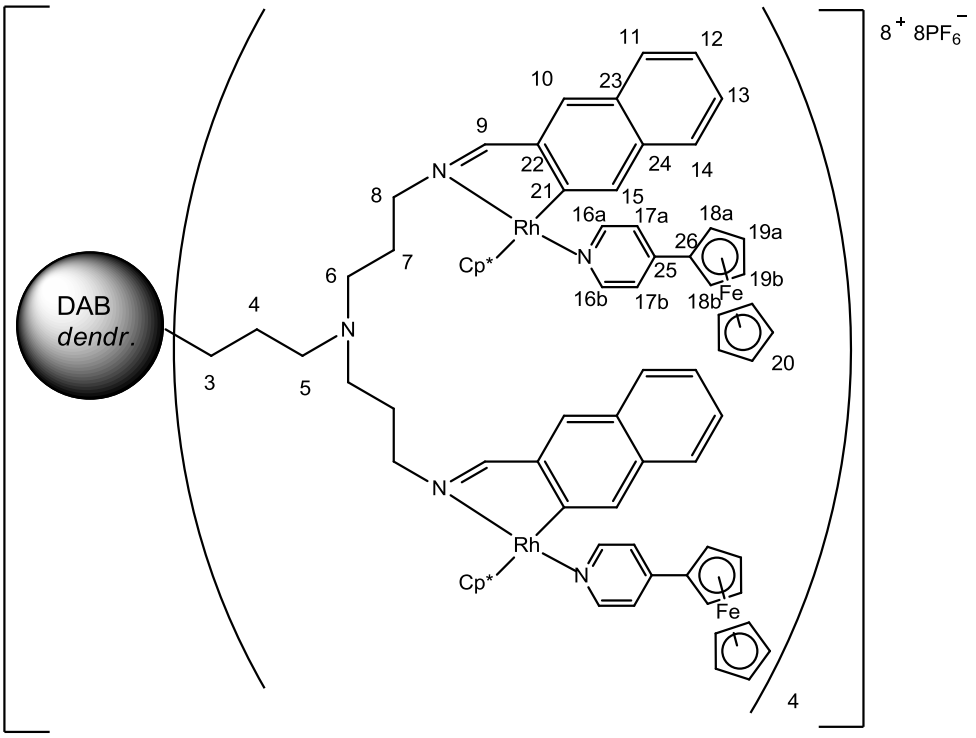

3.14: Dark orange solid. Yield = 0.0475 g (51%). **IR:** (KBr pellets), ν/cm^{-1}: 1608 (C=N), 835 (s, P–F). **^{1}H NMR** (400 MHz, acetone-d$_6$) δ (ppm) = 1.30 (m, 4H, **H$_{core}$**); 1.43 (m, 8H, **H$_4$**); 1.68 (br s, 120H, **Cp***); 2.09 (m, 16H, **H$_7$**); 2.60-3.06 (m, 36H, **H$_{core}$,H$_3$,H$_5$,H$_6$**); 3.87 (m, 16H, **H$_8$**); 3.97 (m, 40H, **H$_{20}$**); 4.54 (br d, 16H, **H$_{19}$**); 4.81 (br d, 16H, **H$_{18}$**); 7.18, 7.47 (m, 24H, **H$_{11}$,H$_{12}$**); 7.72 (m, 16H, **H$_{17}$**); 7.83 (m, 16H, **H$_{13}$,H$_{14}$**); 8.05, 8.12 (m, 16H, **H$_{10}$,H$_{15}$**); 8.36 (m, 16H, **H$_{16}$**); 8.49 (br s, 8H, **H$_9$**).

^{13}C{^{1}H}-NMR (100 MHz, acetone-d$_6$) δ (ppm) = 7.91 (**C$_{core}$**); 8.37 (**Cp***); 14.57 (**C$_4$**); 29.54 (**C$_7$**); 51.11-59.48 (**C$_{core}$,C$_3$,C$_5$,C$_6$**); 67.27 (**C$_{18}$**); 69.97 (**C$_{20}$**); 70.95 (**C$_8$**); 71.41 (**C$_{19}$**); 123.76, 123.93 (**C$_{23}$,C$_{24}$**); 124.74 (**C$_{12}$**); 126.16 (**C$_{17}$**); 127.81 (**C$_{10}$**); 128.95 (**C$_{15}$**); 130.32 (**C$_{11}$**); 130.86 (**C$_{21}$**); 132.70 (**C$_{13}$**); 133.48.25 (**C$_{16}$**); 134.17 (**C$_{26}$**); 135.38 (**C$_{25}$**); 136.13 (**C$_{22}$**); 145.92 (**C$_{14}$**); 174.96 (**C$_9$**). Melting point: 196-198^{o}C.

Elemental Analysis (%): Calc. For $C_{328}H_{360}F_{48}Fe_8N_{22}P_8Rh_8$ (7040.32): C, 55.96; H, 5.15; N, 4.38; Found: C, 53.05; H, 5.02; N, 3.92. **MS** (ESI-HR, m/z): 782.29 $[M\text{-}8PF_6\text{+}HCO_2H]^{8+}$.

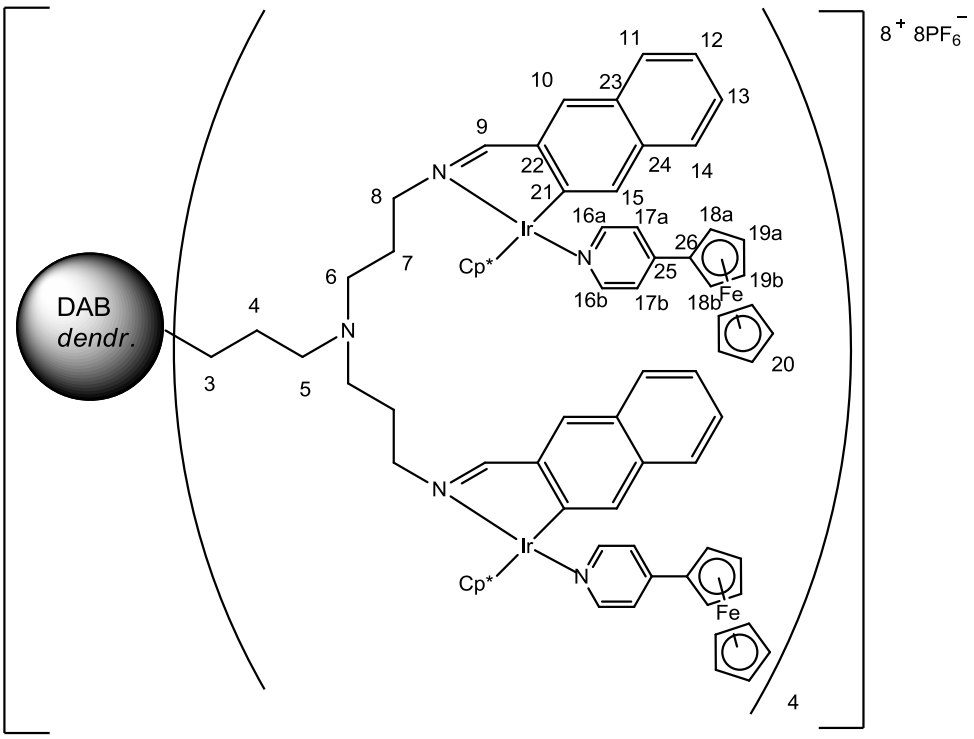

3.15: Dark orange solid. Yield = 0.0800 g (42%). **IR:** (KBr pellets), ν/cm^{-1}: 1610 (C=N), 836 (s, P–F). **^{1}H NMR** (400 MHz, acetone-d$_6$) δ (ppm) = 1.20 (m, 4H, **H$_{\backslash core}$**); 1.30 (m, 8H, **H$_4$**); 1.71 (br s, 120H, **Cp***); 1.82 (m, 16H, **H$_7$**); 2.91 (m, 36H, **H$_{core}$,H$_3$,H$_5$,H$_6$**); 3.94 (m, 40H, **H$_{20}$**); 4.46 (m, 32H, **H$_8$,H$_{19}$**); 4.80 (m, 16H, **H$_{18}$**); 7.42 (m, 24H, **H$_{12}$,H$_{17}$**); 7.57 (m, 8H, **H$_{13}$**); 7.79 (m, 16H, **H$_{11}$,H$_{14}$**); 8.02 (m, 16H, **H$_{10}$,H$_{15}$**); 8.29 (m, 16H, **H$_{16}$**); 8.74 (br s, 8H, **H$_9$**).

$^{13}C\{^1H\}$-NMR (100 MHz, acetone-d_6) δ (ppm) = 8.18 (**Cp^***); 8.62 (**C_{core}**); 27.85 (**C_4**); 32.70 (**C_7**); 51.00 (**C_{core}**); 52.66 (**C_3**); 57.50 (**C_5**); 59.12 (**C_6**); 67.71 (**C_{18}**); 70.25 (**C_{20}**); 71.68, 71.87 (**C_8,C_{19}**); 122.90 (**C_{12}**); 124.57 (**C_{17}**); 126.25 (**C_{10}**); 126.73 (**C_{15}**); 128.13 (**C_{11}**); 129.17 (**C_{14}**); 130.05 (**C_{13}**); 131.80 (**C_{21}**); 135.25 (**C_{26}**); 137.04 (**C_{25}**); 147.88 (**C_{22}**); 153.21 (**C_9**); 176.96 (**C_{16}**). Melting point: 200-202°C.

Elemental Analysis (%): Calc. For $C_{328}H_{360}F_{48}Fe_8Ir_8N_{22}P_8$ (7754.82): C, 50.86; H, 4.68; N, 3.97; Found: C, 47.08; H, 5.65; N, 3.46. **MS** (ESI-HR, m/z): 1058.37 $[M\text{-}6PF_6\text{-}2(Fc\text{-}py)]^{6+}$.

5.5 X-ray diffraction studies

X-ray quality crystals of **2.7**, **2.8**, **2.11** and **2.12** were mounted on a STOE Image Plate Diffraction system equipped with a ϕ circle goniometer, using Mo-Kα graphite monochromated radiation (λ = 0.71073 Å) with ϕ range 0–200°, increment of 1.2 and 0.8° respectively, 2θ range from 3.0–56°, Dmax − Dmin = 12.45–0.81 Å. The structures were solved by direct methods using the program SHELXS-97.[4] Refinement and all further calculations were carried out using SHELXL-97.[4] In all the structures, the H- atoms were included in calculated positions and treated as riding atoms using the SHELXL default parameters and the non H-atoms were refined anisotropically, using weighted full-matrix least-square on F^2. Crystallographic details of complexes were drawn with ORTEP[5] and/or MERCURY[6].

5.6 *In vitro* anticancer activity studies

A2780 (cisplatin-sensitive human ovarian cancer cell line), A2780cisR (cisplatin-resistant human ovarian cancer cell line) and HEK (Human Embryonic Kidney 293) were obtained from the European Collection of Cell Cultures (Salisbury, U.K.). The A2780 and A2780cisR cells were grown routinely in two 50 mL culture flasks in regular RPMI-1640 medium supplemented with 10% heat-inactivated foetal bovine/calf serum (FCS) and antibiotics, 100 μmL penicillin and 100 μm streptomycin. While HEK cells were grown with DMEM medium, with 10% foetal calf serum (FCS) and antibiotics at 37 °C and 5% CO2. One day before experiments, cells were seeded into 96-well plates as monolayers with 100 μL of cell solution (approximately 20 000 cells) per well and preincubated for 24 h in medium supplemented with 10% FCS. The compounds were prepared as DMSO solutions and then dissolved in the PBS buffer culture and serially diluted to the appropriate concentration, to give a final DMSO concentration of 0.5%. A 100 μL portion of the drug solution was added to each well, and the plates were incubated for another 72 h at 37°C. Subsequently, MTT (3-(4,5-dimethyl-2-thiazolyl)-2,5-diphenyl-2H-tetrazolium bromide) (5 mg/mL solution) was added to the cells and the plates were incubated for a further 2 h. The MTT assay was used to quantify the viability of cells. The culture medium was aspirated, and the purple formazan crystals formed by the mitochondrial dehydrogenase activity of vital cells were dissolved in DMSO. The optical density, directly proportional to the number of surviving cells, was quantified at 590 nm using a multiwell plate reader, and the fraction of surviving cells was

calculated from the absorbance of untreated control cells at 590 nm. Mean and standard deviation for the triplicate wells were reported. Each compound was tested at various maximum concentrations ranging from 30-300μM.

5.7 References

1. M. A. Bennett and A. K. Smith, *Dalton Trans.*, 1974, **2**, 233-241.
2. C. White, A. Yates, P. M. Maitlis and D. M. Heinekey, *Inorg. Synth.*, 2007, **29**, 228-234.
3. N. Mungwe, A. J. Swarts, S. F. Mapolie and G. Westman, *J. Organomet. Chem.*, 2011, **696**, 3527-3535.
4. G. M. Sheldrick, *Acta Cryst.*, 2008, **A64**, 112-122.
5. L. J. Farrugia, *J. Appl. Cryst.*, 1997, **30**, 565.
6. I. J. Bruno, J. C. Cole, P. R. Edgington, M. Kessler, C. F. Macrae, P. McCabe, J. Pearson and R. Taylor, *Acta Cryst*., 2002, **B58**, 389-397.

Chapter 6: Conclusions and Future Outlook

6.1 Conclusions

A series of monomeric, first- and second- generation end-group modified *C,N*-chelating bidentate poly(propylenimine) dendritic ligands were prepared. These monomeric and dendritic ligands were fully characterized using a range of spectroscopic and analytical techniques. These ligands were based on a naphthaldimine and benzaldimine Schiff base ligand.

The synthesized monomeric and dendritic ligands were reacted with ruthenium(II), rhodium(III) and iridium(III) precursors to afford air-stable naphthaldimine and semi-air-stable benzaldimine chelating bidentate *C,N*-donor ruthenium(II), rhodium(III) and iridium(III) cyclometalated multinuclear metallodendrimers, which were characterised using analytical and spectroscopic methods.

The naphthaldimine neutral complexes underwent reactivity studies with PTA to afford air-stable naphthaldimine chelating bidentate *C,N*-donor ruthenium(II), rhodium(III) and iridium(III) cyclometalated multinuclear metallodendrimers. A series of heterometallic complexes were synthesized by replacing the chloride ligand with a nitrogen-donor ferrocenyl-pyridine moiety to afford air-stable naphthaldimine chelating bidentate *C,N*-donor rhodium(III) and iridium(III) cyclometalated heterometallic metallodendrimers. These cationic complexes were characterised using analytical and spectroscopic methods.

The molecular structures of the mononuclear neutral ruthenium(II) and rhodium(III) naphthaldimine and rhodium(III) and iridium(III) benzaldimine complexes were determined using single crystal X-ray crystallography which confirmed the pseudo-tetrahedral “piano-stool” geometry around the metal centres.

Subsequent to the synthesis of the neutral and cationic homometallic metallodendrimers, their cytotoxicities against A2780 and A2780cisR human ovarian cell lines, as well as the non-cancerous HEK and KMST-6 cells, were evaluated. The second generation naphthaldimine cationic *C,N*-chelating bidentate octanuclear complexes showed the highest antiprolific

activity against both cell lines. Hence, this study has shown a definite correlation between the size of the metallodendrimer and cytotoxicity, as well as charge and cytotoxicity.

6.2 Future Outlook

From the obtained results, the project has shown great outcomes in the field of ruthenium(II), rhodium(III) and iridium(III) cyclometalated metallodendrimers as biological agents. Through functionalization of the poly(propylenimine) dendritic scaffold with ruthenium(II), rhodium(III) and iridium(III) moieties there was an increase in biological activity, as well as specificity. The benzaldimine complexes proved to be less stable and showed inconclusive antiproliferative results. Hence, the naphthaldimine complexes only underwent reactivity studies with PTA, as well as displacement with a ferrocenyl-pyridine moiety, to produce cationic complexes. Therefore incorporation of water soluble moieties, such as PTA or may increase the water solubility and therefore may result in lower IC_{50} values.[1] Introducing a more water soluble dendritic scaffold, such as PAMAM, may also play a role in increasing the antiproliferative activity of these complexes.[2]

Another alteration that could be changed is the ring-moieties attached to the metal centre. For example a more extended Cp* ring, such as (η^5-$C_5Me_4C_6H_4C_6H_5$), could be incorporated into the rhodium(III) and iridium(III) complexes to improve IC_{50} values by possible DNA intercalation.[3] In addition to this an HMB arene ring can be incorporated onto the ruthenium(II) complexes in order to improve lipophilicity.[4]

In order to confirm the possible drug targets and the mode of action of these ruthenium(II), rhodium(III) and iridium(III) metallodendrimers, further studies need to be undertaken. These studies could include DNA-binding studies, imaging studies (for example fluorescent studies of iridium complexes) and cell uptake studies.

6.3 References

1. C. Scolaro, T. J. Geldbach, S. Rochat, A. Dorcier, C. Gossens, A. Bergamo, M. Cocchietto, I. Tavernelli, G. Sava, U. Rothlisberger and P. J. Dyson, *Organometallics*, 2006, **25**, 756-765.

2. X. Zhao, S. C. J. Loo, P. P.-F. Lee, T. T. Y. Tan and C. K. Chu, *J. Inorg. Biochem.*, 2010, **104**, 105-110.
3. Z. Liu, A. Habtemariam, A. M. Pizarro, G. J. Clarkson and P. J. Sadler, *Organometallics*, 2011, **30**, 4702-4710.
4. P. Govender, A. K. Renfrew, C. M. Clavel, P. J. Dyson, B. Therrien and G. S. Smith, *Dalton Trans.*, 2011, **40**, 1158-1167.